Ethos
14/2/14

RIPHID16

ISSN

THE DEVELOPMENT OF A GENERALISED FINITE ELEMENT SCHEME FOR HEAT TRANSFER AND FLUID FLOW ANALYSIS

BY

FARAMARZ SHEMIRANI, BSc (HONS), MSc

A THESIS SUBMITTED IN PARTIAL FULFILMENT OF THE REQUIREMENTS OF THE COUNCIL FOR NATIONAL ACADEMIC AWARDS FOR THE DEGREE OF DOCTOR OF PHILOSOPHY

DECEMBER 1991

DEPARTMENT OF MECHANICAL ENGINEERING

NOTTINGHAM POLYTECHNIC

Dedicated to my loving parents.

ACKNOWLEDGEMENTS

To my Director of Studies, Dr K Jambunathan, I express my sincere gratitude for his continuous support and encouragement and invaluable advice and guidance throughout this work. I am grateful to my second supervisor and the Head of the Department, Professor BL Button, who allowed unlimited access to the facilities of the department.

I am thankful to the librarian, Mr Jim Corlett, who provided an excellent and comprehensive service during the entire period of this work. I thank Mr Shabir Kapasi for his sincere friendship and the genuine interest he showed to my work. His suggestions and advice are greatly acknowledged. I am grateful to Mrs Shirley Ashforth Frost and Mr Stewart Hartle, who permitted the use of their facilities.

My thanks are also extended to Dr Mehran Pasdari, Dr Richard Edwards, Dr Ali Uzel, Dr Martyn Lacey, Mr David York, Mr Farhad Fassihi and Mr Shahrokh Zangeneh for their advice and friendship.

ABSTRACT

A generalised finite element scheme to analyse two-dimensional fluid flow with heat transfer under the steady state condition has been developed. The Analysis of both laminar and turbulent flow regimes in complicated geometries is facilitated. Imposition of various types of flow boundary conditions is achieved with minimal effort.

Throughout its development, the emphasis has been on making the scheme efficient in terms of computer storage and run-time. In order to achieve this goal, a number of innovations have been introduced both at the finite element discretisation and the solution stages. Advantages have been taken from the recent developments in the Finite Element Method (FEM), as well as adopting some of the established techniques used by the Finite Volume Method (FVM). As a result the scheme is shown to have a computational efficiency comparable with those employing the FVM.

A simple streamline upwind technique is devised in representing the advection terms in the governing transport equations. Verification tests are carried out which demonstrate the accuracy of the streamline technique in treating advection. The upwinding is shown to produce significantly smaller numerical diffusion errors than those arising from previous upwind approximations. The results also show that the technique is unconditionally stable and produces no spurious spatial oscillations. The technique is straightforward and can be added to conventional Galerkin type finite element codes quite readily.

For the solution of the coupled transport equations, an equal order interpolation is used for all variables including pressure. Pressure and velocities are segregated and are obtained separately. A SIMPLER-like algorithm is used to sequentially solve and update velocity components and pressure. The solution is carried out in an iterative fashion. At each iteration, systems of equations are solved by a technique similar to that used in the FVM. A line-by-line Tri-diagonal matrix solution algorithm is developed for the completely unstructured grids that are generated by the FEM. The technique is

particularly efficient in terms of storage requirements and computational speed. It also takes advantage of the nature of the system of equations to be solved.

Several laminar benchmark exercises with and without heat transfer are performed. These include developing and fully developed isothermal duct flow, backward facing step flow, natural convection in square cavity and jet impingement with heat transfer. Results show that the adopted equal order velocity-pressure method can predict the benchmark solutions efficiently and accurately. Spurious pressure modes are also shown to be completely absent.

In modelling turbulent flows, the k-ε two equation eddy viscosity model is employed. The advection part of the k and ε equations are discretised by the upwind technique developed in this research. Special treatment of the source terms eliminate the possibility of producing negative values of k or ε during the iterative solution sequence, which can cause convergence difficulties. By combining the Law of the Wall and the Log Law of the Wall to determine shear stresses near solid regions, the need for an excessively fine mesh in these regions is avoided.

PUBLICATIONS

1. Jambunathan K and Shemirani F (1990), *FIESTA, an Educational Interactive Finite Element Package for Heat Transfer Analysis*, Int J Appl Engng Ed, 6(3), 349-360.

2. Jambunathan K, Shemirani F and Button BL (1990), *FESTAL, a finite element scheme for thermal analysis*, Int J Appl Engng Ed, Accepted.

3. Shemirani F and Jambunathan K (1990), *Conservative monotone streamline upwind formulation using simplex elements*, Int J Numer Meth Fluids, Submitted.

4. Shemirani F and Jambunathan K (1991a), *SIMPLER Finite Element procedure, incorporating equal-order velocity-pressure formulation*, presented at the 7^{th} International Conference on Numerical Methods in Laminar and Turbulent Flow, July 15-19 1991, Stanford, California, USA.

5. Shemirani F and Jambunathan K (1991b), *Regional Alternating-Direction Implicit Solver (RADIS) - A TDMA variant for completely unstructured grids generated by the FEM*, In preparation.

CONTENTS

LIST OF FIGURES

LIST OF TABLES

NOMENCLATURE

A	domain area
A^e	element area
$[A]^e$	element coefficient matrix
A_f	area integral of element shape function
a_{ij}^{ϕ}	members of element coefficient matrix for ϕ
B	constant in the Log Law of the Wall
C, C_1, C_2, C_μ	turbulent model constants
c	specific heat capacity
D	characteristic width
D_x, D_y	absolute sum of shape function x and y derivatives
E	wall smoothness constant
e_i^u, e_i^v	body force vectors excluding pressure gradient terms
F_{ij}, F_{jk}, F_{ki}	normal mass flow rates across element sides
F_P, F_P', F_P''	streamline interpolation factors
f^e	element force vector
f_i^{ϕ}	force vector for ϕ at node i
G	generation term in k-equation
g_x, g_y, g_z	components of gravity in x, y and z directions
H	characteristic height
h	convective heat transfer coefficient
I	turbulent intensity
K_e	non-dimensionalised excess pressure drop
K_i^u, K_i^v	pressure gradient coefficients in x and y directions
k	thermal conductivity, turbulent kinetic energy
k_{air}	thermal conductivity of air
k_{avrg}	average thermal conductivity

k_{solid}	solid thermal conductivity
L	characteristic length
L_e	entrance length
L_i, L_j, L_k	local area coordinates for linear triangular element
ℓ_{ij}	element boundary length
l	turbulent length scale
l_m	turbulent mixing length
M	Mach number
m	number of nodes per element
N	element shape function vector
N_T	lumped element shape function
Nu	Nusselt number
Nu_{max}	maximum wall Nusselt number
Nu_{min}	minimum wall Nusselt number
n	unit outward normal vector
n^e	total number of elements in domain
n_x, n_y	components of n in x and y directions
P	mean pressure
Pe	flow Peclet number
Pe_{cell}	cell Peclet number
p	laminar or fluctuating pressure
p'	instantaneous pressure
$\dot{Q}$	rate of heat generation
Q_c, Q_p	constant terms for heat generation rate
q	outward flux
R	universal gas constant
Ra	Rayleigh number
Re	Reynolds number
R^ϕ	absolute residual for ϕ
R_T^ϕ	total absolute residual

r	radial distance
S_ϕ	source term for ϕ
S_c, S_p	source term constants
s	domain boundaries, tangential streamline coordinate or step height
s_q	flux boundaries
s_ϕ	Dirichlet boundaries
T	temperature
T_{min}, T_{max}	minimum and maximum domain temperatures
T_o	reference temperature
t	time
t_o	sampling time
U	x-component of mean velocity
U_{avrg}	average inlet velocity
U_{max}	maximum velocity in x-direction
u	x-component of laminar or fluctuating velocity
u'	x-component of instantaneous velocity
$\hat{u}$	x-component of hat velocity
u_s	streamline velocity
u_δ	velocity parallel to wall
V	y-component of mean velocity
V_{max}	maximum velocity in y-direction
V_{ref}^{ϕ}	physical reference value for ϕ
V_{jet}	jet inlet velocity
v	y-component of laminar or fluctuating velocity
v'	y-component of instantaneous velocity
$\hat{v}$	y-component of hat velocity
W	z-component of mean velocity or element weight function vector
w	z-component of laminar or fluctuating velocity

w'	z-component of instantaneous velocity
X	x-component of body force
$\overline{X}$	x-component of mean body force
X_R	reattachment point
x	x-coordinate direction
Y	y-component of body force
y	y-coordinate direction
$\overline{Y}$	y-component of mean body force
Z	z-component of body force
$\overline{Z}$	z-component of mean body force
z	z-coordinate direction

GREEK SYMBOLS

α^{ϕ}	relaxation factor for ϕ
β	thermal expansion coefficient
δ	perpendicular distance from wall
δ^{+}	non-dimensional δ
Γ_{ϕ}	diffusion coefficient for ϕ
ε	rate of dissipation of turbulent kinetic energy
η	local coordinate for bi-linear rectangular element
θ	flow angle
$\theta_1, \theta_{ij}, \theta_{ik}$	streamline elevations with respect to x
κ	Kolmogorov constant
λ	element aspect ratio
μ	laminar dynamic viscosity
μ_t	turbulent dynamic viscosity
ν	laminar kinematic viscosity
ν_t	turbulent kinematic viscosity
ξ	local coordinate for bi-linear rectangular element
ρ	reference fluid density

ρ_l	local fluid density
$\sigma_k, \sigma_\varepsilon$	turbulent model constants
$\sigma_x, \sigma_y, \sigma_z$	Reynolds normal stresses
$\tau_{xy}, \tau_{xz}, \tau_{yz}$	Reynolds shear stresses
τ_w	wall shear stress
Φ	dissipation function
ϕ	scalar variable
ϕ^e	element vector of unknown ϕ
ψ_{max}	maximum stream-function value
ψ_{mid}	centre point stream-function value
ω	time-average square of vorticity fluctuation

CHAPTER 1

INTRODUCTION

1.1 Overview and scope of current work

This work is concerned with the Finite Element discretisation of the governing transport equations for fluid flow. The ultimate aim of this research is to provide an efficient and accurate program for the prediction of turbulent flow in general two-dimensional geometries. This has been possible through a number of successive development stages. At each stage, a number of alternative techniques were considered and the most appropriate was selected. The chosen techniques were then altered, modified or refined in order to produce the best possible results. Throughout this research, emphasis has been placed on physical considerations and mathematical manipulations have been deliberately kept to a minimum. It was decided that in this manner the critical evaluation of the results would point directly to the deficiencies of the proposed models.

In this chapter a literature review of the research work in the field of numerical analysis of fluid flow and heat transfer is presented. In section 1.2.1 the recent developments by the Finite Element Method (FEM) are reviewed. In section 1.2.2 the numerical treatment of the advection terms in the transport equations by various methods is presented. A discussion is also given on the effectiveness of such methods in reducing the errors associated with the modelling of advection. Section 1.2.3 provides a broad review of the current methods for turbulence modelling by both the Finite Volume Method

(FVM) and the FEM. It is through these reviews that the most appropriate course of action for this research is selected. The objectives of the current research are presented in the penultimate section. In the final section an outline of the remaining chapters in this dissertation is presented.

1.2 Review of previous work

In this section a review of the relevant research work in the field of Computational Fluid Dynamics (CFD) is presented. The focus of attention is mainly on the FEM. The most recent advances by the FEM are first reviewed. The various FEM models for advection transport are next reviewed. Lastly, the subject of turbulence modelling by the FEM is presented. Also throughout this review, and especially in the area of turbulence modelling, reference is made to the appropriate research carried out with the FVM.

1.2.1 Recent developments in FEM

The FEM was first conceived in the late 1950's as a method of analysing stress distributions within complex structures in the aircraft industry. Since then, the FEM has found its way into countless other applications. Its range of applicability and success rate in many areas of science and technology has, quite simply, been astonishing. Over the past two decades the FEM has emerged as a powerful tool for predicting and analysing complex flow situations. Engineers and researchers alike have benefitted considerably from the freedom, accuracy and ease offered by the FEM in describing complicated geometries and imposing various boundary conditions. The purpose of this review is to list and briefly discuss the implications of the most recent developments in the FEM that are relevant to the

present work. The review is therefore concerned with three specific topics of mesh generation, novel Finite Element formulations and solution techniques.

Mesh generation is one of the key areas where the FEM has been particularly successful. The task of defining complex two-and three-dimensional shapes and their subsequent subdivision into elements is becoming progressively easier, faster and more accurate. Mesh generation is an area where the complete unstructured nature of the FEM has been explored to the full. In most Finite Element codes, mesh generation forms an essential and an integral part of the whole analysis. There are numerous mesh generation techniques currently in use. These techniques are becoming more advanced almost by the day. The following review concentrates on recent papers which deal with the more fundamental aspects of mesh generation. In particular those papers where mesh generation is influenced by the criteria of simplicity, generality, efficiency, accuracy and utilisation in fluid flow analysis are reviewed. Comprehensive surveys of mesh generation routines are carried out by Buell and Bush (1973), Ewing (1986), Hawken (1987) and Shephard (1988).

Akyuz (1970) uses the concept of natural coordinate systems to produce a flexible automatic mesh generation scheme. By dividing the domain of interest into subdomains, Akyuz was able to generate the desired mesh for one-, two- or three-dimensional geometries with curved boundaries. He employed biquadratic quadrilateral subdomains and bilinear rectangular elements. Zienkiewicz and Phillips (1971) used isoparametric curvilinear mapping of quadrilaterals to generate planes and curved surfaces. They used triangular shapes as their basic

elements, which enabled them to discretise any arbitrary shape in space. Their method may be extended to three-dimensions with minor additions. Jones (1974) introduced a mesh smoothing and mesh restructuring technique for two-dimensions. He employed quadrilateral elements and was able to re-number the elements in such a way to minimise the bandwidth of the global matrix and hence improve on machine storage and execution time. Herrmann (1976) developed a combined Laplacian-Isoparametric two-dimensional grid generator. His scheme could be extended to three dimensions, but due to its iterative nature it was rather wasteful of computer time. Bryant (1985) proposed a flexible two-dimensional mesh generator that used triangular elements. Penman and Grieve (1987) based their self-adaptive mesh generator on principles that ensured global error bounds. They sequentially solved the discretised equations, calculated error estimates and refined the mesh until an optimum solution was obtained. Oden et al (1987) developed an adaptive mesh generator that was used throughout the computations with the mesh being continuously refined and re-defined as the solution progressed. Cook (1988) introduced a body-fitted Finite Element mesh generator and demonstrated its accuracy by solving examples in both Cartesian and Cylindrical coordinate systems. Tezuka and Okuda (1988) introduced an adaptive mesh refinement procedure that considered the Finite Element discretisation error. They managed to refine the mesh based on this error analysis without having to introduce more nodes/elements into the domain. The mesh generation routine developed for this research is based on the scheme of Zienkiewicz and Phillips (1971). Jambunathan and Shemirani (1990) used the mesh generator in an interactive Finite Element package for heat transfer analysis in solids. Jambunathan et al (1990) employed the routine in the analysis of isothermal laminar

fluid flow. The routine has been further modified in order to increase its flexibility and accuracy by Shemirani and Jambunathan (1991a). In their method, the mesh generation routine becomes an integral part of the solution algorithm and greatly improves the computer storage and execution time of the solution algorithm as is mentioned later in this section and described in detail in Chapter 5.

The discretisation of the nonlinear governing transport equations by the FEM results in a set of simultaneous linear algebraic equations. The solution to such an equation set can be obtained by either direct or iterative methods. Direct methods such as the Gaussian elimination or the Lower-Upper (LU) decomposition require excessive amounts of computer storage and solution time. For flow situations where a large number of elements must be used, the direct methods become very inefficient and indeed impractical. The relatively slow emergence of semi-direct or iterative solutions for the FEM is due to the unstructured nature of the method. In the FVM on the other hand, a structured grid allows the development of very efficient solution algorithms which possess optimal convergence rates to the exact solution. The most well known of these methods are the Alternating-Direction Implicit (ADI) scheme of Peaceman and Rachford (1955), strongly implicit scheme of Stone (1968), preconditioned conjugate gradient methods such as that of Kershaw (1978), the multigrid method of Brandt (1977) and many more. Some of these solution techniques have been adopted for regularly structured Finite Element meshes. Solution strategies based on the above iterative techniques yet applicable to completely unstructured Finite Element meshes are highly desirable.

Irons (1970) introduced a Frontal solution technique where the Gaussian elimination was combined with a front advancing strategy to solve symmetric positive-definite equations. Hood (1976) later extended this technique to the solution of unsymmetric matrices. The Frontal solution is quite satisfactory for small two-dimensional problems, but becomes very inefficient and time consuming for larger problems. Douglas and Dupont (1971) introduced an Alternating Direction Galerkin method for structured rectangular domains. The implementation of their method to rectangular polygons was performed by Dendy and Fairweather (1975). Deconinck and Hirsch (1979a) used the successive line overrelaxation (SLOR) and the approximate factorisation (AF) in conjunction with FEM for transonic flow calculations. Deconinck and Hirsch (1979b) extended their techniques to the computation of subsonic and transonic cascade flows. Deconinck and Hirsch (1980) then experimented with higher order elements. They showed improved computer efficiency and fast convergence rate, however their method is only suitable for regular Finite Element grids. Some researchers adopted a transient solution strategy, where the steady state solution is obtained in the limit. This allowed nonlinear schemes such as Newton-Raphson or Runge-Kutta to be used very efficiently and without restrictions on the regularity of the Finite Element mesh, see for example Donea (1984), Zienkiewicz et al (1985) and Peraire et al (1986). Preconditioned conjugate gradient methods have also been devised for the FEM. These methods generally require parameter settings which depend on the type of problem at hand, see Carey and Jiang (1987).

For the present research, a novel iterative solution algorithm was devised which is described in detail in Chapter 5. The algorithm

is an implementation of the Alternating-Direction Implicit scheme of Peaceman and Rachford (1955) to the FEM. The algorithm is termed the Regional Alternating-Direction Implicit Solver (RADIS). RADIS is applicable to structured and completely unstructured grids generated by the FEM. RADIS is also applicable to all types of two- and three-dimensional elements. Shemirani and Jambunathan (1991b) show the superiority of the algorithm in terms of computer storage, execution time and convergence rate over the conventional direct or iterative solvers. They also recommend RADIS as a smoother to the Multigrid method, hence improving on its convergence rate.

During the past decade a number of novel Finite Element formulations have appeared in the literature. These formulations generally tend to combine the geometrical flexibility of the FEM with the sequential solution strategy of the FVM. Baliga and Patankar (1980) devised a control volume based formulation with triangular elements for two-dimensional calculations. The formulation was of mixed-order interpolations for velocity and pressure fields. The method was later extended to heat transfer problems by Baliga and Patankar (1983) and Baliga et al (1983). Parakash (1986) introduced the equal-order version of the Baliga and Patankar (1980) method. In this way, he managed to reduce the discretisation errors associated with mixed-order interpolations. Schneider et al (1978b) devised a velocity correction, equal-order finite element formulation, and achieved fast convergence rates. Other equal-order velocity-pressure formulations have also been proposed, see for example Rice and Schnipke (1986) and Schnipke and Rice (1987). Ramaswamy (1988) also used an equal-order velocity-pressure formulation for two-dimensional natural convection analysis.

Other Finite Element workers have concentrated on developing efficient and accurate algorithms for their particular flow arrangements. Obee and Witt (1980) used velocity potential and multi-region arrangement to analyse the impingement of a free jet on a disk. Their method took advantage of the flow conditions in the three different regions of the flow. Allaire et al (1985) employed simplex elements with penalty formulation for accurate analysis of recirculating flows. Betts and Haroutunian (1983) devised a stream function formulation for two-dimensional natural convection, and accurately predicted the variation of the Nusselt number. Dhatt et al (1986) developed a new triangular element for steady and unsteady free surface flows. They employed a Newton-Raphson method to solve the governing nonlinear system of equations. Mochimaru (1986) used the pressure gradient terms in the momentum equations as the dependent variable for the analysis of circular cavity flow. Kawahara and Umetsu (1986) used a two-step explicit FEM in river flow calculations, which contains moving boundaries. Kim (1988) used bilinear rectangles for velocity components and linear triangles for the pressure for the calculation of high Reynolds number flows. Kaluarachchi and Parker (1989) applied the FEM to multiphase flow situations with the help of nonlinear iterative solvers. Kim and Decker (1989) used both velocity-pressure integrated and penalty schemes for high Reynolds Number flows. Finally, Hansen and Hassager (1989) developed a moving FEM which is specially suited for differential equations whose solution contains steep gradients.

The review of the above papers enabled the selection of the most relevant technique for the present work. The criteria of selection were robustness, generality, applicability and possible future

extension to three-dimensions. The selected method was that of Rice and Schnipke (1986). As well as satisfying the above criteria, it also offered a sequential, equal-order velocity-pressure approach in the spirit of the SIMPLER algorithm. This meant that additional transport equations both for the laminar and the turbulent regimes could be included in the formulation without excessive computer requirements. The method of Rice and Schnipke (1986) was based on bilinear quadrilaterals. In order to increase the efficiency and robustness of the formulation for this work, a triangular version of their method was developed. Some novel alterations had to be introduced to increase the accuracy of the formulation. A detailed description of this formulation is given in Chapter 4.

1.2.2 Advection treatment by FEM

The variation of a scalar variable, ϕ, in time and space may be described by a general differential equation that contains rate of change, advection, diffusion and source terms. The temporal variations in ϕ are described by the rate of change term. The source term provides the rate at which ϕ is generated or destroyed. The spatial transport of ϕ is represented by both the advection and the diffusion terms. The diffusive and the advective transport mechanisms are two quite different phenomena- a local disturbance in ϕ is transmitted, in all directions by the diffusion mechanism, and only along characteristic lines by the advection mechanism. The physics of the diffusive transport are adequately captured by the Galerkin weighted residual approach in FEM. In this approach the value of the scalar quantity ϕ at a point is related to ϕ at all the point's neighbours. This in turn ensures that local perturbations in ϕ are made to spread in all directions throughout the diffusive medium - a consistent

reflection of the diffusion transport.

The advection transport, on the other hand, exhibits a directional bias in that the effects of disturbances in ϕ may only travel along characteristic lines. Also the direction of travel is from upstream to downstream locations and not vice versa. This important physical observation may not be immediately deducible from the first order, and generally nonlinear, form of the advection terms in the governing transport equation. Many of the past and present formulations violate the physics of the advection transport resulting in numerical instability and physical inaccuracy that are only too familiar. A major drawback in treating the advection terms is the contamination of the computed variable field by spurious oscillations. For example, in the absence of any source term for ϕ, these oscillations may cause the solution set to waver outside the limiting values of the variable imposed by the boundary conditions which clearly is unacceptable on physical grounds. These oscillations have in the past been referred to as overshoot/undershoot, numerical oscillations, spatial oscillations, wiggles or numerical instability. These oscillations will be referred to as spatial oscillations hereafter. A second drawback, and perhaps not as detectable as the first, is the smearing of the solution set by artificial diffusion. This phenomenon, which is a direct consequence of numerical modelling, acts in a manner analogous to the physical diffusion transport. This artificial diffusion has been referred to as numerical diffusion, crosswind diffusion, false diffusion or numerical smearing. The artificial diffusion will be referred to as numerical diffusion hereafter. In some instances the numerical diffusion can be orders of magnitude greater than the physical diffusion resulting in highly

erroneous solutions.

The deceptively simple form of the advection terms has rendered the numerical treatment of advection an art of compromise between numerical stability and physical accuracy. There is no ideal model of advection which can produce results that are unconditionally free of all spatial oscillations and numerical diffusion. Both the Finite Element and the Finite Volume workers are constantly looking for more accurate and stable, yet more efficient formulations to represent the advection transport. The current review is mainly concerned with the recent advances to this end by the FEM. However, as many of the interesting and innovative ideas have originated from the FVM camp, a brief summary of their research effort is in order.

Initial attempts to approximate the advection terms by the central-difference operators in FVM resulted in unacceptable levels of numerical diffusion and spatial oscillations in cases where the cell Peclet number, Pe_{cell}, exceeded 2. The central-difference scheme can yield reliable results when used in conjunction with very fine grids for which the largest Pe_{cell} is below 2. However, this approach is highly undesirable, and in fact in most engineering applications impractical, as it requires vast amounts of computer resources. To cure this deficiency, countless schemes have been proposed. Patankar (1980) provides a detailed analysis of the earlier models, some of which are still in use today. The simplest advection model is the Upwind scheme first proposed by Courant et al (1952), which approximates the advection terms by the first-order differences taking into account the direction of the velocity vector. The model is accurate for large Pe_{cell}, but breaks down at lower values. The

Exponential scheme of Spalding (1972) relies on the exact one-dimensional solution of the advection-diffusion problem. This scheme is computationally expensive and is not accurate for multi-dimensional situations. The Hybrid scheme of Spalding (1972) is a mixture of the central-difference and the upwind schemes. This scheme can be implemented efficiently, but it gives a poor performance especially around Pe_{cell} of 2. The Power-Law scheme of Patankar (1980) produces the exact solution for one-dimensional situations, but in multi-dimensional situations it too suffers from inaccuracies.

Higher order Finite Volume schemes have also been developed. Amongst these are the second-order upwind differencing (HOU) scheme of Price et al (1966), the quadrature upwind (QUICK) scheme of Leonard (1979) and the streamline upwind (SUD) scheme of Raithby (1976). Hassan et al (1983) produced a mass-flow-weighted skew upwind scheme which is stable and results in little numerical diffusion. In a number of comparison exercises the QUICK scheme has shown to be more accurate than the other schemes, see for example Han et al (1981), Huang et al (1985), Shyy (1985), and Patel and Markatos (1986). QUICK is also being used increasingly in complex two- and three-dimensional turbulent flow calculations, see Leschziner (1989). The QUICK scheme is however computationally expensive and suffers from convergence problems, see Han et al (1986) and Patel et al (1987). Pollard and Sui (1982) improved the convergence properties of the QUICK scheme, but their method is complicated and hence uneconomical. The two major disadvantages of the higher-order schemes are large spatial oscillations at high Pe_{cell} and relatively expensive computer costs in terms of storage and evaluation-time. A variety of composite schemes have been proposed which try to improve the performance of the

higher-order schemes. Leschziner (1989) provides a comprehensive overview of these and many other schemes in connection with the treatment of the advection terms by the FVM.

The evolution of Finite Element schemes in treating the advection transport follows a similar path to that of the FVM. The conventional Galerkin weighted residual approach, akin to the central-difference operator, produces unacceptable levels of spatial oscillation and numerical diffusion. This approach fails to allow for the directional feature of the advection transport. The advection terms are treated in the same manner as the diffusion terms. Hence in a purely advective medium, perturbations in ϕ at a point are incorrectly felt by all of the neighbouring points. The presence of spatial oscillations are more clearly visible in flow situations where downwind Dirichlet boundary conditions are imposed. This difficulty was overcome by one-dimensional upwind schemes, see Christie et al (1976) and Christie and Michell (1978). The generalisation of the one-dimensional schemes to two- and three-dimensions proved to be unsatisfactory, as they resulted in excessive numerical diffusion and spatial oscillation. Hughes and Brooks (1979) introduced a multi-dimensional streamline-upwind/Petrov-Galerkin (SUPG) scheme, which was based on the upwind scheme of Hughes (1978). SUPG had good stability properties and would dampen the numerical diffusion. It also had faster convergence rate than the classical upwind schemes. Brooks and Hughes (1982) demonstrated the use of SUPG in incompressible transient flow calculations. SUPG was later extended to multi-dimensions by Hughes and Mallet (1986a), who also produced precise error estimates of their method for the complete flow Peclet number range. Heinrich and Chung-Chyi (1987) extended the SUPG scheme to time dependent analysis.

They constructed a scheme which is second-order accurate in time and third-order accurate in space for the case of the constant coefficient convection-diffusion equation on a uniform grid with bilinear elements. However, levels of spatial oscillation produced by SUPG generally means its exclusion from applications where sharp boundary and internal layers are present.

More stable solutions may be obtained by Monotone methods. In these methods, monotonicity ensures that new maxima/minima are not introduced in the solution set. In other words, the solution set does not contain values that are outside the physical range imposed by the boundary conditions. Ideka (1983) explains the basic principles of monotone methods. The methods of Hughes et al (1985) and Rice and Schnipke (1985) are good examples of the monotonic property mentioned above. In the latter example, upwinding is performed along the streamline segments passing through the elements. Rice and Schnipke (1985) produced oscillation-free results with minimal numerical diffusion. Unfortunately monotone methods are generally based on arbitrary constraints and do frequently violate the physical laws. For example a major shortcoming of such methods is that they can be non-conservative. In flow cases where the fluid properties are changing, non-conservatism can lead to the global imbalance of the transported quantities. Mizukami and Hughes (1985) introduced a monotone method that uses simplex triangular elements. Their method is conservative and satisfies the requirements of the Petrov/Galerkin method. However the method is complex and its extension to three-dimensions has not yet been reported.

SUPG can be modified so as to capture sharp discontinuities in

the solution domain. Hughes et al (1986a) add a discontinuity capturing term to the element weighting function of the SUPG and produce a nonlinear method. The additional term acts in the direction of the solution gradient rather than in the direction of the streamline. The method shows improved performance over the SUPG on cases with sharp boundary/internal layers. The spatial oscillations are dampened considerably in comparison to SUPG, but are still present at corner points in the domain. The method was generalised to multi-dimensions by Hughes and Mallet (1986b) and obtained accurate solutions to the compressible Euler equations. The method was later used for the Stokes problem by Hughes et al (1986), who employed equal-order interpolation for velocity and pressure. The success of the formulation depends on the correct specification of the stability constants that change from one type of element to another. Also, Hughes et al (1986b) express reservations on their formulation to solve the most general cases of fluid flow which are governed by the Navier-Stokes equations.

Other Finite Element formulations have also appeared in the literature that do not adopt the above concepts. Baliga and Patankar (1980) introduced a control-volume based finite element formulation. They employ three-noded triangular elements for which the element shape function is based on the direction of the local velocity vector. Their method is later extended to three-dimensions by Muir and Baliga (1986) who use tetrahedral elements as their control-volumes. A similar approach is employed by Ramadhyani and Patankar (1985) in conjunction with quadrilateral elements. Idelsohn (1989) achieves upwinding by requiring the satisfaction of a variational principle. He claims that his technique can give clear indication of regions in the

domain where either upwinding is not required, upwinding is necessary and sufficient or upwinding is insufficient and should be replaced by artificial viscosity. Finally, Steffler (1989) introduces a new upwind-weighted element function in the spirit of the QUICK scheme. His element function is influenced by the presence of upwind nodes external to the element. Steffler produces good results for a number of convection-diffusion problems and concludes that the reliability and efficiency of the method should be further investigated.

It can be said that in general the FEM produces less numerical diffusion than the FVM, as is evident from the comparison exercise of Smith and Hutton (1982). This is due to the ability of the method to work with the resultant-velocity direction as opposed to the locally one-dimensional approach of the FVM. Neta and Williams (1986) examined a variety of advection Finite Element formulations and found that the schemes with linear isosceles triangles or bilinear quadrilaterals gave the best results. For the current research, after considering the advantages and disadvantages of the techniques reviewed above, it was decided to employ a monotone upwind technique for the treatment of the advection terms. Monotone techniques are simple to implement and their extension to multi-dimensions is relatively straightforward. They are also computationally economical in terms of storage and evaluation-time. But perhaps the most important feature of these methods is that they do not introduce spatial oscillations. These unphysical oscillations apart from being cosmetically displeasing, can often lead to divergence problems during the course of an iterative process.

The criteria for selecting the appropriate monotone method were

the degree of numerical diffusion, the economy of operations, the generality and the possible extension to three-dimensions. The Monotone Streamline Upwind (MSU) technique of Rice and Schnipke (1985) seemed to satisfy these criteria. However, the MSU technique was non-conservative and was developed in conjunction with the bilinear quadrilateral elements. As is discussed in Chapter 2, these elements can lead to matrices that are not diagonally dominant. This would in turn prohibit the use of fast iterative matrix solvers. Therefore a conservative formulation based on the MSU technique was developed for this research. In this formulation three-noded triangular elements were used to ensure diagonal dominance and to minimise the computational costs. Shemirani and Jambunathan (1990) have applied this formulation to stringent test cases and validated its capability in predicting results with minimal numerical diffusion without spatial oscillations for the entire flow Peclet number range.

1.2.3 Turbulence modelling

Turbulent flows occur at high Reynolds numbers. They are characterised by random and unsteady eddying motions with pressure and velocity fluctuating irregularly in all directions. Rapid diffusion of properties such as mass, heat and kinetic energy are present in a turbulent flow field. A high rate of energy dissipation, i.e. the transfer of the kinetic energy to the internal energy, is also present. Visual observations of turbulent flows show them to consist of eddies of many different sizes or scales. The relative scales of the eddies depend on the geometry and the past history of the flow. In internal flows, the largest eddies have scales of the same order as the width of the flow, whereas the smallest eddies are orders of magnitude smaller than the overall flow dimensions. So to capture the

essential details of such flows directly, very fine computational grids must be employed. Then the solution of the unsteady three-dimensional transport equations for laminar flow would provide the instantaneous distribution of turbulent flow quantities. However as Launder (1972) points out such a direct approach demands computer storage and run-time which exceed today's hardware capabilities. To overcome this problem, numerous turbulence models have been proposed and are in use today. It must be said that none of these models are capable of predicting the turbulent flow characteristics exactly.

Present turbulence models vary greatly in the degree of complexity. Each model has associated with it a set of underlying assumptions. These assumptions ultimately determine the accuracy, generality and applicability of each model. A good turbulence model, is one that relies on as few assumptions as possible, whilst possessing a wide range of applicability. The simpler models are based on the equations that govern laminar flows with no additional transport equations. In the more sophisticated models, additional differential equations are used to describe the transport of turbulent quantities such as the turbulence energy and its dissipation rate. Turbulent models can be classified in several ways. The most popular classification is one where turbulent models are grouped in terms of the number of additional transport equations that are solved along side the equations for mass, momentum and energy, see for example Reynolds (1976) and Rodi (1980). According to this classification there are zero-equation, one-equation, two-equation and turbulent stress/flux-equation models of turbulence. These are the main classes of turbulent models. Rodi (1980) mentions that apart from the above models, there is a newly emerging class of models, called the subgrid

scale models, which show promising results. There are also turbulent models that are based on the integral methods. Before considering the main classes of turbulent models, a brief description of the latter two models will be given.

In the subgrid scale model, it is recognised that the main turbulent transport is governed by the motion of the energetic large scale eddies. A computational grid is then set up to capture such unsteady, three-dimensional motion. The small scale motion, which cannot be captured by this grid, is approximated by an appropriate subgrid model. Examples of the subgrid scale modelling can be found in Deardorff (1971, 1973 and 1975), Schumann (1975), Kwak et al (1975), Love (1978 and 1980) and McMillan and Ferziger (1979). The main drawback of this type of model is its excessive computer requirements, since the computational grid must be fine enough to resolve all but the smallest eddy motions. Additional assumptions may be employed to decrease the grid density. However this diminishes the accuracy and the generality of the method. A typical subgrid model is composed of two components- a main grid scale model and a subgrid scale model. The main grid scale model is used to represent the motion of the large eddies, while the subgrid scale model attempts to model the behaviour of the smallest eddies. These two components are derived from mathematical manipulations involving filtering operations. The filtering may be achieved by a variety of filtering functions such as the Gaussian function, see Love (1980). The two components are substituted into the governing transport equations. The transport equations are then themselves filtered. The nonlinearity of the transport equations results in additional terms which contain the subgrid scales. The subgrid scales can then be described effectively

by simple conventional eddy-viscosity models. The subgrid models are not at present suitable for general turbulence predictions as they place heavy demands on computer memory and run-time. Nevertheless, these models are useful tools in developing and evaluating the more conventional forms of turbulence models.

The models based on the integral methods are used mainly in day-to-day engineering applications. These methods rely on the boundary layer equations which are the simplified versions of the Navier-Stokes equations. The simplifying assumption is that the changes in the flow properties along the stream-wise coordinate are much smaller than those in the cross-stream coordinate. This eliminates the stream-wise dependency and allows for a parabolic rather than an elliptic consideration. The former offers considerable savings in computer storage and execution time as it renders itself to a marching solution procedure as opposed to a sweeping one. Reynolds (1968) reviews a number of these models which were presented at the first Stanford Conference on Computation of Turbulent Boundary Layers in 1968. The most commonly used integral method is the Head's Entrainment Method, Head (1958). In this method the momentum and the continuity equations are integrated with respect to the cross-stream coordinate. With a power-law velocity profile assumption and a skin-friction law, a system of ordinary differential equations is obtained for the boundary layer displacement thickness and the momentum thickness. Other related variables may also be obtained by taking moments of the momentum equation, see Murphy and Rose (1968). The solution of such a system of equations is then obtained by any standard integration algorithm such as Runge-Kutta or Adams Moulton. Green (1968) extended the basic integral method to account for

compressibility. Green et al (1977) introduced an additional differential equation to describe the entrainment rate, hence incorporating the flow history into the method. The integral method models are frequently used in everyday engineering practices where flow parameters such as the pressure distribution and the skin-friction need to be evaluated reasonably accurately and cheaply. They are simple and the turbulence equations can be modified to include new empirical correlations. However, they can only be used for flows where a predominant flow direction exists in the absence of recirculation. The models also lack generality in that they depend strongly on the empirical correlations which change from one flow case to another.

The main classes of turbulent models rely on the time averaged versions of the governing transport equations. The concept of a time-averaged flow field was first introduced by Reynolds (1884). According to Reynolds, an instantaneous turbulent quantity is made up of a mean value and a turbulent fluctuation. By substituting the instantaneous quantities into the transport equations and time-averaging them, a set of coupled differential equations are obtained in terms of the mean values. The time over which the equations are averaged must be larger than the largest turbulent time scale for a particular flow. The time-averaging process produces terms involving the products of the turbulent fluctuations. These terms are the Reynolds stress/flux terms. It is the treatment of these terms that has lead to the development of many turbulent models. The Reynolds stress/flux terms can themselves be described exactly by additional differential equations. These equations are obtained by taking velocity-weighted moments of the momentum equations and

time-averaging them. Unfortunately, this results in equations containing quadratic products of the turbulent terms. This process can be continued to create as many equations as desired. However, at some point the set of equations must be closed by making assumptions about the relationships between the highest order terms and the mean flow quantities. This is known as the turbulent closure problem.

In the zero-, one- and two-equation models the action of the Reynolds stress/flux terms are considered to be similar and additional to those of laminar viscosity/diffusion. In the Reynolds stress/flux models, these terms are themselves governed by algebraic or partial differential equations. There are, in the literature, numerous books and papers on the subject of turbulence modelling, which review and discuss the benefits and the drawbacks of all past and present models. The more recent reviews include: Rodi (1980) who provides a brief and accurate comparative account of the most popular turbulent models and their use in hydraulics, Rodi (1982) lists various models for incompressible turbulent flows, Nallasamy (1987) gives a comprehensive review of turbulence models and their application to internal flows, Launder (1988) concentrates on the problem of heat transfer in turbulent flow calculations, Hutton (1985) highlights the recent advances in the field of turbulent flow predictions by the FEM and Hutton et al (1987) review the role of FEM in the computation of turbulent flows in complex geometries. In the remaining part of this section the main classes of the turbulence models are briefly described. The advantages and disadvantages of each model are also discussed. It is through this discussion that the most appropriate turbulence model for this work is selected.

In the zero-equation models, sometimes referred to as the zero-closure models, the principal governing transport equations are the time-averaged mass, momentum and energy equations. There are no additional equations employed to describe the distribution of the Reynolds stress/flux terms. These terms are modeled via the eddy viscosity/diffusivity concept, where their actions are considered to be similar and additional to their laminar counterparts. The turbulent viscosity and diffusivity may be specified directly from experimental data. They may also be related to the mean-velocity distribution or even take the form of empirical correlations. In the simpler models, the turbulent viscosity and diffusivity are assumed constant everywhere, except at the wall boundaries where they fall to zero. The constant eddy viscosity model offers a simple and crude way of representing turbulence. It over-simplifies the action of the turbulent transport terms and is therefore not widely used. A more advanced model is the Prandtl's mixing length model. In this model the turbulent transport terms are expressed as the product of the turbulent viscosity and the local gradient of the mean flow. Hence for a two-dimensional situation

$$- \overline{uv} = \nu_t \frac{\partial U}{\partial y} \tag{1.1}$$

where ν_t is the turbulent viscosity. ν_t is itself related to the mean velocity gradient

$$\nu_t = l_m^2 \left| \frac{\partial U}{\partial y} \right| \tag{1.2}$$

where l_m is the unknown mixing length, whose variation over the flow field is prescribed empirically. The mixing length model is frequently used for free shear layers and wall boundary layers, see Spalding (1982). Turner Jr and Gunzburger (1988) propose a robust FEM version

of the zero-equation which has a fast convergence rate. In the zero-equation models, the prescription of l_m depends strongly on the type of flow under consideration and becomes increasingly more difficult for recirculating and three-dimensional flows. The important flow features such as curvature, buoyancy and rotation must also be specified empirically. The convective/diffusive transport and the history of turbulence are not accounted for in the mixing length model. Hence, the model has a narrow range of applications and is not suitable as a general purpose turbulence model.

The one-equation models obtain the turbulent velocity scale from an additional transport equation. The most appropriate velocity scale is the turbulent kinetic energy. The turbulent viscosity is expressed in terms of the turbulent kinetic enegry, k, and a length scale, l,

$$\nu_t = C_\mu \sqrt{k}\, l \tag{1.3}$$

where C_μ is an empirical constant. The length scale is flow dependent and must be specified empirically. The differential equation for k is of the same form as for any other transportable quantity, with transient, convective, diffusive and source terms. The one-equation models are generally superior to the zero-equation models as they account for the convective and the diffusive transport of the fluctuating velocity scales. In the case of unsteady flow, the flow-history of the velocity scales is also accounted for by the one-equation models. These models are adequate for shear layer type flows, where the zero-equation models also perform well. The specification of l becomes difficult for the more complex flow situations where separation, streamline curvature or rotation may be present. Algebraic formulae have been used to calculate the length

scale by Gawain and Prichett (1970). However these formulae are complicated and demanding on computer time. Bringen and Abdol-Hamid (1987) apply the one-equation model to free shear flows and produce accurate results for axisymmetric and plane jets, but their agreements with experimental data for the axisymmetric wake is only moderate.

The two-equation models attempt to eliminate the need to empirically describe the length scale in terms of positions in the flow field. This is achieved by introducing a second differential equation. This equation is in effect used to prescribe the length scale. An equation describing the length scale itself can be derived from the Navier-Stokes equations. However this approach is undesirable as it leads to a semi-empirical treatment. Instead, the kinetic energy equation will be supplemented with an equation for another appropriate turbulent quantity. This quantity will be a function of both k and l. Examples of the two-equation models include k-kl, k-ω and k-ε models, where ω is the time-average square of the vorticity fluctuation and ε is the dissipation rate of k, see Launder and Spalding (1974) and Spalding (1977). All of these models, although dissimilar in appearance, are essentially length scale equations. The second quantity, like the turbulent kinetic energy, is governed by a differential equation consisting of transient, convective, diffusive and source terms. The treatment of the near wall regions is different for each model. It is this treatment that often determines the popularity of one model over others. The most popular model in this class is the k-ε model, see Launder and Spalding (1974) and Spalding (1974). The k-ε has been applied to a wide variety of flow situations and is currently the most frequently used turbulence model.

The k-ε model has been successfully incorporated in both the FVM and the FEM. The FVMs with the orthodox coordinate systems, i.e. Cartesian and cylindrical coordinates, have benefitted considerably, e.g. Gosman et al (1977), Leschziner and Rodi (1981), Nallasamy and Chen (1985) and many more. Examples of k-ε with FVMs using the curvilinear coordinate systems include the works of Wachpress (1979), Raithby et al (1986), Demirdzic et al (1980), Demirdzic et al (1986), Demirdzic et al (1987), Burns et al (1988) and Kual and Kwak (1986). Turbulent flow predictions using the k-ε model in conjunction with the FEM are being continuously reported. Larock and Schamber (1981) put forward suggestions for incorporating the k-ε model in the FEM. Taylor et al (1981) consider the turbulent flows with separation. Tong (1982) performs a comprehensive study on the application of the model to recirculating flows. Hutton and Smith (1981) consider the computation of the two-dimensional incompressible turbulent flow using the k-ε model. Smith (1984) reports on the performance of the model with FEM for recirculating flows. Benim and Zinser (1985) apply the model in conjunction with FEM to several confined turbulent flows and obtain good agreements between FEM and FVM. Sharma and Carey (1986) use an efficient FEM discretisation with the k-ε model for boundary layer analysis and produce accurate result on coarse grids. Devantier and Larock (1986) employ the Galerkin FEM with the k-ε model for density driven turbulent flow and express the need for better understanding of the buoyancy production terms in the turbulence closure model. Polansky et al (1987) also experiment with the FEM version of the k-ε model and report convergence difficulties with their high Reynolds number formulation. Their low Reynolds number model behaves well and yields results which are in good agreement with experimental data for two-dimensional channel and backstep geometries. Torbjorn (1988) uses

a mixed Galerkin/Penalty function formulation with the k-ε model for one- and two-dimensional steady-state flows and is able to reasonably predict the major features of the flows.

The original k-ε model of Launder and Spalding (1974) is suitable for the fully turbulent flow regions. In the vicinity of solid boundaries, viscous forces become significant and the flow is no longer turbulent. To account for this, a number of modifications have been introduced. These include the use of various wall functions and near-wall treatments. Jones and Launder (1973) modified the k-ε model to account for laminar, transition and fully turbulent regions. Their low Reynolds number model was further refined by Launder and Sharma (1976) and was reported to perform well in cases studied by Patel et al (1985). Other low Reynolds number models have also been reported which show promising results, e.g. Lam and Bremhorst (1981) and Launder (1986). Nagano and Hishida (1987) improve the performance of the k-ε model of Jones and Launder (1973) for near-wall turbulence by relating the influence of the wall to the local Reynolds number and obtain accurate predictions for isothermal shear flows. Nagano and Kim (1988) also use this model in heat transfer calculations for shear layer flows and show very good agreements with experimental data. Another approach is to divide the near-wall region into two or three layers. Chieng and Launder (1980) adopted a two-layer approach for flow predictions in a pipe expansion. Their two-layer model consisted of a viscous layer beyond which the flow is fully turbulent. Amano (1984) uses a three-layer model consisting of a viscous sublayer, a buffer layer and an overlap layer. Iacovides and Launder (1984) propose a thin Parabolic Sublayer (PSL) model which eliminates the need for wall functions. Nallasamy (1986) expresses that the two- and

three-layer models both improve the heat transfer calculations, but have little advantage over other models in predicting the flow field. However, Chen and Patel (1988) examine the performance of various near-wall treatments and express satisfaction with a two-layer approach, which combines a one-equation near-wall model and the k-ε model, e.g. Richmond and Patel (1987). Djilali et al (1989) compare the performance of several near-wall turbulence models for heat transfer calculations in recirculating turbulent flow and recommend the use of the k-ε model with the three-layer model of Amano (1984).

The k-ε model does not perform well in flow situations where body forces are important. Such body forces may arise as a result of strong streamline curvature, rotation or buoyancy. The reason for the poor performance of the k-ε model has been attributed to its key assumption that the turbulent energy is destroyed where it is created. In other words the k-ε model assumes a local state of isotropy whereby all the stress terms are approximated by one eddy viscosity. This assumption breaks down in cases where a dominant body force is present. The action of such a force is to destroy the local state of isotropy by interacting selectively with different normal and shear stresses. The k-ε model can be modified or refined to capture this anisotropy to some extent. For example, Rodi (1972) replaces the conventional constants in the k-ε model by functional relationships for the case of an axisymmetric jet and observes a significant improvement in his predictions. Nallasamy (1985) in his evaluation of various turbulent models for the flow over a backward-facing step, states that the standard k-ε model always under predicts the reattachment point. Yet, the k-ε model retains its popularity since it allows the user to easily adjust, modify or replace parts of the model in order to

accommodate for a wide range of flow situations. Nallasamy (1986), in his comprehensive review of present-day turbulence models, concludes that the k-ε model is still the most widely used model for internal flow calculations.

The Reynolds stress/flux models no longer adhere to the eddy viscosity concept. Instead, they consider the stress/flux terms individually and are therefore better equipped to analyse a wider range of turbulent flow situations than the k-ε model. Generally, in a turbulent flow field components of the stress/flux tensor can develop differently from one another. Consequently, additional differential equations can be used to describe the transport of each of the turbulent stress/flux terms. These equations are again derived from the mean momentum and energy equations, see for example Hinze (1959). By deriving individual transport equations for the stress/flux terms, flow features such as swirl, streamline curvature and buoyancy are automatically accounted for. However, as mentioned previously, these equations contain higher order terms and to close them, these terms must be related to the mean flow characteristics. In particular the proper modelling of the pressure-strain, the diffusion and the dissipation terms are required. Model proposals include those of Daly and Harlow (1970), Launder et al (1975), Llewellen et al (1976), Lin and Wolfshtein (1977) and Rodi (1981). The solution of the full Reynolds stress/flux equations together with the mass, momentum, energy and dissipation equations requires a vast amount of computer time. Therefore the use of such a model must be justified by its claimed accuracy over the k-ε model. The Reynolds stress/flux models, unlike the k-ε model, have not yet been thoroughly tested and are still in the development stages. Hogg and Leschziner (1988 and 1989)

apply the model to highly swirling confined flow and obtain good agreement with measurement for the velocity and turbulence fields. Leschziner (1989) lists the most recent advances in the Reynolds stress/flux closure models and conclude that flows with large recirculation zones and/or with strong swirl clearly benefit from this type of model.

The algebraic stress/flux models attempt to reduce the computational overheads of the Reynolds stress/flux models by reducing the stress/flux equations to algebraic relations, while maintaining their pertinent features. For example, Rodi (1980) relates the transport of the stress terms to the transport of the kinetic energy, k, and also employs a k-equation to close the system. Rodi et al (1981) obtained a poor performance from an algebraic equation model when applied to several cases with curved and rotating boundaries. In their comparison of three algebraic stress models with the k-ε model, Nikjooy et al (1985) showed only marginal improvements over the k-ε model. Wilkes and Clarke (1987) compare the performance of the algebraic stress model with that of the k-ε model and experimental data for flows in pipes, sudden expansions and cavities. They obtain better predictions of turbulence levels in flows with curved streamlines and recirculation lengths. The algebraic stress models are much more economical than the Reynolds stress/flux models, and yet produce results which are not very different to those obtained by them, see Rodi (1980). Martinuzzi and Pollard (1989) compare the performances of the algebraic stress and the k-ε models for pipe flow and find the k-ε model to be in better agreement with experimental data. The algebraic models do not treat the convective and diffusive transport of the turbulent quantities accurately. In order to cure

this deficiency, Amano and Chai (1988) have recently gone one step further and introduced transport equations for the triple products of the turbulent fluctuations. They claim that in this manner the effects of convection and diffusion in strong shear flows, such as reattaching separated flows, are properly accounted for.

1.3 Objectives of current research

The present research is limited to the numerical prediction of the steady-state incompressible fluid flow in both laminar and turbulent regimes. The flow is two-dimensional and may include complex geometries. The accurate imposition of boundary conditions should be facilitated in an easy manner. The discretisation algorithm should be developed in modular form so that future alterations or additions may be carried out with minimum effort. The discretisation and solution strategies should be efficient in terms of hardware resources. In order to meet these stringent requirements the current research will concentrate on the following subject areas:

1) The discretisation of the governing equations will be performed by the use of the FEM, which allows accurate and efficient representation of complex geometries. Curved or irregular boundaries will be handled with relative ease. The subdivision of the domain into elements in an unstructured manner will provide great flexibility, not offered by any other technique. It also allows the user to refine or re-define parts or whole of the domain with minimum effort. The imposition of various types of boundary conditions follow naturally from the FEM discretisation. Both essential and natural boundary conditions will be imposed simply and accurately.

2) A two-dimensional mesh generation routine will be developed to

divide the domain of interest into triangular elements. The use of triangular elements enables the complete triangularisation of any arbitrary domain. The integral terms for the triangular element will be evaluated exactly and efficiently with minimum amount of repetition. The mesh generation will be flexible enough, so that any element size or orientation may be selected. The mesh generation will become an integral part of the solution strategy, so that iterative solution procedures may be used in place of the direct or the semi-direct solvers. This will greatly reduce the computer storage and run-time requirements.

3) The advection term will be treated so as to follow the physics of the advection transport closely. The treatment of the advection will be conservative and monotonic giving oscillation free results with minimal numerical diffusion. This treatment will be accurate, unconditionally stable and efficient in terms of computer storage and evaluation time. It is only in this manner that the method may be applied confidently to a wide range of flow situations.

4) Unlike the conventional FEM procedures, an equal-order velocity-pressure formulation will be devised. The discretisation procedure will then become significantly simple, as all variables will use the same element shape functions. The variables will also be stored at similar locations in the domain. The equal-order formulation will not produce spurious pressure modes, which contaminate the flow field. A separate pressure equation will be derived. The velocity and pressure fields will be segregated and solved sequentially.

5) A fast iterative solution procedure will be developed for the solution of the linear system of simultaneous algebraic

equations. The procedure will be designed for the completely unstructured grids that are generated by the FEM. The solution procedure will possess a fast rate of convergence, and be efficient in terms of computer storage and execution time. It will be used for all the variables and will not require parameter settings that need changing from one flow case to another.

6) A general turbulence model will be developed. The model will be accurate in capturing the essential features of turbulence in arbitrary domains under various flow conditions. The model must also be flexible enough to allow future modifications to be carried out with minimum effort.

1.4 Outline of remaining chapters

In Chapter 2, the governing set of partial differential equations are presented. These equations describe the fluid motion under both laminar and turbulent flow regimes. For this research, only the two-dimensional form of the equations in Cartesian frame work are considered. In the latter part of this chapter the FEM is introduced. The Galerkin form of this method is then described in detail for the case of the two-dimensional Poisson type differential equation. Based on some computational considerations, the most appropriate element for this work is then selected.

Chapter 3 presents a novel streamline upwind technique that was devised for this research. The case of pure advection is first analysed from a physical stand-point. Its treatment by a variety of methods is briefly mentioned. Reasons for the deficiency of such methods in capturing the physical process of advection are given. The current streamline approach is then described in detail. It is shown

that the technique is able to model the advection phenomenon in a simple and consistent manner. The accuracy and the efficiency of the present technique is demonstrated by way of three stringent test cases. General remarks are made on the performance and the validity of the current streamline technique.

Chapter 4 presents the discretisation of the laminar flow equations by the FEM. The problem of velocity-pressure segregation is first considered. The current equal-order discretisation strategy is then described in detail. A separate pressure Poisson type equation is proposed. A segregate solution procedure where velocity and pressure are obtained sequentially is presented. Lastly, the discretisation of the energy equation and the imposition of the various types of boundary conditions are given.

Chapter 5 begins by outlining the overall computational sequence of the computer code for laminar flow analysis. A novel fast and efficient iterative solver is then described. Computational aspects of the analysis such as relaxation parameters and convergence criteria are then discussed. The current method is applied to several test cases. The case of the laminar jet impingement with heat transfer is also analysed. In the final part of the chapter general remarks on the performance, accuracy and efficiency of the current method are given.

Chapter 6 is dedicated to the analysis of isothermal turbulent flow. The problem of turbulence closure is first addressed. The finite element discretisation of the additional transport equations is then presented. The imposition of boundary conditions for turbulent flows is given. The program flow chart for turbulent flow analysis is next

presented. Two turbulent benchmark exercises as well as the case of confined plane jet impingement are provided in Appendix B.

Chapter 7 provides a discussion on the work contained in this research. Finally, based on the experience gathered here, several recommendations are given for future work.

CHAPTER 2

GOVERNING EQUATIONS AND FINITE ELEMENT METHOD

The governing equations of fluid flow and heat transfer are first presented. These equations describe the flow of fluids in both laminar and turbulent regimes. The assumptions leading to the derivation of these equations are also included. The last section of this chapter presents the adopted finite element discretisation of a typical partial differential equation, the Poisson's equation. Also in the last section it is suggested, based on computational considerations, that the most suitable element is the simplex three-noded triangular element.

2.1 Laminar flow equations

The set of equations governing the flow of fluid in a laminar regime can be found in most fluid mechanics text books, e.g. Schlichting (1960), Hughes and Brighton (1967) and Kay and Nedderman (1974). They are the continuity, momenta, energy and state equations. In their most general form for Newtonian fluids in a three-dimensional Cartesian frame-work, they are (Schlichting (1960))

Continuity
$$\frac{\partial}{\partial t}\rho + \frac{\partial}{\partial x}\rho u + \frac{\partial}{\partial y}\rho v + \frac{\partial}{\partial z}\rho w = 0 \qquad (2.1)$$

X-momentum
$$\begin{aligned}\frac{\partial}{\partial t}\rho u + \frac{\partial}{\partial x}\rho u^2 + \frac{\partial}{\partial y}\rho vu + \frac{\partial}{\partial z}\rho wu &= X - \frac{\partial p}{\partial x} \\ &+ \frac{\partial}{\partial x}\left[\mu\left(2\frac{\partial u}{\partial x} - \frac{2}{3}\left(\frac{\partial u}{\partial x} + \frac{\partial v}{\partial y} + \frac{\partial w}{\partial z}\right)\right)\right] \\ &+ \frac{\partial}{\partial y}\left[\mu\left(\frac{\partial u}{\partial y} + \frac{\partial v}{\partial x}\right)\right] \\ &+ \frac{\partial}{\partial z}\left[\mu\left(\frac{\partial u}{\partial z} + \frac{\partial w}{\partial x}\right)\right]\end{aligned} \qquad (2.2)$$

Y-momentum

$$\frac{\partial}{\partial t}\rho v + \frac{\partial}{\partial x}\rho uv + \frac{\partial}{\partial y}\rho v^2 + \frac{\partial}{\partial z}\rho wv = Y - \frac{\partial p}{\partial y} + \frac{\partial}{\partial x}\left(\mu\left(\frac{\partial v}{\partial x} + \frac{\partial u}{\partial y}\right)\right) + \frac{\partial}{\partial y}\left(\mu\left(2\frac{\partial v}{\partial y} - \frac{2}{3}\left(\frac{\partial u}{\partial x} + \frac{\partial v}{\partial y} + \frac{\partial w}{\partial z}\right)\right)\right) + \frac{\partial}{\partial z}\left(\mu\left(\frac{\partial v}{\partial z} + \frac{\partial w}{\partial y}\right)\right) \tag{2.3}$$

Z-momentum

$$\frac{\partial}{\partial t}\rho w + \frac{\partial}{\partial x}\rho uw + \frac{\partial}{\partial y}\rho vw + \frac{\partial}{\partial z}\rho w^2 = Z - \frac{\partial p}{\partial z} + \frac{\partial}{\partial x}\left(\mu\left(\frac{\partial w}{\partial x} + \frac{\partial u}{\partial z}\right)\right) + \frac{\partial}{\partial y}\left(\mu\left(\frac{\partial w}{\partial y} + \frac{\partial v}{\partial z}\right)\right) + \frac{\partial}{\partial z}\left(\mu\left(2\frac{\partial w}{\partial z} - \frac{2}{3}\left(\frac{\partial u}{\partial x} + \frac{\partial v}{\partial y} + \frac{\partial w}{\partial z}\right)\right)\right) \tag{2.4}$$

where X, Y and Z are components of the body force,

Energy

$$\frac{\partial}{\partial t}\rho cT + \frac{\partial}{\partial x}\rho ucT + \frac{\partial}{\partial y}\rho vcT + \frac{\partial}{\partial z}\rho wcT = \frac{\partial}{\partial x}\left(k\frac{\partial T}{\partial x}\right) + \frac{\partial}{\partial y}\left(k\frac{\partial T}{\partial y}\right) + \frac{\partial}{\partial z}\left(k\frac{\partial T}{\partial z}\right) + \mu\Phi + \dot{Q} \tag{2.5}$$

where $\dot{Q}$ is the rate of heat generation and Φ is the dissipation function. The energy equation, equation (2.5), can accommodate for heat transfer in both solid and fluid media as is shown later. The properties μ, c and k are all known functions of pressure and temperature, and

State

$$\rho = f(p,T) \tag{2.6}$$

For the purpose of this research the above set of equations are simplified according to the following assumptions:

a) Flow is in a two-dimensional Cartesian coordinate system, i.e. w=0, $\partial\phi/\partial z=0$ and Z=0.

b) Flow has reached steady state conditions, i.e. $\partial\phi/\partial t=0$.

c) Viscosity is constant and the influence of variable density appears only in the body force terms, i.e. $\partial u/\partial x + \partial v/\partial y + \partial w/\partial z=0$, $X=(\rho-\rho_1)g_x$ and $Y=(\rho-\rho_1)g_y$.

d) The dissipation function, Φ, which is important in lubrication situations, can be neglected since the flow applications considered here are in the low Mach number region ($M < 0.3$), i.e. $\Phi=0$.

With the above assumptions the set of equations, used in this research, are

Continuity
$$\frac{\partial}{\partial x}\rho u + \frac{\partial}{\partial y}\rho v = 0 \qquad (2.7)$$

X-momentum
$$\frac{\partial}{\partial x}\rho u^2 + \frac{\partial}{\partial y}\rho vu = (\rho-\rho_1)g_x - \frac{\partial p}{\partial x} + \frac{\partial}{\partial x}\left(\mu\frac{\partial u}{\partial x}\right) + \frac{\partial}{\partial y}\left(\mu\frac{\partial u}{\partial y}\right) \qquad (2.8)$$

Y-momentum
$$\frac{\partial}{\partial x}\rho uv + \frac{\partial}{\partial y}\rho v^2 = (\rho-\rho_1)g_y - \frac{\partial p}{\partial y} + \frac{\partial}{\partial x}\left(\mu\frac{\partial v}{\partial x}\right) + \frac{\partial}{\partial y}\left(\mu\frac{\partial v}{\partial y}\right) \qquad (2.9)$$

Energy
$$\frac{\partial}{\partial x}\rho ucT + \frac{\partial}{\partial y}\rho vcT = \frac{\partial}{\partial x}\left(k\frac{\partial T}{\partial x}\right) + \frac{\partial}{\partial y}\left(k\frac{\partial T}{\partial y}\right) + \dot{Q} \qquad (2.10)$$

State
$$\rho_1 = \rho(1-\beta(T-T_\circ)) \qquad (2.11)$$

where equation (2.11) relates the local density, ρ_1, to the reference density, ρ, the temperature difference, $(T-T_\circ)$, and the thermal expansion coefficient, β. Although ρ and μ are constant here, they are retained within the partial derivative terms to accommodate for possible future modifications to the above assumptions. Equations (2.7) to (2.10) are written in their conservative form. This would ensure the conservation of the transported properties, i.e. mass, momentum and energy, in flow cases where fluid properties are not constant. In the case of heat transfer by conduction in solids, the left hand side of equation (2.10) becomes redundant and the appropriate diffusion coefficient, k_{solid}, is inserted.

With equations (2.7) to (2.11), a wide range of problems may be analysed:

a) Isothermal flow, employing equations (2.7), (2.8) and (2.9).

b) Forced convection, decoupling equation (2.10) from the rest.

c) Natural and mixed convection, using all equations (2.7) to (2.11).

d) Heat conduction in solids with heat generation, using refined form of equation (2.10).

e) Conjugate heat transfer/fluid flow, using all equations (2.7) to (2.11).

2.2 Turbulent flow equations

The above set of equations adequately describe fluid motion under laminar regime. However most flows encountered in practice are of turbulent nature and laminar flows are the exceptions. Some examples of turbulent flow are:

- pipe flows,
- flow through pumps, turbines and compressors,
- flow around or in the wake of cars, aircrafts, ships etc.,
- jet flows,
- atmospheric boundary layers,
- upper atmospheric jet streams,
- Ocean currents and many more.

It is therefore necessary to construct a set of equations that can describe the turbulent fluid motion.

In the first chapter, the two alternative numerical methodologies used for treating turbulent flows were put forward. These were to either solve the unsteady differential equations of laminar flow or to consider the time-averaged form of these equations. It was also argued

that, with present-day computational resources, it is only the latter that can efficiently provide solutions to turbulent flow analysis. This is not a crippling factor, since it is the time-mean behaviour of these flows that is usually of practical interest. The method adopted in this research for isothermal flows is now presented.

The time-averaging process begins by assuming that at any instant in time the fluid motion is governed by the laminar flow equations (2.1) to (2.4) and that the velocity vector and the pressure are composed of mean and fluctuating components, such that

$$\begin{aligned} u' &= U + u \\ v' &= V + v \\ w' &= W + w \\ p' &= P + p \end{aligned} \qquad (2.12)$$

where

$$U = \frac{1}{t}\int_{t_o}^{t_o + t} u'\, dt \quad \text{and} \quad \int_{t_o}^{t_o + t} u\, dt = 0 \quad \text{etc ...} \qquad (2.13)$$

Substituting equation (2.12) into equations (2.1) to (2.4) and averaging with respect to time, taking ρ constant, (White (1974))

Continuity
$$\frac{\partial}{\partial t}\rho + \frac{\partial}{\partial x}\rho U + \frac{\partial}{\partial y}\rho V + \frac{\partial}{\partial z}\rho W = 0 \qquad (2.14)$$

X-momentum
$$\begin{aligned} &\frac{\partial}{\partial t}\rho U + \frac{\partial}{\partial x}\rho U^2 + \frac{\partial}{\partial y}\rho VU + \frac{\partial}{\partial z}\rho WU = \bar{X} - \frac{\partial P}{\partial x} \\ &+ \frac{\partial}{\partial x}\left[\mu\left(2\frac{\partial U}{\partial x} - \frac{2}{3}\left(\frac{\partial U}{\partial x} + \frac{\partial V}{\partial y} + \frac{\partial W}{\partial z}\right)\right)\right] \\ &+ \frac{\partial}{\partial y}\left[\mu\left(\frac{\partial U}{\partial y} + \frac{\partial V}{\partial x}\right)\right] \\ &+ \frac{\partial}{\partial z}\left[\mu\left(\frac{\partial U}{\partial z} + \frac{\partial W}{\partial x}\right)\right] \\ &- \frac{\partial}{\partial x}\rho\overline{uu} - \frac{\partial}{\partial y}\rho\overline{uv} - \frac{\partial}{\partial z}\rho\overline{uw} \end{aligned} \qquad (2.15)$$

Y-momentum

$$\begin{aligned}
&\frac{\partial}{\partial t}\rho V + \frac{\partial}{\partial x}\rho UV + \frac{\partial}{\partial y}\rho V^2 + \frac{\partial}{\partial z}\rho WV = \overline{Y} - \frac{\partial P}{\partial y} \\
&+ \frac{\partial}{\partial x}\left[\mu\left(\frac{\partial V}{\partial x} + \frac{\partial U}{\partial y}\right)\right] \\
&+ \frac{\partial}{\partial y}\left[\mu\left(2\frac{\partial V}{\partial y} - \frac{2}{3}\left(\frac{\partial U}{\partial x} + \frac{\partial V}{\partial y} + \frac{\partial W}{\partial z}\right)\right)\right] \\
&+ \frac{\partial}{\partial z}\left[\mu\left(\frac{\partial V}{\partial z} + \frac{\partial W}{\partial y}\right)\right] \\
&- \frac{\partial}{\partial x}\rho\overline{vu} - \frac{\partial}{\partial y}\rho\overline{vv} - \frac{\partial}{\partial z}\rho\overline{vw}
\end{aligned} \tag{2.16}$$

Z-momentum

$$\begin{aligned}
&\frac{\partial}{\partial t}\rho W + \frac{\partial}{\partial x}\rho UW + \frac{\partial}{\partial y}\rho VW + \frac{\partial}{\partial z}\rho W^2 = \overline{Z} - \frac{\partial P}{\partial z} \\
&+ \frac{\partial}{\partial x}\left[\mu\left(\frac{\partial W}{\partial x} + \frac{\partial U}{\partial z}\right)\right] \\
&+ \frac{\partial}{\partial y}\left[\mu\left(\frac{\partial W}{\partial y} + \frac{\partial V}{\partial z}\right)\right] \\
&+ \frac{\partial}{\partial z}\left[\mu\left(2\frac{\partial W}{\partial z} - \frac{2}{3}\left(\frac{\partial U}{\partial x} + \frac{\partial V}{\partial y} + \frac{\partial W}{\partial z}\right)\right)\right] \\
&- \frac{\partial}{\partial x}\rho\overline{wu} - \frac{\partial}{\partial y}\rho\overline{wv} - \frac{\partial}{\partial z}\rho\overline{ww}
\end{aligned} \tag{2.17}$$

where the bar indicates a time-averaged quantity. The above equations are similar to those presented in the previous section for laminar flow. The extra terms appearing on the right hand sides of the momentum equations are the Reynolds stress terms. Written in the matrix form, these additional stresses are

$$\begin{bmatrix} \sigma_x & \tau_{xy} & \tau_{xz} \\ \tau_{yx} & \sigma_y & \tau_{yz} \\ \tau_{zx} & \tau_{zy} & \sigma_z \end{bmatrix} = \begin{bmatrix} -\rho\overline{uu} & -\rho\overline{uv} & -\rho\overline{uw} \\ -\rho\overline{vu} & -\rho\overline{vv} & -\rho\overline{vw} \\ -\rho\overline{wu} & -\rho\overline{wv} & -\rho\overline{ww} \end{bmatrix} \tag{2.18}$$

where σ_x, σ_y and σ_z are the normal stresses and the rest are the shear stresses, all arising from the onset of turbulence. The above matrix is symmetric, hence $\tau_{xy} = \tau_{yx}$, $\tau_{xz} = \tau_{zx}$ and $\tau_{yz} = \tau_{zy}$.

As before, the following assumptions are made for flow situations considered here:

a) Flow is in a two-dimensional Cartesian coordinate system, i.e. W=0, $\partial\phi/\partial z=0$, and $\overline{Z}=0$.

b) Flow has reached steady state conditions, i.e. $\partial\phi/\partial t=0$.

c) Fluid has constant density and viscosity.

e) The body force is due to the gravitational pull, i.e. $\overline{X}=\rho g_x$ and $\overline{Y}=\rho g_y$.

With these assumptions the time-averaged differential equations used in this research are

Continuity
$$\frac{\partial}{\partial x}\rho U + \frac{\partial}{\partial y}\rho V = 0 \tag{2.19}$$

X-momentum
$$\frac{\partial}{\partial x}\rho U^2 + \frac{\partial}{\partial y}\rho VU = \rho g_x - \frac{\partial P}{\partial x} + \frac{\partial}{\partial x}\left(\mu\frac{\partial U}{\partial x} - \rho\overline{uu}\right) + \frac{\partial}{\partial y}\left(\mu\frac{\partial U}{\partial y} - \rho\overline{uv}\right) \tag{2.20}$$

Y-momentum
$$\frac{\partial}{\partial x}\rho UV + \frac{\partial}{\partial y}\rho V^2 = \rho g_y - \frac{\partial P}{\partial y} + \frac{\partial}{\partial x}\left(\mu\frac{\partial V}{\partial x} - \rho\overline{uv}\right) + \frac{\partial}{\partial y}\left(\mu\frac{\partial U}{\partial y} - \rho\overline{vv}\right) \tag{2.21}$$

and the turbulence stress matrix is reduced to

$$\begin{bmatrix} \sigma_x & \tau_{xy} \\ \tau_{xy} & \sigma_y \end{bmatrix} = \begin{bmatrix} -\rho\overline{uu} & -\rho\overline{uv} \\ -\rho\overline{uv} & -\rho\overline{vv} \end{bmatrix} \tag{2.22}$$

ρ and μ are kept inside the partial derivative terms to facilitate future modifications to the above assumptions. The primary concern is to solve the above equations to obtain the mean velocity distributions. However this cannot be done until the Reynolds stress terms are more clearly expressed. As can be seen from equations (2.20) and (2.21), these terms are additional to the viscous stress terms. Therefore it would be plausible to regard them as additional viscosity due to the onset of turbulence. By describing a turbulent viscosity, the above set of equations are closed and could therefore be solved.

Although the flow is considered to be two-dimensional, i.e. W = 0, no assumption about the magnitude of the fluctuating component, w, which may still be nonzero, is made.

2.3 Finite Element Method

The first part of this section presents the finite element discretisation strategy adopted here by considering the diffusion type problems. Reference is also made to the imposition of boundary conditions. It is through this discretisation and simple computational considerations that the choice of the element type is then made in the last part of the section. It is shown that the success of this work depended on this type of element.

2.3.1 Discretisation of Poisson's equation

In general the Finite Element approximation of a set of differential equations may be carried out, based on, (Zienkiewicz (1977)):

a) Variational principles,

b) Weak formulations, or

c) Global physical statements.

Here, a form of the weak formulation method, namely the Galerkin weighted residual approach is adopted. This choice is not an arbitrary one and is based on the ability of this method in treating the sort of boundary conditions that are encountered in fluid flow situations.

For the purpose of presenting the adopted methodology, only the discretisation of the diffusion part of the differential equations is addressed here. The construction of the full finite element set will be completed in the next chapter, where the treatment of the

convection term will be discussed. The discretisation, therefore begins by considering the two-dimensional form of the Poisson's equation in Cartesian coordinate system

$$\frac{\partial}{\partial x}\left(\Gamma_\phi \frac{\partial \phi}{\partial x}\right) + \frac{\partial}{\partial y}\left(\Gamma_\phi \frac{\partial \phi}{\partial y}\right) + S_\phi = 0 \qquad (2.23)$$

where ϕ is a scalar variable with Γ_ϕ and S_ϕ being the diffusion coefficient and the source of ϕ respectively. Both Γ_ϕ and S_ϕ are in general dependent functions of x, y and ϕ. Equation (2.23) is subject to the following boundary conditions:

a) essential boundary conditions,

$$\phi = \phi_{\text{prescribed}} \text{ on } s_\phi \qquad (2.24)$$

b) natural boundary conditions,

$$q = q_{\text{prescribed}} \text{ on } s_q \qquad (2.25)$$

where q is the outward flux of ϕ, and

$$s = s_\phi + s_q \qquad (2.26)$$

with s representing the complete domain boundaries both internal and external. Amongst the physical processes that are governed by equation (2.23) together with equations (2.24) and (2.25) are heat conduction, potential flow, mass diffusion, flow through porous media, lubrication flow and some fully developed duct flows.

Application of the Galerkin weighted residual method to equation (2.23) is now demonstrated. The weak form of this equation is obtained by first multiplying through by the weight function, W, and then integrating the product with respect to x and y, (Taylor and Hughes (1977))

$$\int_A W \left[\frac{\partial}{\partial x} \left(\Gamma_\phi \frac{\partial \phi}{\partial x} \right) + \frac{\partial}{\partial y} \left(\Gamma_\phi \frac{\partial \phi}{\partial y} \right) + S_\phi \right] dA = 0 \qquad (2.27)$$

A is the area of the domain where equation (2.23) is applicable and dA=dxdy. Since first order continuous elements will be used in sub-dividing the domain, the order of the diffusion terms in the above equation is reduced by employing Gauss's theorem. Hence equation (2.27) with elemental sub-divisions becomes

$$\sum_1^{n^e} \left\{ \int_{A^e} \left[\frac{\partial W_i}{\partial x} N_j \Gamma_{\phi j} \frac{\partial N_k}{\partial x} \phi_k + \frac{\partial W_i}{\partial y} N_j \Gamma_{\phi j} \frac{\partial N_k}{\partial y} \phi_k \right] dA^e = \right. \qquad (2.28)$$

$$\left. \int_{A^e} W_i S_\phi \, dA^e + \int_{s_q^e} W_i N_j \Gamma_{\phi j} \frac{\partial N_k}{\partial n} \phi_k \, ds^e + \int_{s_\phi^e} W_i N_j \Gamma_{\phi j} \frac{\partial N_k}{\partial n} \phi_k \, ds^e \right\}$$

where W_i is equal to N_i, and is replaced by N_i hereafter. n is the unit outward normal vector at the element boundary such that

$$\frac{\partial N_k}{\partial n} \phi_k = n_x \frac{\partial N_k}{\partial x} \phi_k + n_y \frac{\partial N_k}{\partial y} \phi_k \qquad (2.29)$$

with n_x and n_y being the direction cosines in the x and y directions respectively. The physical significance of equation (2.29) is that it represents the outward flux of ϕ, i.e.

$$\int_{s_q^e} N_i N_j \Gamma_{\phi j} \frac{\partial N_k}{\partial n} \phi_k \, ds^e = \int_{s_q^e} N_i \, q \, ds^e \qquad (2.30)$$

The second integral on the right hand side of equation (2.28) need only be evaluated on the outside boundaries since internal fluxes cancel each other. On the outside boundaries the value of q is given by equation (2.25). In heat conduction situations where a convective

boundary may exist, q is replaced by

$$q = h\ (\phi_f - \phi_b) \tag{2.31}$$

where h is the convective heat transfer coefficient, ϕ_f is the fluid temperature at a distance away from the boundary surface and ϕ_b is the unknown boundary temperature. It is seen that already as a consequence of the Galerkin formulation the natural boundary conditions are easily catered for. The last integral on the right hand side of equation (2.28) applies to that part of the boundary where ϕ is prescribed and is therefore redundant.

The treatment of the source term, the first term on the right hand side of equation (2.28), is now presented. A proper treatment of the source term is required if the discretisation procedure is to yield a converged solution set (Patankar (1980)). If the source of ϕ, S_ϕ, has a constant value, its treatment becomes trivial and is done in a similar fashion to that of the prescribed flux. However, when S_ϕ is a dependent function of ϕ, a more elaborate treatment is required. S_ϕ may either be a linear or a non-linear function of ϕ. For linear dependency the source term may be expressed as

$$S_\phi = S_c + S_p \phi \tag{2.32}$$

where S_C and S_p are constants. The source integral of equation (2.28) is then split into two parts

$$\int_{A^e} N_i\ S_\phi\ dA^e = \int_{A^e} N_i\ S_c\ dA^e + \int_{A^e} N_i\ S_p\ N_j \phi_j\ dA^e \tag{2.33}$$

The last term on the right hand side is carried over to the left hand side of equation (2.28). Note that with this treatment, unknown variable ϕ only appears on the left hand side of equation (2.28). When

the dependence of S_ϕ on ϕ is non-linear, the source term is linearised. First, S_ϕ is expanded using the Taylor series formula

$$S_\phi = S_\phi^* + \frac{(\phi - \phi^*)}{1!}\left(\frac{dS}{d\phi}\phi\right)^* + \frac{(\phi - \phi^*)^2}{2!}\left(\frac{d^2S}{d\phi^2}\phi\right)^* + \frac{(\phi - \phi^*)^3}{3!}\left(\frac{d^3S}{d\phi^3}\phi\right)^* + \cdots \tag{2.34}$$

where * denotes the evaluation of quantities at the previous stage of the calculation. Inherent in this linearisation technique is the assumption that an iterative solution method is to be used. This presents no further complication, as it was argued in Chapter 1 that an iterative algorithm for the solution of the discretised equations would be used. Then * would refer to quantities evaluated at the previous iteration. Assuming first order approximation for the source term, equation (2.34) is truncated to give

$$S_\phi \simeq S_\phi^* + \frac{(\phi - \phi^*)}{1!}\left(\frac{dS}{d\phi}\phi\right)^* \tag{2.35}$$

This linearisation presents the tangent to the S_ϕ versus ϕ curve at ϕ^*. Equation (2.35) can be rearranged as

$$S_\phi = \left(S_\phi^* - \phi^*\left(\frac{\partial S}{\partial \phi}\phi\right)^*\right) + \phi\left(\frac{\partial S}{\partial \phi}\phi\right)^* \tag{2.36}$$

The term in parentheses, is weighted by the Galerkin method and is integrated, which forms the explicit part of the source integral term in equation (2.28). The implicit part of the source integral is obtained by using the lumped mass approach with Galerkin weighting, which has been shown to improve the solution accuracy (Zienkiewicz (1977)). Hence,

$$\int_{A^e} N_i \, N_j \phi_j \left(\frac{\partial S}{\partial \phi}\phi\right)^* dA^e = \int_{A^e} N_i \, N_T \phi_j \left(\frac{\partial S}{\partial \phi}\phi\right)^* dA^e \qquad (2.37)$$

where

$$N_T = \sum_{j=1}^{m} N_j \qquad (2.38)$$

with m being the number of nodes per element. Returning to equation (2.28), it can be written concisely as

$$\sum_{1}^{n^e} \left\{ [\, A \,]^e \, \phi^e = f^e \right\} \qquad (2.39)$$

where $[A]^e$ is the element coefficient matrix, ϕ^e is the vector containing unknown nodal values of ϕ and f^e is the element force vector. The finite element discretisation as presented above is applicable to all types of elements, regardless of the shape or property of the element.

The discretisation procedure produces a system of simultaneous algebraic linear equations. The solution to such a system may be obtained either by direct or indirect (iterative) methods. However, as discussed in Chapter 1, computer requirements for direct methods make their use restrictive and highly undesirable, especially in two and three dimensional analyses. Therefore it is preferred to employ iterative solution algorithms, whereby requirements on computer storage and time are minimised. Iterative solvers have been widely used in conjunction with finite difference schemes where a structured grid is present (Patankar (1980)). In this research a similar iterative solver, as will be described in Chapter 5, is devised for use with the unstructured mesh which arises from the application of

the FEM.

2.3.2 Choice of element type

In this final part of the section, the appropriate type of element for the adapted discretisation is selected. This selection is based on the following computational considerations:

a) use of an iterative solution algorithm,

b) efficient integration procedure, and

c) adaptation of a simple upwinding scheme.

Although upwinding is not required for purely diffusive type problems, i.e. equation (2.23), it plays an important role in the analysis of fluid flow phenomena. Therefore it is taken into consideration when choosing the element type at this stage.

As is shown below, two types of elements are considered:

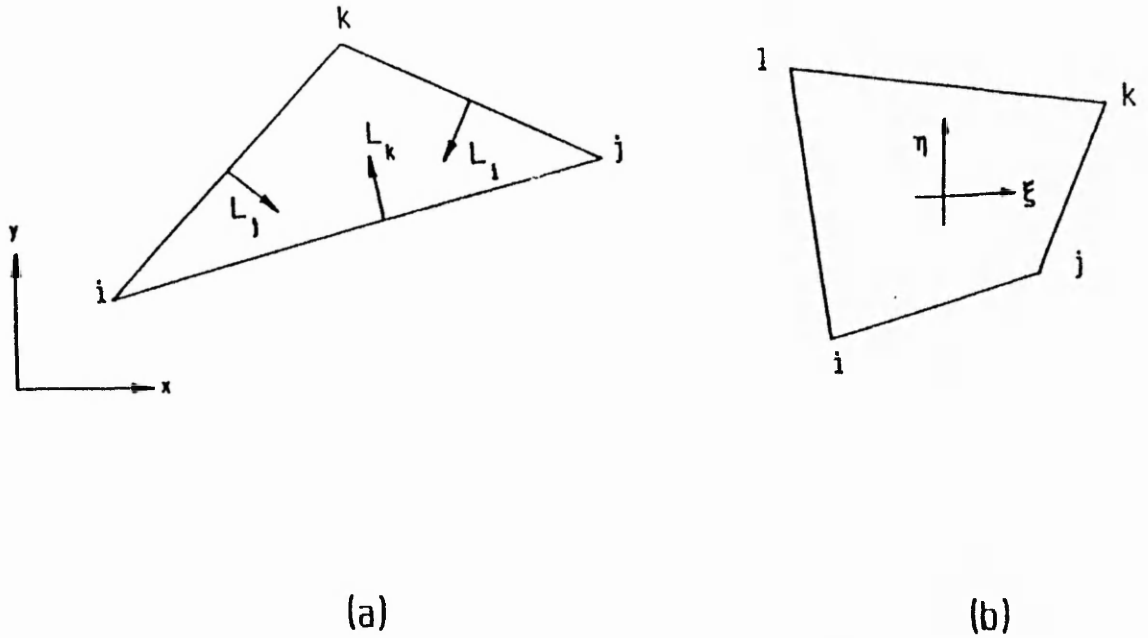

Figure 2.1 Two-dimensional elements, (a) three-noded linear triangle, (b) four-noded bilinear quadrilateral.

a) linear three-noded triangular element, with Φ expressed as

$$\phi = N_i\phi_i + N_j\phi_j + N_k\phi_k \tag{2.40}$$

where ϕ_i, ϕ_j and ϕ_k are nodal values of ϕ, with L_i, L_j, and L_k as local area coordinates, and

$$N_i = L_i \ , \ N_j = L_j \ , \ N_k = L_k \quad \text{and} \quad L_i + L_j + L_k = 1 \tag{2.41}$$

b) bi-linear four-noded rectangular element, with ϕ expressed as

$$\phi = N_i\phi_i + N_j\phi_j + N_k\phi_k + N_l\phi_l \tag{2.42}$$

where again ϕ_i, ϕ_j, ϕ_k and ϕ_l are nodal values of ϕ, and

$$N_i = \frac{1}{4}(1-\xi)(1-\eta) \ , \quad N_j = \frac{1}{4}(1+\xi)(1-\eta) \ , \tag{2.43}$$
$$N_k = \frac{1}{4}(1+\xi)(1+\eta) \ , \quad N_l = \frac{1}{4}(1-\xi)(1+\eta)$$

with ξ and η as local coordinates.

For simplicity the elements shown in Figure 2.2 are considered where they are deliberately oriented with sides ij and jk perpendicular to each other. Also sides ij of both elements are parallel with the x-axis. Let the aspect ratio, λ, for both elements be defined as the ratio of the side lengths L_{ij} and L_{jk},

$$\lambda = \frac{L_{ij}}{L_{jk}} \tag{2.44}$$

Assuming constant unit diffusivity in both x and y directions, i.e. $\Gamma_\phi = 1$, the element coefficient matrix of equation (2.39) then becomes (see Appendix A),

$$\left[A \right]^e_{\text{triangle}} = \frac{1}{2} \begin{bmatrix} \frac{1}{\lambda} & -\frac{1}{\lambda} & 0 \\ -\frac{1}{\lambda} & \frac{1}{\lambda}+\lambda & -\lambda \\ 0 & -\lambda & \lambda \end{bmatrix} \tag{2.45}$$

for the triangular element, and

$$[\,A\,]^{e}_{rectangle} = \frac{1}{6\lambda}\begin{bmatrix} 2+2\lambda^2 & -2+\lambda^2 & -1-\lambda^2 & 1-2\lambda^2 \\ -2+\lambda^2 & 2+2\lambda^2 & 1-2\lambda^2 & -1-\lambda^2 \\ -1-\lambda^2 & 1-2\lambda^2 & 2+2\lambda^2 & -2+\lambda^2 \\ 1-2\lambda^2 & -1-\lambda^2 & -2+\lambda^2 & 2+2\lambda^2 \end{bmatrix} \tag{2.46}$$

for the rectangular element.

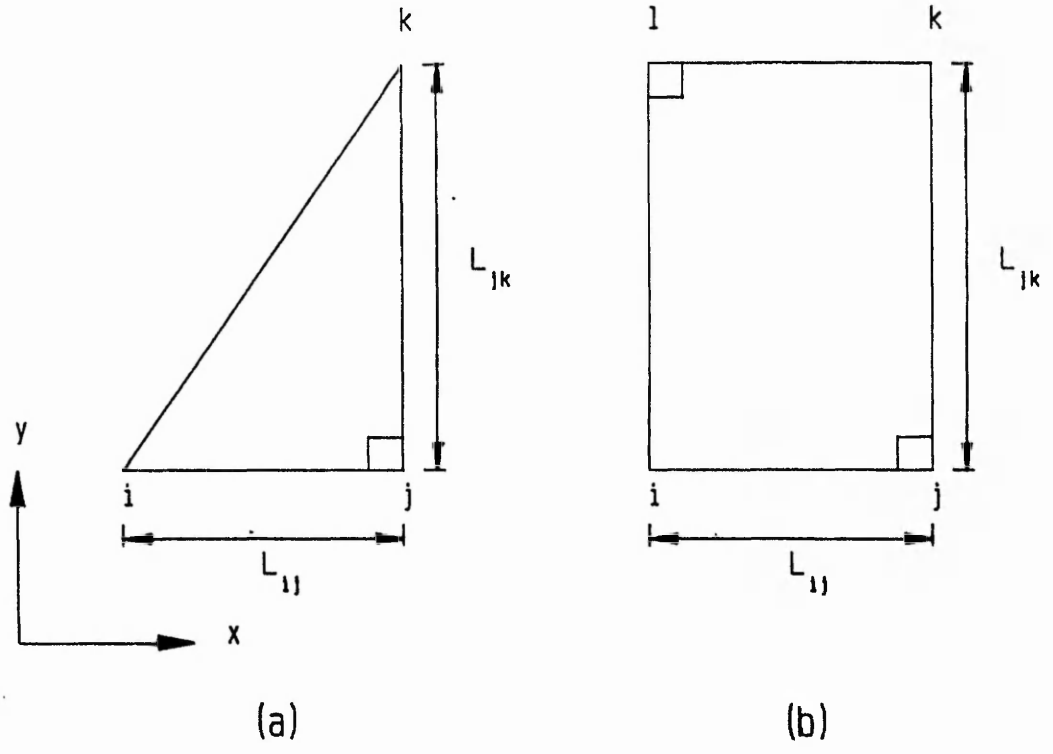

Figure 2.2 Elements oriented with respect to the coordinate system, (a) triangle, (b) quadrilateral.

Close inspection of the coefficient matrix for the triangular element, equation (2.45), reveals that:

a) the diagonal members will always be equal to the absolute sum of the off-diagonal members on each row,

b) the diagonal members have opposite signs to the other members on their corresponding rows, and

c) the absolute value of the diagonal member can never be smaller than

the sum of the absolute values of the off-diagonal members, i.e. the matrix is always diagonally dominant.

Conditions (a) and (b) show the physical consistency of the formulation. Condition (c) satisfies the Scarborough criterion, a sufficient condition for the convergence of the Gauss-Siedel iterative solution method, Patankar (1980). However, for the coefficient matrix of the rectangular element, equation (2.46), although condition (a) above is always satisfied, condition (b) is always violated and condition (c) can be violated depending on the value of the aspect ratio. It can easily be shown from equation (2.44) that condition (c) is violated if λ falls outside the range

$$\sqrt{1/2} \leq \lambda \leq \sqrt{2} \tag{2.47}$$

The global coefficient matrix is the assembly of all element coefficient matrices, i.e.

$$[A] = \sum_{1}^{n^e} [A]^e \tag{2.48}$$

It follows that [A], when fully assembled, will always satisfy the above three conditions if triangular elements are used and may violate them if rectangular elements are employed, Fried (1971). As mentioned earlier, the system of linear equations, whose coefficients are given by [A], will be solved in an iterative manner. In order to ensure a converged solution set by at least one such iterative scheme, e.g. Gauss-Siedel method, it is therefore desirable to use triangular elements which will always lead to an unconditionally stable system of equations. It may be noted that similar analysis carried out on a domain subdivided into linear triangular elements of general shape and arbitrary orientation, would produce a global coefficient matrix with

similar properties as above. This is regardless of the value of the diffusion coefficient in any direction.

The simplex triangular element offers three more advantages in comparison with the bi-linear rectangular element, as well as with most of the other types of elements commonly in use. These advantages arise from the shape and the linear properties of the triangular element (equation (2.40)). This element allows the complete triangularisation of any arbitrary shape in space to be carried out. Exact integration procedures can be easily employed. Exact integrations are much more efficient than their numerical counterparts in terms of computational speed. For the triangular element shown in Figure 2.1, the area integral can be evaluated from

$$\int_{A^e} L_i^a \, L_j^b \, L_k^c \, dA^e = \frac{a!b!c!}{(a+b+c+2)!} \, 2A^e \tag{2.49}$$

Also boundary integrals can be evaluated from

$$\int_{\ell_{ij}} L_i^a \, L_j^b \, d\ell = \frac{a!b!}{(a+b+1)!} \, \ell_{ij} \tag{2.50}$$

where ℓ_{ij} is the element boundary length. Lastly, upwinding of the advection terms, i.e. the left hand side of equations (2.8) to (2.10), becomes very simple. The adopted upwinding technique is described in detail in the next chapter.

CHAPTER 3

STREAMLINE UPWIND TECHNIQUE

The treatment of the advection terms in the governing transport equations is presented. The first section is dedicated to outlining the problems associated with advection treatment. In the second section the appropriate streamline upwind technique is derived from simple physical considerations. The accuracy of the technique is then demonstrated by way of its application to benchmark cases. Finally, in the last section, general comments regarding the present technique and the test results are given.

3.1 Advection consideration

The differential equation governing the transport of a scalar variable, ϕ, in a two-dimensional Cartesian frame-work, can be written in its conservative form as

$$\frac{\partial}{\partial x}(\rho u\phi) + \frac{\partial}{\partial y}(\rho v\phi) = \frac{\partial}{\partial x}\left(\Gamma_\phi \frac{\partial \phi}{\partial x}\right) + \frac{\partial}{\partial y}\left(\Gamma_\phi \frac{\partial \phi}{\partial y}\right) + S_\phi \qquad (3.1)$$

In fluid flow analysis, ϕ may be replaced by the components of the momentum velocity vector, u, v, or temperature T. Γ_ϕ would then represent the dynamic viscosity or the diffusion coefficient respectively. The source term, S_ϕ, represents the pressure gradient and the body forces due to variations in density in the momentum equations (2.8) and (2.9). It can also stand for the generation term in the energy equation (2.10). The treatment of the right hand side of equation (3.1) by the Galerkin method, was described in detail in the

last chapter. It is the treatment of the two terms on the left hand side that is addressed in this section.

The left hand side of equation (3.1) represents the transport of ϕ by advection. The two terms are first order derivatives in contrast to the second order diffusion terms of the right hand side. The advection terms can be non-linear as u, v or ρ may be dependent functions of ϕ itself. Hence, solution to such a non-linear differential equation can only be obtained in an iterative manner.

The discretisation of the advection terms by the Galerkin method limits the applicability of the finite element code to very low Reynolds number flow situations, where advection and diffusion forces are of the same order. For advection dominated flows, i.e. those with high Reynolds numbers, the Galerkin weighted residual approach leads to physically unrealistic results, where numerical diffusion and spatial oscillations contaminate the flow field. The shortcomings of the Galerkin technique lie in its inability to distinguish between the two completely different transport mechanisms which exist for diffusion and advection. The diffusion of ϕ may occur in all directions, which is adequately reflected in the finite element formulation of the diffusion terms by the Galerkin method. However, the advective transport of ϕ can only take place along characteristic lines, i.e. streamlines. Furthermore, small perturbations in ϕ at any point can only be transmitted along such a streamline from an upstream location to downstream locations and not vice versa. The advection mechanism is therefore highly directional and must be treated as such. Its approximation by the Galerkin method would relate ϕ at a point to those at all its neighbouring points. This would in turn result in

numerical diffusion and unphysical spatial oscillations. By using a very fine mesh, i.e. sub-dividing the domain into very small elements, equation (3.1) may be made unconditionally diffusion dominated. This strategy would require excessively fine meshes and is therefore discarded on economical grounds.

As reviewed in the first chapter, a variety of finite element formulations exist which can, to some extent, alleviate the numerical diffusion and spatial oscillations associated with the discretisation of the advection terms. A performance study, carried out on a number of then existing methods by Smith and Hutton (1982), concluded that nearly all the methods considered exhibited numerical diffusion and spatial oscillations to some degree. These so called upwind techniques also required considerable computational effort. In relative terms, effective upwinding may be achieved by the streamline diffusion approach of Hughes and Brooks (1979) and Brooks and Hughes (1982). In this approach, the weighting function in the Galerkin method is modified so as to produce a streamline upwind approximation. This approach also suffers from small magnitude spatial oscillations. Hence its adoption here would diminish the generality of the current finite element code.

One of the most promising upwinding techniques, devised for the finite element method, is the direct streamline upwind approximation of the advection terms themselves of Rice and Schnipke (1985). This monotone upwind streamline approximation, does not suffer from spatial oscillations and is able to predict benchmark cases with a significant increase in accuracy compared to other existing techniques. The upwind approximation method does not require excessive computational effort,

yet its inclusion in the finite element code is straightforward. Also, its application to quite a number of flow cases as well as test cases by Rice and Schnipke (1985 and 1986)) has demonstrated its generality of use.

The above streamline upwind technique is however non-conservative. Its implementation in cases where fluid properties are varying, especially for turbulent flows, may therefore lead to the global imbalance of the transported property. More importantly, the above technique was developed for bilinear rectangular elements. As discussed in Chapter 2, these elements may result in coefficient matrices which are not diagonally dominant. As far as iterative solution algorithms are concerned, these matrices are therefore ill-conditioned. In other words, a converged solution set may not be obtained if iterative schemes are employed to solve such an ill-conditioned matrix. Direct solution methods may be used, but these, as mentioned in Chapter 1, are inefficient in terms of computer storage and execution time. Since it was one of the primary objectives of this research to develop an efficient finite element code, bilinear elements were discarded. For the current research, a conservative streamline upwind approximation, based on the method of Rice and Schnipke (1985), is devised for linear triangular elements.

3.2 Conservative streamline upwind approximation

The treatment of the right hand side of equation (3.1) by the Galerkin method was fully described in the last chapter and is not repeated here. It may be noted that the discretisation of the diffusion terms and the source term is applicable to all types of elements. In approximating the advection terms the linear triangular

element is employed. Hence the following discretisation will be specific only to this type of element and cannot be used directly for any other types of elements.

In the absence of diffusion and source terms, equation (3.1) reduces to

$$\frac{\partial}{\partial x}(\rho u\phi) + \frac{\partial}{\partial y}(\rho v\phi) = 0 \qquad (3.2)$$

i.e. the transport of ϕ can take place purely via the advection mechanism. Supposing that a velocity field is already established, i.e. both u and v are known, and that u varies independent of ϕ, equation (3.1) becomes a first order linear differential equation in ϕ. Equation (3.1) may be expressed in terms of the streamline coordinates shown in Figure (3.1), thus

$$\frac{\partial}{\partial s}(\rho u_s \phi) = 0 \qquad (3.3)$$

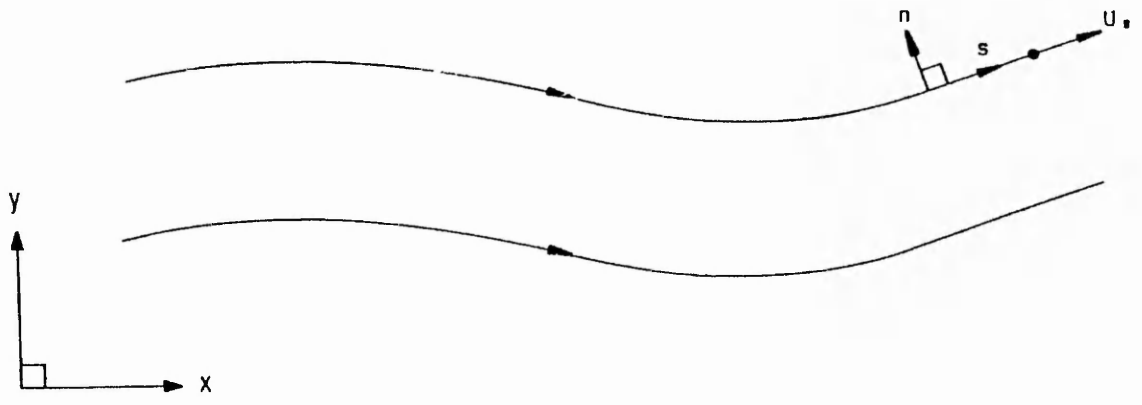

Figure 3.1 Streamline coordinates.

where s is along the tangent to the streamline, and u_s denotes the streamline velocity. Therefore, the two-dimensionality of the advection mechanism in the x-y coordinate system has now been reduced to that of a one-dimensional case in the s direction. Equation (3.3) states that in the absence of diffusion and source terms, $\rho u_s \phi$ is constant along a streamline. This is a characteristic of all pure advection situations, and was the basis for the derivation of the monotone streamline upwind technique of Rice and Schnipke (1985).

Equation (3.3) is weighted and then integrated over the domain area

$$\int_A N \left\{ \frac{\partial}{\partial s} (\rho u_s \phi) \right\} dA = 0 \qquad (3.4)$$

As the domain is made up of small elements, Equation (3.4) can be written as

$$\sum_1^{n^e} \int_{A^e} N_i \left\{ \frac{\partial}{\partial s} (\rho u_s \phi) \right\} dA^e = 0 \qquad (3.5)$$

At this point, in order to progress with the approximation, it is assumed that on the elemental level

$$\frac{\partial}{\partial s} (\rho u_s \phi) = \text{constant} \qquad (3.6)$$

Using (3.6) in equation (3.5), the weighted form of equation (3.3) becomes

$$\sum_1^{n^e} \left\{ \frac{\partial}{\partial s} (\rho u_s \phi) \right\} \int_{A^e} N_i \, dA^e = 0 \qquad (3.7)$$

From equation (3.7) the advection contribution to the global coefficient matrix can be evaluated. The evaluation of the above

expression begins by determining the value of the element constant, i.e. equation (3.6).

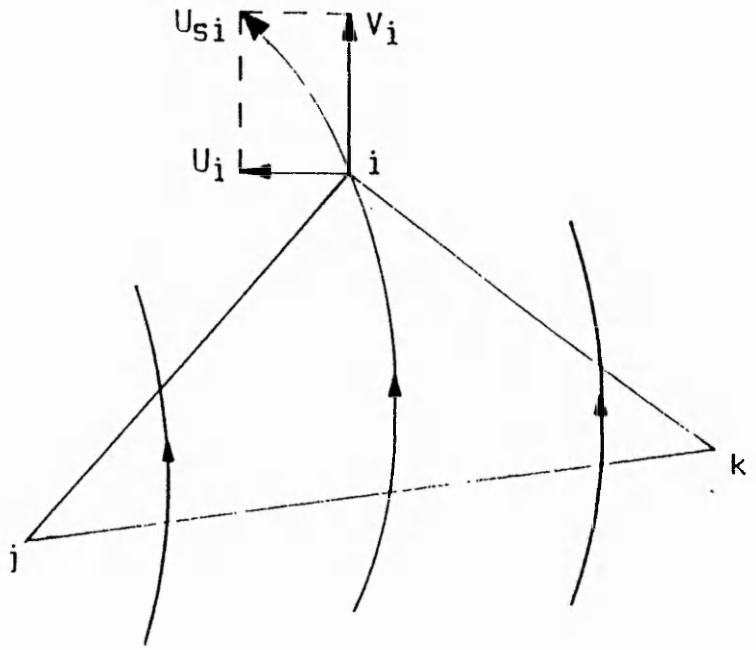

Figure 3.2 Illustration of a downwind node.

Consider the triangular element depicted in Figure 3.2. The streamlines passing through the element are also shown. As illustrated in the figure, node i is a "downwind" node. A node is defined to be a "downwind" node if the negative of the velocity vector at that node points back into the element. It may be noted from Figure 3.2, that the streamlines show some degree of curvature. This curvature is important and plays a significant role where, due to computational constraints, a coarse mesh must be used. For an isolated element within the computational domain, a number of streamline-element configurations are possible. These configurations are illustrated in Figure 3.3. For elements situated in the core of the flow, Figures 3.3(a) and (b), there may exist one, and only one, downwind node. For

elements with one or two sides lying next to a solid boundary, Figures 3.3(c) and (d), no such downwind node exists.

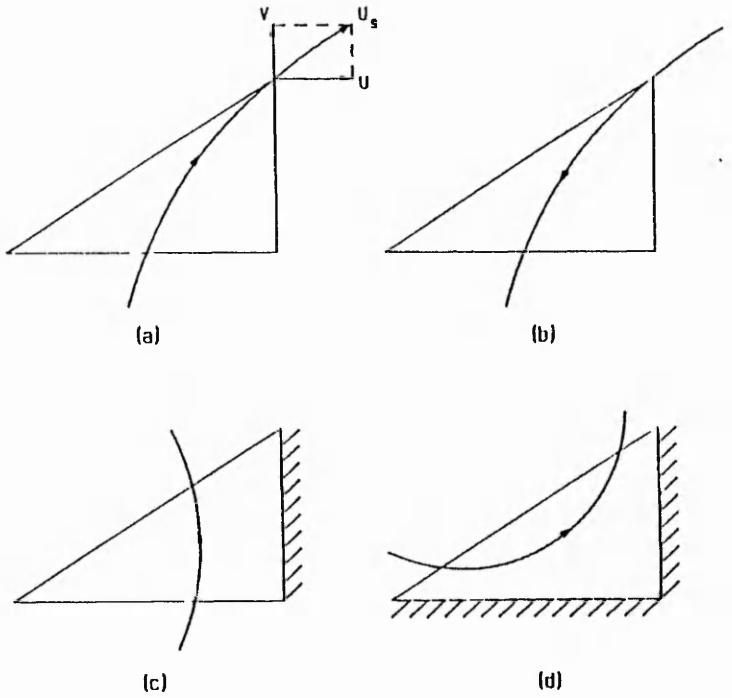

Figure 3.3 Possible streamline-element configurations, (a) one downwind node, (b), (c) and (d) no downwind nodes.

A downwind node on a given element is identified according to the following condition. A node is a downwind node, if the velocity vector at that node has positive outward normal components on both the element sides adjacent to it, i.e. with reference to Figure 3.4,

$$u_i \Delta y_{ik} - v_i \Delta x_{ik} \geq 0 \quad \text{and}$$
$$u_i \Delta y_{ij} - v_i \Delta x_{ij} \geq 0 \qquad (3.8)$$

Alternatively, equation (3.8) implies that

$$\tan \theta_{ij} \leq \tan \theta_i \leq \tan \theta_{ik} \qquad (3.9)$$

Once a node has been identified as a downwind node, the interception of the streamline, passing through that node, with the opposite side is located. As depicted in Figure 3.5, this interception

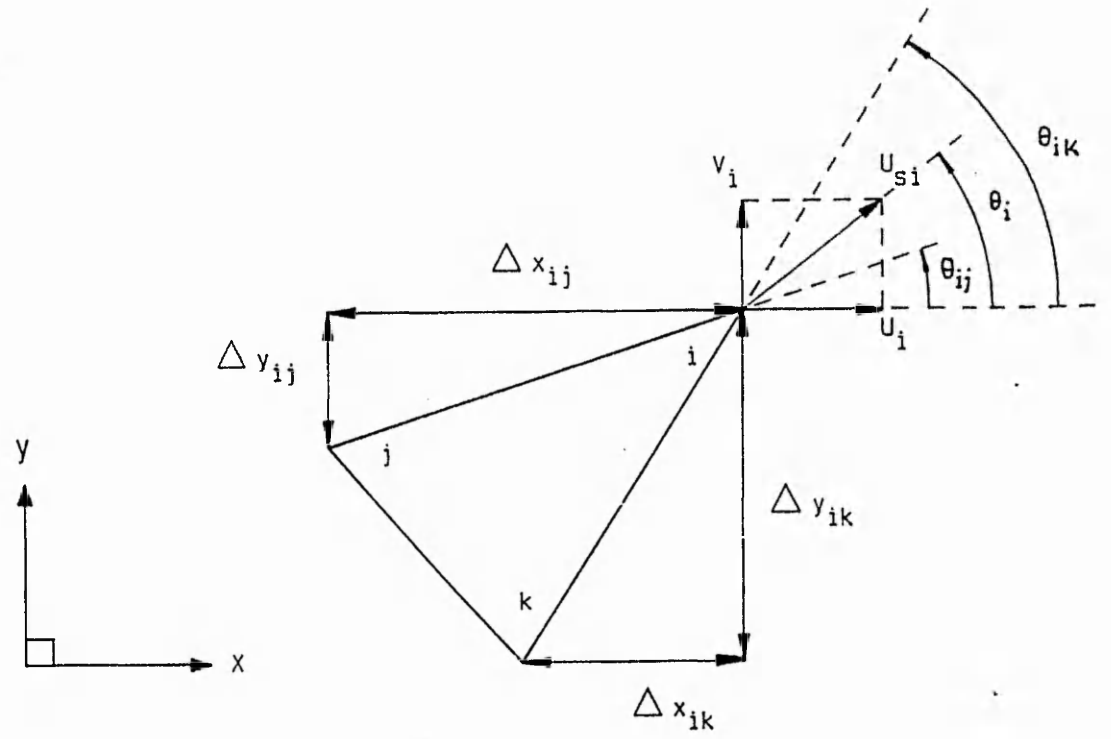

Figure 3.4 Identification of a downwind node.

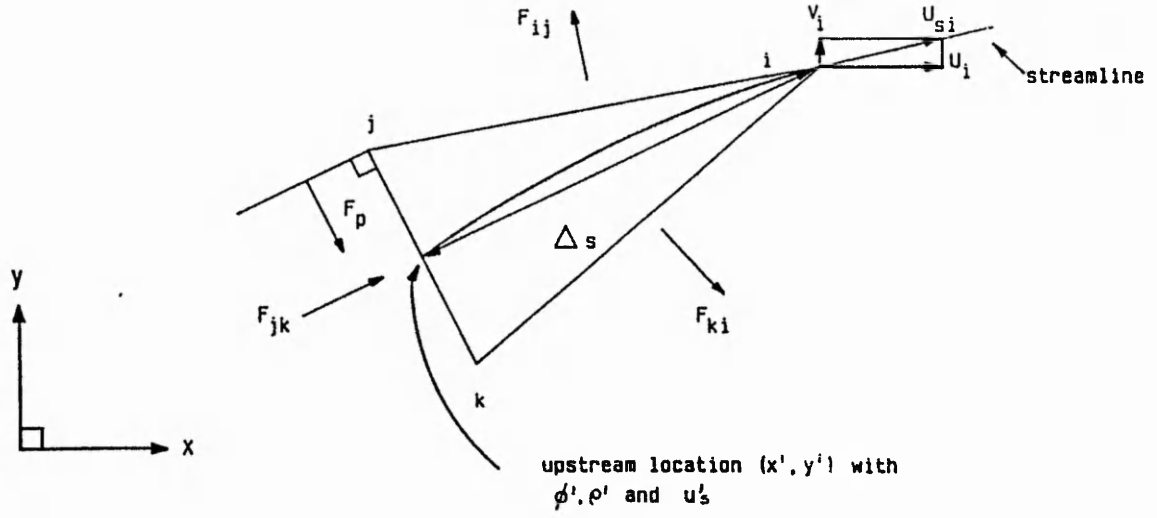

Figure 3.5 Determination of the upstream location.

takes place on side jk at the point with coordinates (x′,y′). This point is the "upstream location". With reference to Figure 3.5, x′ and y′ are determined by employing the interpolation factor, F_p expressed as

$$F_p = \frac{1}{2} (F'_p + F''_p) \tag{3.10}$$

where F'_p and F''_p are obtained by considering the normal mass flow rates across the element sides

$$F'_p = \text{Max} \left\{ \text{Min} \left\{ \frac{F_{ij}}{F_{jk}} , 1 \right\} , 0 \right\} \quad \text{and}$$

$$F''_p = 1 - \text{Max} \left\{ \text{Min} \left\{ \frac{F_{ki}}{F_{jk}} , 1 \right\} , 0 \right\} \tag{3.11}$$

The normal mass flow rates are themselves evaluated using the following surface integrals

$$F_{ij} = \int_i^j - \rho v \, dx + \int_i^j \rho u \, dy$$

$$F_{jk} = - \left\{ \int_j^k - \rho v \, dx + \int_j^k \rho u \, dy \right\} \tag{3.12}$$

$$F_{ki} = \int_k^i - \rho v \, dx + \int_k^i \rho u \, dy$$

Equation (3.12) is obtained by integrating the continuity equation over the element area

$$\int_{A^e} \left\{ \frac{\partial}{\partial x} (\rho u) + \frac{\partial}{\partial y} (\rho v) \right\} dA^e = 0 \tag{3.13}$$

Applying the Green's theorem to equation (3.13), it is rewritten as

$$\int - \rho v \, dx + \int \rho u \, dy = 0 \tag{3.14}$$

It is seen from equations (3.10) and (3.11) that F_p varies between 0 and 1. With reference to Figure 3.5, the coordinates of the upstream location, x′ and y′, are evaluated as

$$\begin{aligned} x' &= (1-F_p)\, x_j + F_p\, x_k \quad \text{and} \\ y' &= (1-F_p)\, y_j + F_p\, y_k \end{aligned} \tag{3.15}$$

From equations (3.15) and (3.16) and Figure 3.5, the upstream location coincides with node j when $F_p = 0$, and coincides with node k when $F_p = 1$. For other values of F_p between 0 and 1, the upstream location would lie somewhere along the side jk, between nodes j and k. Other upstream values are evaluated in a similar manner

$$\begin{aligned} \phi' &= (1-F_p)\, \phi_j + F_p\, \phi_k \\ \rho' &= (1-F_p)\, \rho_j + F_p\, \rho_k \\ u_s' &= (1-F_p)\, u_{sj} + F_p\, u_{sk} \end{aligned} \tag{3.16}$$

with

$$\begin{aligned} u_{sj} &= (u_j^2 + v_j^2)^{1/2} \quad \text{and} \\ u_{sk} &= (u_k^2 + v_k^2)^{1/2} \end{aligned} \tag{3.17}$$

With the above definitions, the advection term in equation (3.7) is approximated for the upwind node shown in Figure 3.5 as

$$\sum_{1}^{n^e} \frac{\partial}{\partial s}(\rho u_s \phi) \int_{A^e} N_i \, dA^e \simeq \frac{(\rho_i u_{si} \phi_i - \rho' u_s' \phi')}{\Delta s} A_f \tag{3.18}$$

where

$$\Delta s = ((x_i - x')^2 + (y_i - y')^2)^{1/2} \tag{3.19}$$

and A_f represents the summation of element shape function integrals for all the elements surrounding an upwind node, i.e.

$$A_f = \sum_{1}^{n^e} \int_{A^e} N_i \, dA^e \tag{3.20}$$

The streamline curvature, as mentioned earlier, is taken into account when determining the upstream location at x′ and y′. However, the length of the streamline segment, Δs, is calculated as a straight line. More accurate evaluation of the streamline arc requires complex iterative procedures. For a quadratic arc, the evaluation time increases by 10 fold and would include a logarithmic calculation as pointed out by Rice and Schnipke (1985). Since such accuracy in the evaluation of Δs, does not greatly improve the approximation of the advection terms, the linear calculation given by equation (3.19) is adopted.

row \ column	*i*	*j*	*k*
i	$\frac{\rho_1 u_{si}}{\Delta s} A_f$	$-(1-F_p)\frac{\rho' u'_s}{\Delta s} A_f$	$-F_p \frac{\rho' u'_s}{\Delta s} A_f$
j	*0*	*0*	*0*
k	*0*	*0*	*0*

Table 3.1 Element coefficient matrix for pure advection.

The element coefficient matrix arising from pure advection can be constructed using equations (3.18) to (3.20), which is shown in Table 3.1. From the table it can be seen that the element matrix is unconditionally diagonally dominant as a consequence of the current

streamline approximation. The global coefficient matrix is then assembled by considering each individual element advection contribution. The global coefficient matrix will also be diagonally dominant irrespective of element sizes or orientations. This in turn will ensure a converged solution set regardless of the chosen iterative solution scheme.

The upwind technique presented above adequately captures the discontinuous nature of the transport mechanism via pure advection. Pure advection involves the transport of quantities along streamlines, which is typical of characteristic value problems. Most of the previous methods modelled the pure advection phenomenon by continuous or semi-continuous approximations. These approximations, as discussed in Chapter 1, result in numerical diffusion and unphysical spatial oscillations. The present formulation in contrast is a discontinuous approximation of the physically discontinuous pure advection mechanism. Other discontinuous methods have also been previously employed, e.g. Hughes and Brooks (1979) and Hughes and Brooks (1982). These methods consider the advection to be discontinuous between elements, and continuous within each element. However, the current formulation is discontinuous not only across elements but also within each individual element. In other words, the upstream value of $\rho u \phi$, as well as the upstream location, are determined as discontinuous functions of their corresponding values at the two opposite nodes. In the next section the results obtained for benchmark test cases using the above upwind technique are presented.

3.3 Validation of results

The applicability and accuracy of the above streamline technique

is validated in this section. The benchmark test cases which are used for this validation are the pure advection skew to mesh, the Smith and Hutton case and the rotating disk. These stringent cases have all been commonly used by previous workers in order to verify their proposed techniques devised for approximating the advection terms.

3.3.1 Pure advection skew to mesh

This test case has been employed previously by several researchers in order to evaluate the accuracy and stability of their techniques for treating the advection terms, e.g. Hughes and Brooks (1979), Leschziner (1980), Baliga and Patankar (1980), Hassan, Rice and Kim (1983) and Rice and Schnipke (1985). The flow domain is shown in Figure 3.6. As can be seen, the domain is a square with a known unidirectional velocity field. The flow angle with respect to the x-axis is θ. The objective of this test case is to investigate the transport of the scalar variable, ϕ, via pure advection mechanism, i.e. in the absence of any diffusion. The boundary conditions for ϕ are also shown in Figure 3.6. Value of 1 is imposed along the bottom side as well as on the lower part of the left hand side. ϕ is set at zero along the remaining part of the left hand side. The boundary condition on the left hand side represent a step discontinuity in the value of ϕ. Since this problem involves only pure advection, there are no boundary conditions required along the exit plane, i.e. the right hand side and the top side of the domain. As ϕ can only be transported via pure advection, any diffusion in the outcome of this analysis will point to the inaccuracy of the proposed technique. Also in the absence of any source terms for ϕ, the value of ϕ cannot exceed its maximum prescribed value of 1 or drop below its minimum value of zero. Therefore the computed values of ϕ which fall outside the imposed

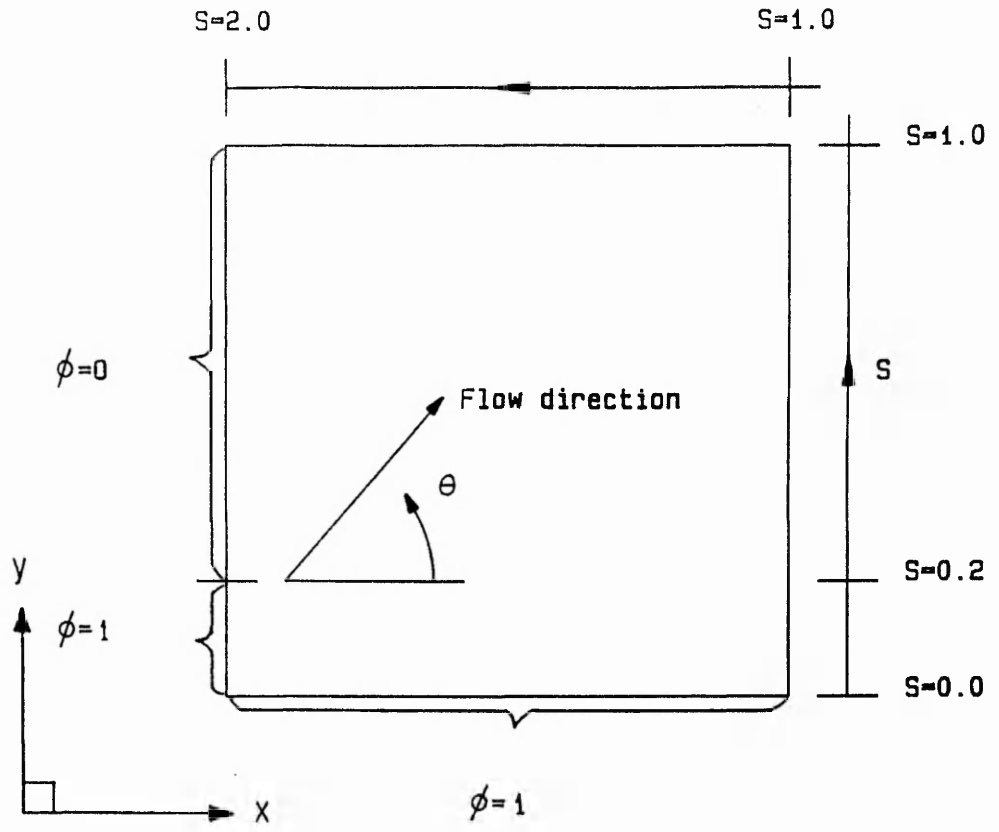

Figure 3.6 Pure advection skew to mesh.

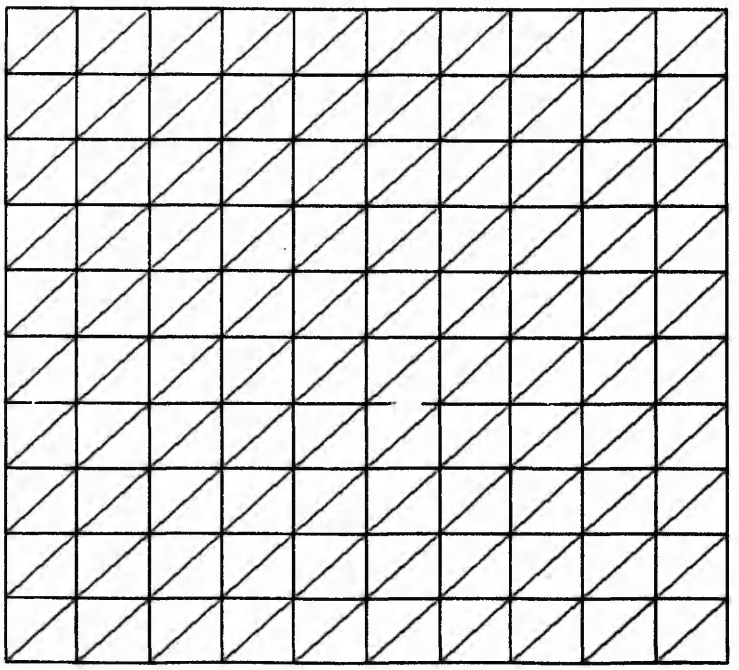

Figure 3.7 Computational grid for pure advection skew to mesh.

range will be unrealistic and will indicate the degree of spatial oscillation in the proposed technique.

To model pure advection, the diffusion coefficient, Γ_ϕ, is set at zero (see equation (3.1)) resulting in an infinite flow Peclet number, $Pe = \rho uL/\Gamma_\phi = \infty$. Consistent with previous works, the domain was divided up into 11 equally spaced rows and columns. This resulted in 11x11 nodes on a regular mesh and 200 triangular elements of equal size. For maximum effectiveness the element diagonals were aligned at 45° to the x-axis as shown in Figure 3.7. This element orientation does not contravene the regular spacing of nodes which was employed by past researchers. The exact solution to this problem is determined by advecting the upwind boundary conditions to the exit planes, taking account of the linear interpolation of ϕ between the nodes. The analysis was performed for three flow angles of 22.5°, 45° and 67.5°.

For $\theta = 22.5^\circ$, Figures 3.8(a) and (b) present the past published results and the result of the current streamline upwind approximation against the exact solution respectively. This flow angle is the worst case for all the methods including the current work. The conventional Galerkin formulation, G, exhibits considerable spatial oscillations as large as 19% with the maximum of 32% numerical diffusion. The streamline upwind approximations of Hughes and Brooks (1979), SU1 and SU2, also show numerical diffusion and spatial oscillations. SU1 has maximum of 23% spatial oscillation and 54% numerical diffusion. Results predicted by SU2 show a maximum spatial oscillation of 6% and maximum numerical diffusion of 25% . The standard upwind technique, U, shows no spatial oscillations, but a considerable numerical diffusion which is as muchas 43%. The monotone streamline upwind

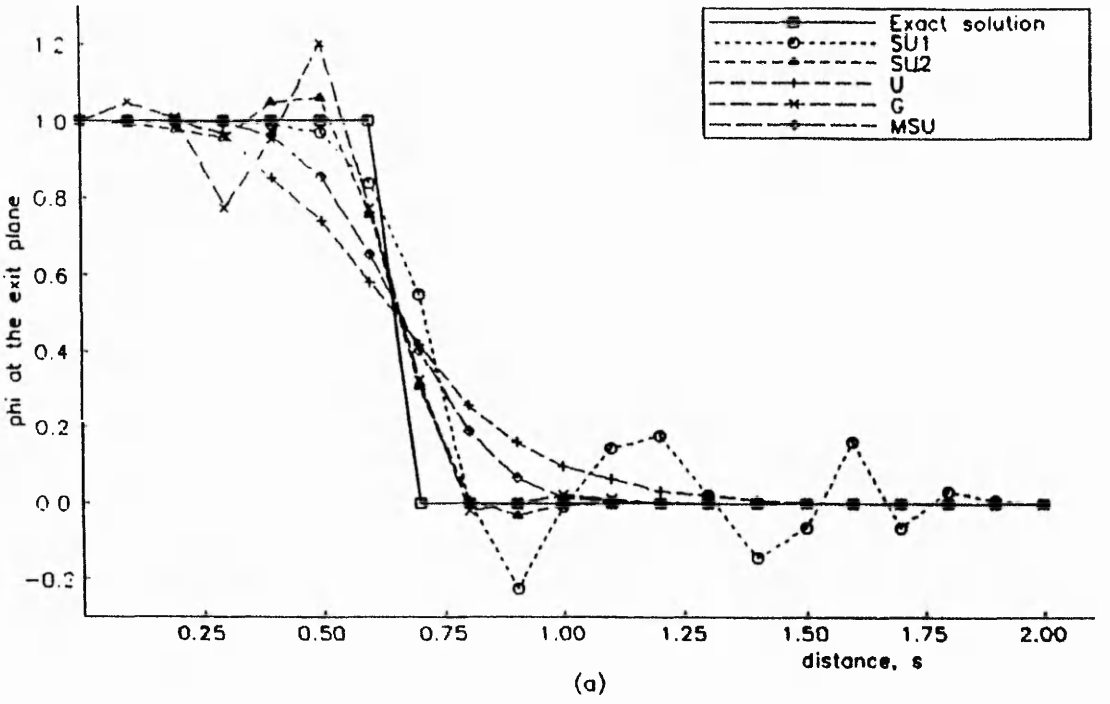

(a)

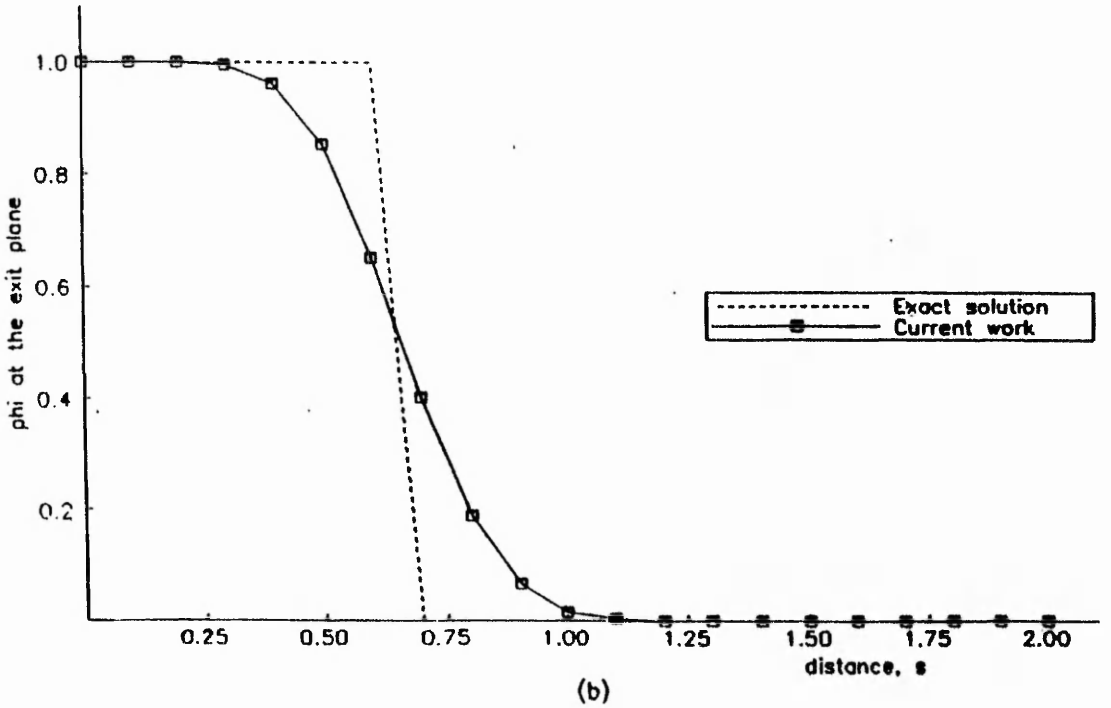

(b)

Figure 3.8 Comparison of results for pure advection skew to mesh at θ = 22.5°, (a) previous results, (b) current method.

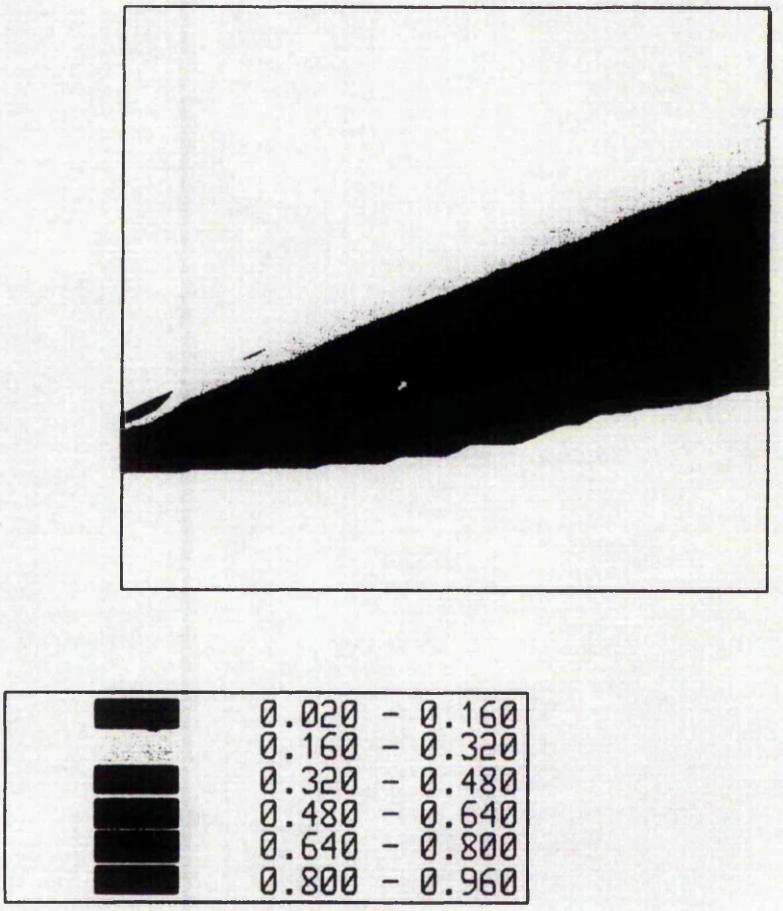

Figure 3.9 *Numerical diffusion in the domain by the current method at* $\theta = 22.5^{\circ}$.

technique of Rice and Schnipke (1985), MSU, produces the best results amongst the previously published results. It exhibits no spatial oscillation and 35% numerical diffusion. The result of the current method, as shown in Figure 3.8(b), also displays no spatial oscillation and maximum of 35% diffusion at the step discontinuity. MSU and the current work show very similar trends. This is to be expected since the current work is essentially the conservative form of MSU adapted for triangular elements. The degree of numerical diffusion in the domain arising from the current method can be seen clearly in Figure 3.9. The widening of the rainbow as the flow progresses from left to right is indicative of the presence of numerical diffusion in the result. For the exact solution, the width of the rainbow would remain unchanged.

For $\theta = 45^{\circ}$, Figures 3.10(a) and (b) present the past published results and that of the current method against the exact solution, respectively. The Galerkin formulation once more fails to produce physically realistic results, showing maximum of 12% spatial oscillation and 19% numerical diffusion. SU1 accurately follows the exact solution with no spatial oscillation or numerical diffusion. SU2 produces results with maximum of 6% spatial oscillation and a high degree of numerical diffusion (35%). U shows no spatial oscillations, but a considerable numerical diffusion which is as much as 49%. Both MSU and the current method reproduce the exact solution. As is evident from Figure 3.11, the rainbow retains its original thickness, indicating that the exact results are reproduced by the current method for $\theta = 45^{\circ}$.

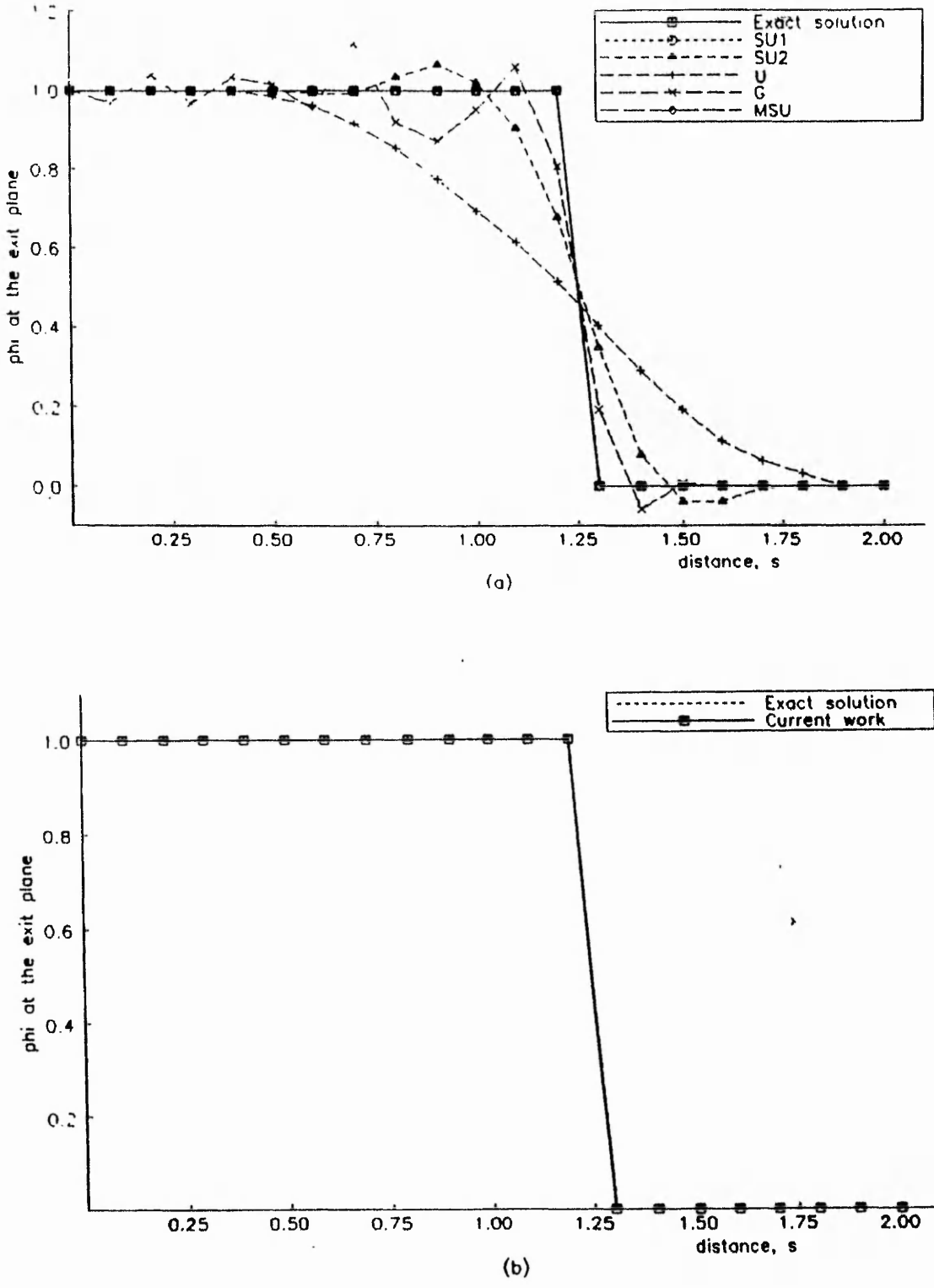

Figure 3.10 Comparison of results for pure advection skew to mesh at θ = 45°, (a) previous results, (b) current method.

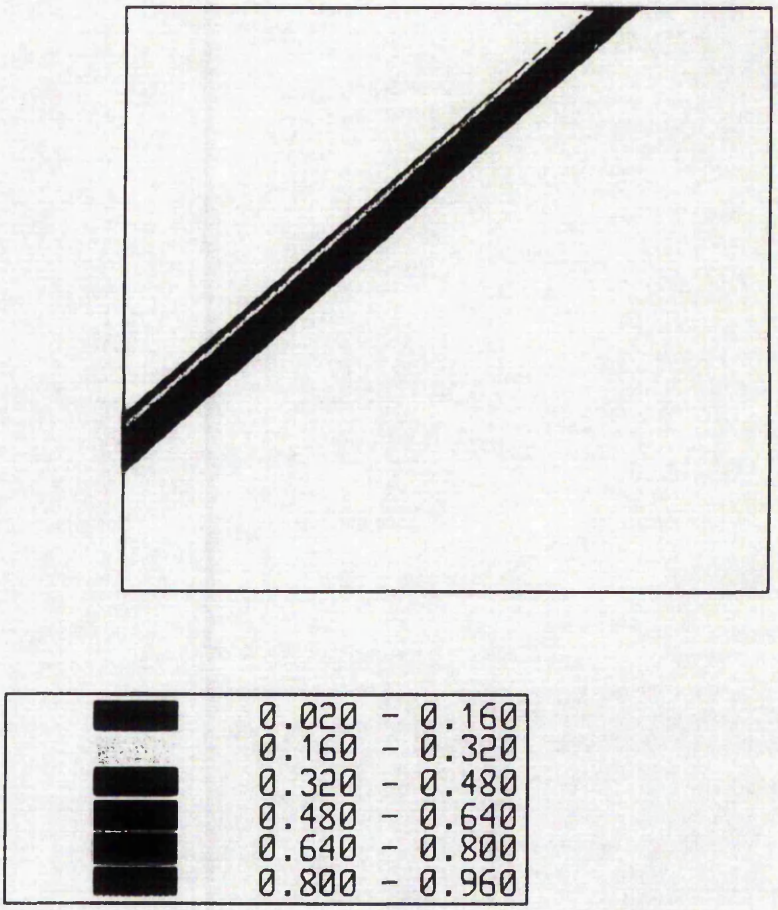

Figure 3.11 *Absence of numerical diffusion in the domain by the current method at* $\theta = 45^{\circ}$.

For $\theta = 67.5^{\circ}$, Figures 3.12(a) and (b) show the results of past workers and that of the current work against the exact solution, respectively. The Galerkin formulation shows no spatial oscillation but a large degree of numerical diffusion at the step discontinuity (52%). SU1 gives rise to oscillatory results with maximum of 33% spatial oscillation and 30% numerical diffusion. SU2 has spatial oscillation of 5% and numerical diffusion of 52% around the step discontinuity. U shows no spatial oscillation and 40% numerical diffusion. The current method, as shown in Figure 3.12(b), also displays no spatial oscillation and maximum of 39% diffusion at the step discontinuity. Figure 3.13 shows the numerical diffusion present in the current work as the rainbow widens towards the exit plane.

From Figures 3.8, 3.10 and 3.12 it is evident that all methods show maximum deviation from the exact solutions at the step discontinuity. The quadrature upwind and the Galerkin methods show excessive numerical diffusion and produce spatial oscillations at one or more flow angles. The streamline upwind methods of Hughes and Brooks (1979) produce better results compared to other two. These also suffer from spatial oscillations and numerical diffusion. The best results are obtained by the monotone streamline upwind approximation of Rice and Schnipke (1985) and the current method. They do not exhibit spatial oscillations at any angle and the numerical diffusion is small in both cases compared to the other methods. This diffusion exists only around the step discontinuity. The error analysis for this test case is concisely summarised in Table 3.2. One other criterion for comparison would be the computational efficiency of each method. However information regarding computational requirements in terms of storage and run-time for the above methods are not available. Even if

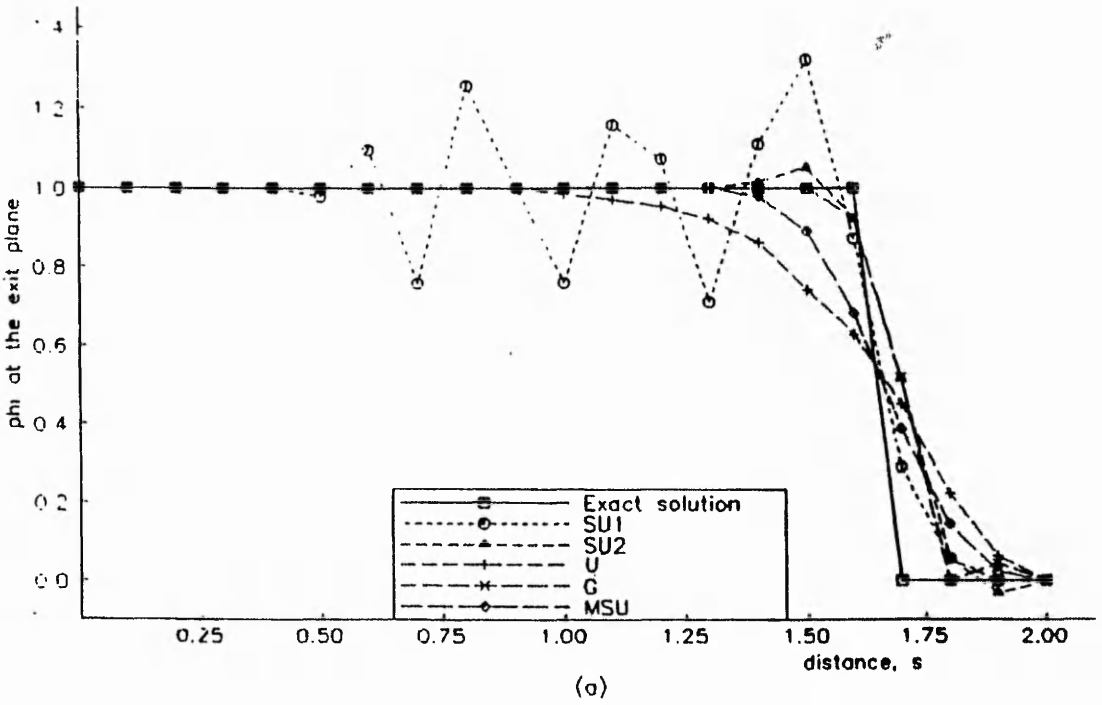

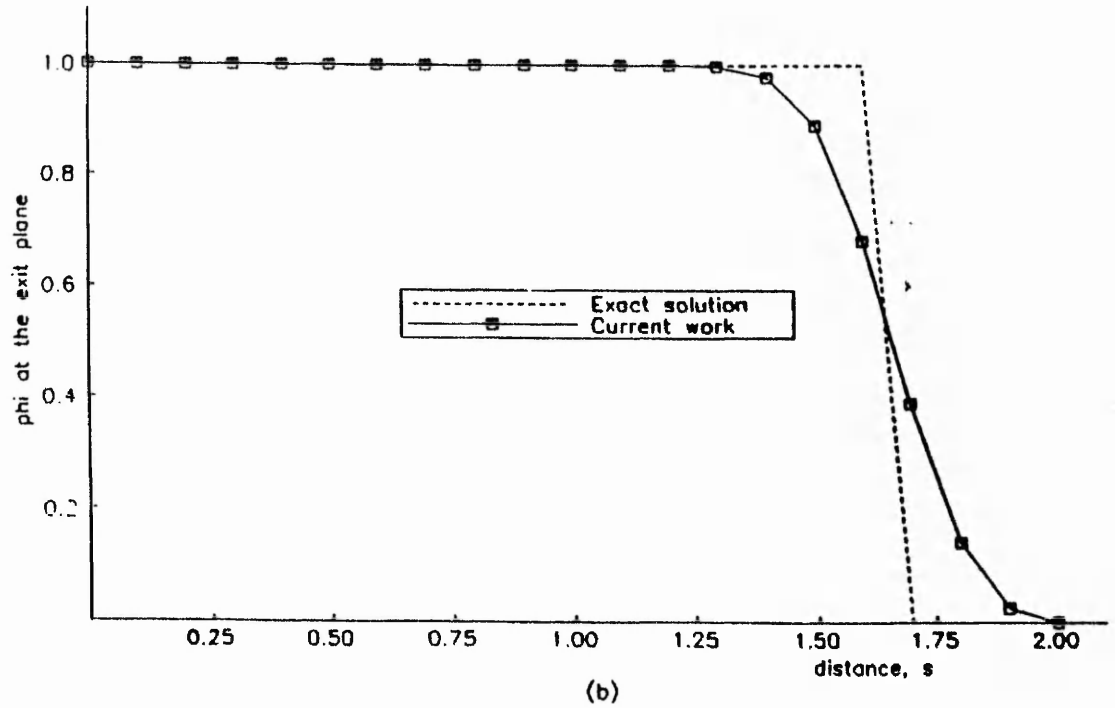

Figure 3.12 Comparison of results for pure advection skew to mesh at θ = 67.5°, (a) previous results, (b) current method.

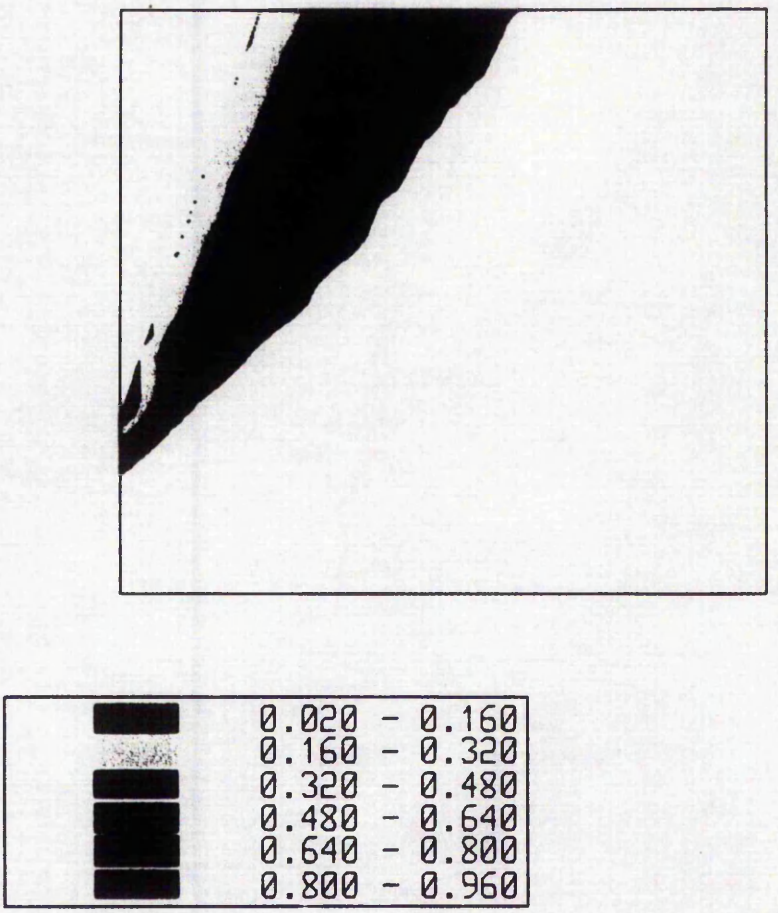

Figure 3.13 Numerical diffusion in the domain by the current method at $\theta = 67.5^{\circ}$.

such information existed, direct comparison could not be easily made as frequently a variety of different machines are in use. For the current method the above analysis was carried out on a Digital VAX-8550 machine. The advection calculations took on average 0.15 milliseconds per element (0.25 milliseconds per node) of the CPU time.

θ	*method*	*maximum percentage spatial oscillation*	*maximum percentage numerical diffusion*
22.5°	*SU1*	*23*	*54*
	SU2	*6*	*30*
	U	*0*	*42*
	G	*19*	*32*
	MSU	*0*	*41*
	Current	*0*	*40*
45°	*SU1*	*0*	*0*
	SU2	*6*	*35*
	U	*0*	*49*
	G	*12*	*19*
	MSU	*0*	*0*
	Current	*0*	*0*
67.5°	*SU1*	*33*	*30*
	SU2	*5*	*52*
	U	*0*	*46*
	G	*0*	*52*
	MSU	*0*	*40*
	Current	*0*	*39*

Table 3.2 Maximum errors for pure advection skew to mesh.

3.3.2 Smith and Hutton test case

The second validation test case considered here is concerned with the transport of the scalar quantity, ϕ, in a more complex flow field than the first test case. This problem was first presented as a comparison exercise by Smith and Hutton (1982), to establish the validity of the then existing codes in treating the advection transport in a flow field with a strong streamline curvature. The flow field together with the boundary conditions for ϕ are shown in Figure

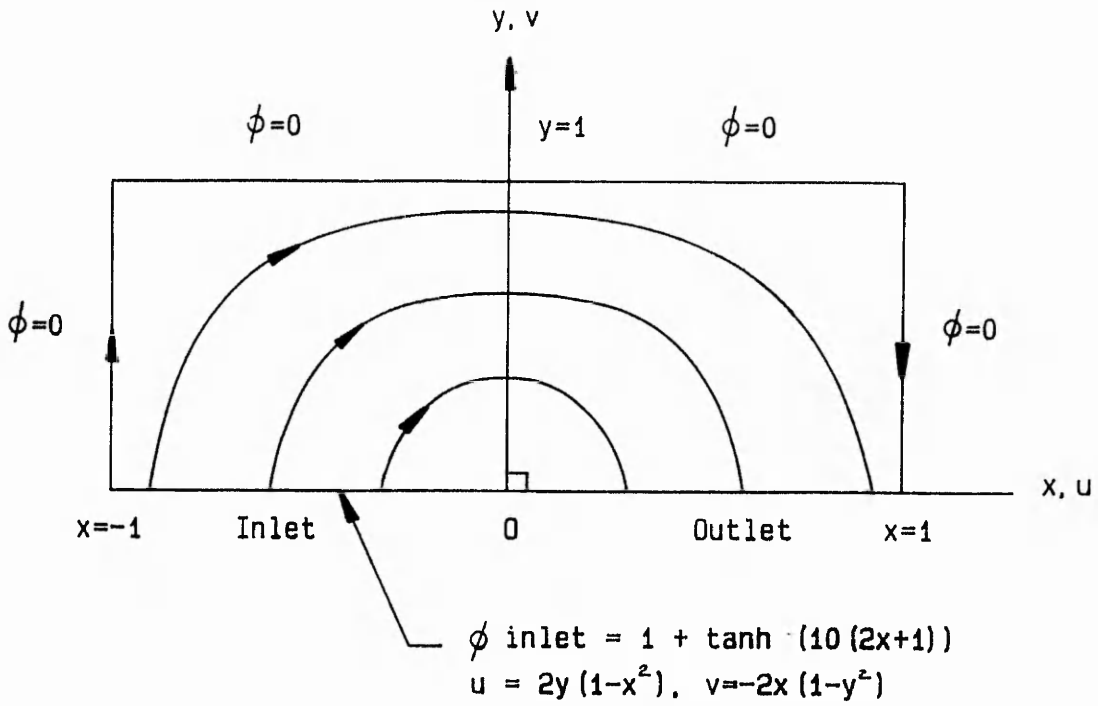

Figure 3.14 Smith and Hutton test case.

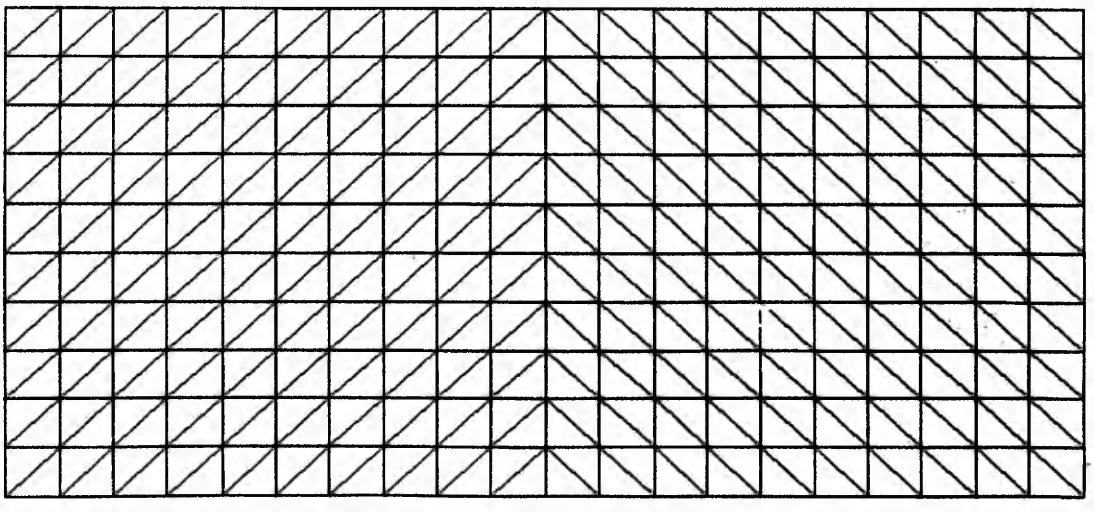

Figure 3.15 Computational grid for Smith and Hutton test case.

3.14. The flow field is specified as

$$u = 2x\,(1-y^2) \quad \text{and} \tag{3.21}$$

$$v = -2y\,(1-x^2)$$

As shown in the figure, with the exception of the outlet part of the boundary, ϕ is specified on the boundary as

$$\phi_{inlet} = 1 + \tanh\,(10(2x+1)) \text{ at } y = 0,\ -1 \le x \le 0$$

and

$$\phi = 0 \quad \text{at} \begin{cases} x = -1\ , & 0 \le y \le 1 \\ y = \ 1\ , & -1 \le x \le 1 \\ x = \ 1\ , & 0 \le y \le 1 \end{cases} \tag{3.22}$$

At the outlet ϕ is unspecified, which is equivalent to the natural boundary condition $\partial\phi/\partial y = 0$.

This test case possesses two important features which are common to most practical problems involving advection and diffusion. The streamlines have a large degree of curvature, a general feature of all recirculating flows. The variation of ϕ at the inlet is highly nonlinear, i.e. ϕ varies sharply over a small distance, possibly due to the presence of a source or mixing of two streams at different temperatures. Consistent with the comparison exercise of Smith and Hutton (1982), the flow domain was divided into 11 rows and 21 columns of equally spaced nodes. This resulted in 231 nodes and 400 triangular elements as shown in Figure 3.15. For maximum effectiveness the elements were aligned with their diagonals along the direction of the streamlines. The current analysis was carried out for two values of the Peclet number, Pe, of 100 and infinity. The results of the current analysis are compared with the reference solution and past published results given in the Smith and Hutton (1982) paper.

For Pe = 100, the variations of ϕ along the outlet plane are shown in Figures 3.16(a) and (b). At this Peclet number both the advection and the diffusion mechanisms equally influence the variation of ϕ in the domain. From Figure 3.16(a), the hybrid upwind differencing technique, HUD, has a maximum of 10% numerical diffusion. The monotone streamline upwind approach of Rice and Schnipke (1985), MSU, results in maximum of 7% numerical diffusion. The current method produces a maximum of 8% numerical diffusion as depicted in Figure 3.16(b). In the comparison study of Smith and Hutton (1982) the best reported result had 4% numerical diffusion. The relative high numerical diffusion of the current method is attributed to the nature of the imposed velocity field being a quadratic function of the space coordinates (equation (3.21)). The overall diffusion in the domain (physical + numerical) is shown in Figure 3.17 for the current method. In the presence of the physical diffusion some gradual widening of the rainbow from the inlet to the outlet is to be expected.

For the infinite Pe, the variations of ϕ along the outlet plane are shown in Figures 3.18(a) and (b). At this Peclet number only the advection mechanism is at work, i.e. the inlet profile of ϕ (equation (3.22)) should be carried round undisturbed to the outlet plane. From Figure 3.18(a), HUD has a very high numerical diffusion of 38% at x = 0.4. In fact HUD fails to capture the pure advection situation by producing results similar to those for Pe = 100 (see Figure 3.16(a)). MSU, results in maximum of 25% numerical diffusion. The current method produces a maximum of 27% numerical diffusion as depicted in Figure 3.18(b). In the comparison study of Smith and Hutton (1985) the best reported result (Sykes (1981)) had 6% numerical diffusion. The degree of numerical diffusion in the domain produced by the current method

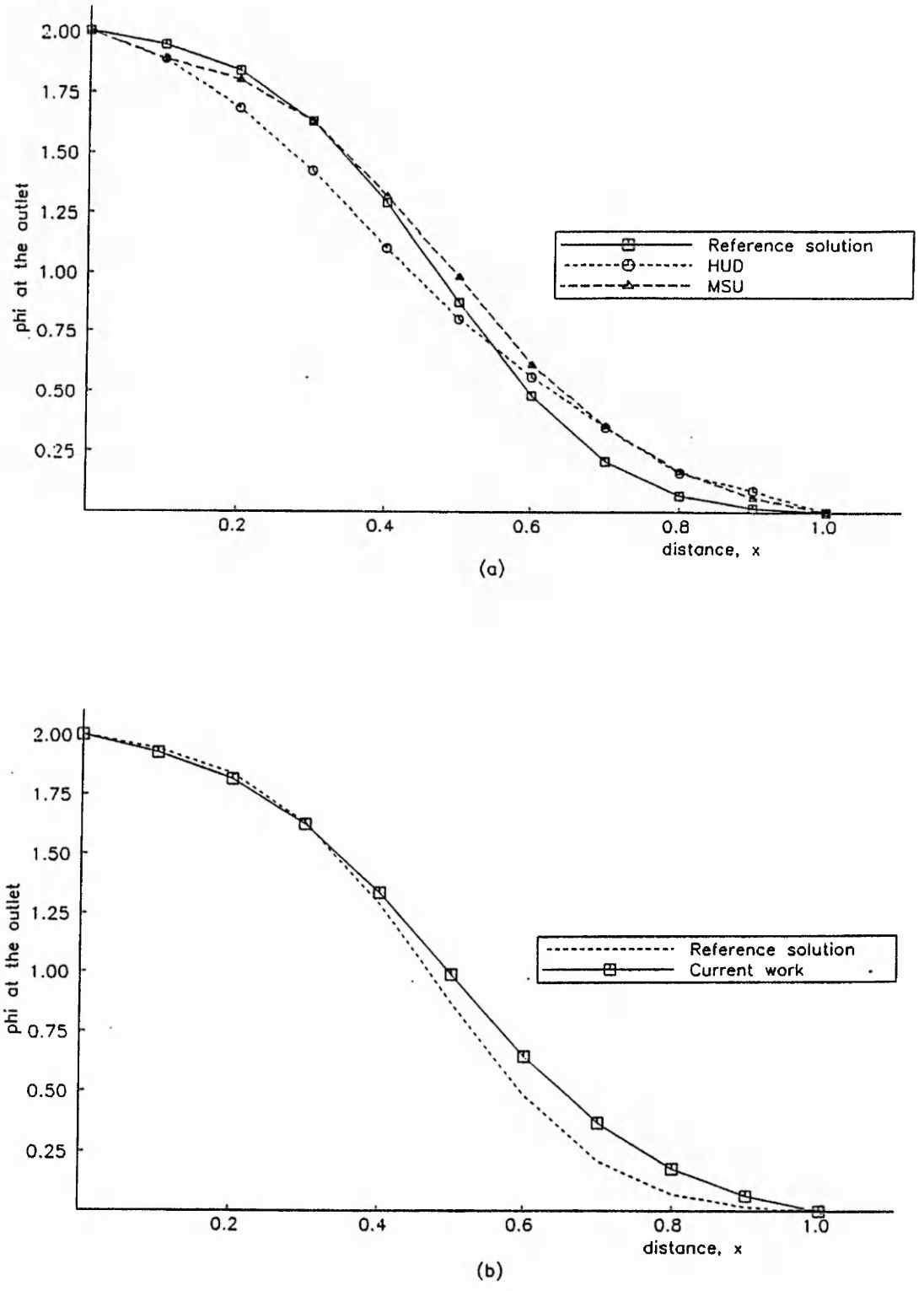

Figure 3.16 Outlet profile of ϕ at Pe = 100 for Smith and Hutton test case, (a) previous results and (b) current work.

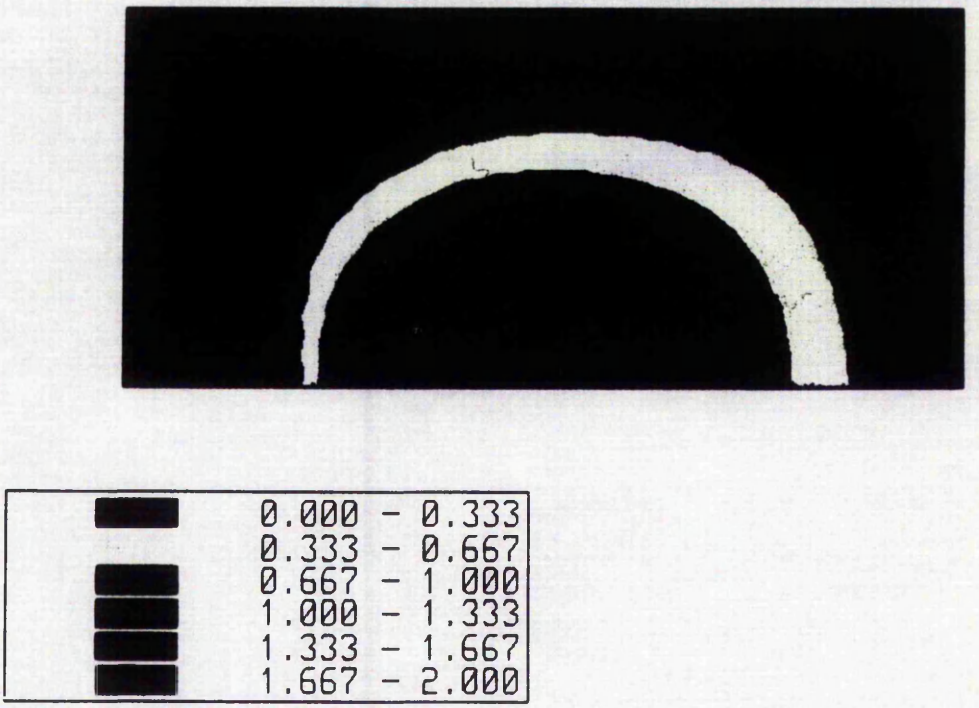

Figure 3.17 Combination of physical and numerical diffusion in the domain at Pe = 100.

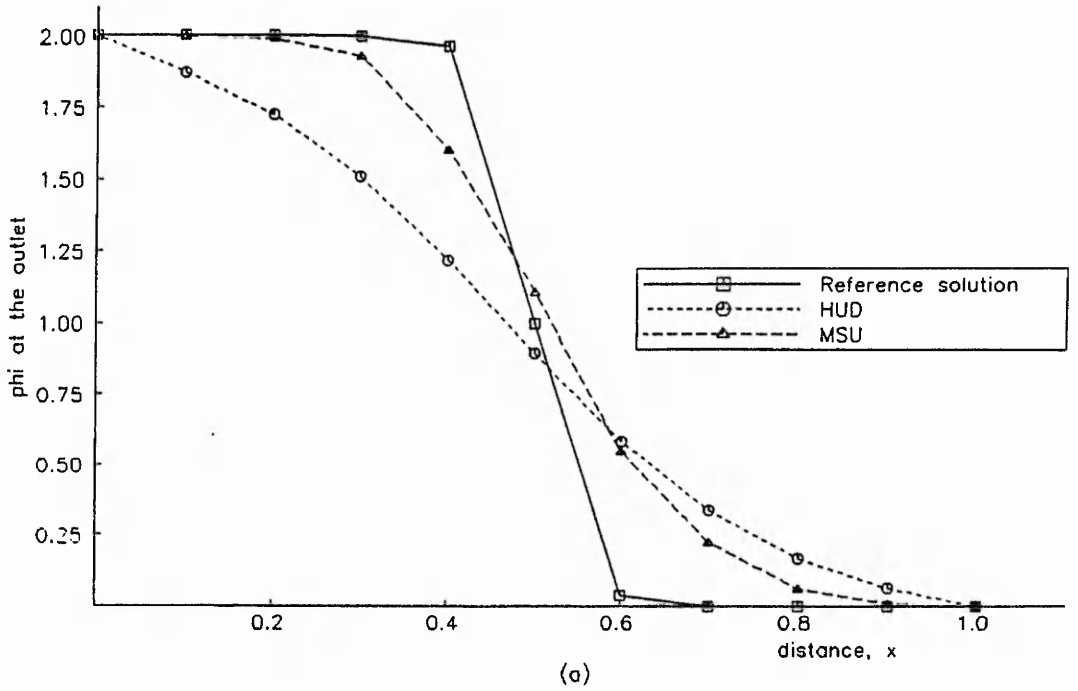

(a)

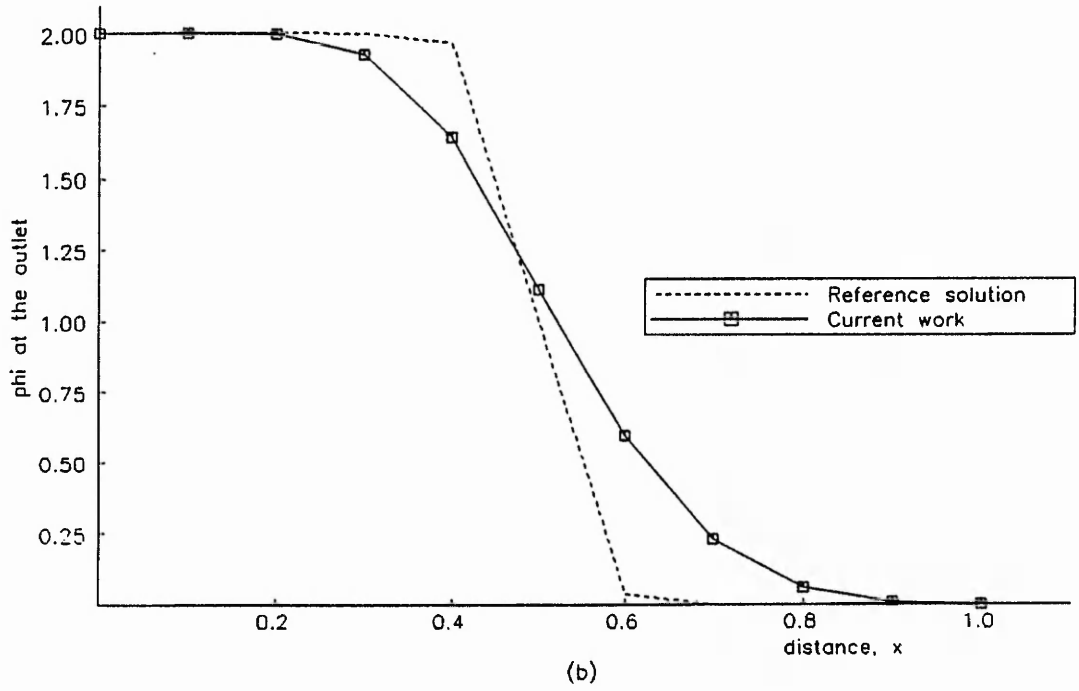

(b)

Figure 3.18 Outlet profile of ϕ at Pe = ∞ for Smith and Hutton test case, (a) previous results and (b) current work.

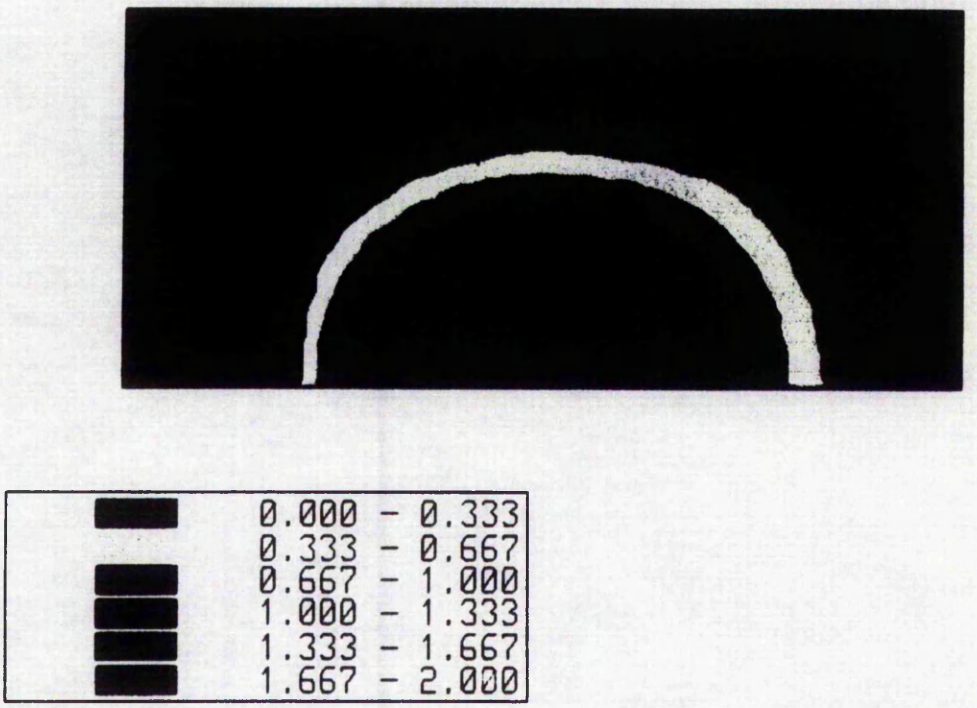

Figure 3.19 Numerical diffusion in the domain at Pe = ∞.

can be seen in Figure 3.19. With no numerical diffusion the rainbow would retain its original width, at the inlet, throughout the domain.

From Figures 3.16 and 3.18 it is seen that none of the methods considered here exhibit spatial oscillations. The conventional upwind technique shows excessive numerical diffusion at the infinite Peclet number. Both the monotone streamline upwind approach of Rice and Schnipke (1985) and the current method capture the physical characteristics of the problem well at the Peclet numbers of 100 and infinity. The former producing marginally less numerical diffusion. The results for the current work were obtained using, as for the first test case, a Digital VAX-8550 machine. Both the advection and diffusion calculations took 0.075 milliseconds per element (0.13 milliseconds per node) of CPU time.

3.3.3 Rotating disk

The last test case is the pure advection transport of the scalar quantity, ϕ, in a rotating flow field. The flow field together with the boundary conditions for ϕ are shown in Figure 3.20. This problem has been previously analysed by Hughes and Brooks (1979). The components of the velocity vector are described as

$$u = -y \ , \ v = x \qquad (3.23)$$

ϕ is set at zero on all four sides and assumes a cosine variation along the OA line as depicted in Figure 3.20. The strong circular curvature of the streamlines as prescribed in equation (3.23) makes this test case a challenging problem for the current method. The exact solution to this problem is obtained by advecting the ϕ profile along the OA line all the way round the flow domain. In other words contours

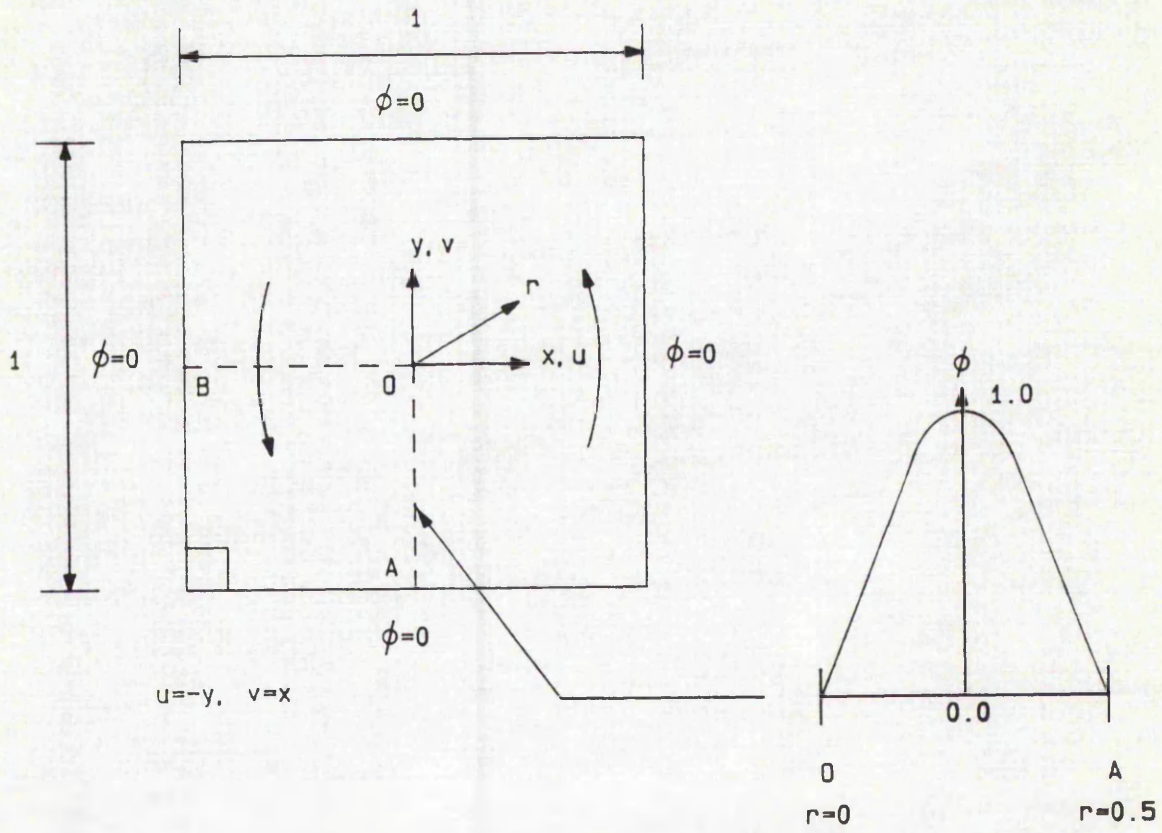

Figure 3.20 Rotating disk with imposed boundary conditions.

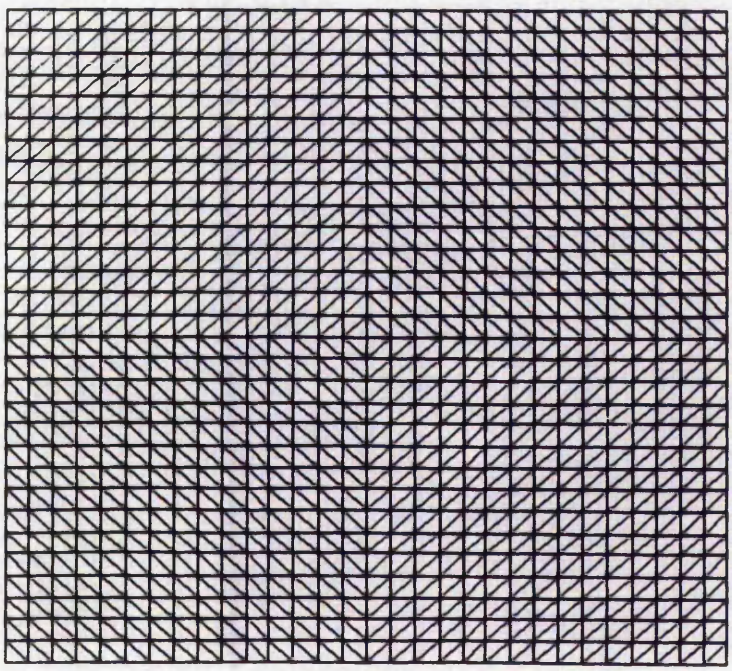

Figure 3.21 Computational grid for the rotating disk.

of ϕ should show circular symmetry about the origin, O. Consistent with the analysis of Hughes and Brooks (1979), the flow domain is divided into 31 rows and 31 columns of equally spaced nodes. This resulted in 961 nodes and 1800 triangular elements of equal size as shown in Figure 3.21. The elements are oriented with their diagonals following the flow direction.

For comparison purposes, the ϕ profile is examined along the OB line against the exact solution, namely ϕ profile along the OA line (see Figure 3.20). Figure 3.22(a) shows the best past results against the exact solution. The streamline upwind method of Hughes and Brooks (1979), SU2, shows no numerical diffusion and reproduces the exact solution. The monotone streamline upwind method of Rice and Schnipke (1985), MSU, results in maximum of 11% numerical diffusion. MSU also shows some degradation in the results at radial distances of 0.033 and 0.467 from the origin. As shown in Figure 3.22(b), the current method has a maximum of 9% numerical diffusion. It too exhibits some degradation in the computed ϕ at the radial distance of 0.467 from the origin. The result of the current analysis is seen to be generally superior to that of Rice and Schnipke (1985) by following the exact solution more closely. The overall numerical diffusion in the flow domain, produced in the current work, is shown in Figure 3.23. As seen in the figure, the narrowing of the colour bands as they turn anti clockwise is an indication of the degree of numerical diffusion present in the result. The exact solution would produce bands which retain their thickness within the flow domain. As with the previous two test cases, this analysis was carried out on a Digital VAX-8550 machine. The advection calculations took 0.10 milliseconds per element (0.19 milliseconds per node) of CPU time.

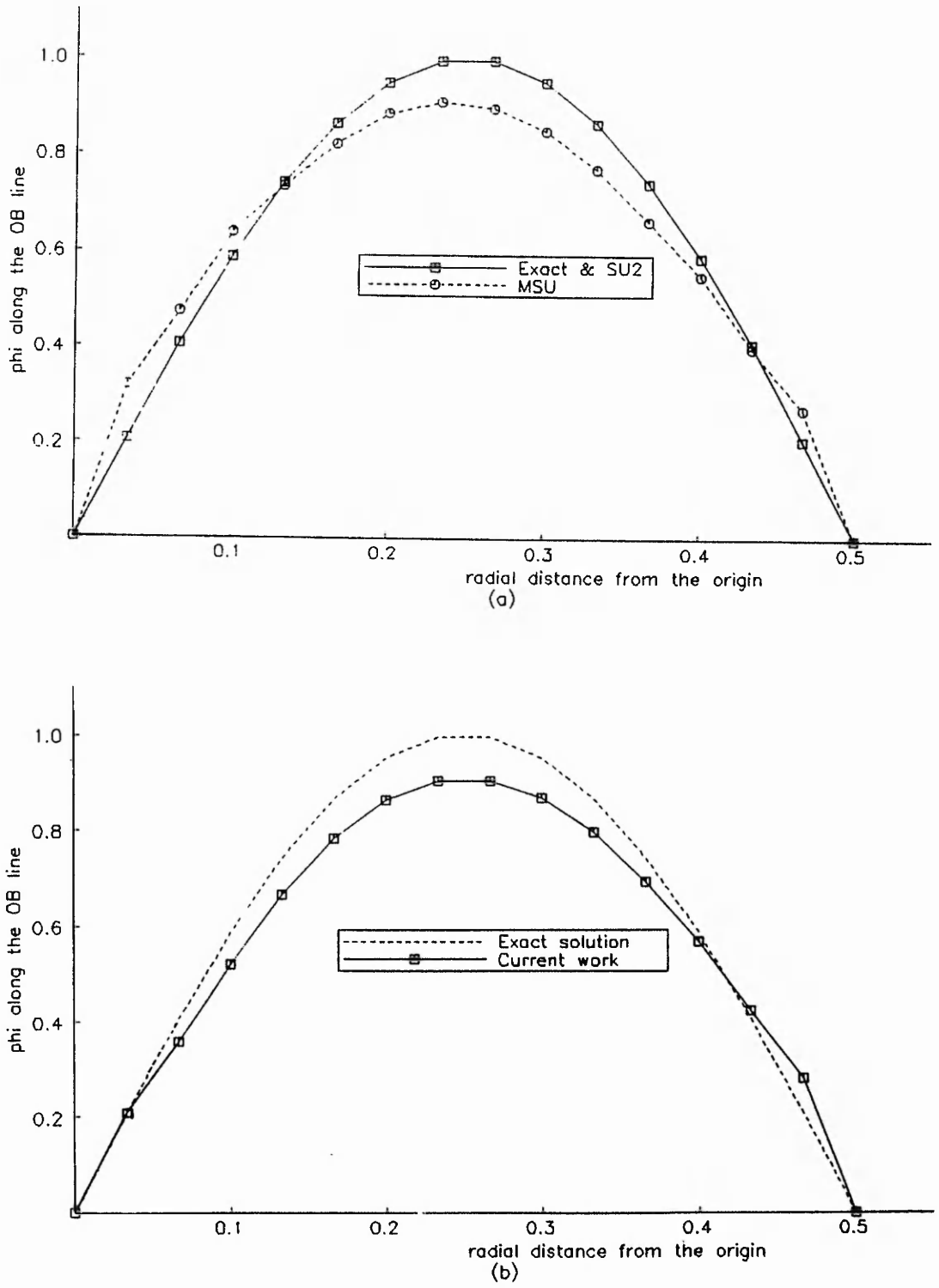

Figure 3.22 ***Profile of ϕ along the OB line for the rotating disk, (a) best previous results and (b) current work.***

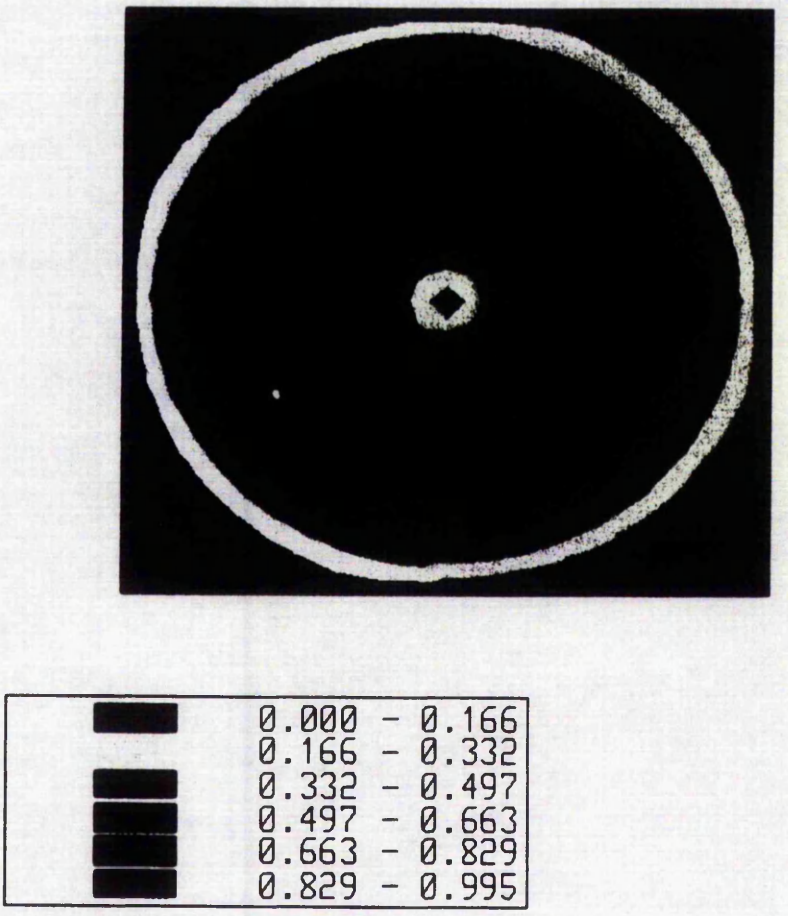

Figure 3.23 Contours of ϕ showing the numerical diffusion for the rotating disk by the current method.

3.4 Remarks on the streamline approximation

In this chapter, a new conservative streamline upwind approximation using linear three-noded triangular elements was developed. The upwinding is based on the physical phenomenon of pure advection transport. The discontinuous nature of the advection transport is adequately captured by the present formulation. This is achieved by modelling the advection mechanism to be discontinuous not only amongst elements but also within each individual element. Most of the previous methods were based on continuous or semi-continuous (discontinuous amongst elements) approximations, which limited their applicability and/or accuracy to certain ranges of the flow Peclet number. The present approximation is equally applicable for all values of the Peclet number. It is also a simple procedure which can be readily incorporated into conventional Galerkin type finite element algorithms.

In section 3.2 it was shown that the present streamline formulation, like the diffusion formulation of Chapter 2, results in a global coefficient matrix, which is unconditionally diagonally dominant. The overall system of the partial differential equations (equation (3.1)), consisting of both diffusion and advection mechanisms, may therefore be discretised to render a system of simultaneous linear algebraic equations which could be solved by any iterative scheme. This is an important outcome of the present formulation, since, as mentioned previously, iterative schemes generally require much less computer requirements in terms of run-time and storage than the direct solution methods.

Three stringent test cases were employed to verify the stability,

accuracy and applicability of the current upwind formulation. These were pure advection skew to mesh, Smith and Hutton case and pure advection on a rotating disk. The results were compared with exact solutions and past published works. The formulation showed unconditional stability in all cases for all Peclet numbers considered ($100 \leq Pe \leq \infty$). The results were all free of spatial oscillations, which had plagued the previous attempts to treat advection mechanism, except that of Rice and Schnipke (1985). The numerical diffusion arising from the current formulation was shown to be small and competitive with the best of the previously published work.

Finally, the use of simplex triangular elements allowed exact integrations to be performed. Exact integrations were employed for both advection and the diffusion terms. This resulted in the overall calculation procedure to become very efficient. Most of the previous workers, in the context of the FEM for fluid flow computations, had employed numerical integration techniques. These numerical techniques are inferior to their exact counterparts on at least two accounts. They may lack accuracy, e.g. use of one-point Gauss quadrature with bilinear elements in the SU1 method of Hughes and Brooks (1979), or they may be accurate at the expense of computational cost, e.g. four-point Gauss quadrature with bilinear elements in the SU2 and MSU methods. To appreciate the efficiency of the exact integration technique employed here, it may be said that the exact integration has the accuracy of the four-point and the efficiency of the one-point Gauss quadratures. Furthermore, the exact integration procedure together with an appropriate iterative solution scheme make the present code competitive with the finite difference (volume) schemes. As demonstrated in Chapter 5, such an iterative solution scheme is

devised for the current research.

CHAPTER 4

FINITE ELEMENT DISCRETISATION OF LAMINAR FLOW EQUATIONS

The finite element discretisation of the governing transport equations for laminar flow is described. To present the current discretisation strategy, the first section is dedicated to isothermal flows. A discussion on the problem of the velocity-pressure interaction is followed by the derivation of a novel equal order velocity-pressure solution procedure. In this procedure, velocity and pressure are segregated and are solved sequentially by a SIMPLER-like algorithm. This procedure forms the core of the discretisation/solution strategy devised for the current research. In the second section the discretisation of the energy equation is described. Imposition of the various types of boundary conditions is presented in the last section.

4.1 Velocity-pressure segregation

Conventional Finite Element practices require the simultaneous solution of the momentum and the continuity equations at each step of an iterative scheme in order to yield velocity and pressure values, see for example Ijam (1977), Chung (1978), Taylor and Hughes (1981) and Olson (1976). The computer storage and execution time for such schemes prohibit their use for problems where, for various reasons, a large number of elements must be employed. Furthermore, the pressure is very often evaluated at fewer points than the velocity components (mixed order interpolation) so as to avoid pressure chequer boarding, see for example Gresho and Lee (1979), Hood and Taylor (1974), Sani et al (1981) and Lee et al (1979). This adds to the complexity of the

scheme and is not entirely effective in eliminating the chequer boarding for simplex triangles or bi-linear quadrilaterals where pressure is assumed constant over the element (Lee et al (1979)). In this research a major departure from the conventional finite element methodology is followed. Pressure and velocity are segregated. A Poisson type pressure equation is developed. The discretisation of the pressure equation is based on element shape functions that are also used to define the velocity components (equal order interpolation). The pressure together with the momentum equations are solved in a sequential manner similar to the SIMPLER algorithm (Patankar (1980). In this section the problem of the velocity-pressure interaction is first discussed. This is followed by the discretisation of the momentum equations. The derivation of the pressure equations is then presented. Lastly, the SIMPLER-like solution sequence is outlined and general remarks are given.

4.1.1 Velocity-pressure interactions

The interaction between the velocity and the pressure fields is best demonstrated by considering the steady state isothermal laminar flow in two-dimensional Cartesian coordinate system. From Chapter 2, the coupled set of differential equations governing such a flow, are

$$\frac{\partial}{\partial x}(\rho u) + \frac{\partial}{\partial y}(\rho v) = 0 \tag{4.1}$$

$$\frac{\partial}{\partial x}\rho u^2 + \frac{\partial}{\partial y}\rho vu = \rho g_x - \frac{\partial p}{\partial x} + \frac{\partial}{\partial x}\left(\mu \frac{\partial u}{\partial x}\right) + \frac{\partial}{\partial y}\left(\mu \frac{\partial u}{\partial y}\right) \tag{4.2}$$

$$\frac{\partial}{\partial x}\rho uv + \frac{\partial}{\partial y}\rho v^2 = \rho g_y - \frac{\partial p}{\partial y} + \frac{\partial}{\partial x}\left(\mu \frac{\partial v}{\partial x}\right) + \frac{\partial}{\partial y}\left(\mu \frac{\partial v}{\partial y}\right) \tag{4.3}$$

The velocity components, u and v, are governed by the momentum equations (4.2) and (4.3) respectively. The pressure gradient terms, $\partial p/\partial x$ and $\partial p/\partial y$, form part of the source terms for the momentum

equations. For a given pressure field, the unknown velocity field may therefore be obtained by solving the momentum equations with the appropriate velocity boundary conditions. Yet, there is no direct equation that describes the variations in pressure. The pressure field is indirectly described by the continuity equation, in that if a correct pressure field was used in the momentum equations, the resulting velocity field would satisfy the continuity equation. This points to a simultaneous solution of the momentum and continuity equations as advocated by the majority of the Finite Element workers. However, such a simultaneous solution is undesirable as it demands excessive computer resources.

One way of overcoming the above difficulty in determining the pressure field is to employ the stream-function/vorticity method (Gosman et al (1969)), where pressure is eliminated from the governing equations. However this method has major disadvantages. The vorticity boundary conditions at a wall are difficult to specify and are often responsible for lack of convergence. The extraction of pressure from the vorticity field requires additional computational effort. Also the method is only applicable to two-dimensional situations, for which the stream-function description exists. The problems just mentioned initiated the Finite Volume workers to derive a direct equation for pressure by suitable conversion of the continuity equation, see for example Patankar (1980). Solution of the momentum and pressure equations would then become part of an iterative scheme. At each iteration, the velocity and the pressure fields are updated sequentially. An improved pressure field is used to obtain better estimates for the velocity field. The velocity field is in turn used to correct the pressure field. Iterations are carried out until

resulting changes in the velocity and the pressure fields are small enough to meet some pre-specified convergence criteria. There are a number of these so called pressure correction methods currently in use. Amongst the most popular, are the SIMPLE and the SIMPLER algorithms of Patankar (1980). To avoid pressure and velocity chequer boarding, the majority of these methods use the staggered grid arrangement first employed by Harlow and Welch (1965). In this arrangement the control volumes for the velocity components and the pressure occupy different spaces surrounding a grid point. This results in an overhead on computer storage and run-time. Since the control volumes for X and Y momentum equations are not the same, the corresponding velocity components, u and v, must be stored at different locations. Furthermore, the discretisation of the X and Y momentum equations will be different, which adds to the complexity of the procedure as well as increasing the required number of computations.

In conventional FEM, the chequer boarding problems are to some extent avoided by the use of mixed order interpolation techniques. These techniques are the finite element counterparts to the staggered grid arrangements employed by the FVM. In mixed order interpolations the pressure field is specified at fewer points than the velocity components. At the elemental level, this results for example in a parabolic variation in the velocity components accompanied by a linear variation in pressure. As mentioned earlier in this chapter, the mixed order interpolation is not totally effective when used in conjunction with simplex triangular or bi-linear elements. Furthermore, as with the staggered grid arrangement, the mixed order interpolation adds to the complexity of the discretisation procedure. With the same element

shape function, the discretisation of the momentum equations becomes identical (except round the boundaries). However, the continuity (pressure) equation requires a different discretisation procedure, as a lower order element shape function must be used.

In order to eliminate the above problems, a number of researchers have in the past devised equal order finite element formulations, see for example Parakash and Patankar (1984), Schneider et al (1978a and 1978b) and Rice and Schnipke (1985). The successful implementation of such formulations has been based on developing a separate Poisson-type equation for pressure. However formulations of this type generally suffer from poor convergence rates as the pressure equation offers no direct constraint on satisfying the continuity, e.g. Schneider et al (1978a). Moreover, the specification of the pressure at the boundaries plays a critical role in obtaining a converged solution set. One of the few equal order velocity-pressure finite element formulations that does not suffer from these difficulties is that devised by Rice and Schnipke (1985). This formulation is based on a Poisson-type pressure equation that does satisfy the continuity. Also, the pressure boundary conditions are imposed in the conventional manner for FEM. The method has been successfully employed for a variety of flow cases in both laminar and turbulent regimes, see Rice and Schnipke (1985), Schnipke and Rice (1985) and Jones et al (1989). In all of the reported cases, the results were shown to be free of spurious pressure modes.

The above method has however several disadvantages. The method was devised for bi-linear quadrilateral elements. As was shown in Chapter 2, these elements, depending on their aspect ratios, may result in non-diagonally dominant coefficient matrices. The diagonal

dominance of the coefficient matrices is an essential condition which must never be violated if iterative solution schemes are to be employed. Also, the method uses numerical integration which is more costly in computational terms than exact integration schemes. The method is also non-conservative in the momentum and the energy equations due to its treatment of the advection terms. For flow cases where the fluid properties vary, this may result in the global violation of conservation of momentum and energy. For the current research, a conservative equal order velocity-pressure equation for simplex triangular elements is developed. This method is based on the original method of Rice and Schnipke (1985).

4.1.2 Momentum equations

As illustrated in Figure 4.1 for a typical momentum element, the variations in u and v within the element, including its sides, are described by

$$u = N_1 u_1 + N_2 u_2 + N_3 u_3$$
$$v = N_1 v_1 + N_2 v_2 + N_3 v_3 \qquad (4.4)$$

where

$$N_1 = \left\{ N_1 \quad N_2 \quad N_3 \right\} \qquad (4.5)$$

is the element shape function vector. As u and v are both stored at the same nodal positions, the discretisation of the advection and the diffusion terms for X and Y momentum equations will be identical. The advection terms in equations (4.2) and (4.3) can be written as

$$\frac{\partial}{\partial x}(\rho u \phi) + \frac{\partial}{\partial y}(\rho v \phi) \qquad (4.6)$$

where ϕ stands for either u or v. The discretisation of the above

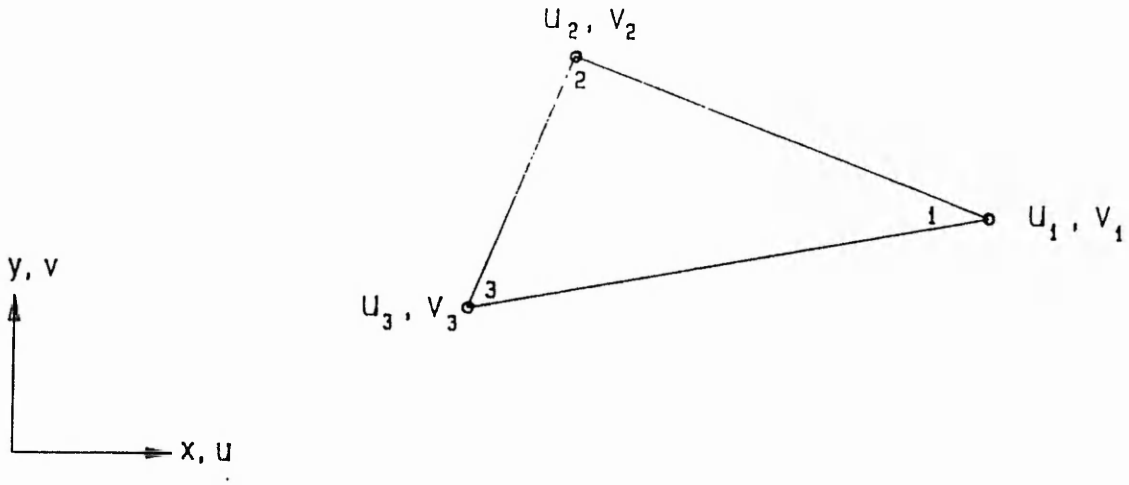

Figure 4.1 Three-noded momentum element.

equation follows the streamline upwind technique developed in the last chapter. Equation (4.6) is expressed in terms of the streamline coordinate system (see Figure 3.1),

$$\frac{\partial}{\partial x}(\rho u\phi) + \frac{\partial}{\partial y}(\rho v\phi) = \frac{\partial}{\partial s}(\rho u_s\phi) \tag{4.7}$$

Equation (4.7) is then weighted and integrated over each element and summed for all the elements in the domain, hence

$$\sum_{1}^{n^e} \int_{A^e} N_i \left\{\frac{\partial}{\partial s}(\rho u_s\phi)\right\} dA^e \tag{4.8}$$

with the differential term approximated conservatively by (see Figure 3.5),

$$\frac{\partial}{\partial s}(\rho u_s\phi) \simeq \text{constant} = \frac{\rho_i u_{si}\phi_i - \rho' u'_s\phi'}{\Delta s} \tag{4.9}$$

The diffusion terms are discretised by the conventional Galerkin weighted residual method described in Chapter 2. The general form of the diffusion terms is

$$\frac{\partial}{\partial x}\left(\mu \frac{\partial \phi}{\partial x}\right) + \frac{\partial}{\partial y}\left(\mu \frac{\partial \phi}{\partial y}\right) \tag{4.10}$$

where as for the advection terms, ϕ may stand for u or v. Equation (4.10) is then weighted and integrated over each element and summed for all the elements in the domain, hence

$$\sum_{1}^{n^e} \int_{A^e} N_i \left\{ \frac{\partial}{\partial x}\left(N_j \mu_j \frac{\partial N_k}{\partial x}\right) + \frac{\partial}{\partial y}\left(N_j \mu_j \frac{\partial N_k}{\partial y}\right)\right\} \phi_k \, dA^e \tag{4.11}$$

As the elements are first order continuous, the order of the element integral in the above equation is reduced by employing the Gauss's theorem, which gives

$$\begin{aligned} &- \int_{A^e} \left\{ \frac{\partial N_i}{\partial x} N_j \mu_j \frac{\partial N_k}{\partial x} + \frac{\partial N_i}{\partial y} N_j \mu_j \frac{\partial N_k}{\partial y} \right\} \phi_k \, dA^e \\ &+ \int_{s^e} \left(N_i N_j \mu_j \frac{\partial N_k}{\partial n} \right) \phi_k \, ds^e \end{aligned} \tag{4.12}$$

The surface integral term is only evaluated for the boundary elements as those arising from the internal elements cancel out.

The first order pressure gradient terms are treated in a discontinuous manner. As with the advection terms, these terms are taken as discontinuous within each element. In the conventional Galerkin method, the element pressure gradient integrals would be distributed equally amongst the element's nodes. Here, each node receives a weighted share of the integral according to

$$- \int_{A^e} N_i \frac{\partial p}{\partial x} \, dA^e = - \frac{A^e}{D_x} \frac{\partial p}{\partial x} \left\{ \left| \frac{\partial N}{\partial x}^1 \right| , \left| \frac{\partial N}{\partial x}^2 \right| , \left| \frac{\partial N}{\partial x}^3 \right| \right\} \tag{4.13}$$

and

$$- \int_{A^e} N_i \frac{\partial p}{\partial y} \, dA^e = - \frac{A^e}{D_y} \frac{\partial p}{\partial y} \left\{ \left| \frac{\partial N}{\partial y}^1 \right| , \left| \frac{\partial N}{\partial y}^2 \right| , \left| \frac{\partial N}{\partial y}^3 \right| \right\} \tag{4.14}$$

where

$$D_x = \sum_{i=1}^{3} \left| \frac{\partial N}{\partial x}^i \right| \tag{4.15}$$

$$D_y = \sum_{i=1}^{3} \left| \frac{\partial N}{\partial y}^i \right| \tag{4.16}$$

and the pressure field is assumed to be known†. This poses no extra difficulty as a converging iterative scheme would continuously provide better estimates for pressure, until the actual pressure field, with which the continuity equation is satisfied, is established. A similar discontinuous treatment of the pressure gradient terms is cited in Baliga and Patankar (1983).

The discretisation of the body force terms is performed by the lumped mass approach outlined in Chapter 2. With the components of the gravity vector, g_x and g_y, taken as constants, the body force integrals become

$$\sum_{1}^{n^e} \int_{A^e} N_i \, N_T \rho_j \, g_x \, dA^e \tag{4.17}$$

† To be correct on an arbitrary finite element mesh, this pressure weighting should be normalised on the sum of the areas of elements surrounding a node, as with the advection upwinding. However on regular meshes and those graded in only one direction, as in most of the tests here, the normalisation scaling is unity and so does not alter the results presented here.

$$\sum_{1}^{n^e} \int_{A^e} N_i \, N_T \rho_j \, g_y \, dA^e \qquad (4.18)$$

with

$$N_T = \sum_{j=1}^{3} N_j \qquad (4.18)$$

The discretised momentum equations can be written as

$$a^u_{ii} u_i = - \sum_{j \neq i} a^u_{ij} u_j + f^u_i \qquad (4.20)$$

$$a^v_{ii} v_i = - \sum_{j \neq i} a^v_{ij} v_j + f^v_i \qquad (4.21)$$

where a^u and a^v are the members of the fully assembled coefficient matrices for X and Y momentum equations. a^u_{ii} and a^v_{ii} denote the diagonal members with a^u_{ij} and a^v_{ij} their corresponding row neighbours. The coefficient matrices only contain contributions from the advection and the diffusion terms in equations (4.8) and (4.12). Hence they are identical except at points where boundary conditions for u or v are specified, and are therefore formed once for both equations. u_i and v_i denote the velocity components at the global node i. u_{ij} and v_{ij} are the velocity components at the nodes surrounding node i. f^u_i and f^v_i are the global right hand side force vectors, which contain contributions from the pressure gradient terms, the body force terms and the surface boundary terms.

4.1.3 Pressure equation

The pressure equation is derived from the continuity equation. Applying the Galerkin weighted residual method to equation (4.1) and reducing the order of the integral gives

$$\int N \left(\frac{\partial}{\partial x} \rho u + \frac{\partial}{\partial y} \rho v \right) dA = \int N \rho \, (u n_x + v n_y) \, ds \qquad (4.22)$$

$$- \int \left(\rho u \frac{\partial N}{\partial x} + \rho v \frac{\partial N}{\partial y} \right) dA$$

$$= 0$$

On the elemental level, the above equation can be written as

$$\int_{A^e} \left(N_i \rho_i N_j u_j \frac{\partial N}{\partial x}_k + N_i \rho_i N_j v_j \frac{\partial N}{\partial y}_k \right) dA^e = \qquad (4.23)$$

$$\int_{s^e} N_i N_i \rho_i \left(N_j u_j N_k n_{xk} + N_j v_j N_k n_{yk} \right) ds^e$$

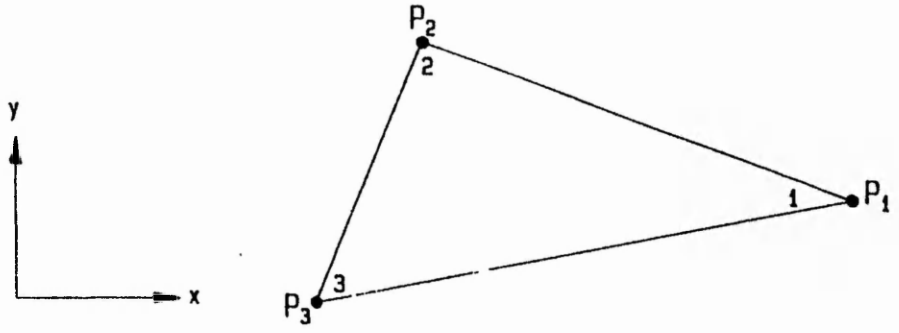

Figure 4.2 Three-noded continuity element.

Equation (4.23) is expressed in terms of the nodal velocity components u_j and v_j. To obtain a direct equation for pressure both u_j and v_j are

replaced by nodal values of pressure. This is achieved by first describing pressure variations within an element with the same shape function used for the velocity components. As is shown in Figure 4.2, the continuity element like the momentum element of Figure 4.1 is a three-noded triangular element for which

$$p = N_1 p_1 + N_2 p_2 + N_3 p_3 \tag{4.24}$$

with the shape function vector, N_i given by equation (4.5) and the pressure field stored at the same nodal positions as the velocity components.

The next step is to write equations (4.20) and (4.21) in a revised form as

$$a^u_{ii} u_i = - \sum_{j \neq i} a^u_{ij} u_j + e^u_i - \int_i N \frac{\partial p}{\partial x} \, dA \tag{4.25}$$

$$a^v_{ii} v_i = - \sum_{j \neq i} a^v_{ij} v_j + e^v_i - \int_i N \frac{\partial p}{\partial y} \, dA \tag{4.26}$$

with e^u_i and e^v_i representing the body force and the surface boundary terms. The pressure gradient terms are now separated from the rest of the right hand side force vectors. Assuming that the pressure gradient terms are known, equations (4.25) and (4.26) can be written as

$$u_i = \hat{u}_i - K^u_i \frac{\partial p}{\partial x} \tag{4.27}$$

$$v_i = \hat{v}_i - K^v_i \frac{\partial p}{\partial y} \tag{4.28}$$

where

$$\hat{u}_i = \frac{1}{a^u_{ii}} \left\{ - \sum_{j \neq i} a^u_{ij} u_j + e^u_i \right\} \tag{4.29}$$

$$\hat{v}_i = \frac{1}{a^v_{ii}} \left\{ - \sum_{j \neq i} a^v_{ij} v_j + e^v_i \right\} \tag{4.30}$$

$$K_i^u = \frac{1}{a_{ii}^u} \left\{ \sum_1^{n^e} \frac{A^e}{D_x} \left| \frac{\partial N_i}{\partial x} \right| \right\} \tag{4.31}$$

$$K_i^v = \frac{1}{a_{ii}^v} \left\{ \sum_1^{n^e} \frac{A^e}{D_y} \left| \frac{\partial N_i}{\partial y} \right| \right\} \tag{4.32}$$

with D_x and D_y given by equations (4.15) and (4.16). Note the approximate relationships between the nodal velocities and the pressure gradient terms as given by equations (4.27) and (4.28). These relationships need not be exact for the iterative scheme to yield a converged solution set. The approximation used here is similar to the secant approximation in a Newton's method.

To derive the pressure equation, equations (4.27) and (4.28) are substituted into equation (4.23), with integrations performed over all elements and summed, hence

$$\begin{aligned} \sum_1^{n^e} \Bigg[& \int_{A^e} \left\{ \frac{\partial N_i}{\partial x} \left(N_j \rho_j N_k K_k^u \frac{\partial N_l}{\partial x} \right) + \frac{\partial N_i}{\partial y} \left(N_j \rho_j N_k K_k^v \frac{\partial N_l}{\partial y} \right) \right\} p_l \, dA^e \\ & = \int_{A^e} \left\{ \frac{\partial N_i}{\partial x} \left(N_j \rho_j N_k \hat{u}_k \right) + \frac{\partial N_i}{\partial y} \left(N_j \rho_j N_k \hat{v}_k \right) \right\} dA^e \\ & - \int_{s^e} N_i N_j \rho_j N_k u_k N_l n_{xl} \, ds^e \\ & - \int_{s^e} N_i N_j \rho_j N_k v_k N_l n_{yl} \, ds^e \Bigg] \end{aligned} \tag{4.33}$$

The above equation is similar to equation (2.28) which was derived from the discretisation of the Poisson's equation. The terms on the left hand side represent a diffusion mechanism for pressure, which corresponds closely to the physically elliptic behaviour of pressure.

The coefficient matrix for equation (4.33), arising from the diffusion terms, is formed by the same procedure used for the diffusion terms in equation (4.12), with $N_j\rho_j\ N_k K^u_k$ and $N_j\rho_j\ N_k K^v_k$ replacing the nodal values of viscosity in X and Y directions respectively. This coefficient matrix is a symmetric positive definite matrix, which renders itself to a number of efficient iterative solvers without having to develop special additional algorithms.

In the classical Galerkin approach the diagonal members of the momentum coefficient matrices, a^u_{ii} and a^v_{ii} in equations (4.20) and (4.21), will be small for convection dominated flows. This will produce large values of K^u_i and K^v_i from equations (4.31) and (4.32). Such large K_i values in equation (4.33) will have a deteriorating effect on the pressure solution. This problem is avoided by the use of the streamline upwind technique for the advection terms. Here, the diagonal members of the momentum equations are never allowed to acquire small values, which in turn ensures reasonable values of pressure diffusion coefficients at all times.

The first term on the right hand side of equation (4.33) represents the source term for pressure. The contributions to the source term arise from the hat velocity components given by equations (4.29) and (4.30). The surface integral terms in equation (4.33) provide a convenient method of specifying boundary conditions for pressure. These terms are identically zero except along the inlet and the outlet boundaries. As equation (4.33) was derived from the continuity equation, it offers a direct constraint on satisfying the continuity. The discretised pressure equation is written concisely as

$$a^{p}_{ii} p_i = - \sum_{j \neq i} a^{p}_{ij} p_j + f^{p}_{i} \qquad (4.34)$$

where a^{p}_{ii} denotes the diagonal members of the pressure diffusion coefficient matrix with their corresponding row neighbours a^{p}_{ij}. p_i is the pressure at the global node i. p_j are pressure values at the nodes surrounding node i. f^{p}_{i} is the pressure right hand side force vector containing the source and the surface boundary integral terms.

4.1.4 SIMPLER-like algorithm

The discretised momentum and pressure equations (4.21), (4.22) and (4.34) are solved sequentially in an iterative manner as commonly employed in FVM. The sequence of operations is as follows:

1. With guessed values of u, v and p, the discretised momentum equations (4.21) and (4.22) are set up and solved to obtain better estimates to u and v. The initial guesses may be zero if no other values are available. The coefficient matrix is set up only once for both the momentum equations. The equation systems for u and v are solved separately by an iterative solver.
2. The hat velocity components from equations (4.29) and (4.30) are evaluated.
3. The discretised pressure equation (4.34) is set up and solved. The pressure diffusion matrix is evaluated using the same procedure that was used in computing the momentum diffusion matrix. Now only the diffusion coefficients are different. Using the newly computed velocity field and hat velocity components the right hand side force vector is formed. The equation system is then solved by an iterative solver.
4. The velocity field is updated using the following relationships

$$u_i = \hat{u}_i - \frac{1}{a^u_{ii}} \sum_1^{n^e} \frac{A^e}{D_x} \left| \frac{\partial N}{\partial x}^1 \right| \frac{\partial p}{\partial x} \qquad (4.35)$$

and

$$v_i = \hat{v}_i - \frac{1}{a^v_{ii}} \sum_1^{n^e} \frac{A^e}{D_y} \left| \frac{\partial N}{\partial y}^1 \right| \frac{\partial p}{\partial y} \qquad (4.36)$$

5. Convergence is then checked. Steps 1 to 4 are repeated until the solution has converged.

The above sequence of operations is akin to the SIMPLER algorithm of Patankar (1980). To form the force vectors in the momentum equations, a known pressure field is assumed. A separate Poisson type equation is used to obtain the pressure field. The pressure equation was derived from the continuity equation and is required to satisfy continuity. The velocity and pressure fields are obtained sequentially. If a correct pressure field were used as the initial guess, the above sequence would yield the correct velocity field at once at the first iteration.

4.2 Energy equation

The energy equation for two-dimensional steady state laminar flow in its conservative form is

$$\frac{\partial}{\partial x} \rho u c T + \frac{\partial}{\partial y} \rho v c T = \frac{\partial}{\partial x} \left(k \frac{\partial T}{\partial x} \right) + \frac{\partial}{\partial y} \left(k \frac{\partial T}{\partial y} \right) + \dot{Q} \qquad (4.37)$$

The three-noded triangular element is again used to define the temperature within each element so that

$$T = N_1 T_1 + N_2 T_2 + N_3 T_3 \qquad (4.38)$$

As before, the left hand side terms of equation (4.37) are converted

to

$$\frac{\partial}{\partial s}\,\rho u_s c T \tag{4.39}$$

On the elemental level, the above term is approximated by the streamline upwind technique developed in the last chapter, so that with reference to Figure 3.5, equation (4.39) becomes

$$\frac{\partial}{\partial s}\,\rho u_s c T \simeq \text{constant} = \frac{\rho_i u_{si} c_i T_i - \rho' u_s' c' T'}{\Delta s} \tag{4.40}$$

with c′ and T′ being the upstream values of the specific heat and temperature respectively. Equation (4.40) is then weighted, integrated over each element and summed for all the elements in the domain, hence

$$\sum_{1}^{n^e} \frac{1}{\Delta s}\left(\rho_i u_{si} c_i T_i - \rho' u_s' c' T'\right) A_f \tag{4.41}$$

The diffusion terms on the right hand side are discretised by the Galerkin weighted residual method as was shown for the viscous terms in the momentum equations, hence

$$\sum_{1}^{n^e}\left[-\int_{A^e}\left\{ \frac{\partial N_i}{\partial x} N_j k_j \frac{\partial N_k}{\partial x} + \frac{\partial N_i}{\partial y} N_j k_j \frac{\partial N_k}{\partial y} \right\} T_k \, dA^e + \int_{s^e} N_i N_j k_j \frac{\partial N_k}{\partial n} T_k \, ds^e \right] \tag{4.42}$$

The surface integral term represents the outward heat flux. It is only evaluated, where non-zero and for elements with sides lying on the domain boundaries.

Treatment of the generation term follows the approach described in Chapter 2. When the term is constant or linearly varying with T, i.e.

$$\dot{Q}(T) = Q_c + Q_p T \tag{4.43}$$

the Galerkin method is adopted explicitly, hence

$$\sum_{1}^{n^e} \left[\int_{A^e} N_i \, Q_c \, dA^e + \int_{A^e} N_i \, Q_p \, N_j T_j \, dA^e \right] \tag{4.44}$$

When the generation term is a non-linear function of temperature, the implicit formulation is employed, hence from equation (2.37)

$$\sum_{1}^{n^e} \int_{A^e} N_i \, \dot{Q} \, dA^e = \sum_{1}^{n^e} \left[\int_{A^e} N_i \left\{ \dot{Q}^* - N_j T_j^* \left(\frac{d\dot{Q}}{dT} \right)^* \right\} dA^e + \int_{A^e} N_i \, N_T T_j \left(\frac{d\dot{Q}}{dT} \right)^* dA^e \right] \tag{4.45}$$

with N_T given by equation (4.19) and * denoting quantities evaluated at the previous iteration.

The system of equations is expressed in terms of the unknown temperature field, which is concisely written as

$$a_{ii}^T T_i = - \sum_{j \neq i} a_{ij}^T T_j + f_i^T \tag{4.46}$$

where a^T are the members of the temperature coefficient matrix containing the advection and the diffusion contributions. The diagonal members, a_{ii}^T, also contain contributions from the implicit part of equation (4.45). The coefficient matrix is unconditionally diagonally dominant, hence allowing for the iterative solution of equation (4.46). The right hand side vector, f_i^T, contains contributions from the surface boundary integrals in equation (4.42) and the explicit parts of the generation integral terms in equations (4.44) and (4.45).

4.3 Imposition of boundary conditions

To complete the definition of velocity, pressure and temperature fields, boundary conditions for these fields are specified. The elliptic nature of the general transport equation requires fixed conditions to be specified along all of the internal and the external boundaries of the domain of interest. Boundary conditions are of either essential (Dirichlet) or natural (Neumann) type. In the former the actual values of the variable are specified. The latter involves the specification of the gradient value of the variable along the boundaries. For the current research both the essential and the natural boundary conditions were employed. Here it is assumed that the complete boundary of a domain consists of five parts: inlet, outlet, wall, convective and plane of symmetry boundaries. The detailed treatment of each of these boundaries is now presented.

4.3.1 Inlet boundaries

The inlet boundary conditions on the momentum and the continuity equations are necessarily interlinked. Such conditions are prescribed by either specifying the inlet mass flow or the inlet pressure. The mass flow is prescribed by fixing the velocity components, u and v, and providing the side lengths of boundary elements. The momentum equations (4.20) and (4.21) therefore reduce to

$$u_i = u_{inlet} \quad , \quad v_i = v_{inlet} \tag{4.47}$$

where i refers to those nodes lying on the boundary. The hat velocity components given by equations (4.29) and (4.30) are adjusted so that

$$\hat{u}_i = u_{inlet} \quad , \quad \hat{v}_i = v_{inlet} \tag{4.48}$$

The pressure diffusion terms given by equations (4.31) and (4.32) are also adjusted to account for the prescribed inlet velocities, hence

$$K_i^u = K_i^v = 0 \tag{4.49}$$

With the above velocities, the inlet boundary condition for pressure are obtained implicitly by evaluating the surface integrals in equation (4.33). From equations (4.48) and (4.49) it can be seen that the hat velocity components are decoupled from the pressure distribution along the inlet boundaries when an inlet mass flow is prescribed.

The prescription of the pressure at the inlet reduces the pressure equation (4.34) to

$$p_i = p_{inlet} \tag{4.50}$$

where as before i refers to the nodes lying on the inlet boundary. The specified inlet pressure is accompanied by zero velocity gradients, i.e. the surface boundary integral in equation (4.12). This type of boundary condition would be relevant to Poiseuille type flow situations. For a given inlet mass flow or pressure, the energy equation (4.46) reduces to

$$T_i = T_{inlet} \tag{4.51}$$

4.3.2 Outlet boundaries

Natural boundary conditions are applied to the momentum and the energy equations along the outlet boundaries. This results in the surface integral terms in equations (4.12), and (4.42) to be zero. In cases where the flow is forced to leave at a specified flow angle, the natural conditions are applied, for example, to the Y-momentum

equation with the essential conditions imposed on the X-momentum equation. Hence,

$$u_i = \hat{u}_i = \theta\, v_i \quad , \quad K_i^u = 0 \tag{4.52}$$

where θ is the specified outlet flow angle.

The pressure boundary conditions along the outlet can be applied in two ways. Here either an outlet pressure or an outlet mass flow is prescribed. The former reduces the pressure equation (4.34) to

$$p_i = p_{outlet} \tag{4.53}$$

where i refers to those nodes lying along the outlet. With a prescribed outlet mass flow, the surface integral terms in equation (4.33) are evaluated. The hat velocity components and pressure diffusion coefficients are also adjusted so that

$$\hat{u}_i = u_{outlet} \quad , \quad \hat{v}_i = v_{outlet} \tag{4.54}$$

and

$$K_i^u = K_i^v = 0 \tag{4.55}$$

4.3.3 Wall boundaries

Along the stationary walls, the two velocity components are set to zero. The hat velocity components together with the pressure diffusion coefficients are adjusted accordingly. Hence,

$$u_i = \hat{u}_i = 0 \quad , \quad v_i = \hat{v}_i = 0 \tag{4.56}$$

and

$$K_i^u = K_i^v = 0 \tag{4.57}$$

For moving wall boundaries, the velocity components are set such that

$$u_i = \hat{u}_i = u_{slip} \quad , \quad v_i = \hat{v}_i = v_{slip} \tag{4.58}$$

with the pressure coefficient given by equation (4.57).

The pressure boundary conditions along the walls become trivial. With both the slip and the no-slip boundaries, the surface integral term of equation (4.34) are zero. The pressure is therefore only constrained by equations (4.56) or (4.58). The wall boundary conditions for the energy equation can either be of the essential or the natural types. These are imposed by prescribing the temperature or its conductive flux along the walls. There are also convective fluxes which are dealt with in the next section. For a known wall temperature the energy equation reduces to one similar to

$$T_i = T_{wall} \tag{4.59}$$

For a given conductive heat flux, usually zero for adiabatic walls, the surface integral term in equation (4.42) is reduced to

$$- \int_{s^e} N_i \, \dot{q}_{wall} \, ds^e \tag{4.60}$$

4.3.4 Convective boundaries

These boundaries are specific to the energy equation and arise from the solid/fluid interfaces. In such cases, the surface integral term in equation (4.42) can be written as

$$\int_{s^e} N_i \, h \, (T_f - T_{wall}) \, ds^e \tag{4.61}$$

where h and T_f are the known convection coefficient and the fluid temperature respectively, and T_{wall} is the unknown temperature along

the interface. Equation (4.61) is split into two parts, with the part containing the unknown temperature, T_{wall}, taken over to the left hand side of equation (4.46), hence

$$\left(a_{ii}^{T} + \int_{s^e} N_i \, h \; ds^e \right) T_i = - \sum_{j \neq i} a_{ij}^{T} T_j + \int_{s^e} N_i \, h T_f \, ds^e \qquad (4.62)$$

4.3.5 Planes of symmetry

Along a plane of symmetry the velocity component normal to the plane, say v, is specified as zero, hence

$$v_i = \hat{v}_i = K_i^v = 0 \qquad (4.63)$$

The surface integral for the tangential momentum equation, i.e. X-momentum, is then set to zero. The surface integral for the pressure equation term will also be zero. The natural boundary condition of zero temperature gradient is imposed along the planes of symmetry giving zero surface integrals in the energy equation.

CHAPTER 5

ITERATIVE SOLUTION PROCEDURE AND LAMINAR FLOW EXAMPLES

The overall computational sequence for the laminar flow calculations is first presented. A novel fast TDMA solver, developed for this work, is then described in detail. The relaxation strategy to avoid solution divergence is presented in section 5.3. In section 5.4 the convergence criteria employed in determining the final solution set is given. Section 5.5 presents the results of a number of laminar flow cases, including the case of the laminar jet impingement with heat transfer.

5.1 Program flowchart

Figure 5.1 shows the overall computational sequence of the finite element program used for the laminar flow calculations. The program starts by reading in a prepared input data file. This file contains information about mesh discretisation, variables to be solved, boundary conditions and control data that govern the course of the overall computation. Some of the more important parameters in the control data set are: number of global iteration loops here referred to as cycles, iterative matrix solution parameters, cycle relaxations, convergence criteria, result print-out rate and evaluation of derived quantities.

An isoparametric automatic mesh generation (Segerlind (1976)), is used to subdivide the domain of interest into simplex elements. Since the elements are of triangular shape, no limitations are imposed on

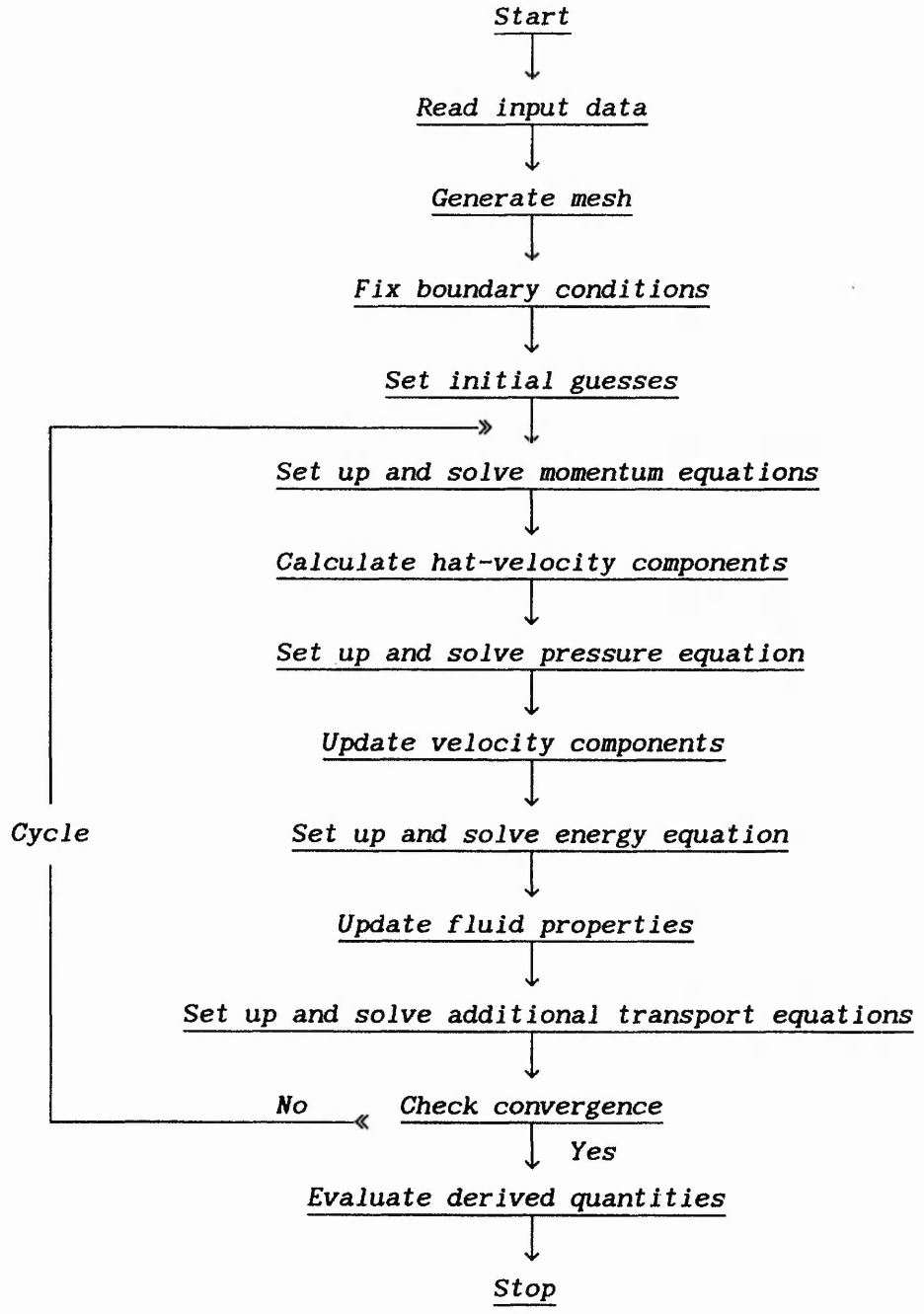

Figure 5.1 Program flowchart for laminar flow calculations.

the shape of the domain to be considered. Therefore the discretisation of complex flow domains can be performed accurately without the need for redundant storage as employed in the FVM, e.g. Patankar (1980). As described later in the next section, the novel matrix solver works independently of the global node and element numbering. This offers an additional flexibility and allows the mesh generation sequence to be completed efficiently with minimal effort at the input data preparation stage.

Boundary conditions are read from the input data file and are stored at the beginning of the program for all variables. Both essential and natural boundary conditions may be specified. This stage is performed only once outside the main iteration loop. This is in contrast to the common practice where fixing of the boundary conditions appears inside the main loop after the equation for each variable is set up.

The initial guesses or the start-up values are also set prior to the main iteration loop. These can be the available analytical or experimental data. For example a developing duct flow can benefit from the analytical solution to the fully developed case. Alternatively, the initial guesses can be a set of results obtained when a computational sequence is terminated before the imposed convergence criteria are fully satisfied. Initial guesses may also be set arbitrarily based on some past knowledge about similar flow situations. The guessed values only help accelerate the convergence to the final solution. The fully converged solution set is independent of the initial guessed values. The iterative solution sequence can start with all variables initially set to zero.

The course of the main iterative computational sequence, the cycle, is governed by the control data supplied at the beginning of the program. Figure 5.1 illustrates a general route thorough the various parts of this cycle. This route may be altered dramatically depending on the flow situation under consideration. The cycle commences by setting up the momentum equations. This consists of evaluating the element coefficient matrices and their assembly into the global coefficient matrix (equations (4.20) and (4.21)). As mentioned in Chapter 4, a^u_{ij} and a^v_{ij} are identical except at points where boundary conditions are specified. Hence, the global coefficient matrix is set up only once for both the X and the Y momentum equations. The elements force vectors, f^u_i and f^v_i, containing the pressure gradient terms, are also evaluated and assembled into the global right hand side vectors. The solution to the simultaneous linear algebraic equations is obtained by a variant of the TDMA which is described in detail in the next section.

The newly computed velocity field is used to evaluate the hat-velocity components (equations (4.29) and (4.30)). The pressure equation (4.34) is set up by first evaluating the pressure diffusion coefficients (equations (4.31) and (4.32)). The right hand side force vector, f^p_i, is evaluated using the velocity field together with the hat-velocity components. These are used to form the boundary integrals and the source terms respectively. The pressure equation, once fully assembled, is also solved using the same iterative solution procedure as for the momentum equations. The new pressure field is used to update the velocity field from equations (4.35) and (4.36). The updated velocity field is used to set up the advective part of the

energy equation (4.37). The discretised energy equation (4.46) is fully formed when the diffusion and the source term contributions are also evaluated. This equation is then solved by the same solution procedure used for the other variables. With all the primitive variables, u, v, p and T computed, the fluid properties e.g. density and viscosity are then updated using auxiliary equations relating them to the primitive variables.

Other quantities which are also governed by the general form of the transport equation (3.1) may also be obtained at the end stages of each cycle. These additional quantities will have associated with them the appropriate diffusion coefficients. Also the source term for each variable must be individually specified. The iterative solution sequence just described employs only four basic routines to set up the transport equations for all the variables including the pressure. These are the advection, diffusion, source and boundary integral routines. This methodology is commonly used in FVM, e.g. Patankar (1980). It is the segregation of the continuity and the momentum equations that has made the present finite element program to be a strong contender with the FVM codes as is seen later in section 5.5. It can also be seen that the extension of the program to include turbulent flow situations follows naturally.

At the end of each cycle, the convergence of the solution set is examined against pre-specified convergence criteria. Cycles are performed until convergence is obtained. The derived quantities such as streamline and heat-flux are then evaluated. A typical cycle as described above is the general route employed for fully elliptic flow cases. This route can be shortened for cases where the flow is

considered to be parabolic, which would result in appreciable savings in both computer storage and run-time. Under the parabolic flow condition only one slab or layer of the flow domain in the predominant flow direction is considered at a time. The pressure gradient term is assumed to be constant in that direction. The pressure gradient in the cross flow direction vanishes and the cross flow velocity is evaluated from the continuity equation. The energy equation and the other transport equations are also solved one slab at a time. Therefore with reference to Figure 5.1, for each slab, cycles are repeated until the convergence criteria are fully met before moving on to the next slab. Also in each cycle there would be no need to evaluate the hat-velocity components or to solve the pressure equation.

5.2 Regional Alternating-Direction Implicit Solver (RADIS)

It was shown in Chapters 2, 3 and 4 that the simultaneous sets of linear algebraic equations arising from the current Finite Element formulation are always diagonally dominant. The diagonal dominance is ensured regardless of element sizes or orientations. The equation sets can therefore be solved iteratively rather than directly provided that some sort of a nodal structure exists. This nodal structure occurs naturally in the FVM. As shown in Figure 5.2, in a typical FVM grid the centre node P(i,j) is surrounded by its neighbours S, E, N and W whose locational subscripts are obtained by either incrementing or decrementing i and/or j by one. This simple structure allows a variety of iterative solution procedures to be employed. A few examples of such procedures are Gauss-Seidel, line-by-line Tri-Diagonal Matrix Algorithm (TDMA) (Patankar (1980)), Alternating- Direction Implicit (ADI) of Peaceman and Rachford (1955) and Strongly Implicit Procedure (SIP) of Stone (1968).

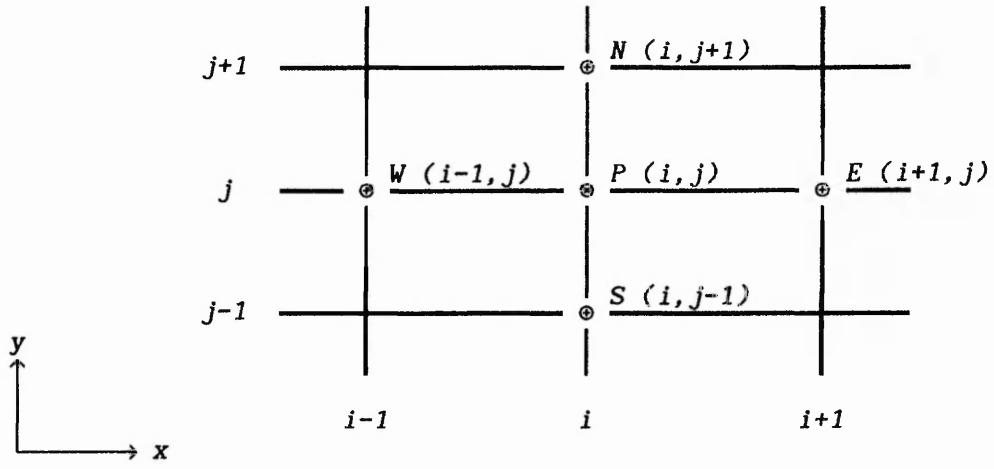

Figure 5.2 Typical orthogonal grid used in FVM.

In general the FEM must work with unstructured grids. The freedom in generating and manipulating such grids is one of the major attractions of the FEM. This is especially true in the field of stress analysis where very often complicated shapes in two- and three-dimensions need to be considered. However, the complete randomness of the Finite Element grid prohibits the use of iterative solvers. As discussed in the first chapter, the conventional FEM resorts to direct solution techniques. These techniques place heavy demands on computer resources.

One of the primary objectives of this work was to develop a Finite Element algorithm that would be competitive with those employing the FVM. To this end a novel line-by-line TDMA, called RADIS, has been developed. The significance of the name will become clear later in this section. This iterative solution algorithm is a variant of the ADI method of Peaceman and Rachford (1955). RADIS is

specifically designed for the "apparently" unstructured grids generated by the FEM. Here, it is shown how a simple grid manipulation during the mesh generation routine has lead to the development of RADIS. As the mesh generation routine forms an integral part of RADIS, a brief description of this routine is given below. However the mesh generation routine in itself carries no claim to novelty.

Figure 5.3(a) shows a single triangular region which is to be subdivided into three-noded triangular elements. The isoparametric subdivision begins by describing the region as an eight-noded bi-quadratic quadrilateral as shown in Figures 5.3(b) and (c). The quadrilateral is divided into the required number of rows and columns in the ξ-η space as shown in Figure 5.3(d). The row and the column strips are arbitrarily graded. The intersection of the row and the column lines results in bilinear quadrilateral elements of varying sizes. Each of these elements is further divided into two triangular elements as shown in Figure 5.3(e). This mesh is then transformed back to the x-y space as shown in Figure 5.3(f), completing the mesh generation routine for the single triangular region.

A complex domain may be subdivided into triangular elements by first dividing the domain into eight-noded quadrilateral regions and then performing the above operation on each of these regions. Figures 5.4(a)-(d) show the mesh generation sequence used for a heavy duty air-cooled first-stage gas turbine blade. This shape was chosen deliberately to demonstrate the RADIS's applicability to complex domains as well as to more regular domains. The blade, shown in Figure 5.4(a), is first divided into isoparametric regions as shown in Figure

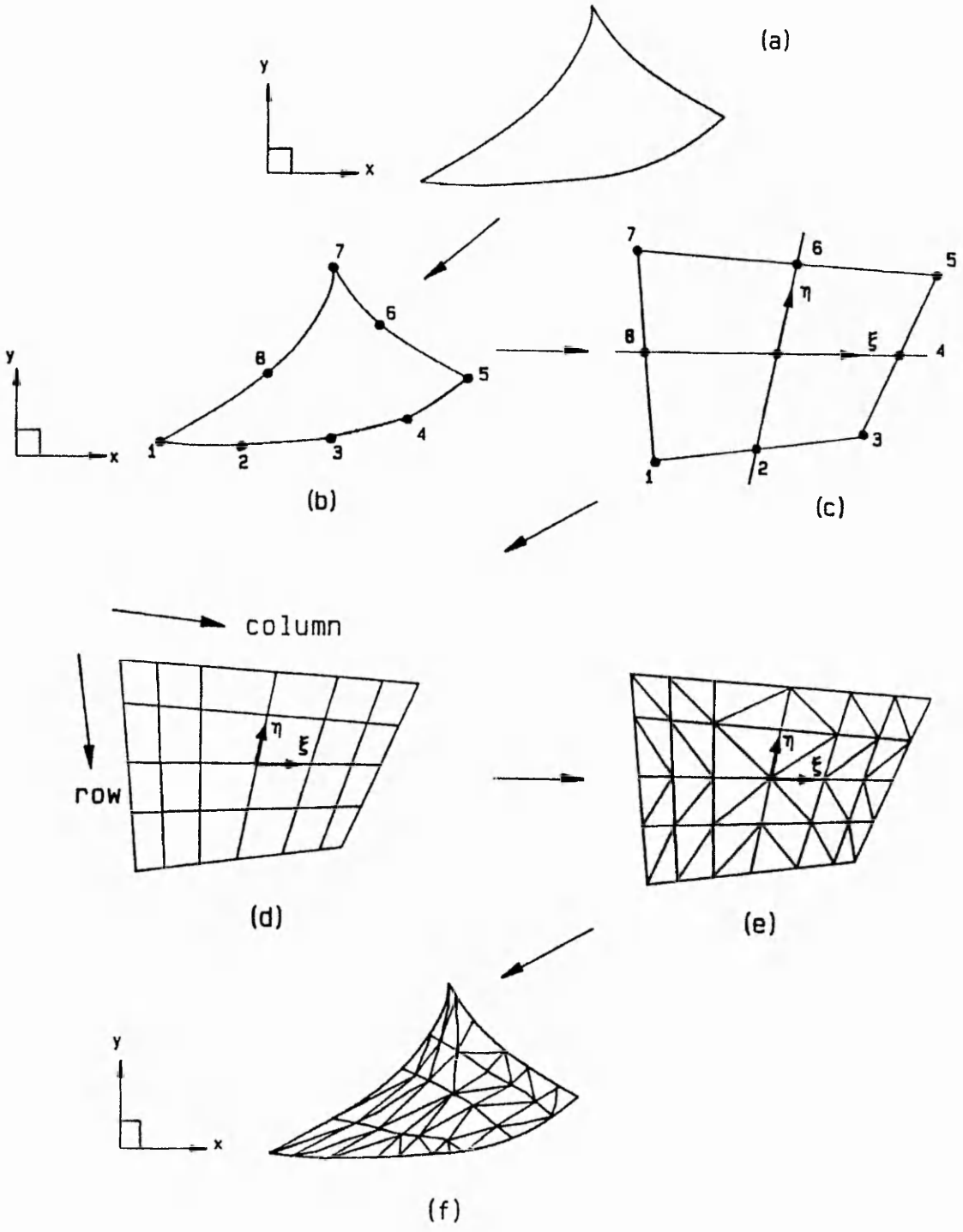

Figure 5.3 *Various stages in the mesh generation routine, (a) triangular region, (b) and (c) region transformation into a quadrilateral, (d) quadrilateral division into rows and columns, (e) further division into triangles and (f) transformation back to the x-y space.*

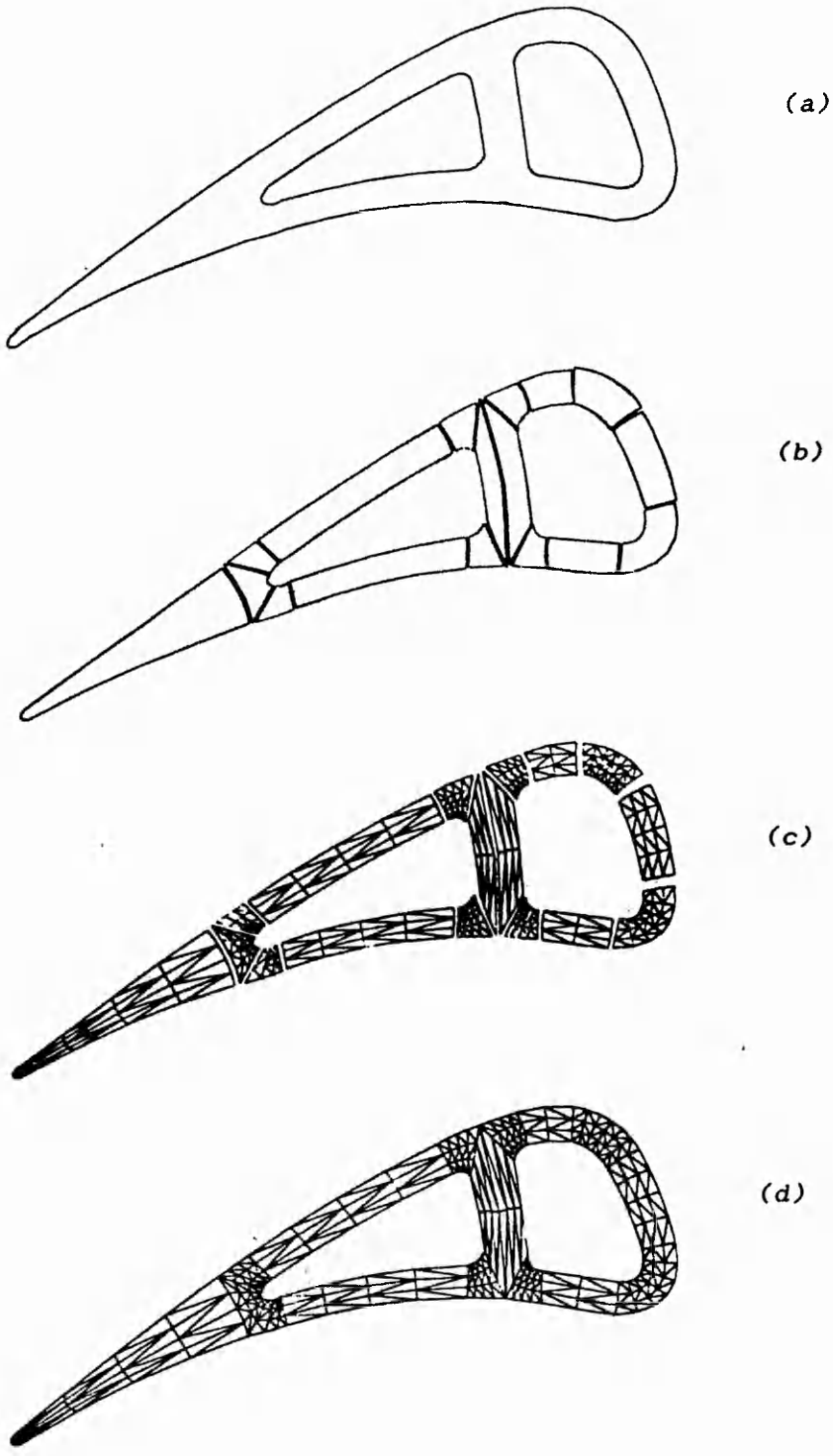

Figure 5.4 *Mesh generation sequence for a complex domain,*
(a) heavy duty air-cooled first-stage turbine blade,
(b) domain division into quadrilateral regions,
(c) regions division into three-noded triangles, and
(d) the complete finite element mesh.

5.4(b). Each region is then subdivided into triangular elements as illustrated in Figure 5.4(c). The regions are then connected together along their external perimeters, resulting in the complete mesh shown in Figure 5.4(d).

The basic methodology behind RADIS is surprisingly simple. That is to perform the ADI procedure for each of the quadrilateral regions, shown in Figure 5.4(c), one at a time. An ADI sweep is completed once all such regions in the domain have been visited. ADI sweeps are repeated until some pre-specified convergence criterion is met. This criterion need not be strict since, at the intermediate cycles (see Figure (5.1)), only a tentative set of coefficients are available. This procedure is named the Regional Alternating-Direction Implicit Solver or RADIS following the above sequence of operations. The ADI procedure itself consists of a number of line-by-line TDMA operations in alternating directions. In a single line-by-line TDMA operation all the nodes falling on a given line are considered collectively. In the FVM these lines are the orthogonal lines used to generate the mesh as is depicted in Figure 5.2. In FEM such lines extending across the domain do not generally exist. RADIS, however, determines its solution direction from the row and the column lines of the quadrilateral regions by considering only one such region at a time.

Figure 5.5 illustrates the selected solution direction and the active line on which a TDMA operation is to be performed for a given region. The figure shows the selected solution direction to advance one column at a time starting with the first column, hence a forward column-sweep. Three other solution directions are also possible: the backward column-sweep and the forward and the backward row-sweeps as

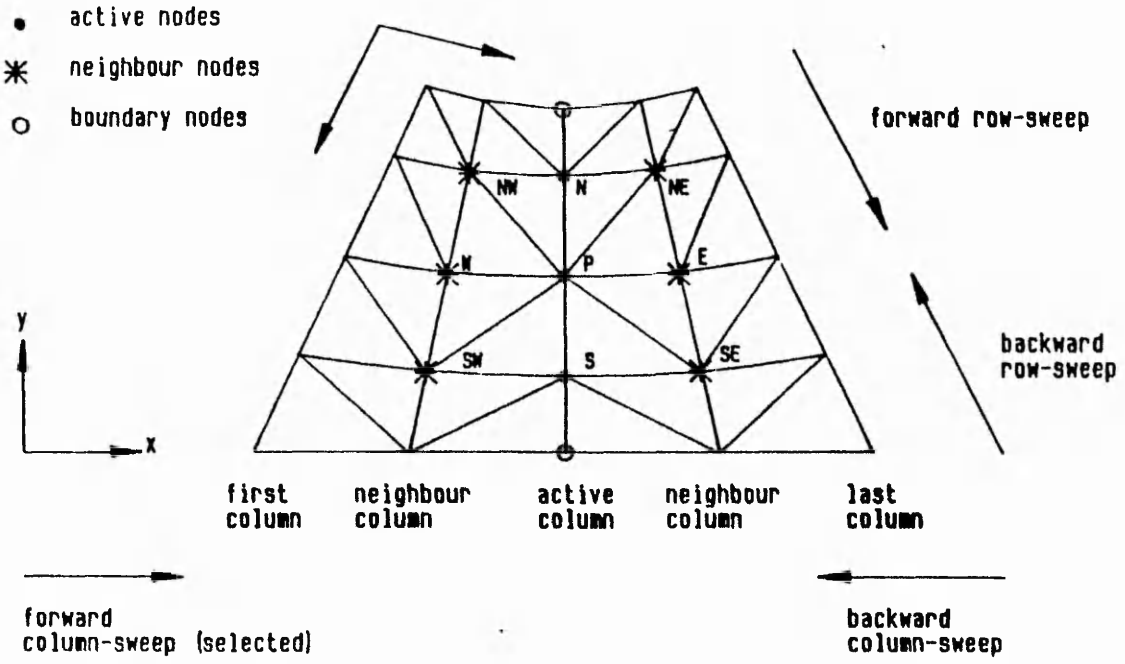

Figure 5.5 The ADI procedure for a single region with the four possible sweep directions.

shown in the figure. For an active point P on the active column there may be a maximum of eight neighbours. The South and the North neighbours, S and N, are themselves active and are handled implicitly in the line-by-line TDMA. The other six neighbours, SE, E, NE, NW, W and SW, are treated explicitly. The two end boundary nodes on the active column are also treated implicitly, unless they fall on the external boundaries of the domain in which case the prescribed boundary conditions are imposed.

RADIS offers several advantages over the direct solution methods.

Only the non-zero elements of the global coefficient matrix need be stored. The storage requirement is hence increased linearly with the total number of nodes in the domain and is unaffected by the element or the node numbering convention used. RADIS is therefore completely band-free. The two additional storage requirements of RADIS are a global node-neighbours matrix and a regional-node matrix. The former determines the neighbours of each node within the domain and the latter specifies the nodes that lie on the rows and columns of each region. Perhaps RADIS's most important feature is its inherent ability to treat each region of the domain quite differently to any other region in the same domain. For example considering a partially elliptic flow case, RADIS can recognize those parts of the domain where the flow is elliptic hence requiring more attention compared to the other parts for which a predominant flow direction exists. RADIS will then perform several row- and column-sweeps in the elliptic regions and will perform only a few row- or column-sweeps in the parabolic regions. In this manner considerable savings in computer time are achieved. The extension of RADIS to three-dimensions follows naturally from the above descriptions and no other novelty need be introduced. With minor modifications, RADIS can be easily adapted to cater for other element types, e.g. six-noded triangles and bilinear or biquadratic quadrilaterals. Although it must be noted that for convergence purposes, the resulting global coefficient matrix should always be (or be nearly) diagonally dominant. Finally, RADIS may also be used in conjunction with the FVM. This is possible if the mesh generation routine described earlier is used to generate orthogonal mesh lines, be it in the x-y or the body-fitted (i.e. curvilinear) coordinate systems. Then all the above mentioned advantages would also apply to the FVM.

5.3 Relaxation

As described in section 5.1, the complete set of results is obtained by an iterative solution procedure consisting of many cycles (see Figure 5.1). The set of partial differential equations are generally coupled and are non-linear (see equations (4.2), (4.3) and (4.37)). Non-linearity arises from the fluid properties being themselves functions of the primitive variables. The source term in equation (4.37) can also be a dependent function of temperature resulting in additional non-linearity. Within each cycle, these equations are linearised and are solved sequentially as has been shown in Chapters 2 and 4. Therefore under-relaxation is employed to minimise the risk of divergence. This results in the slowing down of the rate of change in the computed values at the intermediate cycles. Here, an implicit under-relaxation is employed.

The general form of the linear algebraic equation set

$$a^{\phi}_{ii}\phi_i = -\sum_{j\neq i} a^{\phi}_{ij}\phi_j + f^{\phi}_i \qquad (5.1)$$

is slightly modified to cater for under-relaxation. Equation (5.1) can be written as

$$\phi_i = \frac{1}{a^{\phi}_{ii}}\left\{ -\sum_{j\neq i} a^{\phi}_{ij}\phi_j + f^{\phi}_i \right\} \qquad (5.2)$$

The value of ϕ_i from the previous cycle, ϕ^*_i, is added to and subtracted from the right hand side of equation (5.2), hence

$$\phi_i = \phi^*_i + \frac{1}{a^{\phi}_{ii}}\left\{ -\sum_{j\neq i} a^{\phi}_{ij}\phi_j + f^{\phi}_i \right\} - \phi^*_i \qquad (5.3)$$

The relaxation factor, α^{ϕ} is introduced to the above equation, hence

$$\phi_i = \phi_i^* + \alpha^{\phi} \left[\frac{1}{a_{ii}^{\phi}} \left\{ - \sum_{j \neq i} a_{ij}^{\phi} \phi_j + f_i^{\phi} \right\} - \phi_i^* \right] \tag{5.4}$$

Equation (5.4) is re-written in the following form

$$\frac{a_{ii}^{\phi}}{\alpha^{\phi}} \phi_i = - \sum_{j \neq i} a_{ij}^{\phi} \phi_j + \left\{ f_i^{\phi} + (1 - \alpha^{\phi}) \frac{a_{ii}^{\phi}}{\alpha^{\phi}} \phi_i^* \right\} \tag{5.5}$$

Comparing equation (5.1) and (5.5), the diagonal member of the coefficient matrix, a_{ii}^{ϕ}, and the right hand side force vector, f_i^{ϕ}, are altered in equation (5.1) to account for under-relaxation. Therefore, a_{ii}^{ϕ} is replaced by

$$\frac{a_{ii}^{\phi}}{\alpha^{\phi}} \tag{5.6}$$

and f_i^{ϕ} is replaced by

$$f_i^{\phi} + (1 - \alpha^{\phi}) \frac{a_{ii}^{\phi}}{\alpha^{\phi}} \phi_i^* \tag{5.7}$$

The relaxation factor, α^{ϕ}, takes values between 0 and 1. The appropriate value of α^{ϕ} for each variable depends strongly on the flow situation under consideration. For a correct pressure field, the true velocity field is obtained immediately. Therefore the pressure under-relaxation factor, α^{P}, is the most important parameter. With the correct value for α^{P}, the success of the current formulation is ensured. α^{P} also strongly influences the overall convergence rate. For the cases considered in this research a value of 0.50 was found to give satisfactory convergence rates. Relaxation factors for u, v and T can be set to 0.50 for safe practice. However larger values were also used which resulted in much faster convergence rates. In general the

largest relaxation factor possible should be used to force the fastest convergence rate. Of course too large a value will result in the solution diverging. Also for elliptic or partially elliptic problems a more selective approach must be adopted in order to maximise the convergence rate. Cycles can initially start with low values of α^{ϕ}. Then at later stages, larger values may be used to accelerate the convergence rate.

5.4 Convergence criteria

Three convergence criteria are used to terminate the iterative solution procedure or cycles described in section 5.2. These are the relative change, the total residual check, and the global balance check. The absolute relative change in the variable ϕ at point i is determined from

$$\% \text{ change} = \left| \frac{\phi_1 - \phi_1^*}{\phi_1} \right| \times 100\% \qquad (5.8)$$

where * refers to the previous cycle. The relative change criterion is satisfied when the maximum absolute changes in all variables within the domain fall below a specified limit, e.g.

$$\text{maximum } \% \text{ change} \leq 0.1\% \text{ say} \qquad (5.9)$$

Each primitive variable has its own specified limit. It is usually the pressure for which the strictest control is exercised. The above criterion on its own is not adequate to determine a converged solution set. For cases where heavy under-relaxation is employed to suppress divergence, this criterion may be automatically satisfied. This can give the false impression of convergence.

The second convergence criterion is that of the total residual check. Considering the discretised equation for ϕ_i

$$a_{ii}^{\phi}\phi_i = -\sum_{j\neq i} a_{ij}^{\phi}\phi_j + f_i^{\phi} \tag{5.10}$$

the absolute residual at point i is then

$$R_i^{\phi} = \left| -\sum_{j\neq i} a_{ij}^{\phi}\phi_j + f_i^{\phi} - a_{ii}^{\phi}\phi_i \right| \tag{5.11}$$

R_i^{ϕ} is non-zero if equation (5.10) is not fully satisfied. The total residual is obtained by the addition of all point residuals. Hence

$$R_T^{\phi} = \sum_{i=1}^{n} R_i^{\phi} \tag{5.12}$$

where n denotes the total number of nodes in the domain. The total percentage residual check can then be formed and examined against a prescribed limit, hence

$$\%\ \text{residual check} = \frac{R_T^{\phi}}{V_{ref}^{\phi}} \times 100\% \leq 0.5\% \quad \text{say} \tag{5.13}$$

where V_{ref}^{ϕ} is a physical reference value that must be deducted from the geometry and the conditions of the flow under consideration. For example in the case of pure conduction, ϕ = T and V_{ref}^{T} would be the heat transfer rate, hence with reference to Figure 5.6

$$V_{ref}^{T} = k_{avrg} \left(T_{max} - T_{min} \right) \frac{L}{H} \tag{5.14}$$

Similar expressions for the momentum and pressure equations may be formed, where V_{ref}^{ϕ} would refer to the rates of momentum and mass entering the domain respectively. Equation (5.13) is a good indication of how well the discretised equations are satisfied at each cycle.

The last criterion is the global balance check. This is a very useful convergence indicator especially for the parabolic flow situations. It simply requires that the overall balance of a conserved

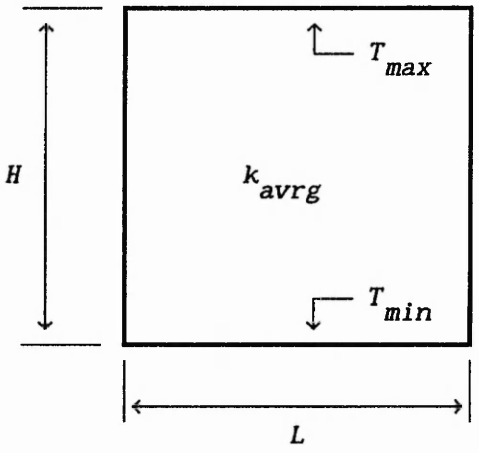

k_{avrg} = *average conductivity*

T_{min} = *minimum domain temperature*

T_{max} = *maximum domain temperature*

L = *domain length*

H = *domain height across which* ($T_{max} - T_{min}$) *acts*

Figure 5.6 Pure conduction in a rectangular plate.

quantity in the domain be satisfied. For a fully converged solution set this means that the mass, momentum and heat transfer rates in and out of the domain must cancel each other out. For example, if the final solution indicates a sizeable imbalance between the total mass entering and the total mass leaving the domain, that solution is not yet converged. At the end of each cycle, the percentage mass flow rate balance is obtained by

$$\% \text{ mass flowrate balance} = \left| \frac{\text{flow}_{in} - \text{flow}_{out}}{\text{flow}_{in}} \right| \times 100\% \qquad (5.15)$$

It is then required that

$$\% \text{ mass flowrate balance} \leq 0.01\% \text{ say} \qquad (5.16)$$

Other balance checks are performed in a similar fashion. In parabolic flow situations the global balance check is the only one carried out. It should be noted that this criterion is only meaningful if the discretisation technique itself conserves quantities such as mass, momentum and energy. As discussed in Chapters 3 and 4, the present Finite Element discretisation is of the conservative form.

5.5 Laminar flow examples

The examples considered here are arranged in the order of increasing complexity. The fully developed and the developing duct flows examine the accuracy of the program against the analytical result and some past predictions respectively. The backward facing step is used to demonstrate the ability of the program to handle a large number of elements efficiently. It also provides the means to comparing present predictions with the existing experimental data. The natural convection in a square cavity is chosen to test the complete set of coupled equations. The results for this case are compared with past predictions. The laminar jet impingement with heat transfer examines the accuracy and the overall efficiency of the solution technique in a conjugate fluid flow/heat transfer situation.

5.5.1 Flow in plane duct

The fully developed or Poiseuille flow in a plane duct is governed by the parabolic velocity profile

$$u = - \frac{1}{2 \mu} \frac{\partial p}{\partial x} y (H - y) \qquad (5.17)$$

where with reference to Figure 5.7, x and y are the streamwise and the cross-stream directions respectively. The plate separation is H. The flow is symmetric about the centre-line as shown in the figure. For

comparison purposes both the full problem and the half problem were considered. The former consists of the plate to plate distance, whereas in the latter only one plate to the axis of symmetry is

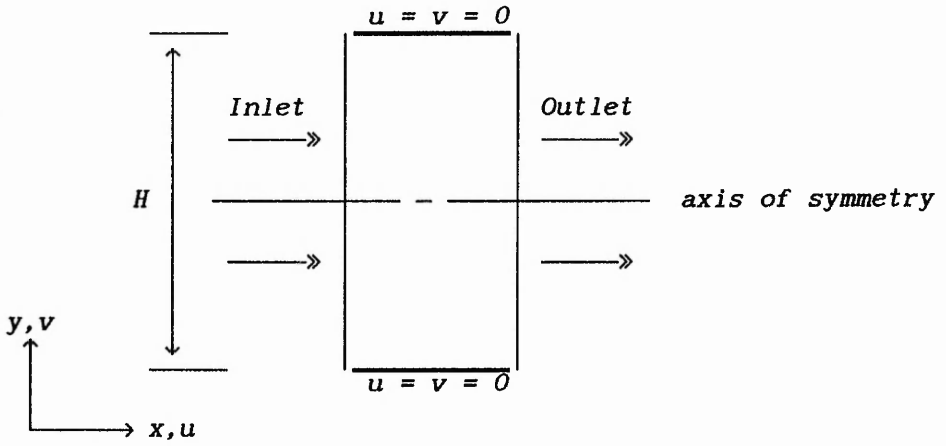

Figure 5.7 Fully developed laminar flow in plane duct.

considered and the velocity gradient along the axis is zero. Two types of boundary conditions were used. First, the velocity field was examined for a specified pressure gradient. The results corresponded exactly to the analytical solution given by equation (5.17) for both the full and the half problem. Secondly, the inlet velocity was prescribed according to equation (5.17) and the outlet pressure was fixed at an arbitrary value. The inlet pressure and the outlet velocity profiles were then examined. Both the pressure and the velocity fields were predicted correctly for the full and the half problems. For this case eight triangular elements of equal size were used. The execution time was below 10 milliseconds.

The developing laminar duct flow was then considered. This problem has been reported in previous works, see for example Wang and

Longwell (1964), Gosman et al (1969), Brandt and Gillis (1966) and Rice and Schnipke (1986). Consistent with the work of Gosman et al (1969), the mesh consisted of 15 equally spaced rows and 21 columns whose x-coordinate positions were determined according to

$$x = 100 \tan (1.55\ w) / \tan (1.55) \qquad (5.18)$$

where w was increased from 0 to 1 in 20 equal increments. This resulted in 560 elements as is shown in Figure 5.8.

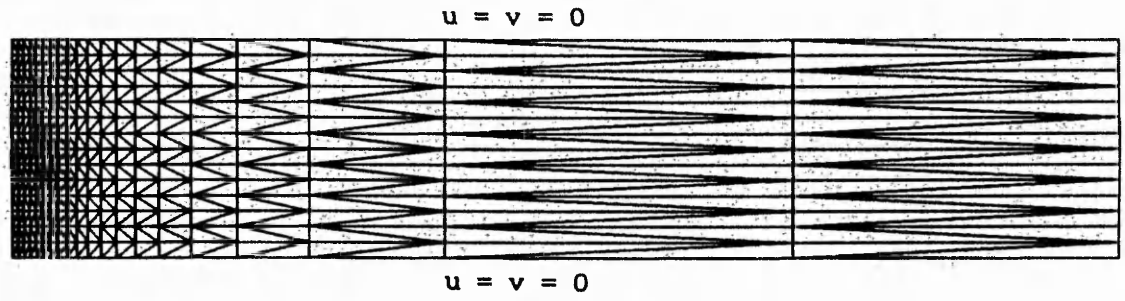

Figure 5.8 Computational mesh for developing laminar duct flow (not to scale).

The average velocity at the inlet was 1. No-slip boundary conditions were imposed along the duct walls. The Reynolds number, based on the plate separation and average inlet velocity was 150. A parabolic solution sequence was used. Hence there were no need for downstream boundary conditions. The centre-line velocity profile is shown in Figure 5.9. It is compared with those of Gosman et al (1969) and Rice

and Schnipke (1986), who used elliptic solution methods. The maximum deviation is about 9%, which is mainly due to the present parabolic flow considerations. Also, Gosman et al (1969) employed the FVM, which results in a slightly different velocity profile at the inlet. The entrance length, L_e, for which the centre-line velocity is 99% of the maximum velocity is given analytically by (White (1974)):

$$\frac{L_e}{H} = 0.04\ Re + 0.5 \qquad (5.19)$$

For Reynolds number of 150,

$$\frac{L_e}{H} = 6.5 \qquad (5.20)$$

The value obtained from the current calculations is 9.11 which is about 29% longer than the above value.

Figure 5.10 shows the calculated pressure drop for this case. As expected a rapid pressure drop is predicted at the inlet. The pressure is quickly adjusted and a constant pressure gradient is observed for most of the flow. The non-dimensionalised excess pressure drop is given analytically by (White (1974)):

$$K_e = \frac{\Delta p - \Delta p_{developed}}{\frac{1}{2}\rho U^2_{avrg}} \qquad (5.21)$$

which for this case should be

$$K_e = 0.738 \qquad (5.22)$$

The value calculated here is 0.720 which is less that 2.5% from the above value. The parabolic solution analysis took 2.47 seconds on a Digital VAX-8550 machine to complete.

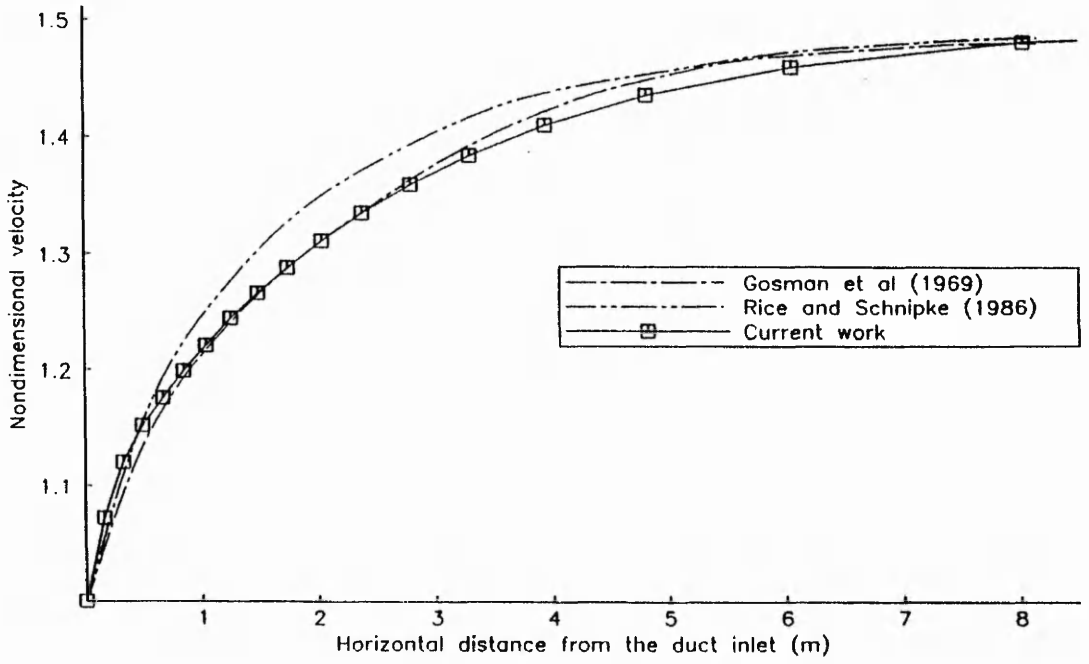

Figure 5.9 Comparison of centre-line velocities for developing laminar duct flow.

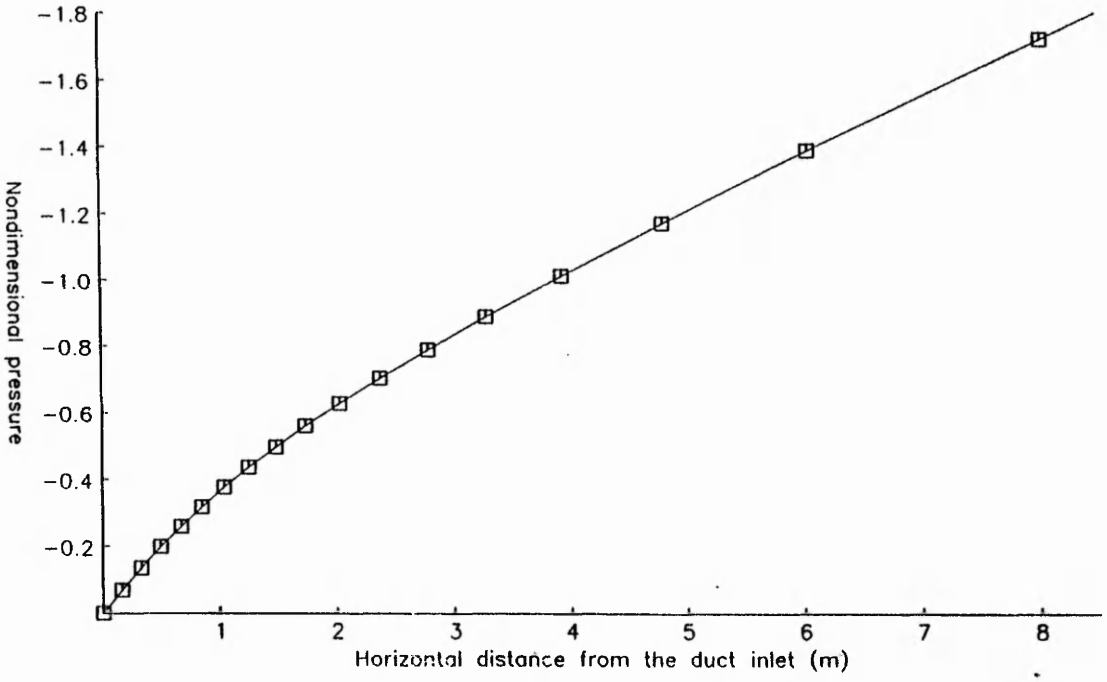

Figure 5.10 Pressure drop for developing laminar duct flow.

5.5.2 Flow over backward facing step

The laminar flow over a backward facing step is characterised by the primary recirculation region near the step. There, flow separation is caused by the sudden change in the cross-sectional area. This flow situation is frequently encountered in engineering practice and has been studied previously by Armaly et al (1983), Rice and Schnipke (1986), Gosman and Pun (1974), Denham and Patrick (1974), Leschziner (1980) and Castro (1978). A comprehensive experimental and theoretical study was conducted by Armaly et al (1983), whose geometry is chosen for the current work.

The geometry and the boundary conditions are shown in Figure 5.11. A parabolic velocity profile is prescribed at the inlet giving an average velocity of 1. No-slip conditions are specified at the top and the bottom. Natural boundary conditions for the velocity components are imposed at the outlet. The pressure is fixed at zero along the outlet. The duct downstream of the step is sufficiently long for the flow to assume a fully developed profile for the range of Reynolds number considered here. The Reynolds number is defined as

$$Re = \frac{U_{avrg} D}{\nu} \qquad (5.24)$$

where U_{avrg} is the average inlet velocity, D is twice the duct opening at the inlet and ν is the kinematic viscosity. The key parameter in this study is the primary reattachment point, whose position was predicted for Reynolds numbers of 100, 200, 400, 600, 800 and 1000.

The computational grid is shown in Figure 5.12. It consists of 717 nodes and 1320 elements in comparison with the 45x45 grid density used by Armaly et al.

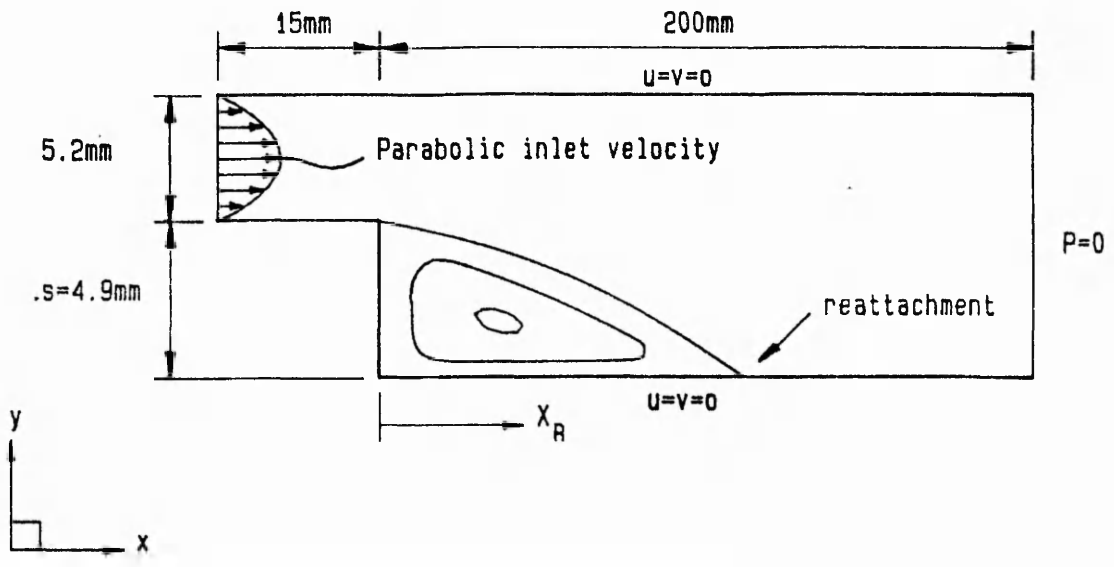

Figure 5.11 *Laminar backward facing step flow with imposed boundary conditions.*

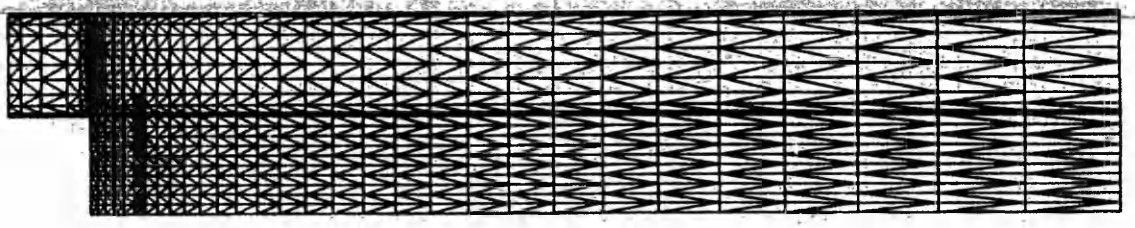

Figure 5.12 *Computational grid for laminar backward facing step flow (not to scale).*

The grid is non-uniform and is dense around the step where sharp gradients in both the velocity and the pressure fields are expected. The mesh was chosen such that further refinements resulted in less than 10% change in the position of the reattachment point for cases with the Reynolds numbers of up to 400. Armaly et al observed that the flow was laminar and purely two-dimensional below Re = 400. Above this value, secondary recirculation regions start to appear both near the top and the bottom walls. The presence of such regions destroys the two-dimensionality of the flow. Hence the results of two-dimensional analyses for Re > 400 should be interpreted with caution. The flow remains laminar up to Re = 1200. As cited by Armaly et al, this peoblem is prone to spurious pressure modes.

To minimise the computational effort, the regions near the step were solved elliptically, and those downstream of the recirculation zone were solved parabolically. This was achieved by employing RADIS which was described in section 5.2. Table 5.1 compares the results of the current analysis with the experimental and the predictive data of Armaly et al. At Re = 100 and 400 the Armaly et al predictions are closer to their measurements than the current results.

	X_R/s		
		Armaly et al (1983)	
Re	*Current work*	*Predictions*	*Measurements*
100	*3.39*	*3.04*	*3.00*
200	*4.87*	*4.88*	*4.79*
400	*6.66*	*7.92*	*8.57*
600	*10.98*	*8.32*	*11.14*
800	*12.87*	*7.60*	*14.29*
1000	*14.20*	*7.36*	*16.00*

Table 5.1 Comparison of reattachment points for laminar backward facing step flow.

The reattachment point is predicted accurately with respect to the measured data for Re = 200 by both the current analysis and that of Armaly et al. For Re > 400, the current analysis follows the experimental data closely. However as mentioned earlier, a direct comparison is not recommended here as the flow is no longer two-dimensional for Re > 400. The predictions of Armaly et al fall far short of their experimental data for Re > 400.

Figures 5.13 (a)-(c) show the graphical representation of the results for Re = 200. Figure 5.13(a) shows the recirculation region very clearly. The velocity quickly develops into a parabolic profile after the reattachment point. The pressure field in Figure 5.13(b) shows the singularity at the step due to flow separation. The pressure field is nearly one-dimensional upstream and downstream of the step. In the vicinity of the step, pressure first rises across the step in the recirculation region and then falls gradually further downstream. As shown in Figure 5.13(c), the primary reattachment point is predicted to be 23.9mm downstream of the step. This value is less than the experimental data by about 2%, see also Table 5.1.

Figures 5.14(a)-(c) show the velocity, pressure and streamline plots for Re = 400 respectively. The same observations as above can be made for this case. It is seen from Figure 5.14(a) that the secondary recirculation region along the top wall is beginning to appear. This is consistent with the experimental observation of Armaly et al. Figure 5.14(b) shows a more rapid pressure change in the proximity of the step than that for Re of 200. From Figure 5.14(c), the reattachment point is predicted at 32.6mm downstream of the step, which is about 22% less than the measured value. The reattachment

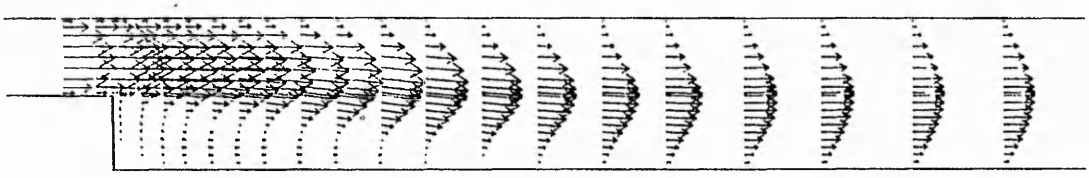

(a)

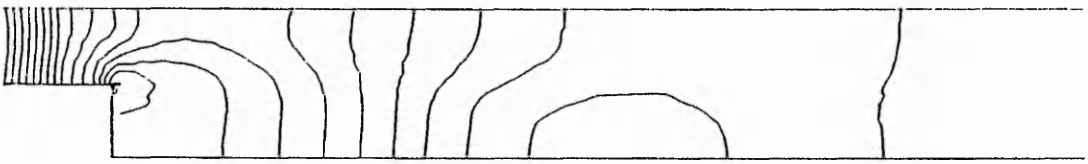

(b)

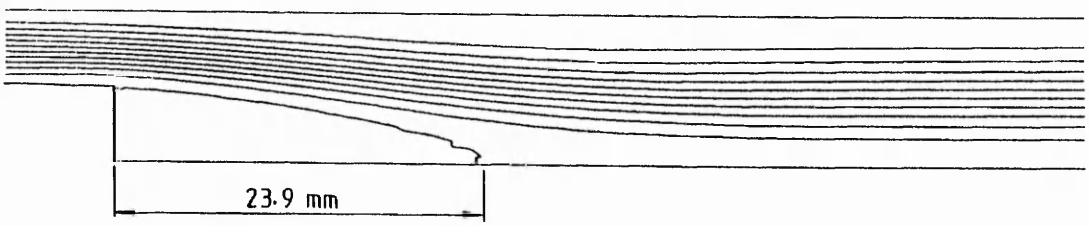

(c)

Figure5.13 *Laminar backward facingstep flow at Re = 200, (a) velocity field, (b)pressure field and (c) streamline plot.*

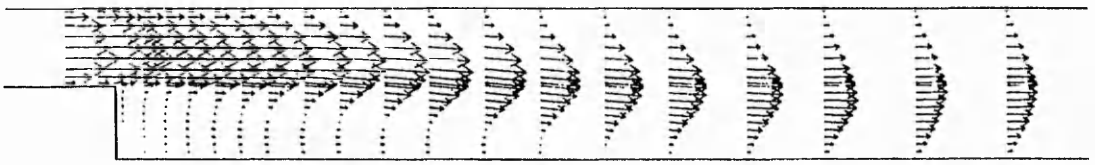

(a)

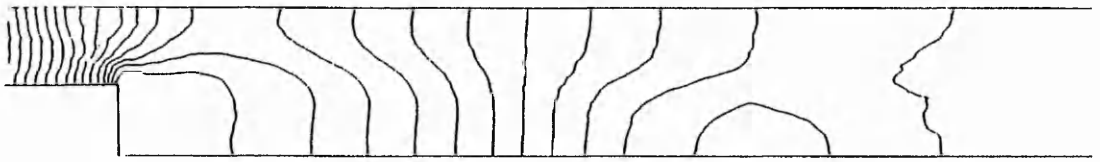

(b)

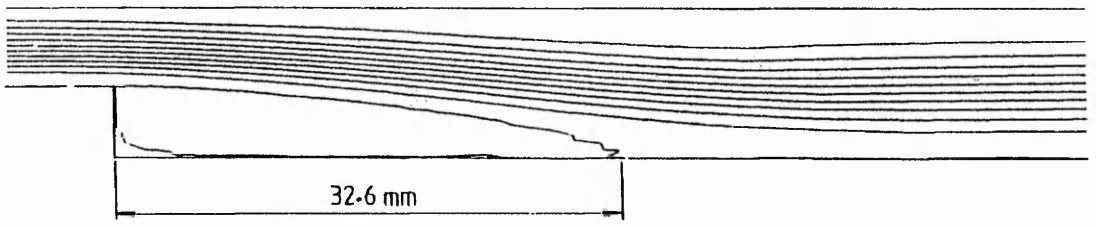

(c)

Figure 5.14 *Laminar backward facing step flow at Re = 400, (a) velocity field, (b) pressure field and (c) streamline plot.*

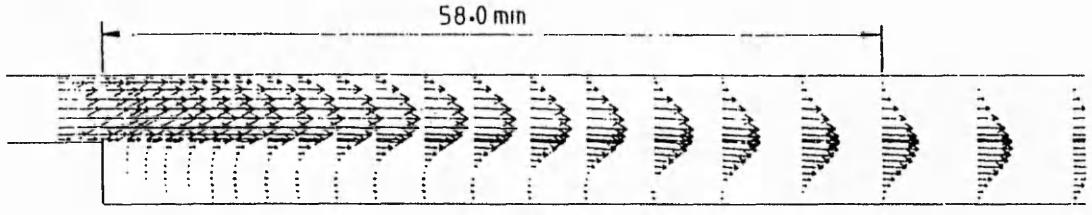

(a)

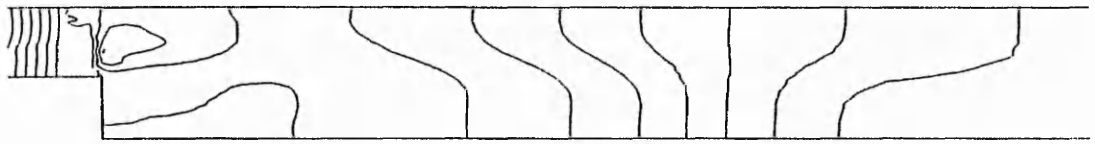

(b)

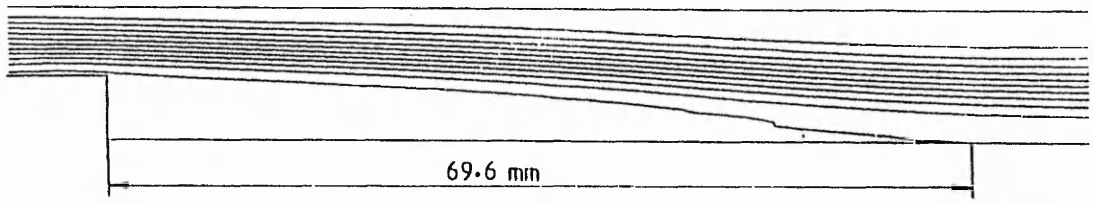

(c)

Figure 5.15 *Laminar backward facing step flow at Re = 1000, (a) velocity field, (b) pressure field and (c) streamline plot.*

point calculated by Armaly et al was shorter than their measurement by about 7% .

Figures 5.15(a)-(c) depict the resulting flow fields for Re = 1000. From Figure 5.15(a), the secondary recirculation region starts at 58.0mm downstream of the step along the top wall. This is in very good agreement with the experimental data of Armaly et al, who found the secondary recirculation to begin at about 65.8mm downstream of the step. The pressure field in Figure 5.15(b) shows a more vigorous rise and fall compared with the other two cases. It also develops into a one-dimensional field much further downstream of the step than for Re of 200 and 400. The primary reattachment point is shown in Figure 5.15(c). It is calculated to be 69.6mm downstream of the step, which is about 11% below that measured by Armaly et al. The numerical analysis of Armaly et al gave a value of 36.1mm for the reattachment point which is 54% below their measured value. It must be noted that the results of the current analysis for Re = 1000 should not be compared directly with the measurements of Armaly et al, since at this Reynolds number the flow is no longer two-dimensional. Nevertheless, these results point to the stability and robustness of the current iterative solution scheme in providing a converged solution set even at such a high Reynolds number. Also the overall results clearly demonstrate the absence of any spurious pressure modes. The pressure field was obtained without any smoothing or any other relaxation techniques.

The above computations were performed on a Digital VAX-8550 machine. The analysis began by obtaining the solution to the lowest Reynolds number case and using it as initial guess for the next

Reynolds number. This procedure was followed until all cases were analysed. The velocity components were relaxed implicitly, see equations (5.5)-(5.7). The pressure was relaxed by underrelaxing the pressure gradient terms, see equations (4.35) and (4.36). The relaxation factors were 0.5 for all variables. The convergence criteria were based on the percentage of the absolute residuals of the discretised equations for momenta and pressure, and the percentage difference between the mass flowrates in and out of the domain, see equations (5.13) and (5.16). In both cases a limiting value of 0.01% was chosen. For Re = 100, the solution took 158 cycles and 1130 CPU seconds to converge. The results were used as initial guesses for Re = 200, which then took a further 110 cycles and 785 CPU seconds to converge. For Re = 400, a further 232 cycles and 1660 CPU seconds yielded the converged solution set. A further 270 cycles and 1935 CPU seconds were required for Re = 600. For Re = 800, 324 additional cycles took 2321 CPU seconds for convergence. At Re = 1000, a further 418 cycles and 2997 CPU seconds provided the final solution. Also the case of Re = 1000 was analysed with no guessed values. This took 1658 cycles and 11630 CPU seconds to converge.

5.5.3 Natural convection in square cavity

Natural convection in differentially heated enclosures is encountered frequently in engineering situations such as reactor insulation, room ventilation and fire prevention. It is therefore of interest to accurately predict the hydrodynamic and thermal characteristics of this type of flow. Numerous experimental and numerical studies of this problem have been conducted in the past. De Vahl Davis and Jones (1983) presented a paper in which the performance of 37 methods were compared with the benchmark solution of De Vahl

Davis (1983), whose geometry and boundary conditions are shown in Figure 5.16.

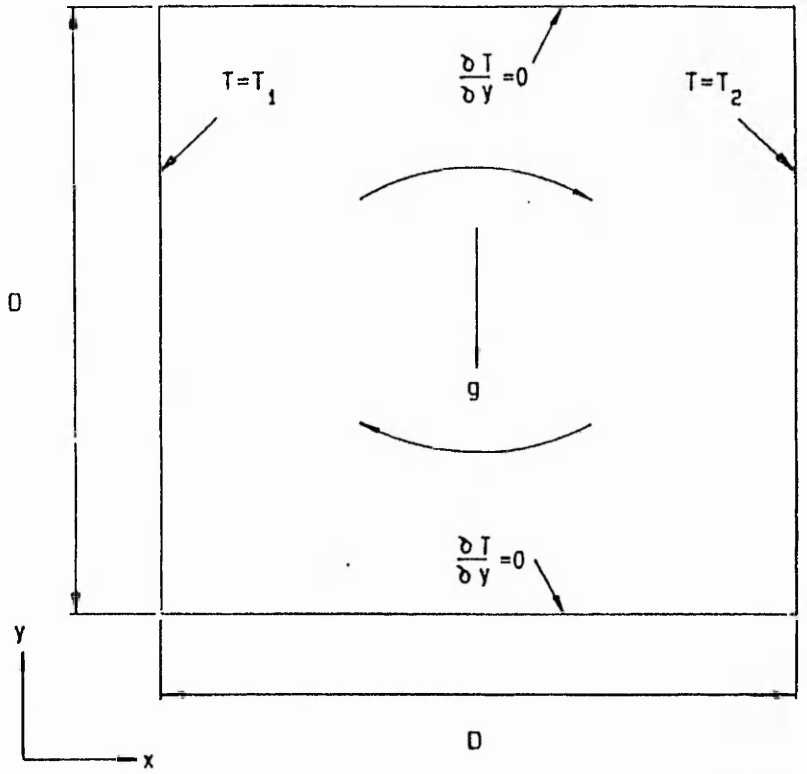

Figure 5.16 Geometry and flow conditions for natural convection in square cavity.

The computational grid used for the present analysis is shown in Figure 5.17. It is a non-uniform grid consisting of 31 equally spaced rows and 31 columns with higher grid density near the side walls, resulting in 961 nodes and 1800 elements. It was necessary to use finer grids near the heated walls in order to predict the Nusselt number variation along the walls accurately. Note also the orientation of the elements with their diagonals following the main direction of the flow. The analysis was carried out for Rayleigh numbers, Ra, of 10^3, 10^4, 10^5 and 10^6 in compliance with the benchmark solutions of De Vahl Davis (1983).

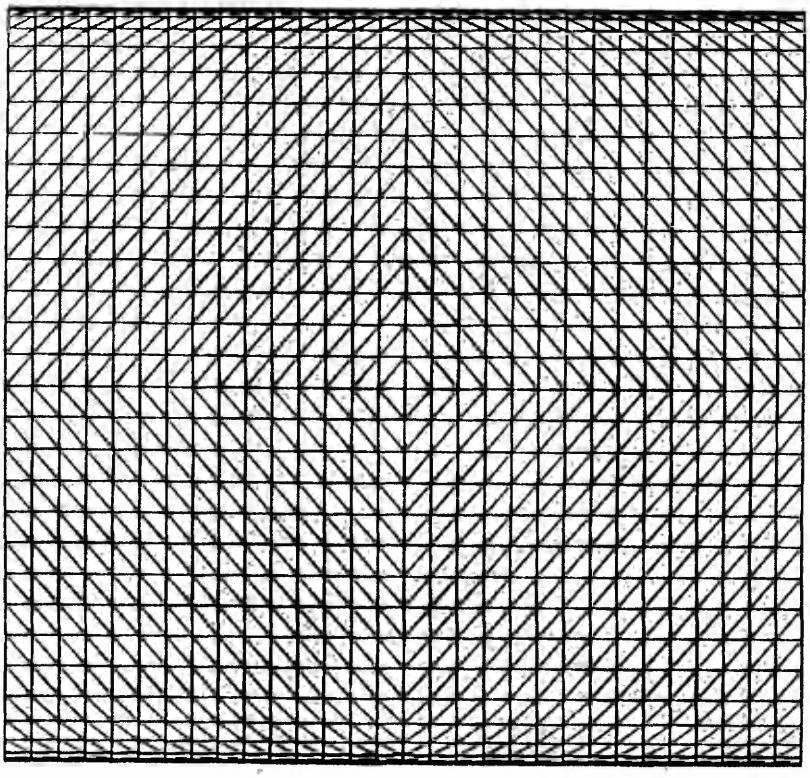

Figure 5.17 Computational grid for natural convection in square cavity.

Figures 5.18 to 5.21 show the results of the present analysis for the above Rayleigh numbers. At lower Rayleigh numbers, i.e. 10^3 and 10^4, the fluid is circulating slowly and the pressure variation is nearly hydrostatic, Figures 5.18(b) and 5.19(b). At Ra of 10^5 and 10^6, the fluid is moving with greater velocities and there are two distinct stagnant regions, above and below the mid plane as is shown in Figures 5.20(a) and 5.21(a). The pressure fields reflect the increase in fluid velocity especially along the top and the bottom walls, Figures 5.20(b) and 5.21(b). As for the backward step flow, no additional smoothing or relaxing techniques were employed for pressure. The pressure contours clearly demonstrate that the present equal-order velocity-pressure formulation does not suffer from pressure chequer boarding.

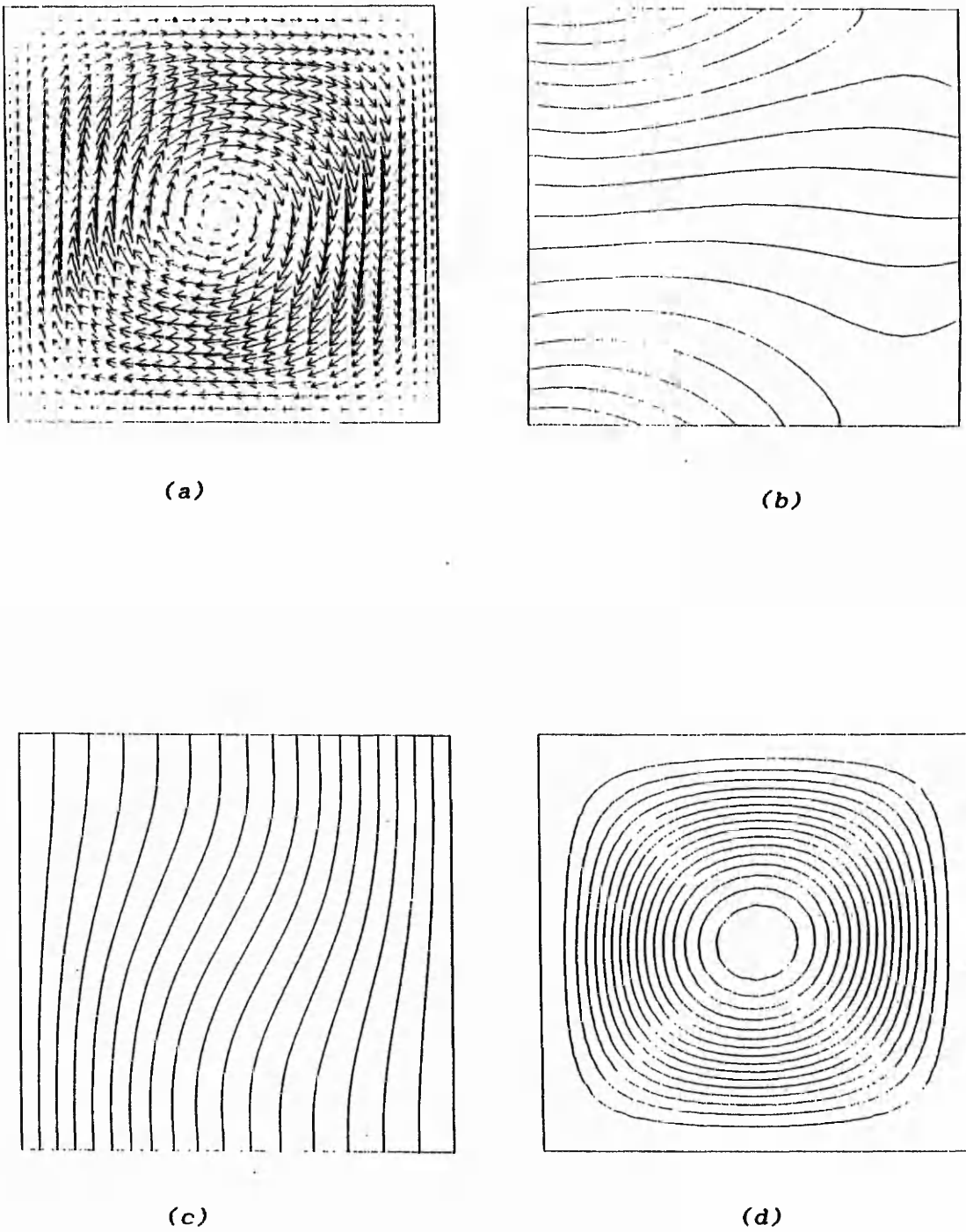

Figure 5.18 Natural convection in square cavity at $Ra = 10^3$, (a) velocity field, (b) pressure field, (c) temperature field and (d) streamline plot.

$Ra = 10^3$					
	Bench mark solution	*Current work*	*Percentage error*	*Gartling*	*Percentage error*
$\lvert\psi_{mid}\rvert$	*1.174*	*1.139*	*2.98*	*1.174*	*0.00*
$\lvert\psi_{max}\rvert$	—	—	—	—	—
x, y	—	—	—	—	—
U_{max}	*3.649*	*3.553*	*2.63*	*3.640*	*0.20*
y	*0.813*	*0.800*	*1.60*	*0.824*	*1.35*
V_{max}	*3.697*	*3.612*	*2.30*	*3.696*	*0.03*
x	*0.178*	*0.169*	*5.06*	*0.176*	*1.12*
$\overline{Nu}$	*1.118*	*1.102*	*1.43*	*1.118*	*0.00*
Nu_{max}	*1.505*	*1.456*	*3.26*	*1.506*	*0.10*
y	*0.092*	*0.100*	*8.69*	*0.080*	*1.23*
Nu_{min}	*0.692*	*0.722*	*4.34*	*0.691*	*0.10*
y	*1*	*0.967*	*3.30*	*0.989*	*1.10*

Table 5.2 *Natural convection in square cavity at Ra = 10^3, comparison of current work with bench mark solution.*

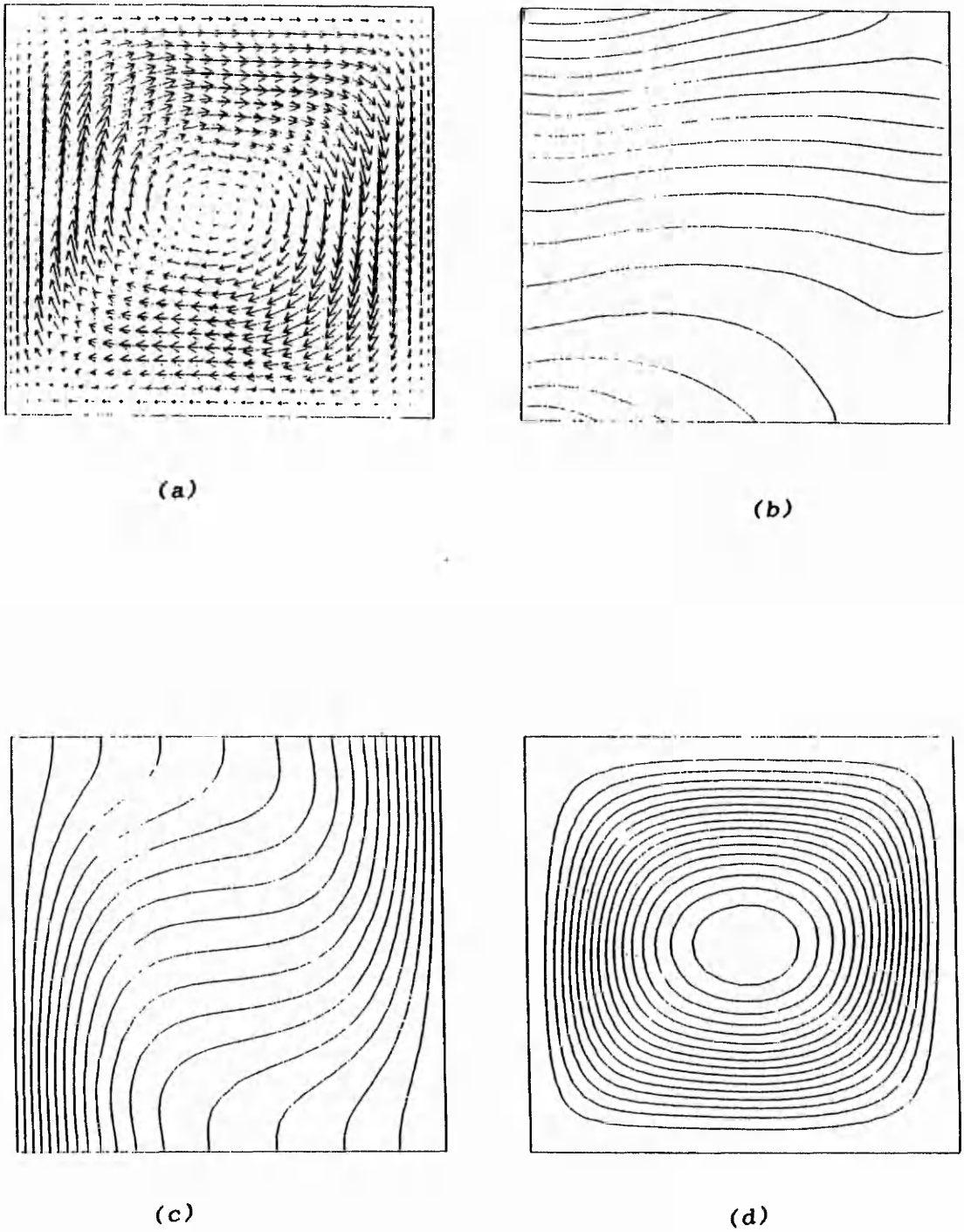

Figure 5.19 *Natural convection in square cavity at Ra = 10^4, (a) velocity field, (b) pressure field, (c) temperature field and (d) streamline plot.*

$Ra = 10^4$					
	Bench mark solution	*Current work*	*Percentage error*	*Gartling*	*Percentage error*
$\lvert\psi_{mid}\rvert$	*5.071*	*5.300*	*4.51*	*5.074*	*0.06*
$\lvert\psi_{max}\rvert$	—	—	—	—	—
x, y	—	—	—	—	—
U_{max}	*16.178*	*17.130*	*5.88*	*16.186*	*0.05*
y	*0.823*	*0.833*	*1.21*	*0.824*	*0.12*
V_{max}	*19.617*	*20.100*	*2.46*	*19.630*	*0.07*
x	*0.119*	*0.128*	*7.56*	*0.119*	*0.00*
$\overline{Nu}$	*2.243*	*2.100*	*6.37*	*2.250*	*0.31*
Nu_{max}	*3.528*	*3.247*	*7.96*	*3.538*	*0.28*
y	*0.143*	*0.200*	*39.86*	*0.133*	*7.34*
Nu_{min}	*0.586*	*0.601*	*2.56*	*0.587*	*0.17*
y	*1*	*0.967*	*3.30*	*0.989*	*1.10*

Table 5.3 *Natural convection in square cavity at Ra = 10^4, comparison of current work with bench mark solution.*

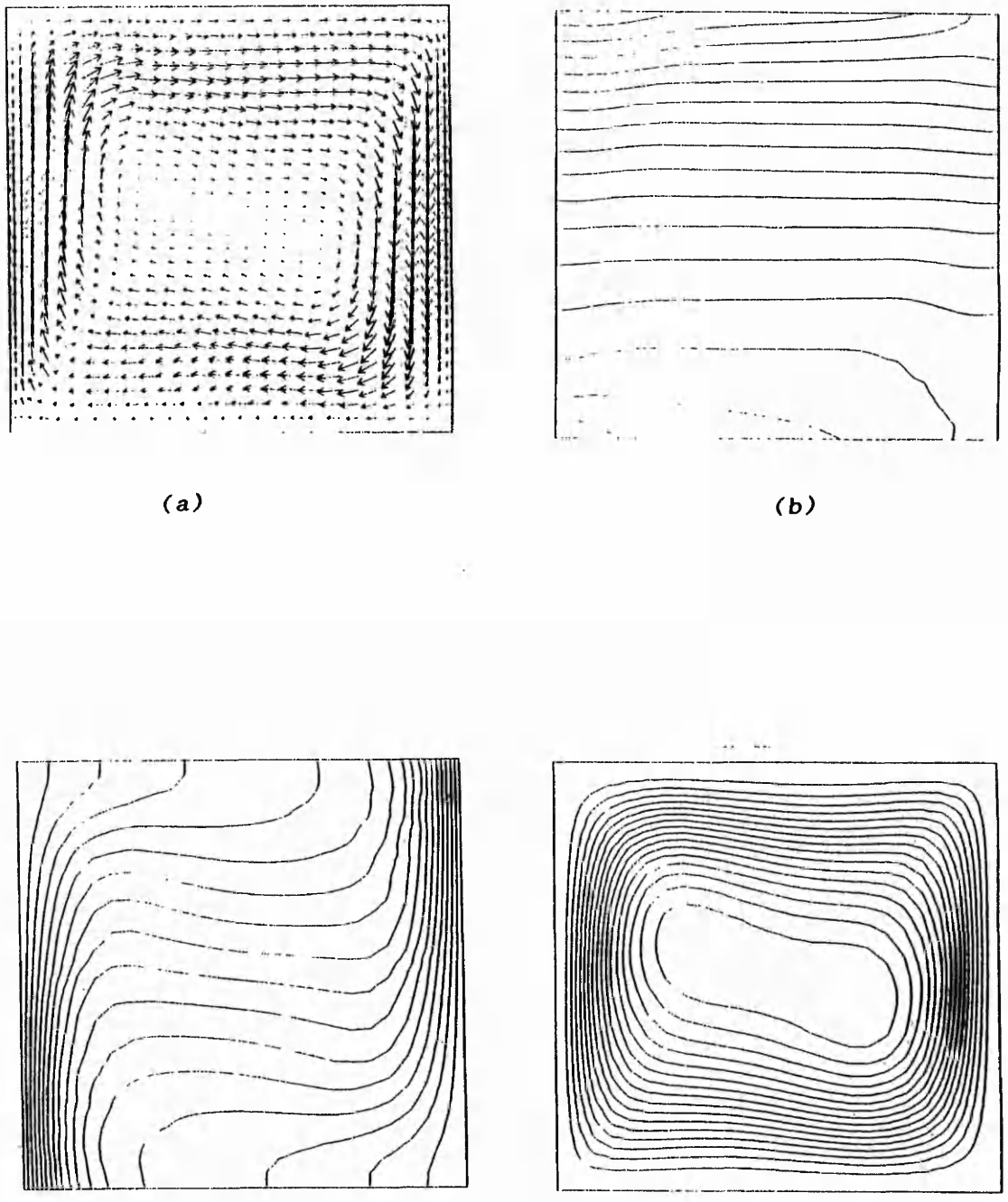

Figure 5.20 *Natural convection in square cavity at Ra = 10^5, (a) velocity field, (b) pressure field, (c) temperature field and (d) streamline plot.*

$Ra = 10^5$					
	Bench mark solution	*Current work*	*Percentage error*	*Gartling*	*Percentage error*
$\lvert\psi_{mid}\rvert$	*9.111*	*11.150*	*22.38*		
$\lvert\psi_{max}\rvert$	*9.612*	*11.290*	*17.46*	*9.603*	*0.09*
x	*0.285*	*0.335*	*17.54*	*0.281*	*1.40*
y	*0.601*	*0.567*	*5.66*	*0.582*	*3.16*
U_{max}	*34.73*	*40.95*	*17.91*	*34.73*	*0.00*
y	*0.855*	*0.867*	*1.40*	*0.854*	*0.12*
V_{max}	*68.59*	*73.78*	*7.57*	*68.63*	*0.06*
x	*0.066*	*0.054*	*18.18*	*0.068*	*3.03*
$\overline{Nu}$	*4.519*	*4.196*	*7.15*	*4.592*	*1.62*
Nu_{max}	*7.717*	*6.704*	*13.13*	*7.873*	*2.02*
y	*0.081*	*0.133*	*64.20*	*0.080*	*1.23*
Nu_{min}	*0.729*	*0.779*	*6.86*	*0.737*	*1.10*
y	*1*	*1*	*0.00*	*0.989*	*1.10*

Table 5.4 *Natural convection in square cavity at Ra = 10^5, comparison of current work with bench mark solution.*

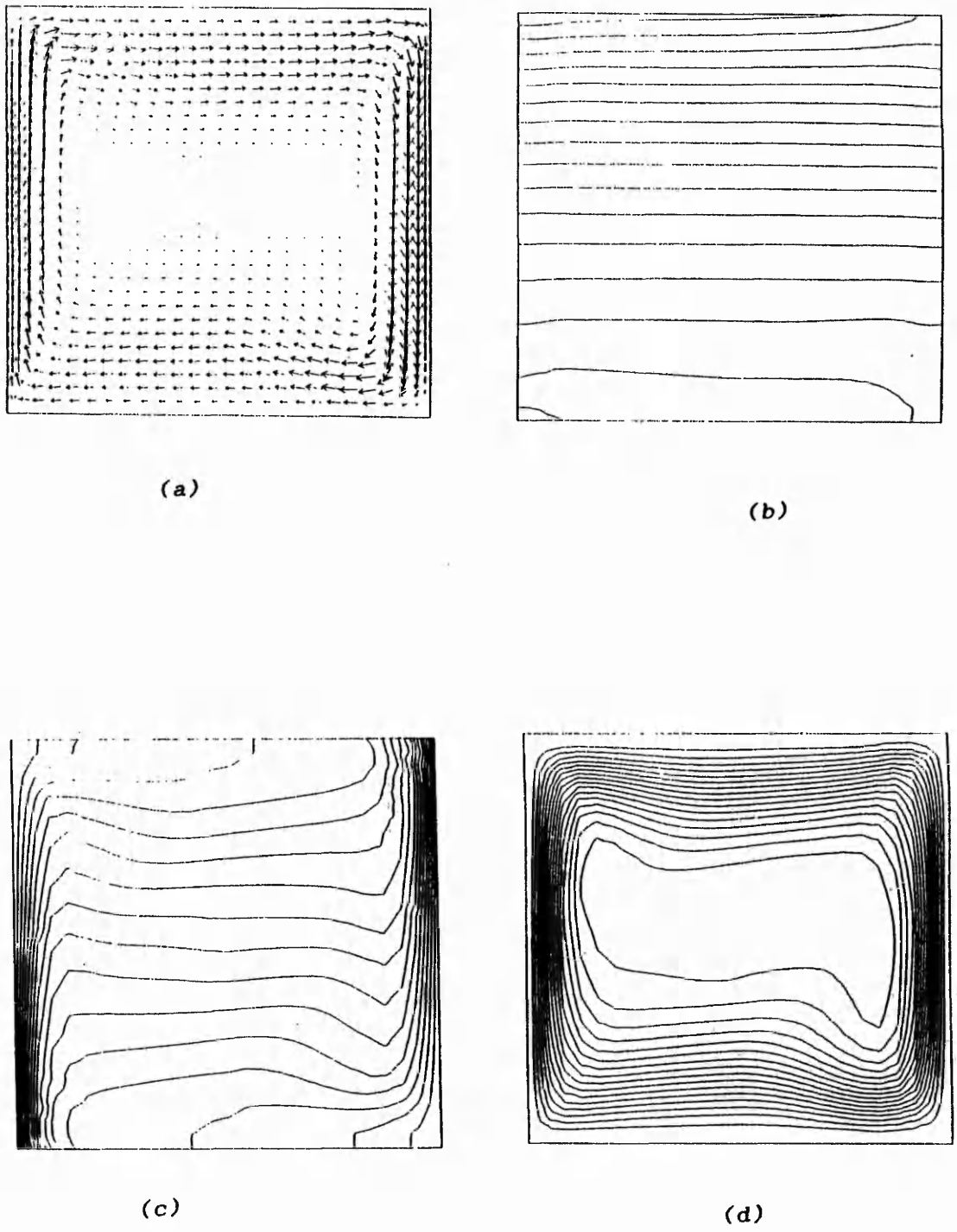

Figure 5.21 *Natural convection in square cavity at Ra = 10^6,. (a) velocity field, (b) pressure field, (c) temperature field and (d) streamline plot.*

$Ra = 10^6$					
	Bench mark solution	*Current work*	*Percentage error*	*Gartling*	*Percentage error*
$\lvert\psi_{mid}\rvert$	*16.32*	*20.51*	*25.67*		
$\lvert\psi_{max}\rvert$	*16.750*	*20.830*	*24.36*	*16.851*	*0.60*
x	*0.151*	*0.458*	*203.31*	*0.146*	*3.31*
y	*0.547*	*0.533*	*2.56*	*0.582*	*6.40*
U_{max}	*64.63*	*89.04*	*37.77*	*64.37*	*0.40*
y	*0.850*	*0.867*	*2.00*	*0.854*	*0.47*
V_{max}	*219.36*	*243.00*	*10.78*	*218.42*	*0.43*
x	*0.0379*	*0.0289*	*23.75*	*0.0430*	*13.46*
$\overline{Nu}$	*8.800*	*8.206*	*6.75*	*9.382*	*6.61*
Nu_{max}	*17.925*	*14.270*	*20.39*	*18.630*	*3.93*
y	*0.0378*	*0.0667*	*76.45*	*0.0322*	*15.34*
Nu_{min}	*0.989*	*1.097*	*10.92*	*1.007*	*1.82*
y	*1*	*1*	*0.00*	*0.989*	*1.10*

Table 5.5 *Natural convection in square cavity at $Ra = 10^6$, comparison of current work with bench mark solution.*

The numerical comparison between the current predictions, the bench mark solutions of De Vahl Davies and the predictions of Gartling , which are both quoted in De Vahl Davies and Jones (1983), are provided in tables 5.2 to 5.5 for Ra = 10^3 to 10^6 respectively. Gartling employed the FEM with the primitive variables on a non-uniform mesh of 16 x 16 isoparametric 8-noded quadrilateral elements. Values of ψ_{mid}, ψ_{max}, U_{max}, V_{max}, Nu_{max} and Nu_{min} are obtained by examining the mesh point values of these variables. The bench mark values are not necessarily the mesh point values and were computed by numerical differentiation, using a fourth-order polynomial

approximation. The heat flux at the wall with T = T_1 was calculated by a three-point forward approximation to $\partial T/\partial x$. The average Nusselt number $\overline{Nu}$ was then evaluated from the $\partial T/\partial x$ variation along the wall using Simpson's rule.

At Ra of 10^3 and 10^4, the agreement was within 9% and 40% of the benchmark solutions for all the predicted values respectively compared with 1% and 7% for Gartling's predictions. At Ra of 10^5 the agreement was within 64% compared to Gartling's 3% . Ignoring field values for x and y below 0.04, at Ra of 10^6, the velocity field was predicted to within 38% with the Nusselt number variation within 20% of the benchmark solution. Gartling's velocity field and Nusselt number variation came to within 0.5% and 7% of the benchmark solution respectively. The large differences in the current predictions at the higher Rayleigh numbers are attributed to the relative coarseness of the grid. With finer grids it would be possible to capture in more detail the flow characteristics in regions where sharp gradients are present, especially near the heated walls. The predictions of Gartling are generally closer to the benchmark solution than those obtained by the current method and do not deviate as much from the benchmark solutions at the higher Rayleigh numbers. The above results are not in general as accurate as some of the results quoted in the comparison exercise of De Vahl Davis and Jones (1983). However, as they point out, a better estimate of accuracy may be based on equal cpu cost, storage or even programming effort.

The predictions were performed, as before, on a Digital VAX-8550 machine. At Ra = 10^3, 188 cycles took 1782 seconds to produce a converged solution. This solution was used as the initial guess for Ra = 10^4. 102 extra cycles took 840 seconds for convergence. The solution

set was then used as the initial guess for Ra = 10^5. In this case a further 138 cycles took 1170 seconds to produce the final result. The last case at Ra = 10^6 used the previous results as the initial guess and after 368 more cycles and 3056 seconds the solution converged. A further run was performed at Ra = 10^6 with no initial guess. This case required 938 cycles and 8990 CPU seconds to converge.

5.5.4 Jet impingement with heat transfer

Rapid heating, cooling or drying of industrial products are often provided by using arrays of impinging jets. Cooling of electronic components or turbine blades, drying of textile and paper, annealing of metal and plastic sheets are among the many industrial applications of impinging jets. In designing an impinging jet system for a specific thermal application, the designer is always faced with a number of possible geometric and flow configurations such as nozzle-to-target surface spacing, position of exhaust ports, surface motion, impingement angle, nozzle design, temperature difference between the jet and the impingement surface and many more. In view of the large number of design parameters, it is clear that a purely experimental approach will be time consuming, expensive and unlikely to yield the optimal solution to the problem. It is therefore necessary to supplement the experimental studies with numerical investigations of the complex impingement transport processes. The success of such numerical investigations depend on the ability of the proposed method to accurately capture and predict the most important features of the flow such as the impingement and the wall jet regions, the recirculation region and the surface skin friction and heat transfer. The accurate prediction of the surface heat transfer is of primary importance since it determines the effectiveness of an

impinging jet system.

The present analysis is chosen to study the accuracy of the method proposed in this research for the conjugate fluid flow/heat transfer situation of a single confined plane laminar jet impinging on the surface of a heated solid block. Laminar jet impingement with heat transfer has been studied extensively, both experimentally and numerically, in the past, see for example van Heiningen et al (1975), Saad et al (1977), Huang et al (1978) and Law (1982). A brief review of the previous work was given in two recent papers by Wang et al (1989a) and (1989b). In most of the previous work on jet impingement heat transfer, only the energy equation for the fluid region is solved and boundary conditions are specified at the fluid-solid interface. However, in engineering applications of jet impingement the temperature or heat flux at the impingement surface is frequently unknown. Therefore, a proper approach should be to solve the energy equation for both the fluid and solid regions simultaneously. Wang et al (1989c) carried out an analytical investigation of the conjugate heat transfer characteristics of a laminar jet impinging on the flat surface of a solid block which was laterally insulated with prescribed temperature along the non-impingement surface. The geometry and boundary conditions of their flow arrangement is depicted in Figure 5.22. It consists of a confined jet of air impinging at right angle on a heated block of copper. The air is issued with a constant velocity and temperature of 20°C. The block of copper is kept at a constant temperature of 100°C along the bottom. The nozzle to impingement surface ratio, D/H, is 1/16. The thickness of the solid block is 0.1 H. The length of the impingement surface is 30 H, which is long enough for the flow to assume a fully developed profile at the exit.

Velocities are set to zero along the confinement plate with the temperature being equal to that of the air jet at the nozzle. Velocities are also set to zero along the impingement surface. The pressure is set to zero along the exit. The solid block is insulated at the exit. The analysis was performed for two inlet Reynolds numbers of 250 and 500, based on the nozzle half width and the air properties at the jet inlet temperature,

$$Re = \frac{V_{jet} D}{\nu} \tag{5.25}$$

The computational grid is shown in Figure 5.23. It is a non-uniform grid consisting of 386 nodes and 700 elements. In the flow region, the elements are oriented so as to follow the main direction of the flow. The grid density is high near the axis of symmetry and the impingement surface where steep gradients are expected. It was necessary to use high grid density along the fluid-solid interface in order to predict the Nusselt number variation there accurately. The grid was modified until further refinements resulted in less that 10% change in the values of the Nusselt number at the stagnation point. The results of this analysis should only serve to give a qualitative estimates of the pressure and Nusselt number variations. This is due to the incorrect weighting of the advection terms in the governing transport equations, see A_f in equation (3.20), which has effectively resulted in the artificial enhancement of the diffusive transport by an approximate factor of two. Here A_f was taken as the area of the element containing the downwind node, see Figure 3.5.

Figure 5.24 shows the streamline plot at Re = 250 for the region close to the impingement region. The streamlines are almost parallel

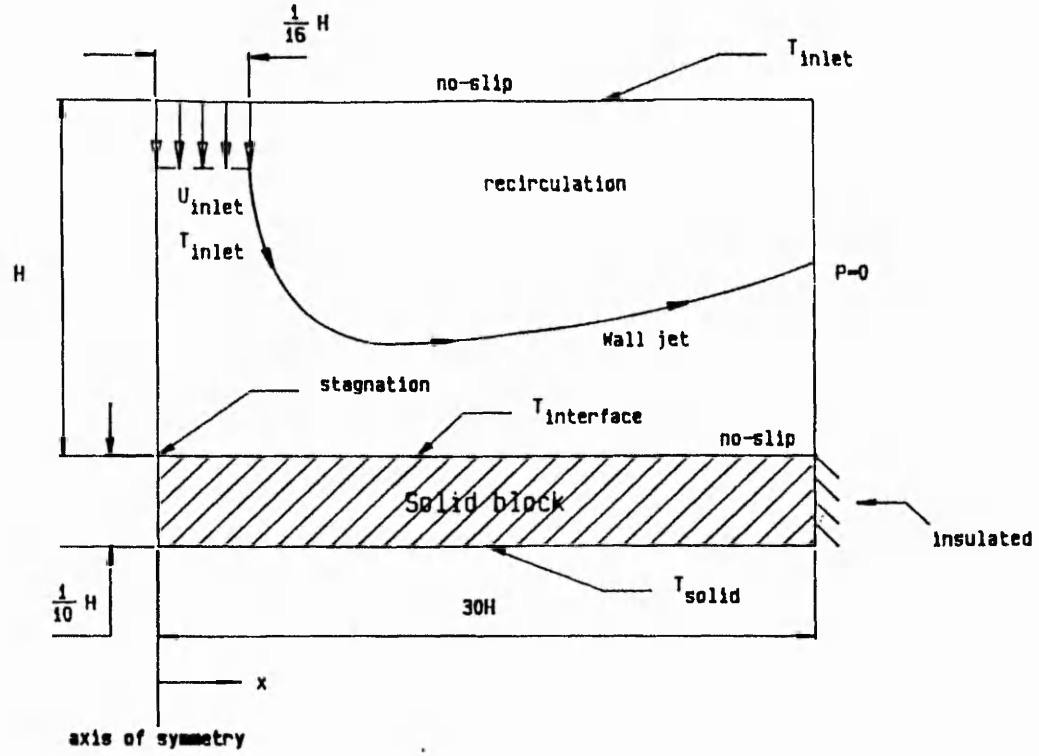

Figure 5.22 Plane laminar jet impingement with heat transfer (not to scale).

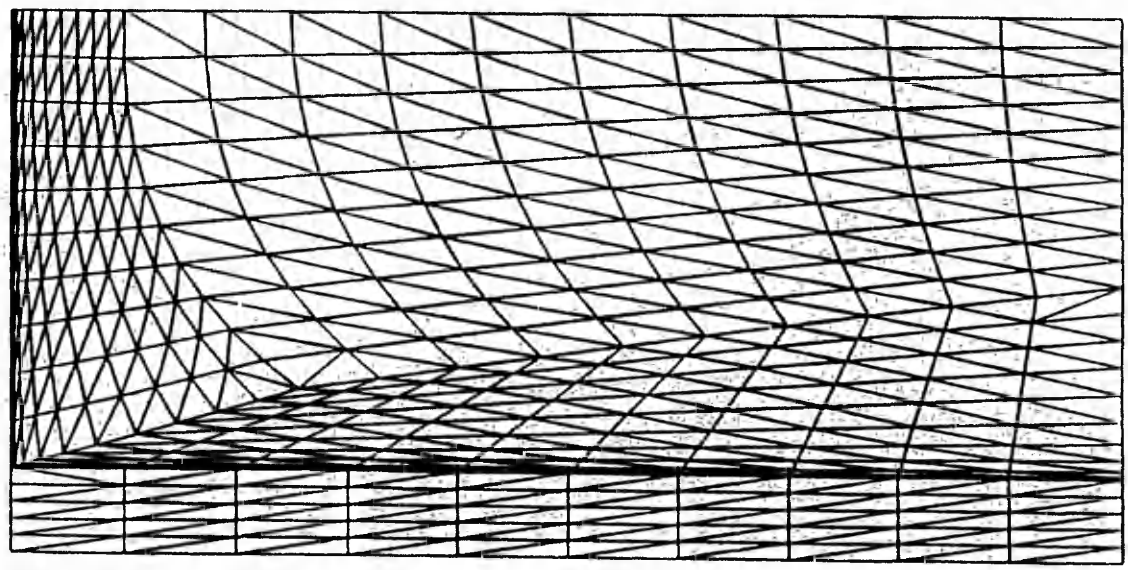

Figure 5.23 Computational grid for laminar jet impingement (not to scale).

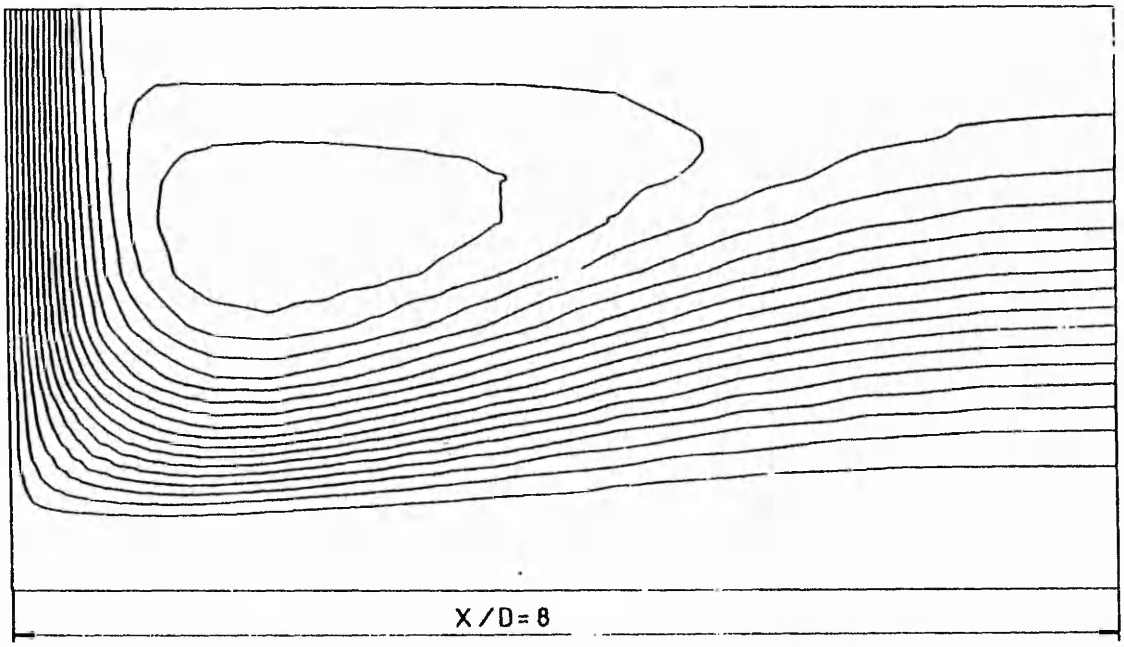

Figure 5.24 Streamline plot for laminar jet impingement at Re = 250.

at x/D = 8, indicating that the flow has nearly reached its fully developed profile there. The recirculation region is situated close to the outer edge of the jet. Figure 5.25(a) shows the variation of pressure along the impingement surface. Pressure is normalised with respect to pressure at the stagnation point. Pressure drops very quickly and is only 0.1% of the stagnation pressure at x/D = 7. The pressure variation is compared with the analytical results of Wang et al (1989c) and the finite element solution of Lipsett and Gilpin (1978). The general agreement between the three predictions is very good and to within 8% . Near the stagnation region, a less steeper pressure drop is predicted by the other two methods. The normalised Nusselt number variation along the impingement surface is shown in Figure 5.25(b). The following definition is used for the Nusselt number,

$$Nu = q_i \, D \left(k_{air} \, (T_{interface} - T_{inlet})\right)^{-1} \qquad (5.26)$$

where q_i is the heat flux at the fluid-solid interface and k_{air} is the thermal conductivity of air. The Nusselt number at the stagnation point was 21. This value was used to normalise the results elsewhere along the impingement surface. The current work indicates that the rate of heat transfer drops to half of its stagnation value by x/D = 3. In other words most of the heat is transferred to the impinging fluid in the stagnation region. Predictions of Lipsett and Gilpin (1978) also show similar trends. Although they indicated a less severe drop in the heat transfer rate. The agreement between the two results is only moderate, which is attributed to the special treatment of the boundary layer region by Lipsett and Gilpin (1978), who employed analytical techniques to obtain the velocity field in this region.

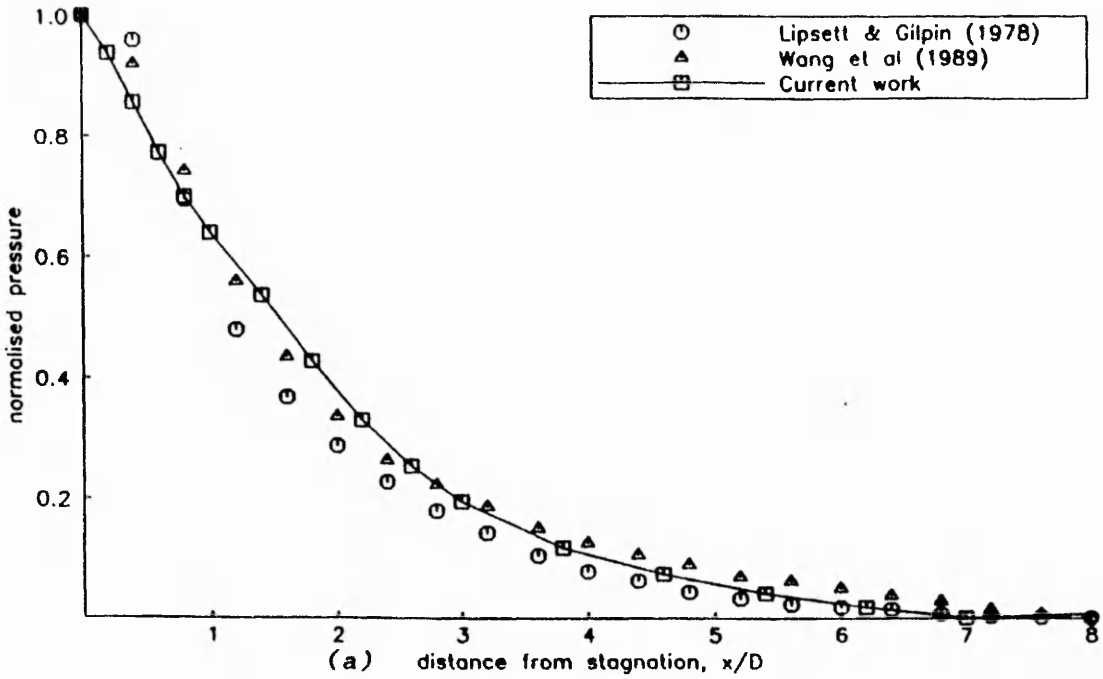

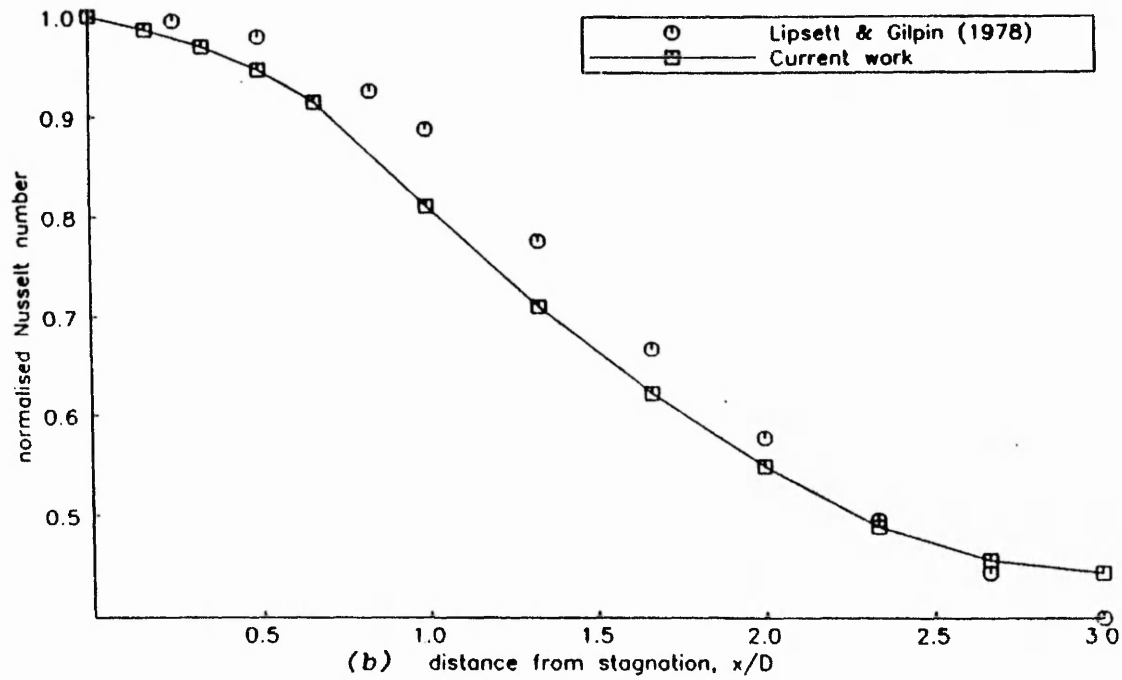

Figure 5.25 *Comparison of results along the impingement surface at Re = 250, (a) pressure variation and (b) Nusselt number variation.*

Figure 5.26 shows the streamline plot for Re = 500. The streamlines in the wall jet region are almost parallel. The recirculation bubble occupies a bigger portion of the near jet region as opposed to the previous case. It extends beyond the x/D = 8 line. The flow is accelerated through the channel-like constraint that is created between the recirculation bubble and the impingement surface.

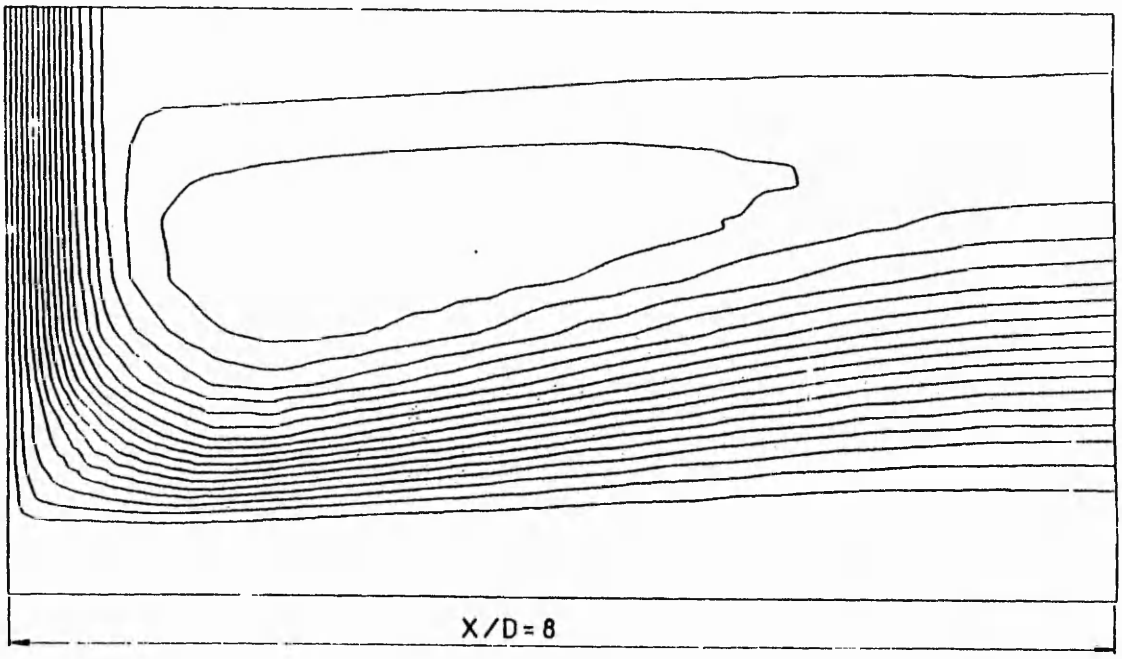

Figure 5.26 Streamline plot for laminar jet impingement at Re = 500.

Figure 5.27(a) shows the pressure variation along the impingement surface. The pressure drop is more rapid than the previous case. Pressure drops below 1% of its stagnation value by x/D = 4.5. The agreement between the current predictions and those of Lipsett and Gilpin (1978) and Wang et al (1989) is very good and to within 4%. Both these workers predict a similar drop in pressure away from the

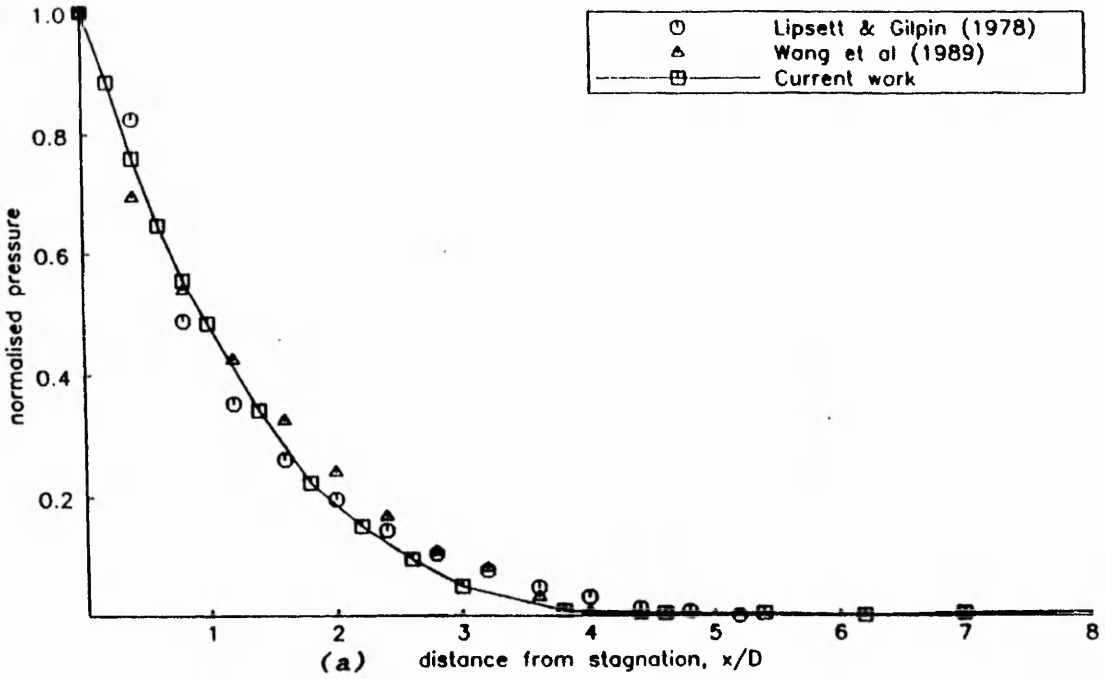

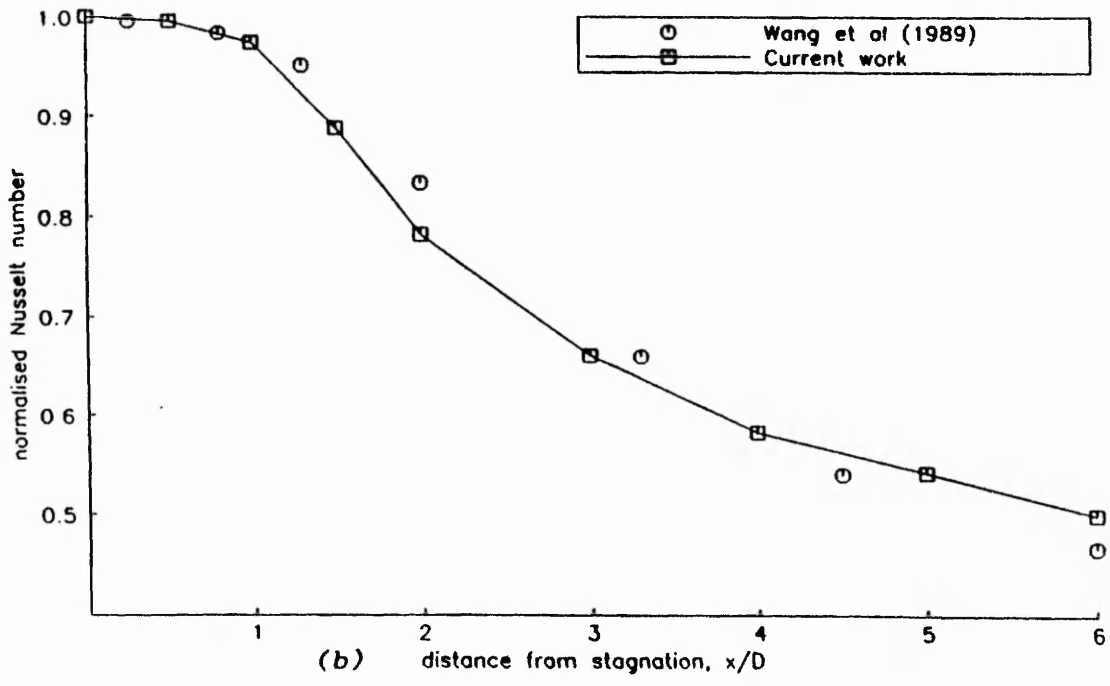

Figure 5.27 *Comparison of results along the impingement surface at Re = 500, (a) pressure variation and (b) Nusselt number variation.*

stagnation point. Figure 5.27(b) compares the predicted Nusselt number variation along the impingement surface with that of Wang et al (1989). The agreement is very good, especially near the stagnation region where there is negligible difference between the two predictions. The stagnation Nusselt number was 27. Compared with Figure 5.25(b), it is seen that a high rate of heat transfer is maintained much further along the impingement surface, dropping to half its stagnation value around x/D = 6.

The computations were performed on a Digital VAX-8550 machine. The jet impingement heat transfer at Re = 250 was started without initial guesses. It took 138 cycles and 1300 CPU seconds to converge. The results were then used as starting values for the second case with Re = 500. This took a further 102 cycles and 910 CPU seconds to complete.

CHAPTER 6

TURBULENT FLOW MODEL

The time-averaged differential equations of turbulent flow are considered. The Reynolds stress terms in the equations are modelled by a new method. The turbulent closure is first reviewed in section 6.1. The adopted approach for turbulent closure is presented. In section 6.2 the discretised form of the equations are presented. Section 6.3 deals with the imposition of the various boundary conditions. The computational aspects of the solution procedure are discussed in section 6.4.

6.1 Turbulent closure

In chapter 1, the turbulent closure problem was considered. This problem arises as the result of time averaging process on the nonlinear advection terms. This problem was clearly demonstrated in Chapter 2. From Chapter 2, the time-averaged equations for steady state, incompressible and two-dimensional mean flow in the Cartesian coordinate system are

Continuity
$$\frac{\partial}{\partial x}\rho U + \frac{\partial}{\partial y}\rho V = 0 \qquad (6.1)$$

X-momentum
$$\frac{\partial}{\partial x}\rho U^2 + \frac{\partial}{\partial y}\rho VU = \qquad (6.2)$$
$$\rho g_x - \frac{\partial P}{\partial x} + \frac{\partial}{\partial x}\left(\mu\frac{\partial U}{\partial x} - \rho\overline{uu}\right) + \frac{\partial}{\partial y}\left(\mu\frac{\partial U}{\partial y} - \rho\overline{uv}\right)$$

Y-momentum $$\frac{\partial}{\partial x}\rho UV + \frac{\partial}{\partial y}\rho V^2 = \rho g_y - \frac{\partial P}{\partial y} + \frac{\partial}{\partial x}\left(\mu\frac{\partial V}{\partial x} - \rho\overline{uv}\right) + \frac{\partial}{\partial y}\left(\mu\frac{\partial V}{\partial y} - \rho\overline{vv}\right) \quad (6.3)$$

The three equations above contain the following unknowns; U, V, P, $\rho\overline{uu}$, $\rho\overline{uv}$, and $\rho\overline{vv}$.

In order to solve the above equations, the Reynolds stress terms must be related to the mean flow quantities U, V and P. The desirable relations are obtained by assuming that turbulence is generated solely due to the transfer of part of the mean flow energy into the energy of the small scale disturbances, see Monin and Yaglom (1971). Following this assumption, the Reynolds stresses must depend on the mean velocities U and V, and result in actions similar to those of viscous stresses. The following relations are then put forward

$$-\rho\overline{uu} = 2\mu_t\frac{\partial U}{\partial x} - \frac{2}{3}\rho k$$

$$-\rho\overline{uv} = \mu_t\left(\frac{\partial U}{\partial y} + \frac{\partial V}{\partial x}\right) \quad (6.4)$$

$$-\rho\overline{vv} = 2\mu_t\frac{\partial V}{\partial y} - \frac{2}{3}\rho k$$

where μ_t is the turbulent or eddy viscosity. μ_t, unlike the laminar viscosity, does not depend on the physical properties of the fluid. It rather depends on the properties of turbulence. It is a function of the velocity and length scale of turbulence, particularly those of the large scale eddies. In consequence its value may not be constant and may even assume negative values (Monin and Yaglom (1971)).

Substituting the relationships given by equation (6.4) in equations (6.2) and (6.3) produces

X-momentum

$$\frac{\partial}{\partial x}\rho U^2 + \frac{\partial}{\partial y}\rho VU = \rho g_x - \frac{\partial P}{\partial x} + \frac{\partial}{\partial x}\left((\mu + \mu_t)\frac{\partial U}{\partial x}\right) + \frac{\partial}{\partial y}\left((\mu + \mu_t)\frac{\partial U}{\partial y}\right) + S_u \tag{6.5}$$

Y-momentum

$$\frac{\partial}{\partial x}\rho UV + \frac{\partial}{\partial y}\rho V^2 = \rho g_y - \frac{\partial P}{\partial y} + \frac{\partial}{\partial x}\left((\mu + \mu_t)\frac{\partial V}{\partial x}\right) + \frac{\partial}{\partial y}\left((\mu + \mu_t)\frac{\partial V}{\partial y}\right) + S_v \tag{6.6}$$

From the above equations it is observed that the effect of turbulent fluctuations on the mean flow is represented as additional mixing or diffusion. S_u and S_v contain the additional turbulent diffusion terms. Equations (6.1), (6.5) and (6.6) may now be solved for the mean flow variables U, V and P, provided that an expression for μ_t exists.

The simplest expression for μ_t is that of a constant value. A constant value eddy viscosity has been employed for free turbulent flows, and is shown to produce reasonable results (Monin and Yaglom (1971)). However, a constant value eddy viscosity yields incorrect results for internal turbulent flows. In these types of flow the effect of constant μ_t is simply the augmentation of the laminar viscosity, resulting in a parabolic velocity profile which of course is in contradiction with the measured profiles for turbulent flow.

To overcome this problem a number of alternative routes for determining the value of μ_t have been employed. These range from simple algebraic expressions to expressions containing several turbulence variables. In the case of multiple scale turbulence, several pairs of these variables are introduced, see for example Fabris and Harsha (1981). One of the most successful of these methods for evaluating μ_t has been the two equation k-ε model of Launder and

Spalding (1972). In this model the eddy viscosity is expressed in terms of empirical constants, the turbulent kinetic energy, k, and its rate of dissipation, ε.

The k-ε model has been successfully applied to a wide range of turbulent flow problems. In the majority of these applications this model has been used together with the conventional upwind discretisation methods. As upwind approximations produce large numerical diffusion, the k-ε model may in fact be able to predict more accurately the turbulent phenomenon than these applications suggest (Hackman et al (1984)). The streamline upwind approximation adopted in this research has been shown to greatly reduce the numerical diffusion. Therefore, the k-ε model may now be more closely assessed.

The relative success of the k-ε model in the past prompted its use in the present research. The turbulent kinetic energy is defined as

$$k = \frac{1}{2}\,\overline{(u^2 + v^2 + w^2)} \qquad (6.7)$$

From Launder and Spalding (1972), the turbulent kinetic energy in Cartesian coordinate system is calculated from the following differential equation

$$\text{k-equation} \quad \frac{\partial}{\partial x}\rho U k + \frac{\partial}{\partial y}\rho V k = \frac{\partial}{\partial x}\left(\frac{\mu_t}{\sigma_k}\frac{\partial k}{\partial x}\right) + \frac{\partial}{\partial y}\left(\frac{\mu_t}{\sigma_k}\frac{\partial k}{\partial y}\right) + \mu_t G - \rho\,\varepsilon \qquad (6.8)$$

where σ_k is a pre-assigned constant and G is the generation term given by the expression

$$G = 2\left[\left(\frac{\partial U}{\partial x}\right)^2 + \left(\frac{\partial V}{\partial y}\right)^2\right] + \left(\frac{\partial U}{\partial y} + \frac{\partial V}{\partial x}\right)^2 \qquad (6.9)$$

The rate of turbulent energy dissipation, ε, is governed by a similar transport equation

$$\varepsilon\text{-equation} \quad \frac{\partial}{\partial x}\rho U\varepsilon + \frac{\partial}{\partial y}\rho V\varepsilon = \frac{\partial}{\partial x}\left(\frac{\mu_t}{\sigma_\varepsilon}\frac{\partial \varepsilon}{\partial x}\right) + \frac{\partial}{\partial y}\left(\frac{\mu_t}{\sigma_\varepsilon}\frac{\partial \varepsilon}{\partial y}\right) + C_1 \mu_t \frac{\varepsilon}{k} G - C_2 \rho \frac{\varepsilon^2}{k} \qquad (6.10)$$

where σ_ε, C_1 and C_2 are pre-assigned constants. Lastly, the eddy viscosity is expressed in terms of k and ε

$$\mu_t = \frac{C_\mu \rho k^2}{\varepsilon} \qquad (6.11)$$

The constants appearing in the above equations take the following values

$$\begin{aligned} C_\mu &= 0.09 \\ \sigma_k &= 1.0 \\ \sigma_\varepsilon &= 1.3 \\ C_1 &= 1.44 \\ C_2 &= 1.92 \end{aligned} \qquad (6.12)$$

6.2 Discretisation of governing equations

The time-averaged equations (6.1), (6.5) and (6.6) have the same form as those for laminar flow, namely equations (2.7), (2.8) and (2.9). Here the laminar viscosity is replaced by an overall viscosity which is the summation of the laminar and the eddy viscosities. Therefore the same velocity-pressure solution procedure developed in Chapter 4 can be employed for the turbulent flow. Since the eddy viscosity is expressed in terms of k and ε, the transport equations

for k and ε, equations (6.8) and (6.10), must also be solved concurrently with the above three equations.

The discretisation of equations (6.8) and (6.10) are carried out in the same manner as for the other transport equations. The advection terms are approximated using the same streamline upwind technique devised in Chapter 3. The standard Galerkin technique described in Chapter 2 is used for the diffusion terms. The source terms require special treatment.

In a turbulent flow field the source terms in the k and ε equations may become significantly larger than the transport terms. For example, in regions of high shear such as those near solid boundaries, the generation term, equation (6.9), can become very large, whereas the transport terms may be small. Also, from equation (6.8), it is possible that k may become negative during the iterations if the dissipation term acquires a large value. This is physically unrealistic and equation (6.7) prohibits such negative values of k. By the same argument, equation (6.10) can also produce negative values of ε, which are again unacceptable based on physical considerations. Therefore, the treatment of the generation term in equations (6.8) and (6.10) should prevent the occurrence of negative values for k and ε. The following procedures for the treatment of the source terms have been successfully implemented by Schnipke (1986) and are adopted here.

The discretised k and ε equations can be written as

$$a_{ii}^{k} k_i = - \sum_{j \neq i} a_{ij}^{k} k_j + \int_i N \mu_t G \, dA - \int_i N \rho \varepsilon \, dA \qquad (6.13)$$

and

$$a^{\varepsilon}_{ii}\varepsilon_i = -\sum_{j\neq i} a^{\varepsilon}_{ij}\varepsilon_j + \int_i N\, C_1\mu_t \frac{\varepsilon}{k} G\, dA - \int_i N\, C_2\rho \frac{\varepsilon^2}{k}\, dA \qquad (6.14)$$

In the above equations only the transport terms have been discretised. In discretising the source terms the above arguments regarding these terms are now taken into consideration. The eddy viscosity expression given by equation (6.11) is used in rewriting the last term in equation (6.13), hence

$$\int_i N\, \rho\, \varepsilon\, dA = \int_i N\, C_\mu\, \rho^2 \frac{k^2}{\mu_t}\, dA \qquad (6.15)$$

The source term linearisation procedure described in Chapter 2 is now used to rewrite equation (6.15) as

$$\int_i N\, C_\mu\, \rho^2 \frac{k^2}{\mu_t}\, dA = \int_i N \frac{C_\mu\, \rho^2}{\mu_t} \left(k^{*2} + 2k^*(k - k^*) \right) dA \qquad (6.16)$$

Rearranging equation (6.16)

$$\int_i N\, C_\mu\, \rho^2 \frac{k^2}{\mu_t}\, dA = \int_i N \frac{C_\mu\, \rho^2}{\mu_t} k^*(2k - k^*)\, dA \qquad (6.17)$$

The independent variables, ρ, μ_t and k are replaced by $N_j\rho_j$, $N_k\mu_{tk}$ and N_lk_l respectively. Also using the lumped mass approach described in chapter 2, equation (6.17) can be written as

$$\int_i N\, C_\mu\, \rho^2 \frac{k^2}{\mu_t}\, dA = -\int_i N_i\, C_\mu \frac{(N_j\rho_j)^2}{N_k\mu_{tk}} (N_Tk_l^*)^2\, dA + \int_i N_i\, C_\mu \frac{(N_j\rho_j)^2}{N_k\mu_{tk}} N_Tk_l^*\, 2N_Tk_l\, dA \qquad (6.18)$$

where

$$N_T = \sum_{l=1}^{3} N_l \tag{6.19}$$

Substituting equation (6.18) into equation (6.13)

$$(a_{ii}^k + b_i^k) k_i = - \sum_{j \neq i} a_{ij}^k k_j + f_i^k \tag{6.20}$$

where

$$b_i^k = \int_i N_i C_\mu \frac{(N_j \rho_j)^2}{N_k \mu_{tk}} 2 N_T k_i^* N_T \, dA \tag{6.21}$$

and

$$f_i^k = \int_i N_i N_j \mu_{tj} \left\{ 2 \left[\left(\frac{\partial N}{\partial x}_k U_k \right)^2 + \left(\frac{\partial N}{\partial y}_k V_k \right)^2 \right] + \left[\frac{\partial N}{\partial x}_k U_k + \frac{\partial N}{\partial y}_k V_k \right]^2 \right\} dA$$

$$+ \int_i N_i C_\mu \frac{(N_j \rho_j)^2}{N_k \mu_{tk}} (N_T k_i^*)^2 \, dA \tag{6.22}$$

Inspection of equations (6.21) and (6.22) reveals that none of the terms in the k equation can now become negative, hence ensuring positive values for k at all times.

The ε equation is treated in a similar manner. Eddy viscosity relation, equation (6.11), is once again invoked to rewrite the fist of the two source terms in equation (6.14), hence

$$\int_i N C_1 \mu_t \frac{\varepsilon}{k} G \, dA = \int_i N C_1 C_\mu \rho k G \, dA \tag{6.23}$$

The second term is linearised and rearranged

$$\int_1 N\, C_2\, \rho\, \frac{\varepsilon^2}{k}\, dA = -\int_1 N\, C_2\, \rho\, \frac{\varepsilon^{*2}}{k}\, dA + \int_1 N\, C_2\, \rho\, \frac{\varepsilon^*}{k}\, 2\varepsilon\, dA \qquad (6.24)$$

Using the lumped mass method and replacing the dependent variables with their discretised form, equation (6.14) can be written as

$$(a_{ii}^{\varepsilon} + b_i^{\varepsilon})\, \varepsilon_i = -\sum_{j \neq i} a_{ij}^{\varepsilon} \varepsilon_j + f_i^{\varepsilon} \qquad (6.25)$$

where

$$b_i^{\varepsilon} = \int_1 N_1\, C_2\, \frac{N_j \rho_j}{N_k k_k}\, 2 N_T \varepsilon_i^*\, N_T\, dA \qquad (6.26)$$

and

$$f_i^{\varepsilon} = \int_1 N_1\, C_2\, \frac{N_j \rho_j}{N_k \mu_{tk}}\, (N_T \varepsilon_i^*)^2\, dA \qquad (6.27)$$

$$+ \int_1 N_1\, C_1\, C_\mu\, N_j \rho_j\, N_k k_k \left\{ 2 \left[\left(\frac{\partial N_1}{\partial x} U_1 \right)^2 + \left(\frac{\partial N_1}{\partial y} V_1 \right)^2 \right] + \left[\frac{\partial N_1}{\partial x} U_1 + \frac{\partial N_1}{\partial y} V_1 \right]^2 \right\} dA$$

Negative values of ε are avoided by the fact that all the terms in equations (6.26) and (6.27) are positive. The discretised equations for k and ε, equations (6.20) and (6.25), are now in forms suitable for turbulent flow analyses.

6.3 Boundary conditions

The types of boundary conditions for turbulent flow are the same as those for laminar flow as discussed in Chapter 4. They are inflow, outflow and solid boundaries and planes of symmetry. The treatment of boundary conditions for the mean flow variables, U, V and P follows exactly from that of section 4.3 and is not repeated here. Boundary conditions for the turbulent quantities, μ_t, k and ε are considered in

this section.

6.3.1 Inlet boundaries

At the inflow boundaries, inlet values of k and ε are specified. From these values the eddy viscosity, μ_t, at inlet is calculated. Prescription of k and ε at these boundaries is not as straight forward as specifying velocities. In the absence of any other information regarding the turbulent nature of the flow at inlet, previously measured values of turbulent intensity and length scales are used to determine values of k and ε. This method has in fact proved most successful in analysing turbulent flows. However, measured values of such quantities are not readily available and dependence on such information restricts the generality of the turbulence model. Alternatively, estimated values of turbulent intensity can be assumed at inlet as suggested by previous workers for a wide ranging classes of flow. In this research a turbulent intensity of 5% is assumed, i.e.

$$I = \frac{u}{U_{inlet}} = \frac{v}{U_{inlet}} = 5\% \qquad (6.28)$$

where U_{inlet} is the predominant mean velocity component at the inlet. It follows that the turbulent kinetic energy, k, at the inlet can be determined from

$$k_{inlet} = \frac{3}{2} (IU_{inlet})^2 \qquad (6.29)$$

The rate of dissipation of turbulent energy, ε, can be determined from

$$\varepsilon_{inlet} = \frac{C\, k_{inlet}^{1.5}}{l} \qquad (6.30)$$

where l is the characteristic length scale and C is a constant. The

commonly used values covering a wide range of flow cases are

$$C = C_{\mu} \quad \text{and} \quad l = 0.01\ D \tag{6.31}$$

where D is the width of flow at inlet. The value of μ_t at inlet can now be evaluated using equation (6.11).

6.3.2 Outlet boundaries

At the outlet boundaries natural boundary conditions are applied for k and ε. The natural boundary conditions arise from the Finite Element discretisation of the diffusion terms in the two transport equations, equations (6.8) and (6.10), similar to those derived in Chapter 2. From equation (6.8), the diffusion term is discretised as

$$\int N \left\{ \frac{\partial}{\partial x} \left(\frac{\mu_t}{\sigma_k} \frac{\partial k}{\partial x} \right) + \frac{\partial}{\partial y} \left(\frac{\mu_t}{\sigma_k} \frac{\partial k}{\partial y} \right) \right\} dA = \tag{6.32}$$

$$\int N \frac{\mu_t}{\sigma_k} \frac{\partial k}{\partial n} ds - \int \left\{ \frac{\partial N}{\partial x} \left(\frac{\mu_t}{\sigma_k} \frac{\partial k}{\partial x} \right) + \frac{\partial N}{\partial y} \left(\frac{\mu_t}{\sigma_k} \frac{\partial k}{\partial y} \right) \right\} dA$$

where the first term on the right hand side is the surface integral term, n being the direction of the outward normal. The natural boundary condition at the outlet implies that the rate of change of k with respect to n is zero. Therefore in imposing this type of boundary condition, the surface integral term in equation (6.32) is set to zero. Similarly the surface integral term for the discretised form of equation (6.10) is also set to zero at the outlets. Note that these surface integrals are identically zero on all internal elemental surfaces.

6.3.3 Solid boundaries

Near solid boundaries the flow of fluid is only partially

turbulent. However, equations (6.8) and (6.10) are only applicable in fully turbulent flow regions. Therefore, in treating regions of flow near solid boundaries, the wall function method is employed. In the wall function approach, the wall shear stress is deduced from the Law of the Wall and the Log Law of the Wall. The two laws in fact govern the variation of velocity very close to and further away from the wall respectively. Hence, the wall shear stress is determined such that the near wall velocity varies according to the above two laws. By combining the two laws, the need for excessively fine mesh near this region is avoided.

The Law of the Wall is (White (1974))

$$u_\delta = \delta \frac{\tau_w}{\mu} \tag{6.33}$$

where δ is the perpendicular distance away from the wall, u_δ is the velocity parallel to the wall, τ_w is the wall shear stress and μ is the laminar dynamic viscosity. The Log Law of the Wall is

$$\frac{u_\delta}{\sqrt{\tau_w/\rho}} = \frac{1}{\kappa} \ln \left(\frac{\delta}{\upsilon} \sqrt{\tau_w/\rho} \right) + B \tag{6.34}$$

where κ is the Kolmogorov constant (= 0.4) and B is a non-dimensional constant which is taken to have the logarithmic form

$$B = \frac{1}{\kappa} \ln E \tag{6.35}$$

where E is a non-dimensional constant (= 9.0 for smooth walls) and introducing δ^+

$$\delta^+ = \frac{\delta}{\upsilon} \sqrt{\tau_w/\rho} \tag{6.36}$$

equation (6.34) can be written as

$$\frac{u_\delta}{\sqrt{\tau_w/\rho}} = \frac{1}{\kappa} \ln E\delta^+ \qquad (6.37)$$

Equations (6.34) and (6.37) are combined into one equation and written as

$$\tau_w = \mu_w \frac{u_\delta}{\delta} \qquad (6.38)$$

where

$$\mu_w = \mu \cdot \text{Max} \left\{ 1 , \frac{\kappa \delta^+}{\ln E\delta^+} \right\} \qquad (6.39)$$

In this way the perpendicular distance from the wall determines which law is selected for subsequent calculations. The wall function approach outlined above has been employed by a number of researchers, e.g. Hutton (1979) and Pun and Spalding (1977). The deficiency of equation (6.39) is that δ^+ depends on τ_w. This deficiency is overcome by employing the Generalised Log Law of Launder and Spalding (1974), that is δ^+ can be written as

$$\delta^+ = \frac{C_\mu^{0.25} \rho \, k^{0.5}}{\mu} \delta \qquad (6.40)$$

At the solid boundaries mean velocity components are set to zero. At the near wall regions, effective viscosity expressed by equation (6.39) is used in the diffusion terms of the mean velocity transport equations.

In the k equation, at the wall region, the generation term, G, is expressed in terms of the wall shear stress τ_w

$$G = \tau_w \frac{u_\delta}{\delta} \qquad (6.41)$$

where τ_w itself is calculated from equations (6.38) and (6.39). The eddy viscosity, μ_t, is replaced by μ_w in the dissipation source term of the k equation, equation (6.22), for near wall regions. At the wall, values of k are decoupled from those at the near wall region and do not contribute to the solution for k. Therefore a zero gradient boundary condition for k is effectively imposed at the wall.

The dissipation rate, ε, is dominated by the turbulent length scale near the wall. For near wall regions, ε is calculated from (Pun and Spalding (1977))

$$\varepsilon_\delta = \frac{C_\mu^{0.75}\, k_\delta^{1.5}}{\kappa\, \delta} \qquad (6.42)$$

6.3.4 Planes of symmetry

At planes of symmetry, the natural boundary conditions, i.e. zero gradients, are used for both k and ε. Hence their treatment follows those of outlet boundaries.

6.4 Computational aspects

The overall computational sequence for isothermal turbulent flow analysis is shown in Figure 6.1. It differs slightly from the flowchart for laminar flow calculations shown in Figure 5.1. The energy equation becomes redundant and two other differential equations, namely those for k and ε, are now solved during each cycle. The imposition of boundary conditions for mean velocity components and mean pressure follow exactly from Chapter 4. The inlet values for k and ε are specified through equations (6.29) and (6.30) respectively. Zero gradient boundary conditions are applied for k and ε along the solid boundaries and the outlets. The initial values for k and ε

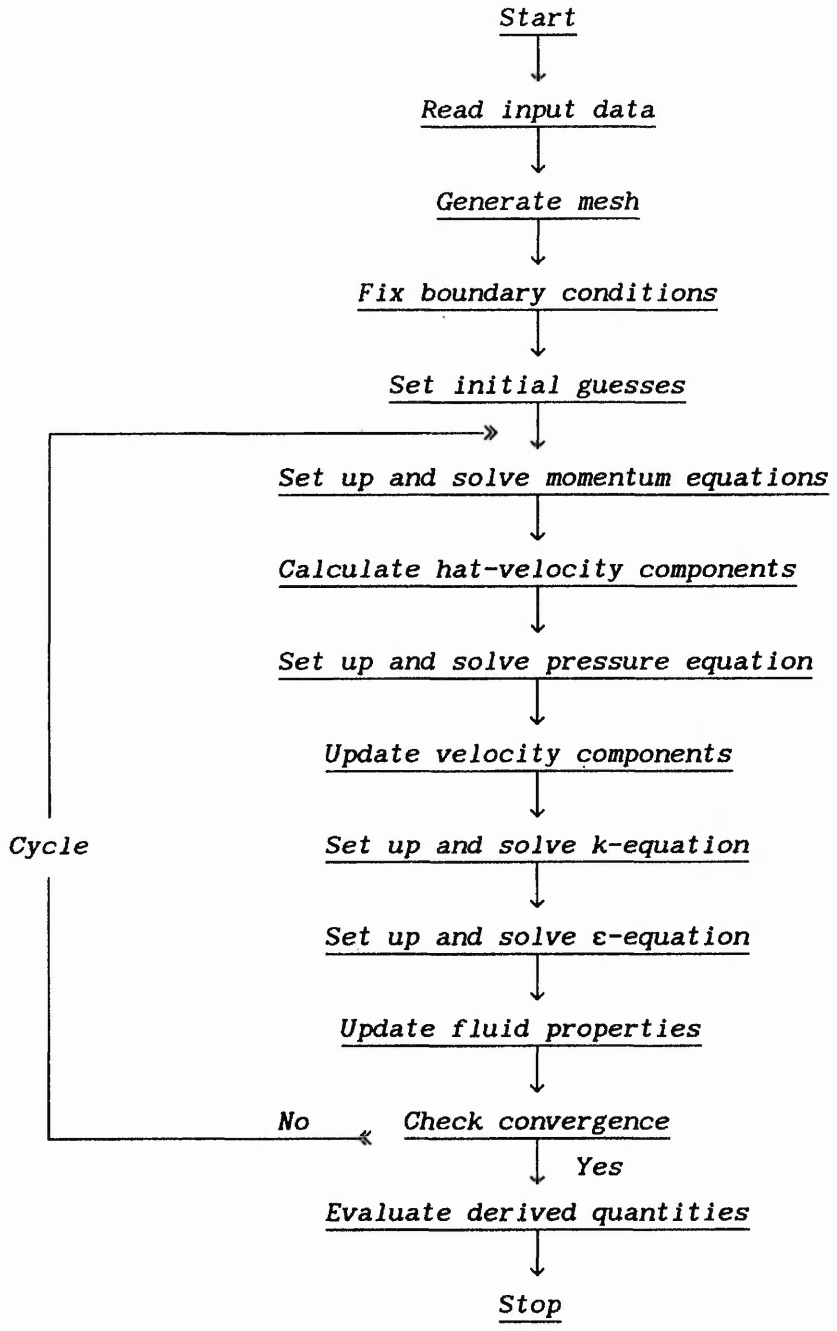

Figure 6.1 Program flowchart for turbulent flow calculations.

elsewhere within the domain may be set equal to the inlet values in the absence of any other data. This will provide a better starting point for the calculations than zero fields. The momentum and pressure equations are solved by the same procedure outlined in Chapter 4. In setting up the k-equation, the source term, G, for the near wall region is modified according to equation (6.41). Similarly, the turbulent dissipation rate, ε, near the wall region is determined from equation (6.42). The discretised equations for the turbulent quantities (equations (6.20) and (6.25)) are solved by the same line-by-line TDMA method described in Chapter 5. From the newly calculated values of k and ε, the turbulent viscosity, μ_t, is updated according to equation (6.11) in the fully turbulent region. The near wall viscosity is calculated from equation (6.39). Solution convergence is ensured by the use of under-relaxation for k and ε. Under-relaxation is performed implicitly as described in section 5.3. The amount of under-relaxation is strongly dependent on the flow conditions. A value of 0.5 was found to provide a satisfactory convergence rate. Although higher values were also employed to produce faster convergence properties. The above cycle is repeated until the pre-specified convergence criteria were fully satisfied. The convergence checks for the mean velocity and pressure fields were those discussed in section 5.4. The only convergence criterion used for the turbulent quantities was the percentage residual check (equation (5.13), where the inlet values of k and ε provided the reference data.

Similar to the laminar case, the above cycle shows the general route through the various parts of the program. Under parabolic flow conditions, this route is shortened considerably. The solution is

obtained in a marching fashion, where only one slab of the domain in the streamwise direction is considered at a time. The streamwise velocity is obtained with a guessed pressure gradient. The cross-stream velocity is calculated from the continuity equation. The pressure equation becomes redundant and the turbulence quantities are also evaluated for the given slab. A new estimate to the pressure gradient is calculated and the procedure is repeated until the convergence criteria are fully satisfied before moving on to the next slab.

CHAPTER 7

SUMMARY AND RECOMMENDATIONS

7.1 Summary

This research was concerned with the development of an efficient Finite Element program for the analysis of conjugate fluid flow/heat transfer problems. The fluid flow conditions were limited to that of an incompressible, steady state two-dimensional laminar/turbulent flow. In Chapter 2, the general sets of governing transport equations for both laminar and turbulent transient flow regimes in three-dimensional Cartesian coordinate system were presented. The sets were simplified for the cases of steady-state two-dimensional laminar flow with heat transfer and isothermal turbulent flow. In deriving the turbulent flow equations a time-averaging approach was followed. The sets of equations were then used as the basic flow equations in the subsequent chapters. The Galerkin weighted residual approach was presented by discretising the Poisson's equation in two-dimensions. It was shown that the Galerkin apprcach was the most appropriate method for this research. It offered the accurate imposition of boundary conditions encountered in fluid flow analysis. The linear three-noded triangular shape was selected as the basic element for this research. The selection was based on physical, computational and geometrical considerations. The use of triangular elements ensured the unconditional dominance of the diagonal terms in the fully assembled global coefficient matrix, hence allowing the use of efficient iterative solution tecniques.

A new advection model was introduced in Chapter 3. The model was monotonic and conservative and was based on the physical processes involved in the advection transport. The model used upwinding along the streamline segment passing through each element. The model was thus discontinuous not only amongst elements but also within each individual element. The upwinding resulted in the diagonal dominance in the element matrix. This in turn ensured diagonal dominance in the fully assembled global coefficient matrix. Three stringent test cases were employed to determine the accuracy, stability and efficiency of the proposed model. These were the pure advection skew to mesh, the Smith and Hutton case and the pure advection on a rotating disk. The results were compared with other formulations currently in use. This exercise showed that the present model captures the physics of the advection phenomenon more accurately. The degree of numerical diffusion in the model was minimal and comparable with the best of the previously published results. The model also showed unconditional stability by predicting results without any spatial oscillation for the entire range of the flow Peclet number. Exact integrations were employed in evaluating the element integrals, which increased the computational efficiency of the model. The upwinding used the same element shape functions as those in the Galerkin method. This allows for the straightforward incorporation of the present advection model into other Finite Element programs which employ the Galerkin method.

A new equal-order velocity-pressure formulation was presented in Chapter 4. The velocity and pressure fields were segregated and solved sequentially. The solution sequence is similar to the SIMPLER algorithm employed in FVM. The momentum equations were discretised by employing the streamline upwind model for the advection terms and the

conventional Galerkin method for the viscous terms. The pressure gradient terms were approximated by assuming a known pressure field. A separate Poisson-type pressure equation was derived from the continuity equation. The pressure equation hence carried the physical constraint of satisfying the mass conservation. The discretisation of the energy equation was similar to that for the momentum equations. The velocity components were first obtained with a guessed pressure field. New estimates to the pressure were calculated from the pressure equation. The velocity fields were then updated with the new pressure field. The solution to the energy equation provided the temperature field. The above sequence would be repeated until the velocity, pressure and temperature fields converged to a final solution. The imposition of both essential and natural boundary conditions for all the variables were also given. The discretisation processes for all the variables produced diagonally dominant matrices, which could then be solved by an efficient iterative scheme as opposed to direct or semi-direct solvers.

In Chapter 5, the overall format of the laminar flow program was shown. This format is similar to other programs employing the FVM. The format is modular and future alterations or additions to the program are easily facilitated. The program was organised in such a way as to take advantage of the nature of the flow under consideration thereby minimising the required computational effort. For elliptic flows, the full solution sequence described above would be employed. Under parabolic flow conditions a marching solution sequence would be activated. The solution would then proceed one layer at a time along the predominant flow direction. An iterative solution procedure named RADIS and based on the TDMA solution sequence was developed. RADIS was

designed for completely unstructured grids generated by the FEM. RADIS worked on individual regions within the domain of interest, hence distinguishing between the different flow regimes present in those regions. RADIS required minimum computer storage which increased linearly with the number of nodes in the domain with only the non-zero coefficients being stored. The computer storage was unaffected by the global node/element numbering. RADIS had a convergence rate similar to that of the conventional ADI procedure.

The accuracy, efficiency and robustness of the program in predicting the flow characteristics for several laminar flow cases were examined. These were parallel duct flow, flow over backward facing step, thermal cavity and plane jet impingement with heat transfer. The current predictions were compared with the analytical values or previously published experimental or numerical data. The fully developed duct flow was predicted exactly. The developing duct flow predictions were very close to past numerical data and were to within 2.5% of the analytical results. The backward facing step flow was analysed for the Reynolds number range of 100 to 1000. The primary reattachment point was predicted to within 22% of the experimental data in all cases. The thermal cavity flow was analysed for the Rayleigh number range of 10^3 to 10^6. The agreement between the current predictions and the benchmark results was to within 38% . The analysis of the plane jet impinging on a heated flat plate provided the Nusselt number variation along the fluid/solid interface. The Nusselt number predictions came to within 8% of the previous experimental and numerical data. However due to the incorrect weighting of the advection terms for the jet impimngement case, the results should only serve to provide a qualitative estimate of the pressure and Nusselt

number variations along the impingement surface.

Spurious pressure modes were absent in all of the current predictions. The pressure field was obtained without the need for any additional relaxing or smoothing procedures. The robustness of the program in providing converged solutions under varying flow configurations and boundary conditions was established. The overall efficiency of the program in handling large numbers of elements was demonstrated.

In Chapter 6, the turbulence closure was presented. The two equation k-ε model was employed to calculate the turbulent viscosity. In the vicinity of solid walls, the Law of the Wall and the Log Law of the Wall were combined. This eliminated the need for excessive mesh refinement near solid walls. The imposition of boundary conditions for the turbulent kinetic energy and its dissipation rate were described. Three cases of turbulent flow were analysed. These were developing duct flow, backward facing step flow and plane jet impingement. The results of all the turbulent cases were provided separately in Appendix B. This was due to an incorrect weighting of the advection terms and the omittion of some of the turbulent diffusion terms. The adopted turbulence model was capable of providing the major features of turbulent flows in a variety of flow configurations and boundary conditions.

In general, the present research has demonstrated the ability of the FEM in predicting the main flow characteristics for different geometries and boundary conditions, accurately and efficiently. Some novel features had to be introduced in order to achieve this goal.

These were the stable treatment of the advection terms, the equal-order velocity pressure formulation, the velocity-pressure segregation and the use of an iterative solution algorithm. The relative simplicity of the present formulation was maintained by the use of simplex elements for which exact integration formulae exist.

7.2 Recommendations for further work

The following recommendations are aimed to provide possible directions for future work with respect to the present research:

1. The accuracy and the stability of the streamline upwind formulation should be examined more rigorously. This might be achieved by considering other test cases possibly in the presence of a source term. To examine the degree of conservatism offered by the formulation, test cases with variable fluid properties could be employed.
2. The extension of the streamline upwind formulation to three-dimensions and also to other coordinate systems, especially the cylindrical system, should be investigated. The time-dependent version of the formulation could open more insight into its behaviour.
3. The application of the segregated velocity-pressure formulation should be examined more thoroughly. This should include the examination of the laminar jet impingement with heat transfer with the correct advection weighting. Problems which include fluids with variable properties, and even non-Newtonian fluids should be considered. Compressible versions of the formulation could be developed. Its extension to other coordinate systems and to three-dimensions should be relatively easy and would require mathematical manipulations without the need for further novelties.

The transient version of the formulation could be derived by employing inertial relaxation techniques.

4. The convergence properties of the velocity-pressure formulation should be examined closely. Any improvement on the convergence rate would obviously make the whole program more efficient. Algorithms based on SIMPLEST (Spalding (1980)), SIMPLEC (van Doormaal and Raithby (1984)) or PISO (Issa (1985)) schemes could quite readily be formulated.
5. The iterative solver may be made to converge faster by increasing the spatial coupling between the nodes. This could be achieved by, say the SIP (Stone (1968)) scheme. Also, a Multigrid method could be developed for which the current solver would act as the initial smoother.
6. The adaptation of the iterative solver for other element types in both two- and three-dimensions could provide a very efficient solution method for the unstructured grids frequently encountered in the FEM.
7. The accuracy of the k-ε model in conjunction with the FEM should be investigated by incorporating the correct weighting for the advection terms and including the missing turbulent diffusion terms. Since, the streamline upwind formulation provided an accurate approximation to the advection terms, the applicability of the k-ε model itself could then be assessed more precisely. This could include the revision of the constants used in the model.
8. The segregated approach of the present Finite Element formulation allows the efficient examination of other turbulence models in conjunction with the FEM. In particular, the performance of the Algebraic Stress or the Reynolds Stress models could be investigated.

APPENDIX A

EVALUATION OF ELEMENT COEFFICIENT MATRIX

Assuming unit diffusivity, i.e. $\Gamma_\phi = 1$, from equations (2.28) and (2.39) the element coefficient matrix reduces to

$$[\,A\,]^e = \int_{A^e} \left(\frac{\partial N_i}{\partial x} \frac{\partial N_j}{\partial x} + \frac{\partial N_i}{\partial y} \frac{\partial N_j}{\partial y} \right) dA^e \qquad (A.1)$$

A.1 Triangular element

Evaluating the above integral for a triangular element produces (see Segerlind (1976))

$$[\,A\,]^e = \frac{1}{4\Delta} \begin{bmatrix} b_i b_i & b_i b_j & b_i b_k \\ & b_j b_j & b_j b_k \\ \text{Sym} & & b_k b_k \end{bmatrix} + \frac{1}{4\Delta} \begin{bmatrix} c_i c_i & c_i c_j & c_i c_k \\ & c_j c_j & c_j c_k \\ \text{Sym} & & c_k c_k \end{bmatrix} \qquad (A.2)$$

where, for the element shown in Figure 2.2(a),

$$\Delta = \text{area of triangle} = \frac{1}{2} L_{ij} L_{jk} \qquad (A.3)$$

and

$$b_i = y_j - y_k = -L_{jk} \;,\; b_j = y_k - y_i = L_{jk} \;,\; b_k = y_i - y_j = 0 \quad \text{and}$$
$$c_i = x_k - x_j = 0 \;,\; c_j = x_i - x_k = -L_{ij} \;,\; c_k = x_j - x_i = L_{ij} \qquad (A.4)$$

Using equations (A.3) and (A.4) in (A.2)

$$[\,A\,]^e = \frac{1}{2\, L_{ij} L_{jk}} \begin{bmatrix} L_{jk}^2 & -L_{jk}^2 & 0 \\ -L_{jk}^2 & L_{jk}^2 & 0 \\ 0 & 0 & 0 \end{bmatrix} + \frac{1}{2\, L_{ij} L_{jk}} \begin{bmatrix} 0 & 0 & 0 \\ 0 & L_{ij}^2 & -L_{ij}^2 \\ 0 & -L_{ij}^2 & L_{ij}^2 \end{bmatrix} \qquad (A.5)$$

With aspect ratio, λ, defined as

$$\lambda = \frac{L_{ij}}{L_{jk}} \qquad (A.6)$$

equation (A.5) finally becomes

$$[\,A\,]^e = \frac{1}{2}\begin{bmatrix} \frac{1}{\lambda} & -\frac{1}{\lambda} & 0 \\ -\frac{1}{\lambda} & \frac{1}{\lambda}+\lambda & -\lambda \\ 0 & -\lambda & \lambda \end{bmatrix} \tag{A.7}$$

A.2 Rectangular element

Evaluating the integral in equation (A.1) using 2x2 Gauss quadrature for the rectangular element shown in Figure 2.2(b), produces (see Segerlind (1976))

$$[\,A\,]^e = \frac{1}{6}\frac{L_{jk}}{L_{ij}}\begin{bmatrix} 2 & -2 & -1 & 1 \\ -2 & 2 & 1 & -1 \\ -1 & 1 & 2 & -2 \\ 1 & -1 & -2 & 2 \end{bmatrix} + \frac{1}{6}\frac{L_{ij}}{L_{jk}}\begin{bmatrix} 2 & 1 & -1 & -2 \\ 1 & 2 & -2 & -1 \\ -1 & -2 & 2 & 1 \\ -2 & -1 & 1 & 2 \end{bmatrix} \tag{A.8}$$

Using λ as defined by equation (A.6), the above equation reduces to

$$[\,A\,]^e = \frac{1}{6\lambda}\begin{bmatrix} 2+2\lambda^2 & -2+\lambda^2 & -1-\lambda^2 & 1-2\lambda^2 \\ -2+\lambda^2 & 2+2\lambda^2 & 1-2\lambda^2 & -1-\lambda^2 \\ -1-\lambda^2 & 1-2\lambda^2 & 2+2\lambda^2 & -2+\lambda^2 \\ 1-2\lambda^2 & -1-\lambda^2 & -2+\lambda^2 & 2+2\lambda^2 \end{bmatrix} \tag{A.9}$$

APPENDIX B

TURBULENT FLOW EXAMPLES

Three test cases were used to validate the accuracy of the turbulence model. The developing flow in a plane duct was chosen to test the parabolic solution sequence. The backward facing step provided the measure of accuracy, stability, efficiency and robustness of the overall formulation for a recirculating flow condition. Finally the case of a plane isothermal jet was analysed and results were compared with available experimental data. While analysing the above cases, the advection terms in the governing transport equations were incorrectly weighted by the area of the element containing the downwind node shown in Figure 3.5, rather than the correct value given by equation 3.20. This has in effect enhanced the diffusive transport by an approximate factor of two. Also there are parts of the turbulent diffusion terms, S_u and S_v in equations 6.5 and 6.6, which were omitted. Therefore the results should only be interpreted qualitatively.

B.1 Developing duct flow

This flow condition has been the subject of numerous experimental and numerical investigations in the past, e.g. Laufer (1950), Launder and Spalding (1974), Pun and Spalding (1977), Hutton (1979) and Schnipke (1986). The flow arrangement is depicted in Figure B.1, which corresponds to the experimental rig of Laufer (1950). The flow is between two smooth parallel plates separated by a distance H. The domain length is 50 H, which is long enough for the flow to assume a fully developed profile. No-slip boundary conditions are imposed along

the walls. A flat velocity profile is specified at the inlet. With 5% turbulent intensity, the inlet values of k and ε are evaluated from equations (6.29) and (6.30). The zero gradient boundary condition is specified for k along the walls. No outlet boundary conditions were required as a parabolic solution sequence was employed, see section 6.4.

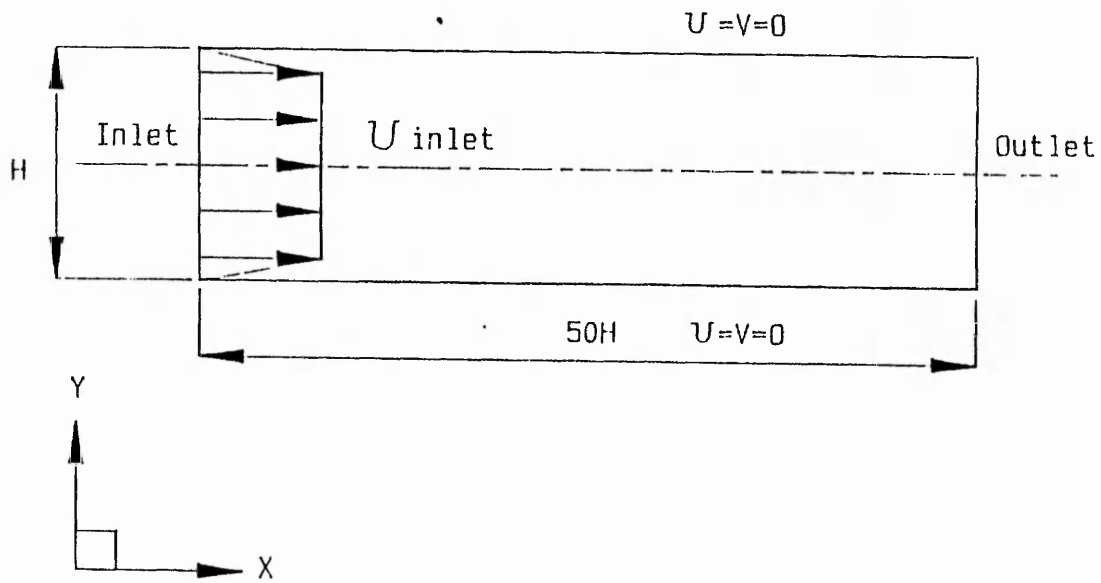

Figure B.1 Geometry and boundary conditions for developing turbulent duct flow (not to scale).

The computational domain is shown in Figure B.2. It consists of 25 rows and 31 columns giving 775 nodes and 1440 elements. The mesh is non-uniform being denser in the developing and the near wall regions, where sharp gradients in the velocity, k and ε fields are expected. Finer meshes were also employed which resulted in less than 1% change in the axial position where the centreline velocity reached 99% of its maximum value. For the current analysis a single slab, i.e. one column of elements in the x-direction, was considered at a time before moving

on to the next slab. The solution convergence was based on the mass flowrate check given by equation (5.15) with 0.01% maximum difference between the in-flow and the out-flow for each slab. The analysis was carried out with an inlet Reynolds number of 24600 based on the plate separation and the mean inlet velocity.

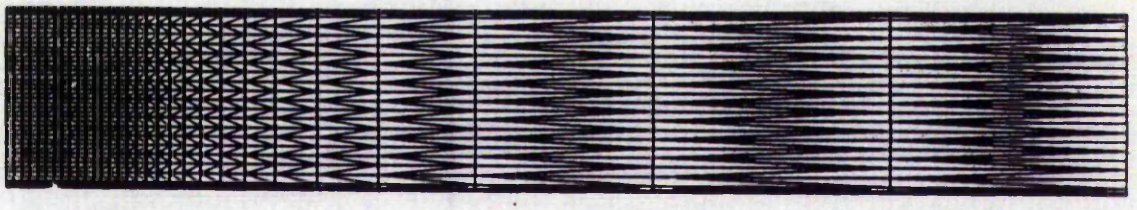

Figure B.2 Computational mesh for developing turbulent duct flow (not to scale).

The computed velocity profile at the outlet is compared with the experimental data of Laufer (1950) and the numerical prediction of Schnipke (1986) as shown in Figure B.3. The values are normalised against the centre line velocity. The agreement between the three sets of data in the near wall region is very good. The same agreement is also observed in the core of the flow around the centre line. The maximum deviation from the experimental data is 4% at x/H = 0.385. The overall agreement between the current parabolic solution and the elliptic prediction of Schnipke (1986) is also very good with a maximum difference in the predicted velocities of 9% at x/H = 0.425.

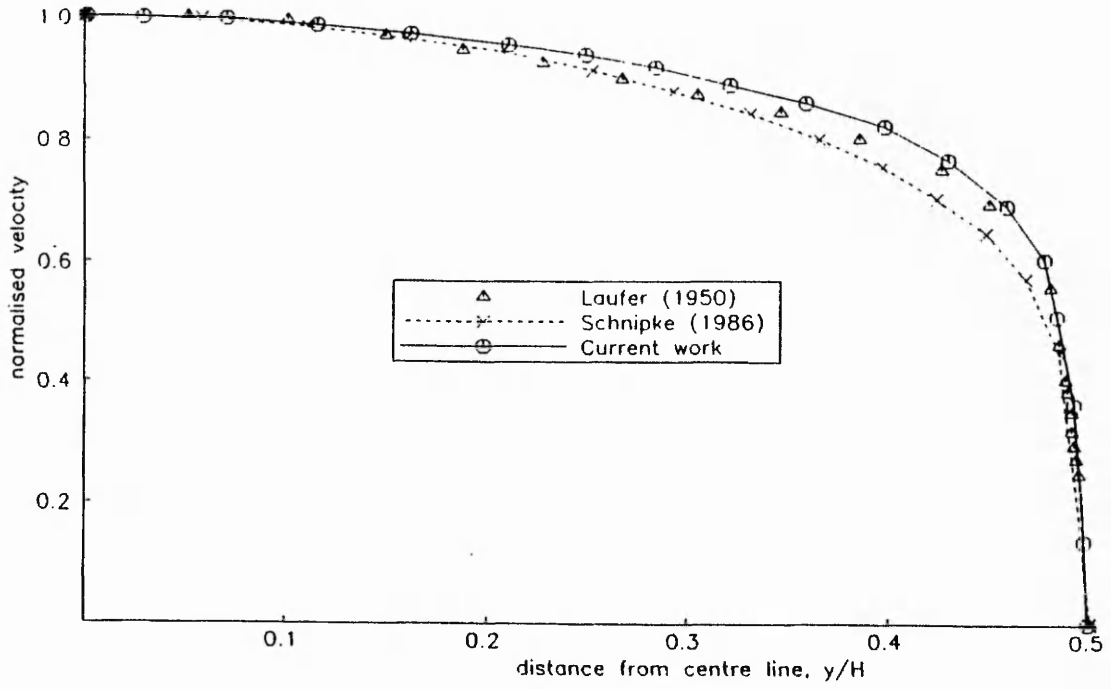

Figure B.3 Comparison of outlet velocity profiles for developing turbulent duct flow.

The above parabolic analysis was performed on a Digital VAX-8550 machine and took 13.48 seconds to complete.

B.2 Backward facing step flow

This flow is characterised by a large recirculation region downstream of the step caused by the sudden expansion in the cross sectional area. This recirculation region will strongly influence the rates of heat and mass transfer in the vicinity of the step as shown by Sparrow and Kaljes (1977). The accurate prediction of such a region is therefore of prime importance. The turbulent backward facing step flow has been studied in detail both experimentally and numerically in the past, e.g. Castro (1978), Leschziner (1980) and Armaly et al (1983). It was also the subject of the 1980-81 Stanford Conference on complex turbulent flows, Nallasamy (1985). It presents a challenging

test for the current turbulent formulation and will determine its accuracy in predicting the position of the reattachment point against the available experimental data.

The geometry and boundary conditions for this flow is shown in Figure B.4, which corresponds to the experimental rig of Armaly et al (1983). With reference to Figure B.4, they noticed that the velocity profile along the inlet channel was parabolic up to 4s behind the step. The length of the inlet channel before the step is 15mm. In the absence of any other data, the inlet velocity profile was taken as the fully developed velocity profile shown in Figure B.3. The inlet values for k and ε also corresponded to those calculated for the previous example. No-slip boundary conditions were imposed along the top and

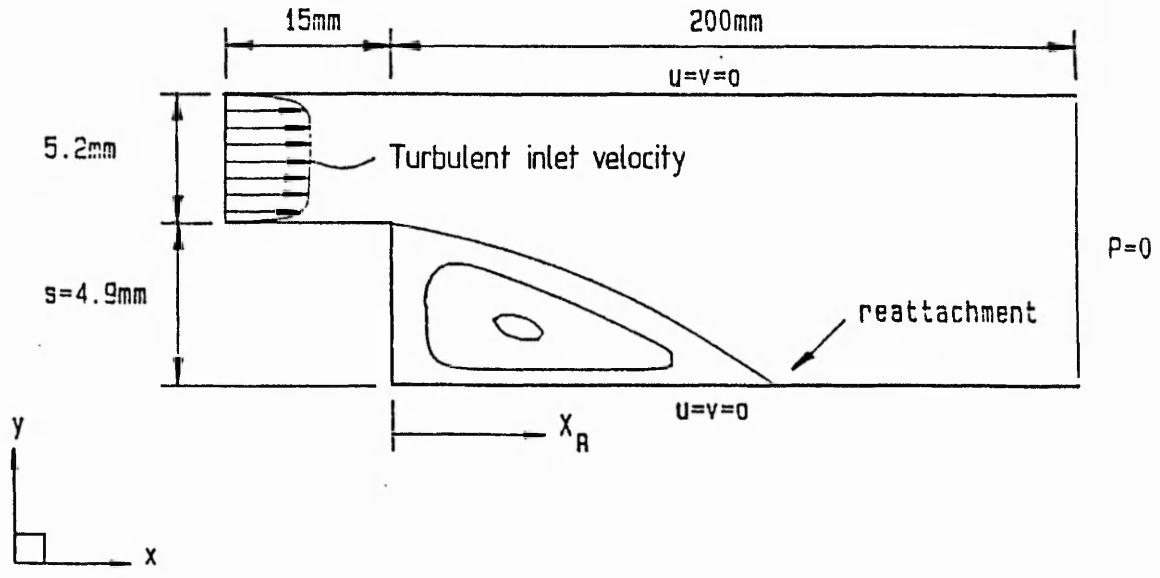

Figure B.4 Geometry and boundary conditions for turbulent backward facing step flow (not to scale).

the bottom walls. The length of the channel downstream of the step is 200mm, which is sufficiently long for the flow to approach a fully developed profile. Natural boundary conditions were used for velocity, k and ε fields at the outlet with pressure fixed at zero. The inlet Reynolds number is given by

$$Re = \frac{U_{avrg} D}{\nu} \qquad (B.1)$$

where U_{avrg} is two-thirds of the maximum inlet velocity, D is twice the channel opening at the inlet and ν is the kinematic viscosity. Armaly et al (1983) observed that the flow was fully turbulent for Re > 6600. The current analysis was performed for Re = 7000. The computational mesh is shown in Figure B.5. It is a non-uniform mesh consisting of 1682 nodes and 3190 elements. The mesh is dense around the step and near the top and bottom walls. Finer meshes were also employed which did not result in more than 5% change in the position of the reattachment point.

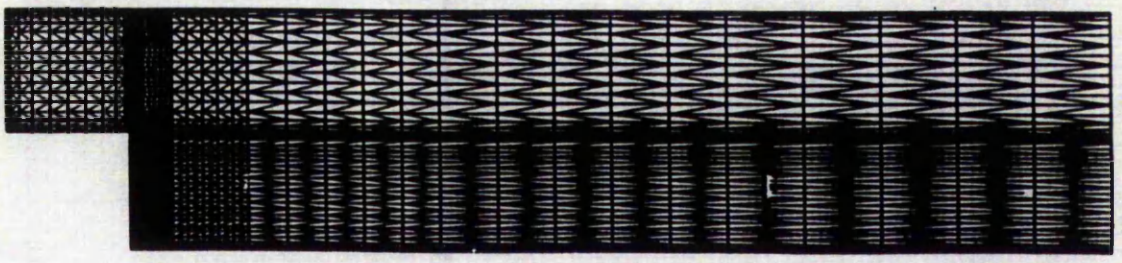

Figure B.5 Computational mesh for turbulent backward facing step flow (not to scale).

A fully elliptic solution sequence was employed for this analysis, see Figure 6.1. To avoid solution divergence, implicit under-relaxation was employed for all variables except pressure, see equation (5.5). The pressure field was relaxed through the pressure gradient terms, see equations (4.13) and (4.14). The relaxation parameters were set to 0.5 for all variables. Computations were terminated when the maximum percentage residuals and the percentage mass flowrate balance given by equations (5.13) and (5.15) respectively fell below 0.05%. The starting values for the velocity, k and ε fields throughout the domain were set to their respective maximum values prevailing at the inlet.

Figures B.6(a) and (b) show the pressure and the streamline plots near the step respectively. The pressure field is nearly one dimensional upstream of the step becoming singular at the step. It then rises through the expansion and subsequently falls further downstream of the step. Also a one-dimensional pressure field was observed along the main portion of the channel downstream of the reattachment point (not shown in the figure). The pressure field was obtained without any additional relaxing or smoothing techniques. This clearly demonstrates the success of the present formulation in providing realistic pressure fields in the absence of spurious pressure modes. The predicted location of the reattachment point on the bottom wall is shown in Figure B.6(b). This point is predicted to be 43.6mm (X_R/s = 8.8) downstream of the step. The value measured by Armaly et al (1983) was about 39.2mm ($X_R/s \simeq 8$). The current analysis is therefore overpredicting the reattachment point by about 10%. This difference is mainly attributed to the discrepancy between the prescribed inlet boundary conditions and the experimental conditions

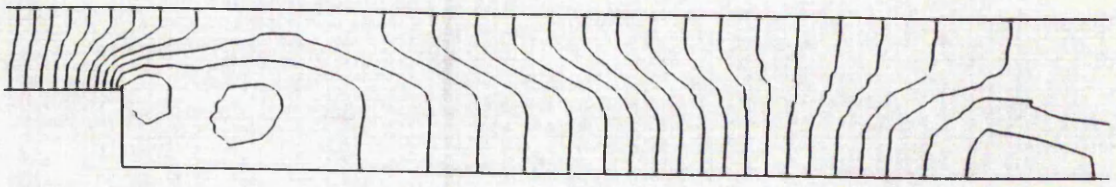

(a)

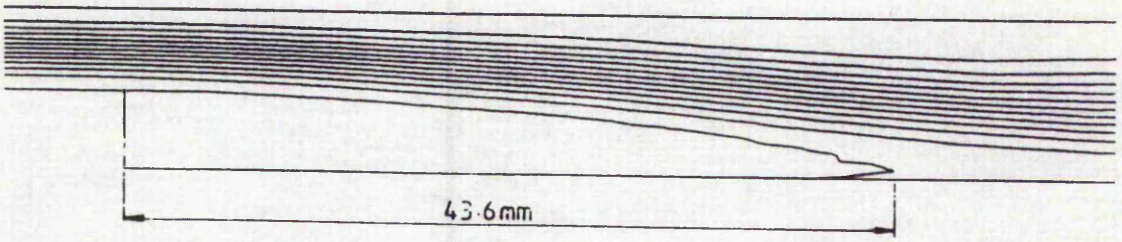

(b)

Figure B.6 Turbulent backward facing step flow at Re = 7000, (a) pressure field and (b) streamline plot.

of Armaly et al (1983). As illustrated by Hackman et al (1984), the position of the reattachment point, as well as being a function of the inlet Reynolds number, also depends strongly on the inlet conditions including those of the turbulent quantities. Nallasamy (1985) in his summary of the results for the backward facing step flow at the 1980-81 Stanford Conference, reported that even the best methods were underpredicting the reattachment point by about 10%. The computations were performed on a Digital VAX-8550 machine. The solution converged after 205 cycles and 5890 seconds.

B.3 Confined plane jet impingement

The final test case is that of a confined isothermal plane turbulent air jet impinging on a smooth flat surface. Jet impingement on a solid wall is commonly encountered in engineering practice, e.g. jets issuing from hydraulic outlet works, vertical take-off aircrafts, vectoring of fighter planes, chemical combustion devices and many more. Flow situations near solid boundaries depend strongly on the impingement conditions such as nozzle width, nozzle-to-surface separation, nozzle exit velocity and turbulent intensity and impingement angle. It is both time consuming and expensive to conduct extensive experimental studies on a case-by-case basis. Numerical modelling can on the other hand provide relatively inexpensive means of understanding the basic structure of impinging jet flow fields.

One-equation models have been employed to predict the flow characteristics under an impinging turbulent jet. These models require the specification of the turbulent length scale which must be determined from simple empirical relations, e.g. Wolfshtein (1967), Russell and Hatton (1972) and Lampinen (1985). In the latter, the

height of the channel formed between the confinement plate and the impingement surface was used as a limiting value for the length scale. The major drawback with the one-equation models is the empirical determination of the turbulent length scale which, as in the case of the turbulent velocity scale, has transport and history effects. The high Reynolds number version of the k-ε model has been most popular in analysing two-dimensional plane turbulent jets, e.g. van Heiningen (1982), Guo and Maxwell (1984) and Polat et al (1985). The algebraic stress model has also been employed, however this was shown by Looney and Walsh (1984) to perform badly in the stagnation region, where results differed markedly from the measurements.

The flow configuration for the present analysis is shown in Figure B.7. The flow is symmetric about the centre line. The separation distance between the confinement plate and the impingement surface is H. The nozzle half-width, D, is 0.125 H. The flow is extended to 30 H downstream of the stagnation point. At the inlet, a flat velocity profile is specified. With 5% turbulent intensity, inlet values of k and ε are calculated from equations (6.29) and (6.30). Along the confinement plate and the impingement surface velocities are set to zero and natural boundary conditions are imposed for k and ε. Pressure is fixed at the outlet with zero gradients for all other variables. Figure B.8 shows the non-uniform computational mesh used for this analysis. The mesh consists of 721 nodes and 1350 elements. Fine mesh grading was employed around the centre line and in the near wall regions along the confinement plate and the impingement surface. The grid independency of the results were checked for this mesh, where finer meshes resulted in less than 5% change in values of all variables at the stagnation point.

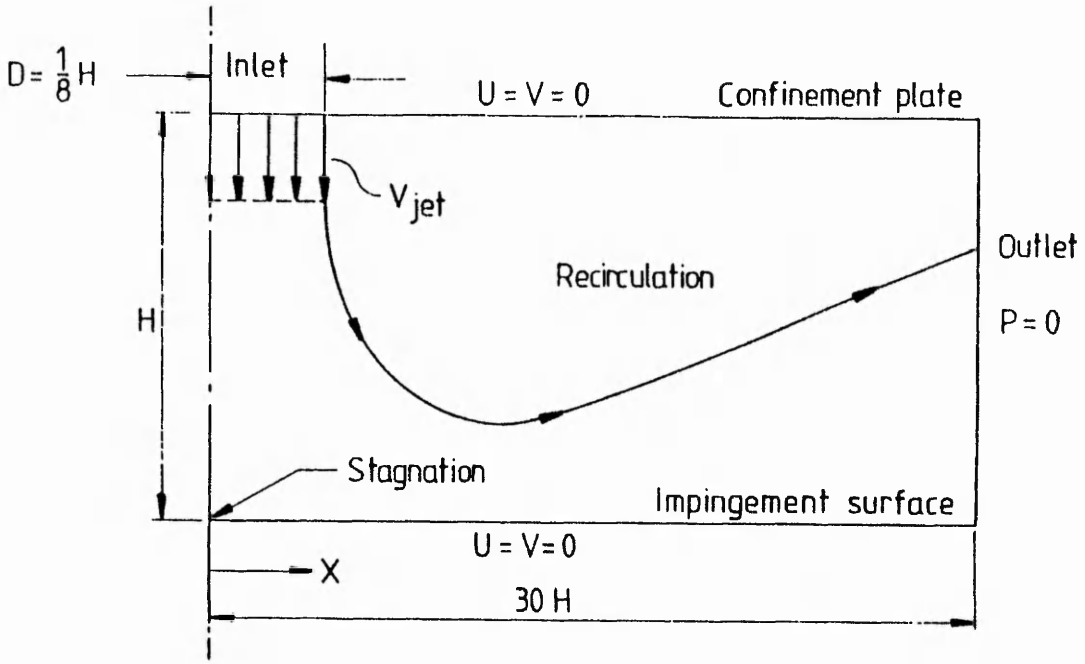

Figure B.7 Geometry and boundary conditions for confined plane turbulent jet (not to scale).

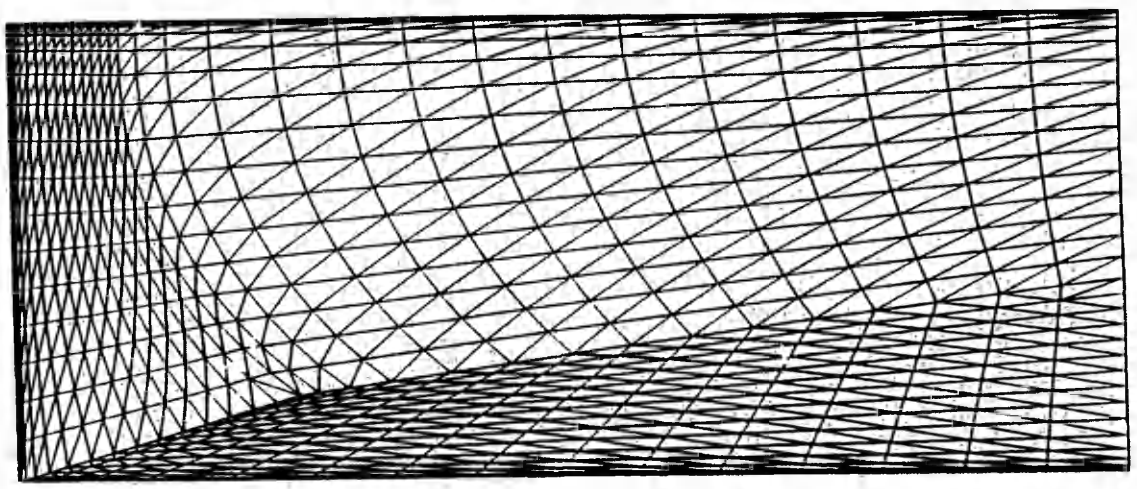

Figure B.8 Computational mesh for confined plane turbulent jet (not to scale).

The jet inlet Reynolds number is calculated as

$$Re = \frac{V_{jet} D}{\nu} \qquad (B.2)$$

where V_{jet} is the jet inlet velocity, D is the nozzle half-width and ν is the kinematic viscosity. Gardon and Akfirat (1966) regarded the plane jet to be turbulent for Re > 1000. In accordance with the studies of Gardon and Akfirat (1965), Wolfshtein (1970) and Hwang and Liu (1989), this analysis was performed for Re = 5500 and 11000.

Figures B.9(a) and (b) show the velocity vector and streamline plots for Re = 5500 respectively. The velocity field was obtained by interpolating between the nodal values of velocity along the lines of constant x. The fluid, after impinging on the bottom surface, is made to accelerate through the channel like constraint formed between the recirculation bubble and the impingement surface. The recirculation region extends to x/D = 34 and represents a very low velocity circulating fluid. The growth of the wall jet along the impingement surface is clearly visible from Figure B.9(a). This region occupies about 80% of the longitudinal flow by x/D = 34. Further downstream of this point the flow is essentially that of a developing duct flow. Figures B.10(a) and (b) show the pressure and shear stress variations along the impingement surface. From Figure B.10(a), the agreement between the experimental data of Gardon and Akfirat (1965), predictions of Hwang and Liu (1989) using FVM and the current work is very good and to within 5%. The shear stress variation is also predicted to within 3% of the previous data up to x/D = 2.5, see Figure B.10(b). The current analysis indicates a sharper fall in the shear stress after x/D =2.5, compared to the other two sets of data.

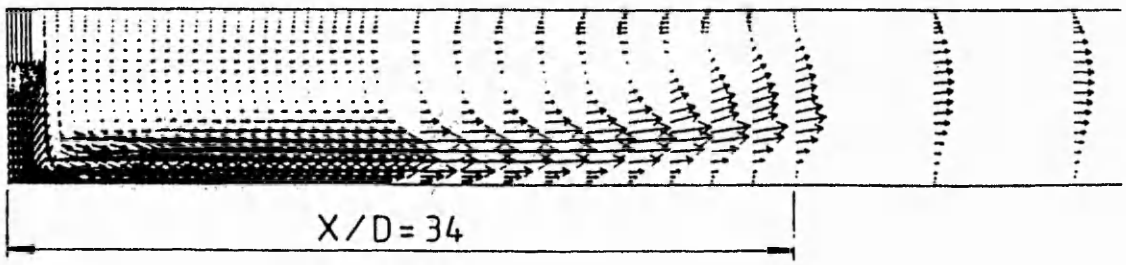

(a)

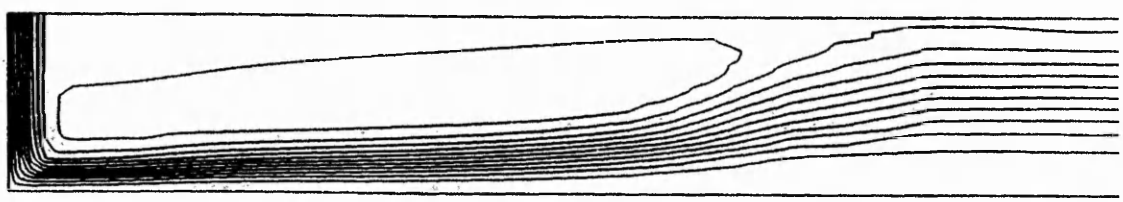

(b)

Figure B.9 *Confined plane turbulent jet at Re = 5500, (a) velocity field and (b) streamline plot.*

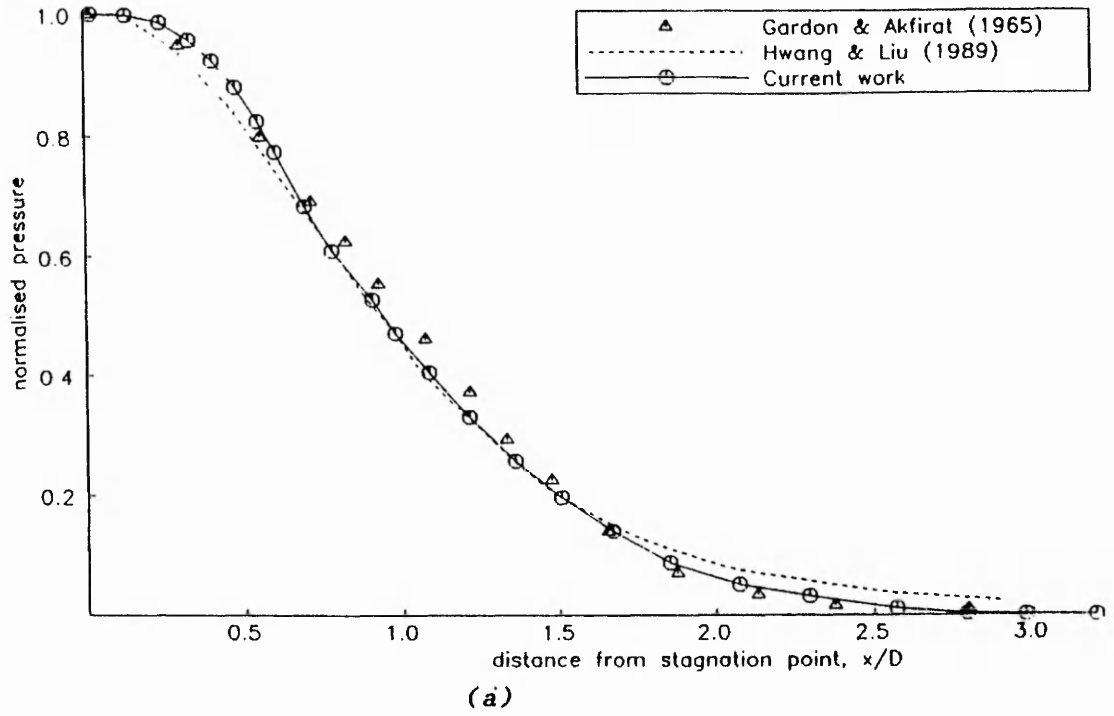

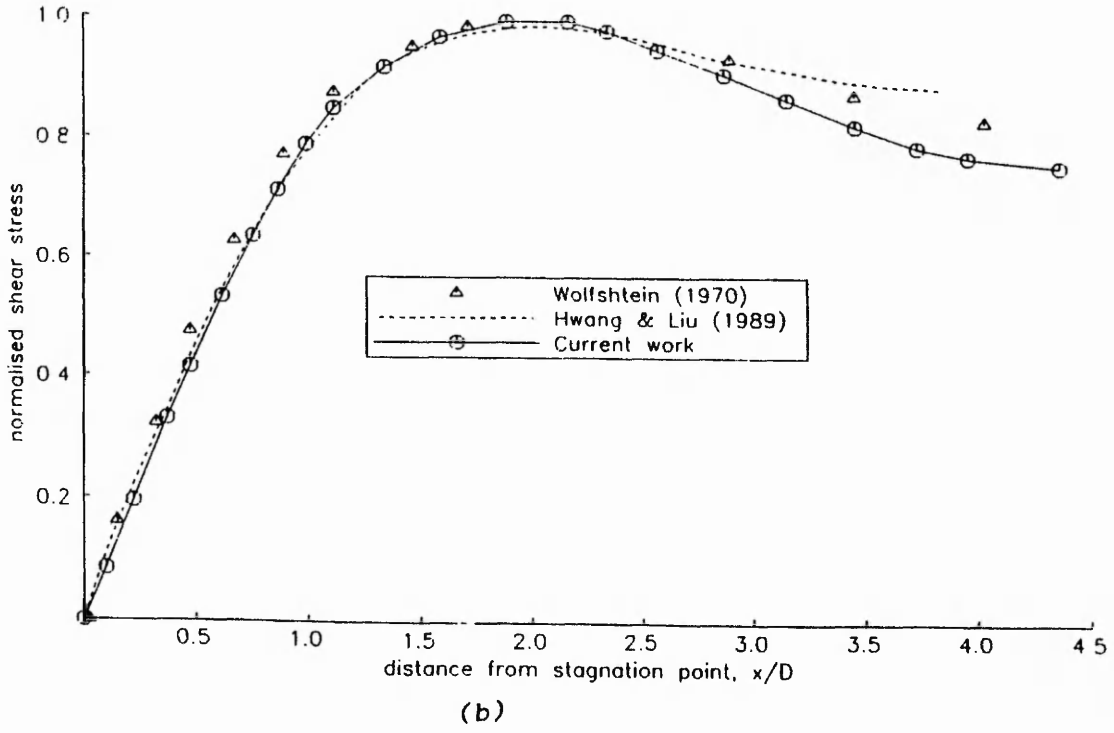

Figure B.10 Comparison of results for confined plane turbulent jet at Re = 5500, (a) pressure and (b) shear stress variations along the impingement surface.

The peak in shear stress is predicted to be at about x/D = 2, which is in excellent agreement with the other results.

Figures B.11(a) and (b) show the velocity and streamline plots for Re = 11000 respectively. The recirculation region extends to x/D = 45. The fluid outside the wall jet region is almost stagnant. Figures B.12(a) and (b) show the comparison between the current work and the previous results for Re = 11000. From Figure B.12(a), the pressure variation along the impingement surface up to x/D = 1.5 is predicted to within 5% of the experimental data of Gardon and Akfirat (1965) and the numerical solution of Hwang and Liu (1989). The results for x/D > 1.5 start to deviate from those of Hwang and Liu (1989), but remain very close to the measurements of Gardon and Akfirat (1965). The pressure drops to about 0.1% of its stagnation value at x/D = 3.0. The shear stress variations along the impingement surface are shown in Figure B.12(b). The current predictions are in very good agreement with the measurements of Wolfshtein (1970) and to within 5%. The same agreement is observed with the numerical solution of Hwang and Liu (1989) up to x/D = 1.5 after which the results start to deviate slightly. The maximum shear stress is predicted to occur at about x/D = 1.25 which is in excellent agreement with the other two data.

As for the previous test cases, the above computations were performed on a Digital VAX-8850 machine. The confined turbulent jet with Re = 5500 was started with the U-velocity, k and ε fields set initially to their corresponding maximum values at the inlet. Under-relaxation of 0.5 was used for all variables including pressure. The solution converged after 245 cycles which took 2990 seconds of the CPU time. The solution set was used as the starting point for Re =

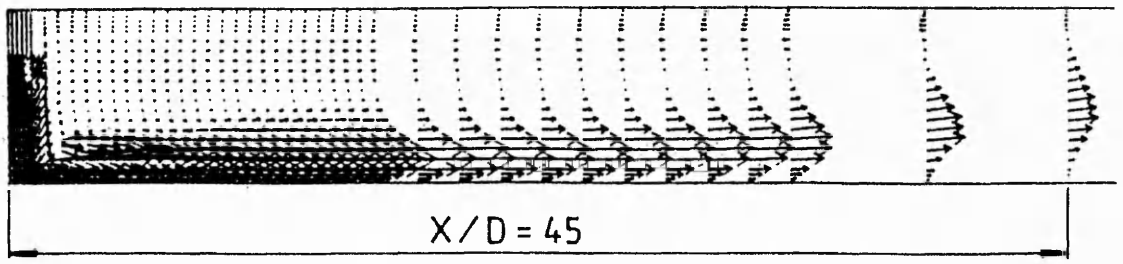

(a)

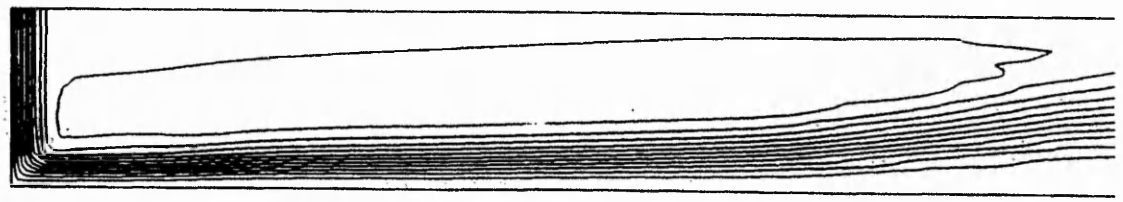

(b)

Figure B.11 Confined plane turbulent jet at Re = 11000, (a) velocity field and (b) streamline plot.

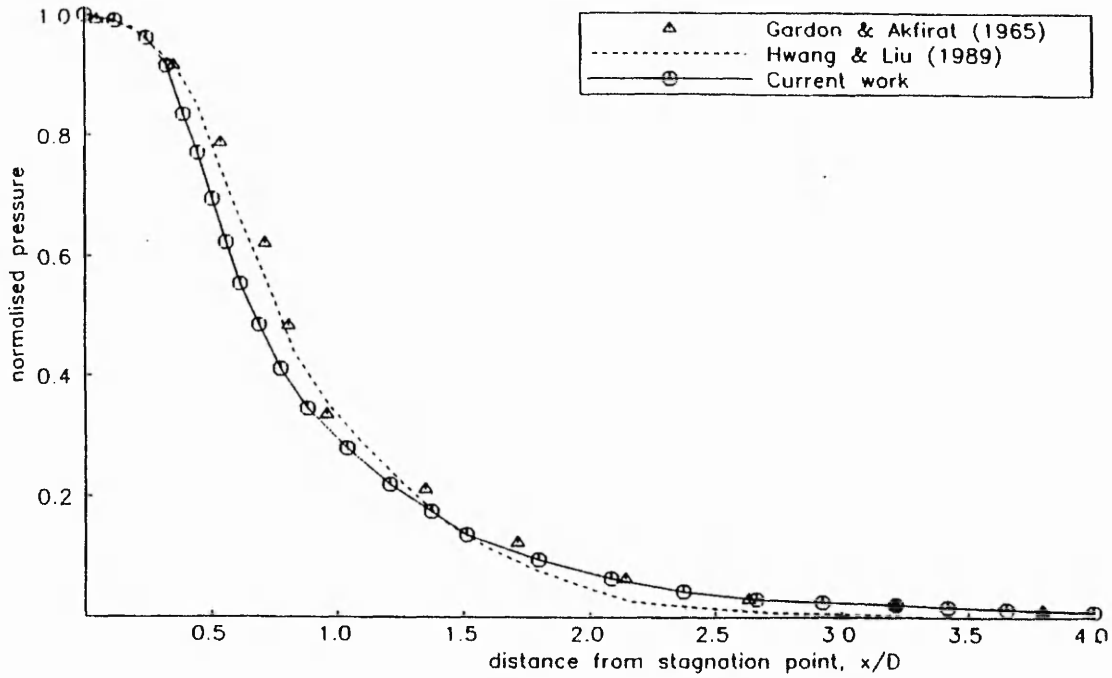

(a)

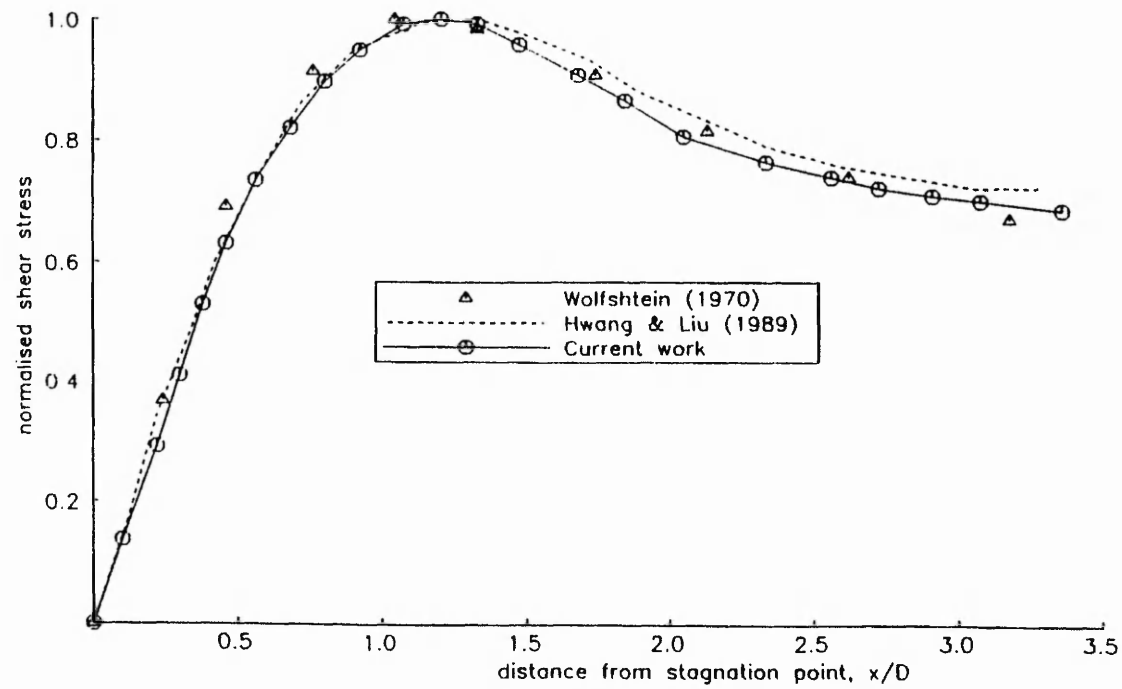

(b)

Figure B.12 Comparison of results for confined plane turbulent jet at Re = 11000, (a) pressure and (b) shear stress variations along the impingement surface.

11000. A further 185 cycles took 2100 seconds to yield the final converged solution. The convergence criteria were those of maximum percentage change and the percentage residual check with the limiting values of 0.5% and 0.05% respectively, see equations (5.8) and (5.13).

REFERENCES

1. Akyuz FA (1970), *Natural coordinate systems - An automatic input data generation scheme for a finite-element method*, Nuclear Engineering and Design, 11, 195-207.

2. Allaire PE, Rosen MC and Rice JG (1985), *Simplex Finite Element Analysis of Viscous Incompressible Flow with Penalty Function Formulation*, Finite Elements in Analysis and Design, 1, 71-88.

3. Amano RS (1984), *Development of a turbulence near-wall model and its application to separated and reattached flows*, Numer Heat Transfer, 7, 59-75.

4. Amano RS and Chai JC (1988), *Transport models of turbulent velocity-temperature products for computations of recirculating flows*, Numer Heat Transfer, 14, 75-95.

5. Armaly BF, Durst F, Periera JCF and Schonung B (1983), *Experimental and theoretical investigation of backward-facing step flow*, J Fluid Mech, 127, 473-496.

6. Baliga BR and Patankar SV (1980), *A new finite element formulation for convection-diffusion problems*, Numer Heat Transfer, 3, 393-409.

7. Baliga BR and Patankar SV (1983), *A Control Volume Finite-Element Method for Two-Dimensional Fluid Flow and Heat Transfer*, Numer Heat Transfer, 6, 245-261.

8. Baliga BR, Pham TT and Patankar SV (1983), *Solution of Some Two-Dimensional Incompressible Fluid Flow and Heat Transfer Problems Using a Control Volume Finite-Element Method*, Numer Heat Transfer, 26, 263-282.

9. Benim AC and Zinser W (1985), *Investigation into the finite element analysis of confined turbulent flows using a k-ω model of*

turbulence, Comp Meth Appl Mech Engrg, 51, 507-523.

10. Betts PL and Haroutunian V (1983), *A Stream Function Finite Element Solution for Two-Dimensional Natural Convection with Accurate Representation of Nusselt Number Variation Near a Corner, Int J Numer Meth Fluids*, 3, 605-622.

11. Biringen S and Abdol-Hamid K (1987), *Modeling and calculation of turbulent transport in free-shear flows*, Numer Heat Transfer, 11, 57-76.

12. Brandt A (1977), *Multi-Level Adaptive Solutions to Boundary-Value Problems*, Math Comp, 31(138), 333-390.

13. Brandt A and Gillis J (1966), *Magnetohydrodynamic flow in the inlet region of a straight channel*, Physics of Fluids, 9(4), 690-699.

14. Brooks AN and Hughes TJR (1982), *Streamline upwind Petrov/Galerkin formulations for convection dominated flows with particular emphasis on the incompressible Navier-Stokes equations*, Comp Meth Appl Mech Engrg, 32, 199-259.

15. Bryant CF (1985), *Two dimensional automatic triangular mesh generation*, IEEE Transactions on Magnetics, MAG-21(6), 2547-2550.

16. Buell WR and Bush BA (1973), *Mesh Generation - A Survey*, Transactions of the ASME, J Engng Industry, 332-338.

17. Burns AD, Clarke DS, Jones IP, Simcox S and Wikes NS (1988), *Turbulent flow computations in complex geometries, in: Computational Fluid Dynamics*, Eds de Vahl Davis G and Fletcher G, Elsevier Science Publishers BV, 315-327.

18. Castro IP (1978), *The numerical prediction of recirculating flows*, Proc Int Conf on Numerical Methods in Laminar and Turbulent Flow, London, UK.

19. Chen HC and Patel VC (1988), *Near-wall treatment models for*

complex flows including separation, AIAA J, 26(6), 641-648.

20. Chieng CC and Launder BE (1988), *On the calculation of turbulent transport downstream from an abrupt pipe expansion*, Numer Heat Transfer, 3, 189-207.

21. Christie I, Griffiths DF, Mitchell AR and Zienkiewicz OC (1976), *Finite Element Method for Second Order Differential Equations with Significant First Derivatives*, Int J Numer Meth Engrg, 10, 1389-1396.

22. Christie I and Mitchell AR (1978), *Upwinding for Higher Order Galerkin Methods in Conduction-Convection Problems*, Int J Numer Meth Engrg, 12, 1764-1771.

23. Chung TJ (1978), *Finite Element Analyses in Fluid Dynamics*, McGraw-Hill.

24. Courant R, Issacson E and Rees M (1952), *On the Solution of the Non-linear Hyperbolic Differential Equations by Finite Differences*, Comm Pure Appl Math, 5, 243-256.

25. Daly BJ and Harlow FH (1970), *Transport Equations in Turbulence*, The Physics of Fluids, 13(11), 2634-2649.

26. De Vahl Davis G (1983), *Natural convection of air in a square cavity: a benchmark numerical solution*, Int J Numer Meth Fluids, 3, 249-264.

27. De Vahl Davis G and Jones IP (1983), *Natural convection in a square cavity: a comparison exercise*, Int J Numer Fluids, 3, 227-248.

28. Deardorff JW (1971), *On the Magnitude of the Subgrid Scale Eddy Coefficient*, J Computational Physics, 7, 120-133.

29. Deardorff JW (1973), *The Use of Subgrid Transport Equations in a Three-Dimensional Model of Atmospheric Turbulence*, Transactions of the ASME, J Fluids Engng, 429-438.

30. Deardorff JW (1975), *Three-dimensional numerical study of the height and mean structure of a heated planetary boundary layer*, Boundary Layer Meteorology.

31. Deconinck H and Hirsch C (1979a), *Finite Element Methods for Transonic Flow Calculations*, Proceedings III GAMM Conference on Numerical Methods in Fluid Mechanics, DFVLR, Koln, 66-77.

32. Deconinck H and Hirsch C (1979b), *Subsonic and Transonic Computation of Cascade Flows*, Proceedings IV International Symposium on Computing Methods in Applied Sciences and Engineering, IRIA, Paris, 175-195.

33. Deconinck H and Hirsch C (1980), *Transonic Flow Calculations with Higher Order Finite Elements*, Proceedings VII International Conference on Numerical Methods in Flow Dynamics, Stanford, California, 138-143.

34. Demirdzic I, Gosman AD and Issa RI (1980), *A finite volume method for the prediction of turbulent flow in arbitrary geometries*, Proceedings of 7^{th} International Conference on Numerical Methods in Fluid Dynamics, Stanford, 144-150, Springer, New York.

35. Demirdzic I, Gosman AD and Issa RI (1986), *Suitability of some general coordinate versions of the fluid transport equations for numerical solution*, Imperical College Fluid Section Report FS/86.

36. Demirdzic I, Gosman AD, Issa RI and Peric M (1987), *A calculation procedure for turbulent flow in complex geometries*, Computers and Fluids, 15(3), 251-273.

37. Dendy Jr JE and Fairweather G (1975), *Alternating-Direction Methods for Parabolic and Hyperbolic Problems on Rectangular Polygons*, SIAM J Numer Anal, 12(2), 144-163.

38. Denham MK and Patrick MA (1974), *Laminar flow over a backward-facing step in a two-dimensional flow channel*, Trans Inst Chem Engrs, 52, 361.

39. Devantier BA and Larock BE (1986), *Modeling a recirculating density-driven turbulent flow*, Int J Numer Meth Fluids, 6, 241-253.

40. Dhatt G, Soulaimani A, Ouellet Y and Fortin M (1986), *Development of a New Triangular Elements for Free Surface Flows*, Int J Numer Meth Fluids, 6, 895-911.

41. Donea J (1984), *A Taylor Galerkin method for convective transport problems*, Int J Numer Meth Engng, 20, 101-120.

42. Douglas J and Dupont T (1971), *Alternating Direction Galerkin Methods on Rectangles*, Proceeding Symposium on Numerical Solution of Partial Differential Equations II, Ed Hubbard B, Academic Press, New York, 133-214.

43. Ewing RE (1986), *Efficient Adaptive Procedures for Fluid Flow Applications*, Comp Meth Appl Mech Engng, 55, 89-103.

44. Fabris G and Harsha PT (1981), *Multiple scale turbulence modelling of free turbulence flows*, ASME paper No 81-FE-20.

45. Fried I (1971), *Condition of finite element matrices generated from nonuniform meshes*, AIAA J, 10.

46. Gardon R and Akfirat JC (1965), *The Role of Turbulence in Determining the Heat-Transfer Characteristics of Impinging Jets*, Int J Heat Mass Transfer, 8, 1261-1272.

47. Gardon R and Akfirat JC (1966), *Heat Transfer Characteristics of Impinging Two-Dimensional Air Jets*, J Heat Transfer, 88, 367-375.

48. Gawain TH and Prichett JW (1970), *A unified heuristic model of fluid turbulence*, J Computational Physics, 5, 383-405.

49. Gosman AD, Khalil EE and Whitelaw JH (1977), *The Calculation of Two-Dimensional Turbulent Recirculating Flows*, Symposium on Turbulent Shear Flows, Penn State University, 1335-1345.

50. Gosman AD and Pun WM (1974), *Lecture notes for course entitled: Calculation of recirculating flows*, Heat Transfer Rep HTS/74/2, Imperial College, London, UK.

51. Gosman AD, Pun WM, Runcha AK, Spalding DB and Wolfshtein M (1969), *Heat and Mass Transfer in Recirculating Flows*, Academic Press, London, UK.

52. Green JE (1968), *The Prediction of Turbulent Boundary Layer Development in Compressible Flow*, J Fluid Mech, 31(4), 753-765.

53. Green JE, Weeks DJ and Brooman JWF (1977), *Prediction of Turbulent Boundary Layers and Wakes in Compressible Flow by a Lag-Entrainment Method*, Aero Res Counc R&M 3791.

54. Gresho PM and Lee RL (1979), *Don't supress the wiggles- They're telling us something*, in: Finite Element Methods in Convection Dominated Flows, Ed Hughes TJR, Winter annual meeting, ASME.

55. Guo CY and Maxwell WHC (1984), *Numerical Modeling of Normal Turbulent Plane Jet Impingement on a Solid Wall*, J Eng Mech, 110(10), 1498-1509.

56. Hackman LP, Strong AB and Raithby GD (1984), *The calculations of the properties of flow over a backward facing step with the k-f model of turbulence*, Transactions af the CSME, 8(3), 165-170.

57. Han T, Humphrey JAC and Launder BE (1981), *A Comparison of Hybrid and Quadratic-Upstream Differencing in High Reynolds Number Elliptic Flows*, Comp Meth Appl Mech Engrg, 29, 81-95.

58. Hansen JA and Hassager O (1989), *A New Moving Finite Element Method Based on Quadratic Approximation Functions*, Int J Numer Meth Engng, 28, 415-430.

59. Harlow FH and Welch JE (1965), *Numerical calculation of time-dependent viscous incompressible flow of fluid with free surface*, Phys Fluids, 8, 2182-2189.

60. Hassan YA, Rice JG and Kim JH (1983), *A stable mass-flow-weighted two-dimensional skew upwind scheme*, Numer Heat Transfer, 6(4), 395-408.

61. Hawken DF (1987), *Review of adaptive-grid techniques for solution of partial differential equations*, Prog Aerospace Sci, 24, 29-49.

62. Head MR (1958), *Entrainment in the Turbulent Boundary Layer*, Aero Res Counc R&M 3152.

63. Heinrich JC and Chung-Chyi Yu (1987), *On the solution of the time-dependent convection-diffusion equation by the finite element method*, Adv Water Resources, 10, 220-224.

64. Herrmann LR (1976), *Laplacian-Isoparametric Grid Generation Scheme*, J Engng Mechanics Division, EM5, 749-756.

65. Hinze O (1959), *Turbulence*, McGraw-Hill, New York.

66. Hogg S and Leschziner MA (1988), *Second-moment-closure calculation of strongly swirling confined flow with large density gradients*, Int J Heat Fluid Flow, 10(1), 16-27.

67. Hogg S and Leschziner MA (1989), *Computation of Highly Swirling Flow with a Reynolds Stress Turbulence Model*, AIAA J, 27(1), 57-63.

68. Hood P (1976), *Frontal solution program for unsymmetric matrices*, Int J Numer Meth Engng, 10, 379-399.

69. Hood P and Taylor C (1974), *Solution of Navier-Stokes equations using mixed interpolation*, Proc 1st Int Conf on FEM in Flow Problems, Swansea, 1974.

70. Huang B, Douglas WJM and Mujumdar AS (1978), *Heat Transfer Under a Laminar Swirling Impinging Jet - A Numerical Study*, Proc 6th Int Heat Tr Conf, 5, Toronto, 311-316.

71. Huang PG, Launder BE and Leschziner MA (1985), *Discretisation of*

Nonlinear Convection Processes: a Broad-Range Comparison of Four Schemes, Comp Meth Appl Mech Engrg, 48, 1-24.

72. Hughes WF and Brighton JA (1967), *Fluid Dynamics*, Schaum's outline series, McGraw-Hill.

73. Hughes TJR (1978), *A Simple Scheme for Developing 'Upwind' Finite Elements*, Int J Numer Meth Engrg, 12, 1359-1365.

74. Hughes TJR and Brooks AN (1979), *A multi-dimensional upwind scheme with no crosswind diffusion*, in: Finite Elements for Convection Dominated Flows, Ed Hughes TJR, AMD, 34, 19-35, ASME, New York.

75. Hughes TJR, Mallet M, Taki Y, Tezduyar T and Zanutta R (1983), *A one dimensional shock capturing finite element method and mutidimensional generalization*, in: Proceedings Workshop on Numerical Methods for the Compressible Euler Equations, INRIA, Rocquencourt, Dec 1983 (SIAM, Philadelphia, PA, 1985).

76. Hughes TJR, Mallet M and Mizukami A (1986a), *A new finite element formulation for computational dynamics: II. Beyond SUPG*, Comp Meth Appl Mech Engrg, 54, 341-355.

77. Hughes TJR and Mallet M (1986a), *A new finite element formulation for computational fluid dynamics: III. The generalized streamline operator for multidimensional advective-diffusive systems*, Comp Meth Appl Mech Engrg, 58, 305-328.

78. Hughes TJR and Mallet M (1986b), *A new finite element formulation for computational fluid dynamics: IV. A discontinuity-capturing operator for multidimensional advective-diffusive systems*, Comp Meth Appl Mech Engrg, 58, 329-336.

79. Hughes TJR, Franca LP and Balestra M (1986b), *A new finite element formulation for computational fluid dynamics: V. Circumventing the Babuska-Brezzi condition: A stable Petrov-Galerkin formulation of the Stokes problem accommodating equal-order interpolations*, Comp Meth Appl Mech Engrg, 59, 85-99.

80. Hutton AG (1979), *Progress in the development of a finite element wall model for high Reynolds number turbulent flow*, Appl Math Modelling, 3, 322-326.

81. Hutton AG (1985), *Current progress in the simulation of turbulent incompressible flow by the Finite Element Method*, Numerical Methods in Laminar and Turbulent Flow, 289-305.

82. Hutton AG and Smith RM (1981), *On the finite element simulation of incompressible turbulent flow in general two-dimensional geometries, in: Numerical Methods in Laminar and Turbulent Flow*, Eds Taylor C and Schrefler BA, Pineridge Press.

83. Hutton AG, Smith RM and Hickmott S (1987), *Finite Elements in Fluids*, 7, Eds Gallagher RH, Glowinski R, Gresho PM, Oden JT and Zienkiewicz OC, John Wiley & Sons Ltd, 289-309.

84. Hwang CJ and Liu JL (1989), *Numerical Study of Two-Dimensional Impinging Jet Flowfields*, AIAA Journal, 27(7), 841-842.

85. Iacovides H and Launder BE (1984), *PSL - An economical approach to the numerical analysis of near-wall, elliptic flow*, J Fluids Engng, 106, 241-242.

86. Idelsohn SR (1989), *Upwind techniques via variational principles*, Int J Numer Meth Engrg, 28, 769-784.

87. Ijam A (1977), *Finite elements in incompressible viscous flow including heat transfer*, PhD Thesis, University of Wales, Swansea, UK.

88. Ikeda T (1983), *Maximum Principle in Finite Element Models for Convection-Diffusion Phenomena*, North-Holland, Amsterdam.

89. Irons BM (1970), *A frontal solution program for finite element analysis*, Int J Numer Meth Engng, 2, 5-32.

90. Issa RI (1985), *Solution of the Implicitly Discretised Fluid Flow Equations by Operator-Splitting*, J Computational Physiscs, 62,

40-65.

91. Jambunathan K and Shemirani F (1990), *FIESTA, an Educational Interactive Finite Element Package for Heat Transfer Analysis*, Int J Appl Engng Ed, 6(3), 349-360.

92. Jambunathan K, Shemirani F and Button BL (1990), *FESTAL, a finite element scheme for thermal analysis*, Int J Appl Engng Ed, Accepted.

93. Jones RE (1974), *A Self-Organizing Mesh Generation Program*, Transactions of the ASME, J Pressure Vessel Technology, 193-199.

94. Jones WP and Launder BE (1973), *The prediction of laminairization with a two-equation model of turbulence*, Int J Heat Mass Transfer, 5, 301-314.

95. Jones JH, Schnipke RJ and Rice JG (1989), *FLOW2D-T-PC: A two-dimensional finite element turbulent flow PC computer code*, Comp Eng Proc ASME Int Comput Eng Conf 3, 2, 407-417.

96. Kaluarachchi JJ and Parker JC (1989), *An Efficient Finite Element Method for Modeling Multiphase Flow*, Water Resources Research, 25(1), 43-54.

97. Kaul UK and Kwak D (1986), *Computation of internal turbulent flow with large separated flow region*, Int J Numer Meth Fluids, 6, 927-937.

98. Kay JM and Nedderman RM (1974), *An Introduction to Fluid Mechanics and Heat Transfer*, Third edition, Cambridge University Press.

99. Kawahara M and Umetsu T (1986), *Finite Element Method for Moving Boundary Problems in River Flow*, Int J Numer Meth Fluids, 6, 365-386.

100. Kershaw DS (1978), *The incomplete Cholesky-conjugate gradient method for the iterative solution of systems of linear equations*,

J Comp Physics, 26, 43-65.

101. Kim SW (1988), *A Fine Grid Finite Element Computation of Two-Dimensional High Reynolds Number Flows*, Computers & Fluids, 16(4), 429-444.

102. Kim SW and Decker RA (1989), *Velocity-Pressure Integrated Versus Penalty Finite Element Methods for High-Reynolds-Number Flows*, Int J Numer Meth Fluids, 9, 43-57.

103. Kwak D, Reynolds WC and Ferzinger JH (1975), *Three-dimensional time-dependent calculation of turbulent flow*, Stanford University, Dept Mechanical Engineering Report TF-5.

104. Lam CKG and Bremhorst KA (1981), *Modified Form of the k-ω Model for Predicting Wall Turbulence*, Transactions of the ASME, J Fluids Engng, 103, 456-460.

105. Lampinen MJ (1985), *Application of Turbulence Theory to the Determination of Heat Transfer Coefficients in an Airofoil Dryer*, Drying Technology, 3(2), 171-219.

106. Larock BE and Schamber DR (1981), *Approaches to the finite element solution of two-dimensional turbulent flows*, in: Computational Techniques in Transient and Turbulent Flow, Eds Taylor C and Morgan K, Pineridge Press.

107. Laufer J (1950), *Some Recent Measurements in Two-Dimensional Turbulent Channel*, Journal of Aeronautical Sciences, 17(5), 277-287.

108. Launder BE (1972), *Mathematical Models of Turbulence*, Academic Press, London, UK.

109. Launder BE (1975), *On the effect of a gravitational field on the turbulent transport of heat and momentum*, J Fluid Mech, 67, 569-581.

110. Launder BE (1986), *Low-Reynolds-Number Turbulence Near Walls*,

University of Manchester Institute of Science and Technology, Thermo-Fluids Division, Report TFD/86/4.

111. Launder BE (1988), *On the computation of convective heat transfer in complex turbulent flows*, Transactions of the ASME, J Heat Transfer, 110, 1112-1128.

112. Launder BE, Reece GJ and Rodi W (1975), *Progress in the Development of a Reynolds-Stress Turbulence Closure*, J Fluid Mechanics, 68(3), 537-566.

113. Launder BE and Sharma BI (1976), *Application of the energy dissipation model of turbulence to the calibration of flow near a spinning disc*, Letters in Heat Mass Transfer, 1, 131-138.

114. Launder BE and Spalding DB (1972), *Mathematical Models of Turbulence*, Academic Press, London, UK.

115. Launder BE and Spalding DB (1974), *The numerical computations of turbulent flows*, Comp Meth Appl Mech Engrg, 3, 269-289.

116. Law HS (1982), *Mass Transfer Due to a Confined Laminar Impinging Two-Dimensional Jet*, PhD Thesis, University of Alberta.

117. Lee RL, Gresho PM and Sani RL (1979), *Smoothing techniques for certain primitive variable solutions of the Navier-Stokes equations*, Int J Numer Meth Engrg, 14, 1785-1804.

118. Leonard BP (1979), *A Stable and Accurate Convective Modelling Procedure Based on Quadratic Upstream Interpolation*, Comp Meth Appl Mech Engrg, 19, 59-98.

119. Leschziner MA (1980), *Practical evaluation of three finite difference schemes for the computation of steady-state recirculating flows*, Comp Meth Appl Mech Engrg, 23, 293-312.

120. Leschziner MA (1989), *Modeling turbulent recirculating flows by finite-volume methods - current status and future directions*, Int J Heat Fluid Flow, 10(3), 186-202.

121. Leschziner MA and Rodi W (1981), *Calculation of annular and twin parallel jets using various discretization schemes and turbulence model variations*, J Fluids Engng, 103, 352-360.

122. Llewellen WS, Teske M and Donaldson C du P (1976), *Variable density flows computed by a second-order closure description of turbulence*, AIAA J, 14(3), 382-387.

123. Lin A and Wolfshtein M (1977), *Theoretical Study of the Reynolds Stress Equations*, Symposium on Turbulent Free Shear Flows, Penn State University, 431-438.

124. Looney MK and Walsh JJ (1984), *Mean Flow and Turbulent Characteristics of Free and Impinging Jet Flows*, J Fluid Mech, 147, 397-429.

125. Love MD (1978), *An Introduction to the Large Eddy Simulation Technique*, J Inst Nuclear Engineers, 20(2), 35-42.

126. Love MD (1980), *Subgrid Modelling Studies with Burgers' Equation, J Fluid Mech*, 100(1), 87-110.

127. Martinuzzi R and Pollard A (1989), *Comparitive Study of Turbulence Models in Predicting Turbulent Pipe Flow, Part I: Algebraic Stress and k-ω Models*, AIAA J, 27(1), 29-36.

128. McMillan OJ and Ferzinger JH (1979), *Direct Testing of Subgrid-Scale Models*, AIAA J, 17(12), 1340-1346.

129. Mizukami A and Hughes TJR (1985), *A Petrov-Galerkin finite element method for convection-dominated flows: an accurate upwinding technique for satisfying the maximum principle*, Comp Meth Appl Mech Engrg, 50, 181-193.

130. Mochimaru Y (1986), *Application of a Pressure Gradient Method to an FEM Flow Analysis*, Int J Numer Meth Fluids, 6, 351-364.

131. Monin AS and Yaglom AM (1971), *Statistical Fluid Mechanics: Mechanics of Turbulence*, The MIT Press, Cambridge, Massachusetts.

132. Muir BL and Baliga BR (1986), *Solution of Three-Dimensional Convection-Diffusion Problems Using Tetrahedral Elements and Flow-Oriented Upwind Interpolation Functions*, Numer Heat Transfer, 9, 143-162.

133. Murphy JD and Rose WC (1968), *Application of the Method of Integral Relations to the Calculation of Incompressible Turbulent Boundary Layers*, 1, Proceedings of Computation of Turbulent Boundary Layers, 1968 AFOSR-IFP-Stanford Conference.

134. Naano Y and Hishida M (1987), *Improved Form of the k-ω Model for Wall Turbulent Shear Flows*, Transactions of the ASME, J Fluids Engrg, 109, 157-160.

135. Nagano Y and Kim C (1988), *A Two-Equation Model for Heat Transport in Wall Turbulent Shear Flows*, Transactions of the ASME, J Heat Transfer, 110, 583-589.

136. Nallasamy M (1985), *A critical evaluation of various turbulence models as applied to internal fluid flows*, NAS 1.60:2474.

137. Nallasamy M (1987), *Turbulence models and their applications to internal flows: A review*, Computers and Fluids, 15(2), 151-194.

138. Nallasamy M and Chen CP (1985), *Studies on effects of boundary conditions in confined turbulent flow predictions*, NASA CR-3929.

139. Neta B and Williams RT (1986), *Stability and Phase Speed for Various Finite Element Formulations of Advection Equation*, Computers & Fluids, 14, 393-410.

140. Nikjooy M, So RMC and Hwang BC (1985), *A Comparison of Three Algebraic Stress Closures For Combustor Flow Calculations*, ASME paper No 85-WA/FE-3.

141. Obee TN and De Witt KJ (1980), *Finite Element Analysis of Free Jet Impingement*, Int J Numer Meth Engng, 15, 63-85.

142. Oden JT, Strouboulis T and Devloo PH (1987), *Adaptive finite*

element methods for high-speed compressible flows, Finite Element in Fluids, 7, Eds Gallagher RH, Glowinski R, Gresho PM, Oden JT and Zienkiewicz OC, 223-239.

143. Olson MD (1976), *Comparison of various finite element solution methods for the Navier-Stokes equations*, Proc Int Conf on Finite Elements in Water Resources, Princeton University.

144. Parakash C (1986), *An Improved Control Volume Finite Element Method for Heat and Mass Transfer, and for Fluid Flow Using Equal-Order Velocity-Pressure Interpolation*, Numer Heat Transfer, 9, 253-276.

145. Parakash C and Patankar SV (1984), *A control volume based finite element method for solving the Navier-Stokes equations using equal order velocity-pressure interpolation*, ASME paper No 84-WA/HT-39, ASME, New York, 1-9.

146. Patankar SV (1980), *Numerical Heat Transfer and Fluid Flow Analysis*, McGraw- Hill, New York.

147. Patel MK, Cross M, Markatos NC and Mace ACH (1987), *An Evaluation of Eleven Discretization Schemes for Predicting Elliptic Flow and Heat Transfer in Supersonic Jets*, Int J Heat Mass Transfer, 30, 1907-1925.

148. Patel MK and Markatos NC (1986), *An Evaluation of Eight Discretization Schemes for Two-Dimensional Convection-Diffusion Equations*, Int J Numer Meth Fluids, 6, 129-154.

149. Patel VC, Rodi W and Scheuerer G (1985), *Turbulence models for near wall and low Reynolds number flows: A review*, AIAA J, 23, 1308-1319.

150. Peaceman DW and Rachford HH (1955), *The numerical solution of parabolic and elliptic differential equations*, J Soc Ind Appl Math, 3, 28-41.

151. Penman J and Grieve MD (1987), *Self-adaptive mesh generation*

technique for the finite-element method, IEE Proceedings, 134, Part A(8), 634-649.

152. Peraire J, Zienkiewicz OC and Morgan K (1986), *Shallow water problems: a general mixed formulation*, Int J Numer Mech Engng, 22, 547-574.

153. Polansky GF, Lamb JP and Klein DE (1987), *Finite element simulation of recirculating flows with heat transfer*, Communications in Appl Numer Meth, 3, 17-22.

154. Polat S, Mujumdar AS and Douglas WJM (1983), *Heat Transfer Distribution under a Turbulent Impinging Jet - A Numerical Study*, Drying Technology, 3(1), 15-38.

155. Pollard A and Siu ALW (1982), *The Calculation of Some Laminar Flows Using Various Discretization Schemes*, Comp Meth Appl Mech Engrg, 35, 293-313.

156. Price HS, Varga RS and Warren JE (1966), *Applications of Oscillation Matrices to Diffusion-Correction Equations*, J Mathematics and Physics, 45, 301-311.

157. Pun WM and Spalding BD (1977), *A general computer program for two-dimensional elliptic flow*, Imperial College, Mech Eng Department Report HTS/76/2, London, UK.

158. Raithby GD (1976), *Skew Upwind Differencing Schemes for Problems Involving Fluid Flow*, Comp Meth Appl Mech Engrg, 9, 153-164.

159. Raithby GD, Gaplin PF and Van Doormal JP (1986), *Prediction of Heat and Fluid Flow in Complex Geometries Using General Orthogonal Coordinates*, Numer Heat Transfer, 9, 125-142.

160. Ramadhyani S and Patankar SV (1985), *Solution of the Convection-Diffusion Equation by a Finite-Element Method Using Quadrilateral Elements*, Numer Heat Transfer, 8, 595-612.

161. Ramaswamy B (1988), *Finite Element Solution for Advection and*

Natural Convection Flows, Computers & Fluids, 16(4), 349-388.

162. Reynolds O (1884), *On the dynamical theory of incompressible viscous fluids and the determination of the criterion*, Philos Trans, Ser A, 186, 123.

163. Reynolds WC (1968), *A Morphology of the Prediction Methods, Computation of Turbulent Boundary Layers*, 1968 AFOSR-ISP-Stanford

164. Reynolds WC (1976), *Computation of turbulent flows*, Ann Rev Fluid Mech, 8, 183-208.

165. Rice JG and Schnipke RJ (1985), *A monotone streamline upwind finite element method for convection-dominated flows*, Comp Meth Appl Mech Engrg, 48, 313-327.

166. Rice JG and Schnipke RJ (1986), *An equal-order velocity-pressure formulation that dose not exhibit spurious pressure modes*, Comp Meth Appl Mech Engrg, 58, 135-149.

167. Richmond MC and Patel VC (1987), *Pressure Gradient and Surface Curvature Effects in Turbulent Boundary Layers*, AIAA Paper 87-1301.

168. Rodi W (1972), *The prediction of free turbulent boundary layers by use of a two-equation model of turbulence*, PhD Thesis, University of London, UK.

169. Rodi W (1980), *Turbulence models and their application in hydraulics*, Presented by the IAHR - Section on Fundumentals of Division II: Experimental and Mathematical Fluid Dynamics.

170. Rodi W (1981), *Stress/Strain Relations in Differential Methods for Turbulent Flows, 1980-81 AFOSR-HTTM Stanford Conference on Complex Turbulent Flows*, Eds Kline SJ, Cantwell BJ and Lilley GM, Stanford University, 681-690.

171. Rodi W (1982), *Examples of turbulence models for incompressible flows*, AIAA J, 20, 872-879.

172. Rodi W, Celik F, Demuren AO, Seheuerer G, Leschziner MA and Rastogi AK (1981), *Summary Report from the 1980-81 AFOSR-HTTM Stanford Conference on Complex Turbulent Flows*, Sept 1981, 1495-1516.

173. Russell PJ and Hatton AP (1972), *Turbulent Flow Characteristics of an Impinging Jet*, Proc Instn Mech Engnrs, 186(52), 635-644.

174. Saad NR, Mujumdar AS and Douglas WJM (1977), *Prediction of Heat Transfer Under an Axisymmetric Laminar Impinging Jet*, Ind Eng Chem Fund, 16(1), 148-154.

175. Sani RL, Gresho PM, Lee RL and Griffiths DF (1981), *The cause and cure (!) of the spurious pressures generated by certain FEM solutions of the incompressible Navier-Stokes equations: Part I*, I.J.M.M.F, 1, 1.

176. Schlichting H (1960), *Boundary Layer Theory*, Fourth edition, McGraw-Hill.

177. Schneider GE, Raithby GD and Yovanovich MM (1978a), *Finite element analysis of incompressible fluid flow incorporating equal order velocity and pressure interpolation*, in: Proc Int Conf on Numerical Methods in Laminar and Turbulent Flows, Swansea, UK.

178. Schneider GE, Raithby GD and Yovanovich MM (1978b), *Finite element solution procedures for solving the incompressible Navier-Stokes equations using equal order variable interpolation*, Numer Heat Transfer, 1, 433-451.

179. Schnipke RJ (1986), *A Streamline Upwind Finite Element Method for Laminar and Turbulent Flow*, PhD Thesis, University of Virginia, Charlottesville, USA.

180. Schnipke RJ and Rice JG (1985), *Examination of a new finite element method applied to convective heat transfer*, Finite Element in Analysis and Design, 1, 227-239.

181. Schnipke RJ and Rice JG (1987), *A Finite Element Method for Free*

and Forced Convection Heat Transfer, Int J Numer Meth Engng, 24, 117-128.

182. Schnipke RJ, Rice JG and Flack RD (1987), *Finite element analysis of vaned radial diffuser*, Int J Heat Fluid Flow, 8(3), 187-194.

183. Schumann U (1975), *Subgrid scale model for finite difference simulation of turbulent flows in plane channels and annuli*, J Computational Physics, 18, 376-404.

184. Segerlind LJ (1976), *Applied Finite Element Analysis*, John Wiley.

185. Sharma M and Carey GF (1986), *Turbulent boundary-layer analysis using finite elements*, Int J Numer Meth Fluids, 6, 769-787.

186. Shemirani F and Jambunathan K (1990), *Conservative monotone streamline upwind formulation using simplex elements*, Int J Numer Meth Fluids, Submitted.

187. Shemirani F and Jambunathan K (1991a), *SIMPLER Finite Element procedure, incorporating equal-order velocity-pressure formulation*, presented at the 7^{th} International Conference on Numerical Methods in Laminar and Turbulent Flow, July 15-19 1991, Stanford, California, USA.

188. Shemirani F and Jambunathan K (1991b), *Regional Alternating-Direction Implicit Solver (RADIS) - A TDMA variant for completely unstructured grids generated by the FEM*, In preparation.

189. Shepard MS (1988), *Automatic Generation and Control of Finite Element Meshes*, Rensselaer Polytechnic Institute, Troy, New York, Report No 880912, 223-236.

190. Shyy W (1985), *A Study of Finite Difference Approximations to Steady-State, Convection-Dominated Flow Problems*, J Computational Physics, 57, 415-438.

191. Smith RM (1984), *On the finite-element calculation of turbulent flow using the k-ω model*, Int J Numer Meth Fluids, 4, 303-319.

192. Smith RM and Hutton AG (1982), *The numerical treatment of advection: A performance comparison of current methods*, Numer Heat Transfer, 5, 439-461.

193. Spalding DB (1972), *A Novel Finite-Difference Formulation for Differential Expressions Involving Both First and Second Order Derivatives*, Int J Numer Meth Engrg, 4, 557-559

194. Spalding DB (1974), *Turbulent Modelling: Solved and Unsolved Problems, Turbulent Mixing in Nonreactive and Reactive Flows*, A Project SQUID Workshop, Ed Murphy SNB, Plenum Press.

195. Spalding DB (1977), *Turbulence Models*, 3rd issue, Imperial College of Science and Technology, Report No HTS/76/17, London, UK.

196. Spalding DB (1980), *Mathematical Modelling of Fluid Mechanics, Heat Transfer and Mass Transfer Processes*, Report No HTS/80/1, Mechanical Engineering Department, Imperial College, London, UK.

197. Spalding DB (1982), *Turbulence Models - A Lecture Course*, Imperial College of Science and Technology, London, UK.

198. Sparrow EM and Kaljes JP (1977), *Local convective transfer coefficients in a channel downstream of a partially constructed inlet*, Int J Heat Mass Transfer, 20, 1241-1259.

199. Steffler PM (1989), *Upwind basis finite elements for convection-dominated problems*, Int J Numer Meth Fluids, 9, 385-403.

200. Stone HL (1968), *Iterative solution of implicit approximations of multi-dimensional partial differential equations*, SIAM J Num Anal, 5, 530-559.

201. Sykes J (1981), paper 357, presented at the HFTS Research Symposium, Oxford, UK, September 1981, AERE Report R10199.

202. Taylor C and Hughes TG (1981), *Finite Element programming of the*

Navier-Stokes Equations, Pineridge Press Ltd, Swansea.

203. Taylor C, Thomas CE and Morgan K (1981), *Analysis of turbulent flow with separation using finite element method*, in: Computational Techniques in Transient and Turbulent Flow, Eds Taylor C and Morgan K, Pineridge Press.

204. Tezuka A and Okuda O (1988), *An Adaptive Mesh Refinement for the Finite Element Method (Trial by the r-Method)*, JSME Int J, Series 1, 31(1), 50-55.

205. Tong GD (1982), *Computation of turbulent recirculating flow*, PhD Thesis, Dept Civil Engineering, University College of Swansea, UK.

206. Torbjorn U (1988), *Two-equation (k,ω) turbulence computations by the use of a finite element model*, Int J Numer Meth Fluids, 8, 965-975.

207. Turner Jr JC and Grunzburger MD (1988), *An analysis of finite element approximations for an algebraic model of turbulence*, Comput math Applic, 15(11), 945-951.

208. van Doormaal JP and Raithby GD (1984), *Enhancements of the SIMPLE Method for Predicting Incompressible Fluid Flows*, Numerical Heat Transfer, 67, 147-163.

209. van Heiningen ARP (1982), *Heat Transfer under an Impinging Slot Jet*, PhD Thesis, McGill University, Montreal.

210. van Heiningen ARP, Mujumdar AS and Douglas WJM (1975), *Numerical Prediction of the Flow Field and Impingement Heat Transfer Due to a Laminar Slot Jet*, ASME paper, No 75-WA/HT-99.

211. Wachpress EL (1979), *The numerical solution of turbulent flow problems in general geometry*, Knolls Atomic Power Laboratory Report, KAPL-4116.

212. Wang YA and Longwell PA (1964), *Laminar flow in inlet section of*

parallel plates, AI Ch E Journal, 10(3), 323-329.

213. Wang XS, Dagan Z and Jiji LM (1989a), *Heat transfer between a circular free impinging jet and a solid surface with non-uniform wall temperature or wall heat flux - 1. Solution for the stagnation region*, Int J Heat Mass Transfer, 32, 1351-1360.

214. Wang XS, Dagan Z and Jiji LM (1989b), *Heat transfer between a circular free impinging jet and a solid surface with non-uniform wall temperature or wall heat flux - 2. Solution for the boundary layer region*, Int J Heat Mass Transfer, 32, 1361-1371.

215. Wang XS, Dagan Z and Jiji LM (1989c), Conjugate heat transfer between a laminar impinging liquid jet and a solid disk, Int J Heat Mass Transfer, 32, 2189-2197.

216. White FM (1974), *Viscous Fluid Flow*, McGraw-Hill, New York.

217. Wikes NS and Clarke DS (1987), *Turbulence flow predictions using algebraic stress models*, Harwell Report AERE R 12694, Engineering Sciences Division, Harwell Laboratory, UK.

218. Wolfshtein M (1967), *Convection Processes in Turbulent Impinging Jets*, PhD Thesis, Imperial College, London, UK.

219. Wolfshtein M (1970), *Some Solution of the Plane Turbulent Impinging Jet*, ASME Transactions, Journal of Basic Engineering, 92D, 915-922.

220. Zienkiewicz OC (1977), *The Finite Element Method*, Third edition, McGraw-Hill.

221. Zienkiewicz OC, Lohner RL and Morgan K (1985), *High speed inviscid compressible flow by the finite element method*, The Mathematics of Finite Elements and Applications, Ed Whiteman JR, Academic Press, 1-25.

222. Zienkiewicz OC and Phillips DV (1971), *An automatic mesh generation scheme for plane and curved surfaces by isoparametric co-ordinates*, Int J Numer Mech Engng, 3, 519-528.